Final Report

INVESTIGATION OF BRIDGE DECK CRACKING IN VARIOUS BRIDGE SUPERSTRUCTURE SYSTEMS

FHWA/IN/JTRP-2002/25

by

Robert J. Frosch
Principal Investigator

and

David T. Blackman, Graduate Research Assistant
Roger D. Radabaugh, Graduate Research Assistant

School of Civil Engineering
Purdue University

Joint Transportation Research Program
Project No. C-36-56YY
File No. 7-4-50

SPR-2404

Prepared in Cooperation with the
Indiana Department of Transportation and the
U.S. Department of Transportation
Federal Highway Administration

Purdue University
West Lafayette, Indiana 47907
February 2003

TECHNICAL REPORT STANDARD TITLE PAGE

1. Report No.	2. Government Accession No.	3. Recipient's Catalog No.
FHWA/IN/JTRP-2002/25		

4. Title and Subtitle	5. Report Date
Investigation of Bridge Deck Cracking in Various Bridge Superstructure Systems	February 2003
	6. Performing Organization Code

7. Author(s)	8. Performing Organization Report No.
Robert J. Frosch, David T. Blackman, and Roger D. Radabaugh	FHWA/IN/JTRP-2002/25

9. Performing Organization Name and Address	10. Work Unit No.
Joint Transportation Research Program 1284 Civil Engineering Building Purdue University West Lafayette, IN 47907-1284	
	11. Contract or Grant No. SPR-2404

12. Sponsoring Agency Name and Address	13. Type of Report and Period Covered
Indiana Department of Transportation State Office Building 100 North Senate Avenue Indianapolis, IN 46204	Final Report
	14. Sponsoring Agency Code

15. Supplementary Notes

Prepared in cooperation with the Indiana Department of Transportation and Federal Highway Administration.

16. Abstract

Many bridges in the state of Indiana have been identified to have cracking in the concrete deck. Cracking has been identified in the negative and positive moment regions of bridges on both the top and bottom surfaces and can appear before or shortly after the opening of the structure to live loads. Significant crack widths and various degrees of cracking exist in different bridge systems including both concrete and steel superstructures. This research project was divided into five phases to determine the factors affecting transverse and longitudinal bridge deck cracking, as well as, to develop design recommendations that minimize or prevent these types of bridge deck cracking. The research focused on the design and construction of new bridge decks. However, an overview of overlay cracking is also presented. The first phase was a field evaluation to investigate the scope of the problem. Using the information gathered from the first phase, the second phase instrumented a typical bridge structure to provide an understanding of the behavior of transverse cracks in a concrete bridge deck. With the findings from the previous two phases, the third phase conducted a laboratory investigation to study the effects of shrinkage and restraint of a concrete deck and to determine the contribution of stay-in-place steel forms to the formation of transverse cracking. The fourth phase evaluated the effect of formwork type on restrained shrinkage. In the final phase, the effect of reinforcing bar spacings and epoxy thickness on crack width and spacings were evaluated. Based on the research investigation, transverse deck cracking is caused by restrained shrinkage of the concrete deck while longitudinal cracking is caused by a combination of factors including restrained shrinkage and a construction detail that turns the leg of an angle used to support stay-in-place formwork into the deck. Design and construction recommendations are provided to minimize transverse, longitudinal, and overlay map cracking.

17. Key Words	18. Distribution Statement
bridge deck, transverse cracking, longitudinal cracking, overlay cracking, bridge decks, restrained shrinkage, shrinkage, restraint, restrained shrinkage, shrinkage and temperature reinforcement	No restrictions. This document is available to the public through the National Technical Information Service, Springfield, VA 22161

19. Security Classif. (of this report)	20. Security Classif. (of this page)	21. No. of Pages	22. Price
Unclassified	Unclassified	265	

Form DOT F 1700.7 (8-69)

TABLE OF CONTENTS

LIST OF TABLES

LIST OF FIGURES

ACKNOWLEDGEMENTS

This work was supported by the Joint Transportation Research Program (JTRP) administered by the Indiana Department of Transportation (INDOT) and Purdue University through contract SPR-2404. The support of the Indiana Department of Transportation (INDOT) and the Federal Highway Administration (FHWA) are gratefully acknowledged. The authors would like to extend thanks to Dr. Tommy Nantung from the INDOT Division of Research for his support throughout the project. In addition, thanks are extended to members of the Study Advisory Committee for their participation and thoughtful comments throughout the project. These members include Youlanda Belew, Mike Byers, Khalil Dughaish, Sherwood Garrison, Jaffar Golkhajeh, John Jordan, Jim Karr, Don Leonard, John McCrary, George Snyder, and Val Straumins.

CHAPTER 1
INTRODUCTION

1.1 Bridge Deck Cracking

Many bridges in the state of Indiana have been identified to have cracking in the concrete deck. Cracking has been identified in the negative and positive moment regions of bridges on both the top and bottom surfaces. In some structures, only top surface cracking is visible due to the use of stay-in-place steel forms. The cracking can appear before or shortly after the opening of the structure to live loads. Significant crack widths and various degrees of cracking exist in different bridge systems including both concrete and steel superstructures. Figure 1.1 shows a bridge with multiple transverse cracks.

Figure 1.1: Transverse Cracking (Bridge 3)

In the United States, many concrete bridge decks have experienced cracking soon after construction (McDonald, Krauss, and Rogalla 1995). From a survey of 52 state and other transportation agencies, it is estimated that more than 100,000 bridges in the United States have developed early transverse deck cracking. This deck cracking has been reported in a variety of geographical locations and climates as well as on different superstructure types. Cracks typically occur before the concrete is one month old and are transverse, full depth, and spaced 3-ft to 10-ft. apart.

1.1.1 Crack Types in Concrete Bridge Decks

In general, a crack will form in a concrete bridge deck once the cumulative stress in the deck exceeds the tensile strength of the concrete. Cracks in concrete bridge decks can typically be divided into three types: transverse cracks, longitudinal cracks, and map cracks. Transverse cracks are those that generally run perpendicular to the girders of the superstructure. Transverse cracks can also exist parallel to the skew of the bridge near

the end abutments. Transverse crack widths have been reported in the range of 0.004-in. to 0.020-in. Longitudinal cracks are those that run parallel to the girders of the superstructure. Longitudinal cracks commonly form directly above the edges of the girders in the superstructure. Map cracks, as the name implies, look like a map showing the haphazard arrangement of roads or waterways. These map cracks are random and run in various directions.

1.1.2 Bridge Deck Cracking Concerns

In recent years, cracking has increased in newly constructed concrete bridge decks (Babaei and Fouladgar 1997). Cracking in the deck provides a route for intrusion of water and chlorides that can potentially lead to corrosion of deck reinforcement, a primary cause of bridge deterioration. In addition, full depth deck cracking allows water and chlorides to penetrate through the deck and can lead to deterioration of the superstructure as well as the substructure. According to Purvis et al. cracks wider than 0.007-in. contribute to the deterioration of the concrete deck and corrosion of the reinforcing steel in the presence of deicing chemicals (Purvis et al. 1995). Surface concrete spalling can also occur at the location in which two cracks intersect one another (NCHRP 380 1996).

The corrosion of the reinforcing steel in the deck can lead to cracks in the top surface of the deck above an individual reinforcing bar or cracks around a large delaminated area due to internal pressure from the expansive corrosion products. To diminish the threat of corrosion of the reinforcing steel and deck deterioration, epoxy coated reinforcing steel is an alternative to normal black reinforcing steel. Also, the minimum clear cover on the top reinforcing steel mat of a slab specified by the American Association of State Highway and Transportation Officials (AASHTO) requirement in the *AASHTO LRFD Bridge Design Specifications,* 2nd Edition is 2.5 in. for deck surfaces exposed to deicing salts (AASHTO 1998). The clear cover for the reinforcing steel requires the water and chlorides to penetrate deep into the deck before it could potentially corrode the reinforcing steel and cause cracking.

1.2 Transverse Deck Cracking

Transverse cracks are the most frequently observed cracks in concrete bridge decks. According to the Portland Cement Association, relatively few transverse cracks have been observed in the positive moment region of bridge decks supported by concrete girders (PCA 1970). In the negative moment region, very fine transverse cracks have been noted in continuous concrete bridges. On decks with a steel superstructure, transverse cracking has been observed along the entire length of the bridge at regular intervals in both simple- and continuous-span construction. NCHRP Report #380 (1996) reported more transverse cracking had been observed on concrete bridge decks with precast concrete girders compared to cast-in-place concrete girders. Also, more transverse cracking was noted on steel superstructure bridges when stay-in-place steel forms were used than if removable plywood forms were used. Concrete decks incorporating composite action supported on either steel wide-flanged girders or steel plate girders cracked much more that those constructed on any other system.

From core samples studied by Purvis et. al. (1995), two observations were made. First, the transverse cracks were predominately over the top transverse reinforcing bars. Second, cracks passed through the coarse aggregate particles. This study demonstrated that the cracks were formed in the hardened concrete state. If the cracks passed through only the cement paste and not through the coarse aggregate, the cracks would have likely formed in the plastic concrete phase.

The restraint of hardened concrete during both drying- and thermal-shrinkage is the main source of tensile stresses causing transverse cracking. This concrete restraint stems from the reinforcing steel in the deck and the support girders (PCA 1970). Work performed by Schmitt and Darwin (1995) studied the effect of live loads and the vibrations caused by live loads on cracking in concrete decks. Neither live loads nor the vibrations caused by live loads were found to cause transverse deck cracks.

1.3 Concrete Shrinkage

Concrete is made with four primary components: cement, aggregate, admixtures, and water. Individually, these materials do not shrink, but in combination, they do. The majority of concrete shrinkage is caused by a complex, internal, build-up of pressures from both the loss and movement of water within the capillaries of the concrete matrix.

Shrinkage begins with the loss of water from the capillaries that is not physically bound (known as free water), resulting in internal relative humidity gradients (Franco 2001). The empty capillaries attract water molecules (known as absorbed water) from the surface of the calcium silicate hydrates (C-S-H). This process creates attraction forces between the C-S-H particles, causing the concrete mass to shrink during both the fresh state of the concrete (plastic shrinkage) and the hardened state of the concrete (drying shrinkage). Therefore, the volume change is indirectly proportional to the free water loss. If no free water is lost during hydration, shrinkage will not occur. Therefore, because the magnitude of free water loss is due to the difference in relative humidity from the internal concrete to the external environment, concrete shrinkage is proportionate to the external relative humidity (Mindess and Young 1981). If external relative humidity was continuously 100%, concrete shrinkage would theoretically not take place. Figure 1.2 displays two graphs that relate relative humidity to shrinkage.

Two less predominate factors to the final magnitude of concrete shrinkage are carbonation and autogeneous shrinkage. Carbonation shrinkage is caused by a chemical reaction from atmospheric carbon dioxide with hardened concrete. Because it is believed that carbonation shrinkage can only have a significant effect in the long term, its relationship with early-aged-cracking is insignificant (Mindess and Young 1981)

Autogeneous shrinkage can occur if no additional water is provided during the mixing of the concrete, which, allows the mix to dry out even if no water is lost to the environment. This type of shrinkage is considered rare and not a major component to the total concrete shrinkage (Mindess and Young 1981; Wiegrink, Shashidhara, and Surendra 1996).

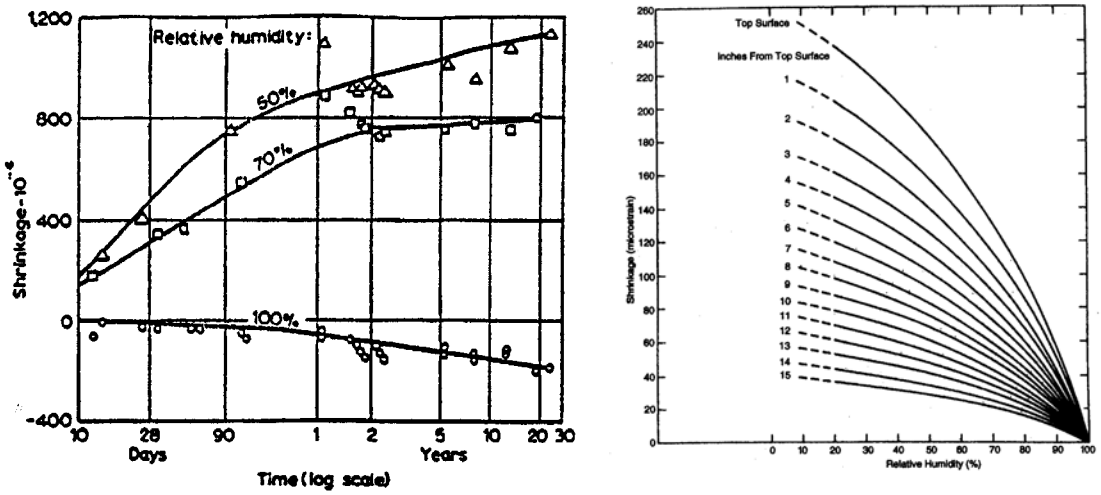

Figure 1.2: Relative Humidity vs. Shrinkage (ACI 224 2001; Suprenant 2002)

1.3.1 Restrained Shrinkage

By themselves, shrinkage and temperature changes are not detrimental to the integrity of concrete. If a concrete slab were allowed to move freely, shrinkage strains would not induce significant stresses. However, in reality concrete is never truly allowed to move freely. In every situation where concrete is used, it is restrained in some way. The amount of restraint will reflect how much movement is restricted and also determine the magnitude of stresses developed in the section. Full restraint will allow no movement. A simple example of restrained concrete is shown in Figure 1.3 (ACI 224 2001).

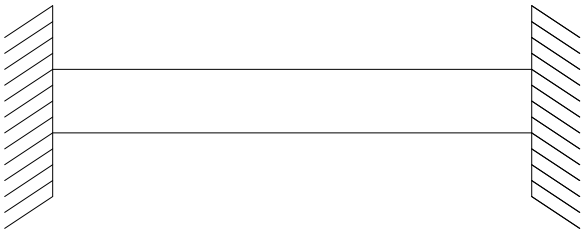

(a) Before Shrinkage

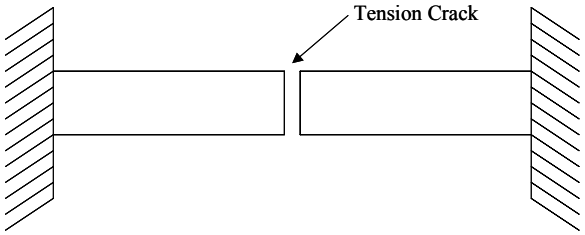

(b) After Shrinkage

Figure 1.3: End Restrained Concrete Slab

In this case, as the concrete mass shrinks, stresses build up within the section. This type of restrained shrinkage is fairly easy to visualize, and stresses can easily be calculated. Unfortunately, this simple scenario is seldom encountered in actual construction.

1.3.1.1 External Restraint

External restraint can come in many different sources. A simple example was explained above. A more complex type of restrained shrinkage results from a fairly new type of bridge design. For decades concrete bridge decks were designed solely to span from girder to girder and to create a durable driving surface. Since the 1970s, economics has forced the majority of bridges to use the bridge deck as a major structural component of the bridge. Bridge decks are now constructed compositely with the girders, which substantially reduce girder depths. This method, however, also has its disadvantages.

Because the deck and girders act compositely, the girders can substantially restrain the concrete deck when it shrinks. This restraint is different from that shown in Figure 1.3 as bridge girders induce longitudinal restraint along the full length of the bridge deck. Both types of restraint can cause transverse cracking, but the manner of which it happens is different.

There are two main differences between the two different types of restraint. If the concrete member was only restrained at its ends, when the tensile stress capacity of the concrete is exceeded due to shrinkage, the specimen will crack exactly in the center of its length. If the specimen contained no reinforcement, the stress caused by shrinkage would be lost when the crack formed. Consequently, the specimen would break into two pieces that could continue to freely shrink without restraint (Figure 1.3). If the specimen were to contain reinforcement, the specimen would also crack near the center when tensile stresses caused by shrinkage are large enough to exceed the tensile strength of the concrete. After which, there are two possibilities.

If the cross-sectional area of the reinforcement is large enough to exceed the tensile capacity of the concrete, the crack will only open to a minor extent and some strain energy would be lost from the system (referred to as over-reinforced). Then the two concrete pieces, connected by reinforcement, will act as separate members restrained at each end, but with half the length of the original member. If each piece of concrete continues to shrink, another two cracks should open at the quarter points of the original length of the uncracked specimen. This process continues until the total shrinkage is accommodate both by cracks and strain between cracks (Hughes and Mahmood 1988).

If the original specimen contained reinforcement, but its total area is not sufficient to exceed the concrete's tensile capacity without yielding, the behavior of the specimen would be different (referred to as under-reinforced). When the strain induced by shrinkage exceeds the tensile strength of the concrete, a crack will occur at the center of the specimen. However, because the section is under-reinforced, the steel will yield. The width of the crack will increase until the total shrinkage displacement is accommodated at the crack location. In this case, only one crack is generated. Under substantial shrinkage strains, an under-reinforced section can produce very large crack sizes.

A continuously restrained concrete slab will behave differently under shrinkage loads. Figure 1.4 illustrates a continuously restrained concrete member, which is significantly different from the end-restrained member shown in Figure 1.3.

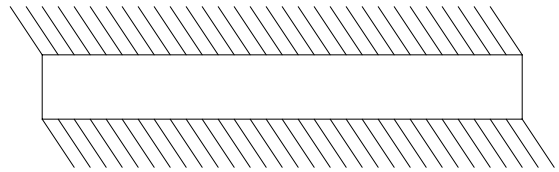

(a) Before Shrinkage

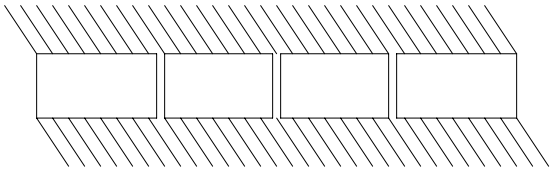

(b) After Shrinkage

Figure 1.4: Concrete Slab Restrained Along its Full Length

Because a concrete bridge deck is typically reinforced, its behavior without reinforcement will not be examined. As explained before, a concrete slab can be under- or over-reinforced. Just as for the end restrained specimen, as tensile stresses induced by shrinkage exceed the tensile capacity of the concrete, the specimen will crack. Depending if the specimen is over- or under-reinforced, the specimen can crack in many locations. It is likely that more than one crack will initiate at the same time. The number of cracks depend on the length of specimen, the strength/stiffness/creep of the concrete, the amount of restraint, and the magnitude of the shrinkage. Restraint provided along a member's full length is more easily understood if thought of as having a development length (Hughes and Mahmood 1998). The first crack(s) will develop when there is enough shrinkage strain induced along a certain length that exceeds the tensile capacity of the concrete. If the specimen is very short, cracking may never occur. If the specimen is very long (like a bridge deck), cracking should occur at evenly spaced intervals along the length. At the location of the crack, two things may happen. If under-reinforced, the reinforcement will yield (local debonding will occur), and at the crack location the concrete will no longer be restrained. Crack width will depend on the amount of reinforcement in the section. If there is additional shrinkage, and the length of continuous restraint between cracks is long enough to develop tensile stresses that exceed the concrete's tensile capacity, new cracks will initiate approximately at the midpoints of the uncracked sections.

If the specimen is over-reinforced, the size of the original crack(s) should not open significantly. Therefore, if additional shrinkage is induced in the specimen, and the uncracked section is long enough to develop tensile stresses greater than the concrete tensile capacity, the specimen will crack. Cracking will continue to occur between cracks until the length of the uncracked section is small enough so that the developed restraint is not capable of generating tensile stresses greater than the concrete tensile strength.

Therefore, both an over- and under-reinforced slab will crack at certain uniform intervals, but if over-reinforced, the crack spacing and widths will be smaller.

A major difference, however, between the restraint provided in Figure 1.3 and Figure 1.4 when compared to a bridge deck, is that the actual restraint is only provided from the bottom section of the slab (Figure 1.5). This restraint creates a more complicated behavior. If the concrete is allowed to shrink uniformly, the bottom section of the slab will be restrained similarly to Figure 1.4, however the top section is not restrained. Therefore, cracking should initiate at the location of greatest restraint, the bottom of the slab. The bottom side of a concrete bridge deck should crack similarly to Figure 1.4. If the slab were only restrained at the bottom section of the slab, cracks should initiate on the bottom surface and continue increasing in depth until the amount of restraint is not adequate to restrict the shrinkage or cause stresses exceeding the tensile strength of the concrete. Figure 1.6 presents a relationship published by ACI Committee 207 of the degree of restraint (fully restrained = 1.0) through the depth of a concrete slab with continuous base restraint.

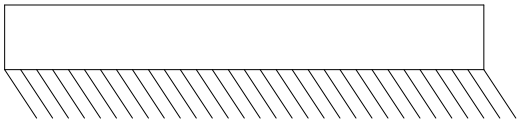

Figure 1.5: Continuous Restraint Along the Bottom Section of a Slab

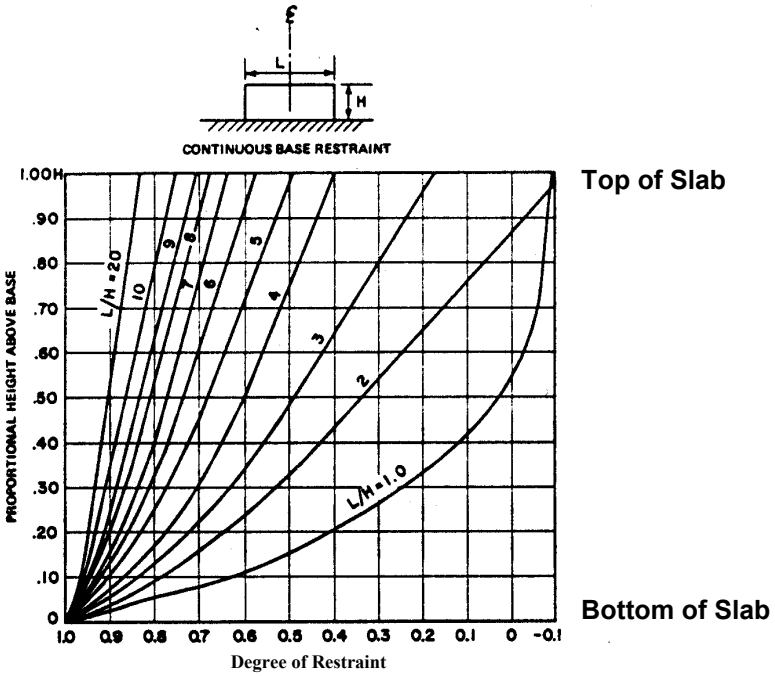

Figure 1.6: Degree of Restraint vs. Depth of Slab (ACI 207)

Figure 1.6 illustrates that even though the top surface of a slab may not be externally restrained, the restraint provided at the bottom of the slab can also significantly restrain the top surface.

1.3.1.2 Internal Restraint

A commonly overlooked type of concrete shrinkage restraint is internal restraint. The primary way internal restraint is provided is through the concrete itself. In some cases, if a concrete member is large enough and not properly cured, this type of restraint alone can cause cracking within a bridge deck. Internal restraint caused by the concrete mass is produced from the manner in which concrete shrinks. As mentioned previously, immediately after a bridge deck has been cast, shrinkage can begin. Concrete must be exposed for shrinkage to occur. If the exposed surface has less than 100% relative humidity, moisture can escape from the concrete. Since all of the concrete is not exposed to a surface, shrinkage can vary. Because exposed sections of concrete will shrink more (and at a faster rate), internal stresses can be created within a concrete slab without any external restraint or reinforcement. Figure 1.7 illustrates how concrete can act as a source of restraint and can create tension and compression through the depth of a slab (ACI 224 2001; PCA 1970; Mindess and Young 1981; ACI 207).

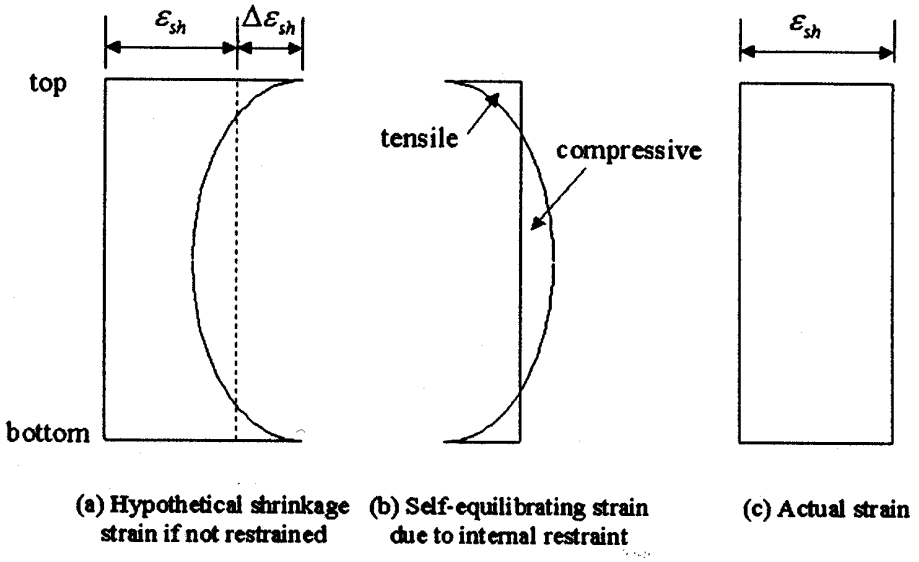

Figure 1.7: Internal Restraint Stress Distribution (ACI 224 2001)

Because the amount of exposed surface relates to how a concrete member will shrink (rate and magnitude), it is common for concrete members to be compared using their surface-to-volume ratio. As the ratio increases, the amount and rate of shrinkage will also increase. Figure 1.8 shows how the surface-to-volume ratio can directly affect shrinkage over time.

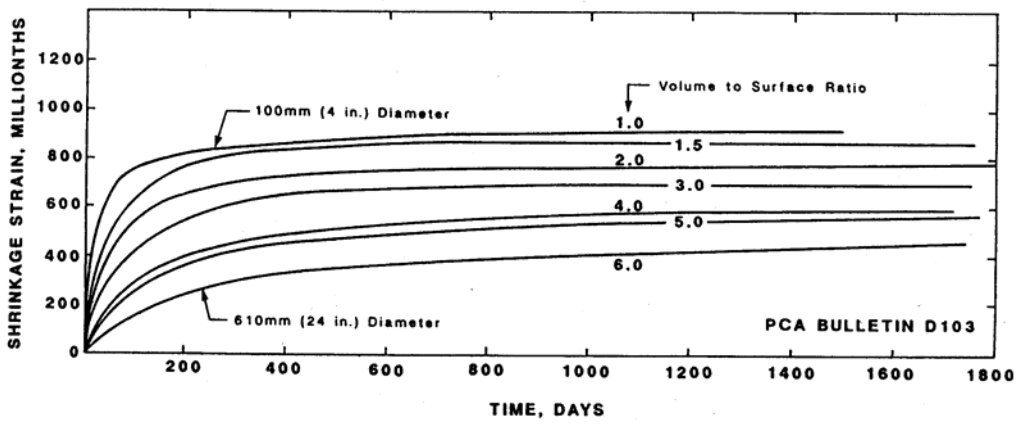

Figure 1.8: Shrinkage vs. Surface-to-Volume Ratio (NCHRP 380 1996)

1.4 Factors Affecting Deck Cracking

The major factors causing early age cracking have not been agreed upon, primarily because of the number of variables involved. Past research has resulted in identification of various primary factors. These factors can be broken down into four categories: environmental, construction technique, design specifications, and material properties. In 1994, the Minnesota Department of Transportation conducted a nation-wide survey of both state and national agencies and bridge design firms, seeking to identify the primary reasons for bridge deck cracking. The results of this survey, which is considered the most comprehensive study of transverse cracking, can be found in Figure 1.9 (NCHRP 380 1996). The reason for the large number of factors reportedly contributing to early-age-cracking is because each factor influences the magnitude of concrete shrinkage, shrinkage restraint, or bridge deck hydration temperatures. Restrained concrete shrinkage is generally accepted as the primary basis of early-age transverse cracking of bridge decks.

Factors	Effect			
	Major	Moderate	Minor	None
Design				
Restraint	✓			
Continuous/simple span		✓		
Deck thickness		✓		
Girder type		✓		
Girder size		✓		
Alignment of top and bottom reinforcement bars		✓		
Form type			✓	
Concrete cover			✓	
Girder spacing			✓	
Quantity of reinforcement			✓	
Reinforcement bar sizes			✓	
Dead-load deflections during casting			✓	
Stud spacing			✓	
Span length			✓	
Bar type—epoxy coated			✓	
Skew			✓	
Traffic volume				✓
Frequency of traffic-induced vibrations				✓
Materials				
Modulus of elasticity	✓			
Creep	✓			
Heat of hydration	✓			
Aggregate type	✓			
Cement content and type	✓			
Coefficient of thermal expansion		✓		
Paste volume—free shrinkage		✓		
Water-cement ratio		✓		
Shrinkage-compensating cement		✓		
Silica fume admixture		✓		
Early compressive strength			✓	
HRWRAs			✓	
Accelerating admixtures			✓	
Retarding admixtures			✓	
Aggregate size			✓	
Diffusivity			✓	
Poisson's ratio			✓	
Fly ash				✓
Air content				✓
Slump†				✓
Water content				✓
Construction				
Weather	✓			
Time of casting	✓			
Curing period and method		✓		
Finishing procedures		✓		
Vibration of fresh concrete			✓	
Pour length and sequence			✓	
Reinforcement ties				✓
Construction loads				✓
Traffic-induced vibrations				✓
Revolutions in concrete truck				✓

† within typical ranges

Figure 1.9: Factors Influencing Cracking of Bridge Decks (NCHRP 380 1996)

1.4.1 Design

1.4.1.1 Structural

The properties of the deck are important. The thickness of the bridge deck can affect the formation of transverse deck cracks. In a study performed by French et al. (1999), decks thinner than 6.25 in. had more observed cracks than thicker decks. Also, the use of smaller reinforcing steel bars (#5 or #6) in the deck spaced closer together (5.5 in. to 7 in.) reduces the risk of transverse deck cracking.

1.4.1.2 Form Type

Two types of forms are typically used for the construction of bridge decks. Concrete commonly is formed with wood, but SIP metal deck pans have also been used as formwork for concrete construction. SIP forms have been adopted for bridge deck design in Indiana. In comparison with wood forms, SIP forms are very easy to construct and cost effective. Consequently, even though both types of formwork are acceptable for bridge construction, the use of SIP forms has become more common.

Form type not only influences economics. As explained in Section 1.2, concrete shrinkage also can be affected by form type. Because SIP deck forms are not removed from a bridge deck and wood forms are removed shortly after casting, surface-to-volume ratios can vary significantly depending on construction technique. A SIP formed bridge deck should have approximately one half the surface-to-volume ratio of a bridge deck formed with wood forms. Therefore, a bridge deck constructed with wood forms should shrink more than one constructed with SIP forms.

If the surface area of a bridge deck (constructed with SIP forms) was decreased evenly by sealing both the top and bottom surfaces of the bridge deck, the deck would be less susceptible to early-age cracking. However, because a SIP deck pan only seals a bridge deck on its bottom face, the shrinkage profile becomes less symmetrical and may be more inclined to crack if restrained. Carrier and Cady (1975), measured the average moisture content of two slabs, one constructed with wood forms (after the removal of the forms) and the other with SIP forms. The results of this experiment are presented in Figure 1.10.

These diagrams illustrate that a bridge deck constructed with SIP forms will result in an asymmetric moisture gradient. The varying moisture gradient will result in varying shrinkage through the depth of a slab and will produce a behavior that is known as curling (Weiss, Yang, and Shah 1998). Figure 1.11 illustrates this behavior.

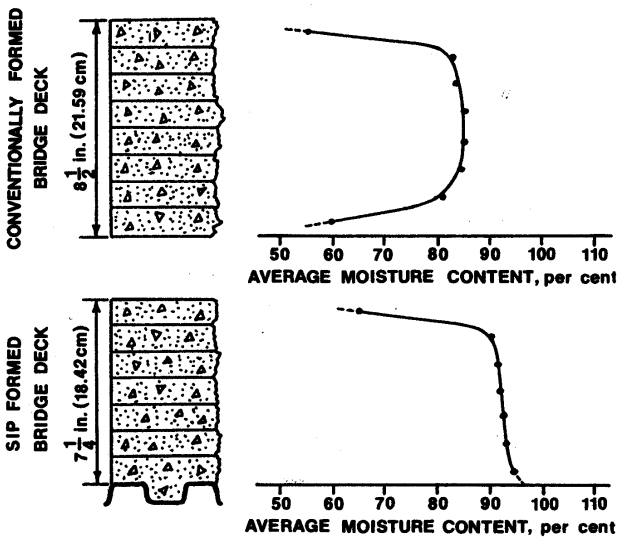

Figure 1.10: Moisture Gradient Within a Bridge Deck (Carrier and Cady 1975)

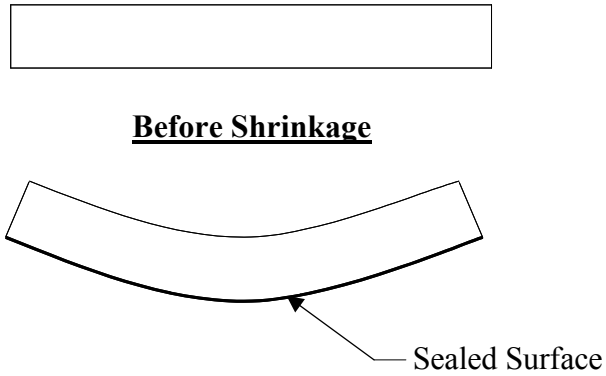

Figure 1.11: Curling

Because the top surface shrinks and the bottom surface does not, the slab will curl so that plane sections will remain plane. If the slab is completely free to move, no internal stresses should develop within the slab. If, on the other hand, the slab is restrained such as from a bridge deck, internal stresses will develop. Because the slab wants to curl, but is restrained from bending on its bottom surface, tensile stresses will develop on the top face of the slab. In reality, some shrinkage will occur on the bottom face of concrete even if it is completely sealed, because water within that section can still migrate to the top surface. Therefore, a non-symmetric stress gradient is likely to form across the depth of the section, with the largest tensile stress located at the top surface. These tensile forces have been estimated to be larger than those created from symmetrical shrinkage, even though the total shrinkage of a wood formed deck will be larger (NCHRP 380 1996). Therefore, the question arises, which type of formwork decreases the likelihood of early-age cracking?

The literature reviewed provided limited information concerning the relationship of early-age cracking and form type. NCHRP Report 380 (1996) only discusses the topic briefly. In the list of reasons reported from their survey (Figure 1.9), form type was mentioned as having a "minor" affect. The report did not discuss if this category referred directly to how the form type affected shrinkage or to other issues such as subsistence due to form deflection.

NCHRP 380 report (1996) references two surveys that mention the effect of form type. One found that less transverse cracking occurred when SIP forms were used (Pfeifer Landgren, and Krauss 1992), while another found no correlation between the two (Wiss et al. 1992). NCHRP 380 report concludes that "A SIP steel form will (1) cause deck shrinkage that is more linear (nonuniform) than uniform, (2) produce larger tensile stresses at the upper surface of a the deck, and (3) may increase the risk or severity of transverse deck cracking".

Pennsylvania State University conducted a survey on the durability of bridge deck concrete in 1971 (Cady et al. 1971). This study references Larson and Malloy (1966) and Love, Barnoff, and Larson (1967). These reports suggest that SIP forms increase the structural stiffness (providing composite action in the lateral direction) of a bridge deck; therefore, these decks performed better than those constructed with wood forms. It was reported that bridge decks formed with conventional forms exhibited more than three times as much transverse cracking as decks formed with corrugated metal SIP forms. It was also suggested that SIP forms could slow moisture loss from the fresh concrete.

Based on the literature review, it was established that there is limited and inconsistent information and research relating early age shrinkage to form type. Therefore, there is limited understanding on the effect of form type on early-age bridge deck cracking.

1.4.1.3 Shrinkage and Temperature Reinforcement

Bridge decks are exposed to severe environmental conditions; consequently, they must be properly designed to endure these conditions. One of the primary factors relating directly to the overall durability of a bridge deck is the crack widths. If a crack is too wide, water and deicing salts can penetrate to the depth of the reinforcement. Typical acceptable crack widths for structures subjected to deicing salts range from 0 to 0.008 in. (NCHRP 380 1996). Regardless of precautions taken to minimize shrinkage, a composite bridge deck will likely crack. Cracking, however, does not have to be significantly detrimental to the life span of a bridge.

The most common way to limit transverse crack widths in a bridge deck is by placing reinforcement longitudinal to the traffic. Reinforcement cannot stop a bridge deck from cracking, but it can control both the crack spacing and crack widths. When shrinkage or temperature changes create tensile forces large enough to exceed the capacity of the concrete, the reinforcement can limit crack widening. Bridge deck shrinkage and temperature (S&T) reinforcement is required by current codes; however, problems related to early-age cracking still exist.

It has been established that minimum deck reinforcement increases the durability of a bridge deck; therefore, it is mandatory in most codes. Table 1.1 presents the required minimum area of shrinkage and temperature steel and maximum bar spacings commonly specified.

Table 1.1: Code Requirements for Shrinkage and Temperature Reinforcement

	AASHTO 16th Ed.	AASHTO (LRFD) 2nd Ed.	ACI 318 - 99
Shrinkage and Temperature Reinforcement Requirements	Section 8.2 $A_s \geq 1/8$ in^2/ft Spacing $\leq 3h$ ≤ 18"	Section 5.10.8 $A_s \geq 0.11*(A_g/f_y)$ Spacing $\leq 3h$ ≤ 18"	Section 7.12.2.1 $A_s \geq 0.0018b*h$ Spacing $\leq 3h$ ≤ 18"
Equivalent S&T Reinforcement Design For a Bridge Deck Similar to I65 over SR25	#4 Bars @ 18" (Two layers)	#4 Bars @ 13.5 (Two layers)	#4 Bars @ 13.5" (Two layers)

Notes: - AASHTO 16th Ed. and 2nd Ed. also require a minimum area of longitudinal distribution reinforcement for bridge decks.
- ACI 318 requires that when S&T movements are significantly restrained, an equivalent factored load shall be applied to the structure.

Beyond code requirements, suggested values of reinforcement to limit crack widths in bridge decks were obtained from the literature review. NCHRP 380 suggests that to control transverse cracking, S&T reinforcement should consist of at least size 10M (#4 bar) bars placed at a maximum of 6 in. MacGregor suggests that 3 times the ACI limitation ($A_s = 0.0054A_g$) should be used to limit shrinkage cracks (MacGregor 1997). ACI Committee 224 (2001) indicates that "the minimum-reinforcement percentage, which is between 0.18 and 0.20%, does not normally control cracks to within generally acceptable design limits. To control cracks to a more acceptable level, the percentage requirement needs to exceed about 0.60%." This value is in general agreement with that proposed by MacGregor.

1.4.1.4 Epoxy Coating

Another method to increase the durability of a bridge deck is by providing an epoxy coating on the reinforcement. ASTM-A775-97 requires that a coated bar must have an epoxy thickness ranging between 0.005 in. and 0.012 in. The primary function of this coating is to protect the reinforcing bars from the environment so they do not rust. Therefore, bridges in Indiana use epoxy-coated bars to increase the durability of the deck. However, the epoxy coating on the reinforcement may decrease the bond characteristics and consequently aggravate deck cracking by producing larger crack spacings and widths. Epoxy coated bars have only been used since the 1970s (Cleary and Ramirez 1993); consequently, there has been a limited amount of research involving the effect of epoxy coated bars on crack widths.

Johnston and Zia performed static and fatigue tests of slabs containing both #6 and #11 epoxy and uncoated (black) bars. The slab specimens showed little difference in spacing, crack width, deflection, or ultimate strength (Johnston and Zia 1982).

R.A. Treece and J.O. Jirsa also performed tests on beams with varying epoxy-coated reinforcement (Treece and Jirsa 1987). They concluded that epoxy coating significantly increased the width and spacing of cracks. For specimens with #6 bars, the average width of cracks were twice that of the uncoated. Figure 1.12 displays some of the results from the tests. The specimen notation is as follows: the first number is coating thickness in mils, the second is the bar size, and the third is the concrete compressive strength (ksi).

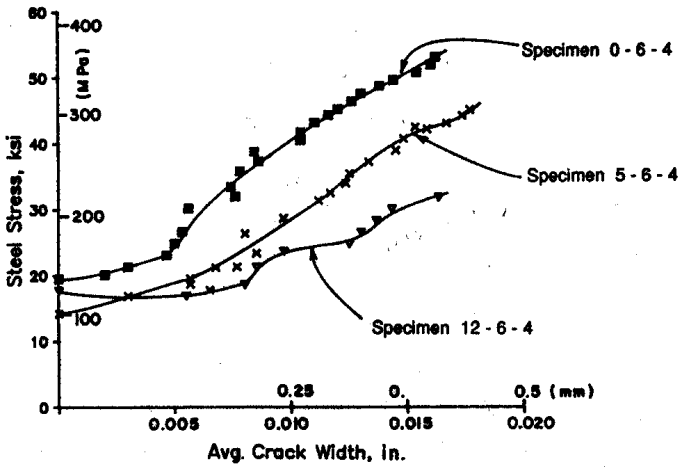

Figure 1.12: Test Results From Treece and Jirsa (1987)

Cleary and Ramirez (1993) also tested beams with varying epoxy-coated reinforcement thickness. The test results found that even though the total widths of all cracks in the constant moment region were found to be approximately equal for each type of reinforcement, the average crack width for a beam with epoxy coated bars was larger (up to 23%) than for beams with uncoated bars.

1.4.2 Materials

1.4.2.1 Basic Materials

The concrete mix design is a very important factor in the control of cracking. The major mix design parameters affecting the tendency towards cracking include cement content, water-to-cement ratio, cement type, cement fineness, and aggregate size and quality.

High strength concrete in the range of 5000 – 7000 psi is commonly used for bridge decks. To achieve this higher concrete strength, more cement is utilized. The additional cement requires extra water and produces more cement paste. The extra cement paste will undergo more shrinkage, as well as, generate a higher heat of hydration. High strength concrete will also develop higher stresses for a given

temperature change or amount of shrinkage. The lowest possible cement content to meet the specified requirements will minimize the cracking tendency by reducing shrinkage, heat of hydration temperatures, and thermal stresses (McDonald, Krauss, and Rogalla 1995).

The water-to-cement ratio also affects the concrete strength. With a given amount of cement, a higher water-to-cement ratio produces more cement paste generating a weaker yet more workable concrete. The lowest possible water-to-cement ratio to meet the workability requirements will minimize the cracking tendency by reducing shrinkage (McDonald, Krauss, and Rogalla 1995).

The type of concrete used in the concrete will influence the heat of hydration. High early heats of hydration cause additional thermal stresses in the concrete deck. Type II or IV cement (low heat of hydration) will reduce the heat of hydration; however, Type III cement (high early strength) increases the heat of hydration. Reducing the thermal stress at early ages will minimize the likelihood of cracking in the deck (McDonald, Krauss, and Rogalla 1995).

Another factor affecting the heat of hydration in concrete is the fineness of the cement. The finer the cement is ground, the higher the heat of hydration. The fineness of the cement varies between manufacturers. Careful selection of a cement manufacturer based on the fineness could affect the cracking tendency by lowing the thermal stresses generated in the deck (McDonald, Krauss, and Rogalla 1995).

The aggregate used in the concrete mix also impacts the concrete shrinkage. The largest possible size of a high quality, low-shrinkage aggregate will help minimize shrinkage. Larger aggregate requires less cement paste to coat the particles, reducing the amount of cement and water required. With less cement paste, the concrete experiences less shrinkage (McDonald, Krauss, and Rogalla 1995).

1.4.2.2 Concrete Admixtures

Admixtures can also have an effect on the cracking tendencies of concrete decks. Admixtures are added to the concrete mix immediately before or during the mixing process to improve one or more of the concrete's characteristics. The primary admixtures that affect this cracking tendency are air entrainment, water reducers, retarders, accelerators, and silica fume.

Air entrainment of 4 to 6 percent yields protection against cracking due to freeze-thaw cycles by encapsulating tiny air bubbles in the hardened concrete. As the water in the capillaries starts to freeze, the water is forced into the air voids. With sufficient voids, internal pore water pressure is alleviated and prevents cracking. As a side effect to freeze-thaw protection, air entrainment yields either a more workability or higher strength concrete. If the same water-to-cement ratio is used, the addition of air entrainment will produce a more workable concrete. If the original workability is desired, the addition of the air entrainment allows for the use of less water, yielding a lower water-to-cement ratio and a higher concrete strength. The lower water-to-cement ratio reduces shrinkage and cracking tendency (McDonald, Krauss, and Rogalla 1995).

Water reducers and high range water reducers (superplasticizers) also reduce the water-to-cement ratio. Water reducers permit a decrease in quantity of mix water required to reach a desirable concrete workability. This lower water-to-cement ratio

again reduces the amount of cement paste and minimizes the cracking tendency (McDonald, Krauss, and Rogalla 1995).

Retarders slow the setting time of concrete; therefore, reducing the temperature gain of the deck. The lower temperature generation reduces the likelihood of thermal cracking. Retarders, however, can increase the susceptibility of plastic shrinkage cracking (McDonald, Krauss, and Rogalla 1995).

As opposed to retarders, accelerators diminish the setting time of the concrete. The shortened setting time increases the heat of hydration, early concrete strength development, and early concrete shrinkage. Therefore, accelerators increase the possibility of deck cracking (McDonald, Krauss, and Rogalla 1995).

Another admixture that increases the heat of hydration is silica fume. The increased early age temperature will increase thermal stresses and the risk of cracking in the deck. Silica fume also reduces the bleed water (McDonald, Krauss, and Rogalla 1995).

1.4.3 Construction

1.4.3.1 Weather

The weather during placement of the concrete bridge deck can affect the tendency towards cracking. The acceptable temperature range for deck casting is recommended to be between 40^{o} F to 90^{o} F. Also, concrete placement should be avoided on days when the temperature range between high and low temperature exceeds 50^{o} F, because additional thermal stresses will be produced in the deck (French et al. 1999). In addition, thermal stresses can be generated when concrete is cast on girders in cold weather due to the differences in temperature of the girders and the heat of hydration of the concrete deck. In hot weather and on windy days rapid surface evaporation can lead to plastic shrinkage cracks or drying shrinkage cracks in the near future. By monitoring the evaporation rate, precautions can be taken to reduce concrete moisture losses using sunscreens, windbreaks, fog mist, and chemical curing films (McDonald, Krauss, and Rogalla 1995). Early evening or night casting can also help to reduce the cracking tendency.

1.4.3.2 Curing

The curing process is very important to eliminate plastic shrinkage cracking and to reduce drying shrinkage cracking. In the early stages of concrete curing, the hydration process is relatively slow and requires the cement to be saturated with water. If water is allowed to evaporate from the surface, the concrete will not acquire any additional strength.

Immediately after finishing the deck, wet curing of the concrete should begin. Curing can be accomplished by ponding water on the deck or by covering the deck with wet burlap covered with plastic sheeting. The deck must remain wet until the curing process is complete. The longer the deck is cured, the higher the concrete strength, the lower the shrinkage, and the less likely transverse cracks will form. From studies performed by McDonald et al. (1995), moist curing is recommended to last at least seven days.

1.5 Crack Width Calculation

Analytical methods used to calculate crack widths can be useful in evaluating parameters that effect and can be used to control crack widths. The most commonly used crack width equations were developed by Gergely and Lutz (1968) and Kaar and Mattock (1963). In each method, crack width calculation is largely based on the steel stress level, effective area around a bar, and cover. Figure 1.13 presents both crack width equations.

Gergely and Lutz

$$w_b = 0.076 \beta f_s \sqrt[3]{d_c A}$$

Kaar and Mattock

$$w_b = 0.115 \beta f_s \sqrt[4]{A}$$

where

w_b = maximum bottom crack width, 0.001 in

β = ratio of distances to neutral axis from extreme tension fiber and from centroid of reinforcement

f_s = steel stress calculated by elastic crack section theory, ksi

d_c = bottom cover measured form center of lowest bar, in; and

A = average effective concrete area around reinforcing bar, having same centroid as reinforcement, in.^{2}

Figure 1.13: Gergely and Lutz (1968), and Kaar and Mattock (1963) Crack Width Equations

Because both equations were derived from a limited amount of test results, and neither has been verified with sections of cover greater than 2.5 in., crack width calculation was revisited by Frosch (1999). This approach is shown in Figure 1.14.

$$w_c = \frac{f_x}{E_x} S_c \quad \text{and} \quad S_c = \psi_x d^*$$

where:

w_c = crack width

f_S = reinforcing steel stress

E_s = reinforcing steel modulus of elasticity

S_c = crack spacing

d^* = controlling cover distance

ψ_s = crack spacing factor: 1.0 for minimum crack spacing; 1.5 for average crack spacing; and 2.0 for maximum crack spacing

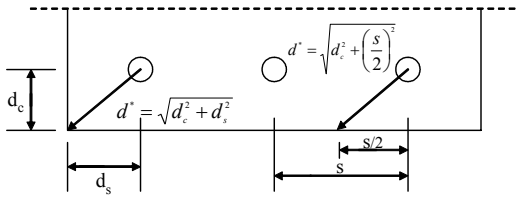

Figure 1.14: Frosch Crack Width and Spacing Equation (Frosch 1999)

This procedure also uses the crack spacing to determine widths of cracks. It seems logical that crack spacing and crack size should be related. If two specimens that only differed in reinforcement were subjected to similar loads, the summation of all crack widths in each specimen should theoretically be equal. However, the size and width of the cracks should vary. Frosch incorporated the work on crack spacing conducted by Broms (1965). It was found that the minimum crack spacing will be equal to the dimension labeled d^* in Figure 1.14. Additionally, Broms found that the maximum crack spacing will be twice the minimum. Following this rationale, it seems that the size of the reinforcing bar does not have as much affect as the spacing of the reinforcement. Other researchers have also supported this line of reasoning (Karr and Mattock 1963; Clark 1955; Broms 1965; Gergely and Lutz 1968). Therefore, the spacing and cover of the reinforcement are important parameters that affect the crack spacing and width. The current ACI provisions are based on the model presented by Frosch.

1.6 Overlay Cracking

Up to this point, the discussion has concentrated primarily on one-part bridge deck construction. However, two-part bridge deck construction is also common and deserves mention. Concrete overlays on a bridge deck also exhibit significant cracking. Of primary importance in this type of construction is map cracking. It should be noted that cracks in overlays do not always translate to failure and are expected in nearly all concrete construction. In general, cracks may be regarded as a problem if they are aesthetically unacceptable, make the structure non-watertight, and affect the durability of the structure (Concrete Society 1982).

There are three types of overlays that have similar cracking problems associated with each, but also with identified differences. As a result, it is also important to evaluate overlays on an individual basis instead of merely as a whole. According to the ACI 224 (2001), the three groups of overlays are: (1) portland cement overlays; (2) polymer and epoxy mortars or concretes; and (3) polymer-impregnated concrete (PIC). Portland cement overlays include: Low-slump dense concrete (LSDC), polymer-modified concrete (also called latex-modified concrete) and fiber-reinforced concrete (FRC). Latex-modified concrete overlays are the most common type found in Indiana. Polymer-impregnated concrete overlays will not be discussed in this report as they have not become generally effective, economical, or practical (ACI 224 2001). Observations of all three types of overlays have shown different types of cracking, the most common and frequently observed being map cracking.

Map cracking can be described as a random pattern of fine cracks which if fully developed begin to resemble the borders of countries on a map. These are non-structural cracks which often appear as early as a few hours after placing the concrete and are most likely due to differential shrinking. Map cracking in and of itself does not damage the integrity of the existing structure nor that of the overlay. Over time, however, these cracks are likely to increase and/or widen. Moisture and other substances such as salts used during the winter can penetrate the overlay and reach the reinforcement possibly causing corrosion and ultimate failure of the overlay. This cracking can be unacceptable on an aesthetic level as well.

Other types of cracking observed include transverse and reflective cracking as well as delamination which is a result of cracking in overlays and boundaries. On occasion, transverse cracking in overlays has been observed in some bridge decks using latex- and epoxy-modified concrete overlays. These cracks are spaced 3 to 4 ft (0.9 to 1.2 m) apart and have caused concern in terms of aesthetics but have not been the cause of overlay failure (ACI 224 2001). However, as in the case of map cracking, the durability of the overlay decreases as more cracks are generated and thus can be another cause for concern.

Reflective cracking although mentioned briefly in several research studies, has not been found to be a common issue. These cracks are worth mentioning, however, because of their damaging possibilities including failure of the overlay. Delamination, also known as debonding, only occurs at cracks in the overlay or at boundaries, normally at very early ages and will spread with time. Delamination/debonding can be failure by itself and/or also be caused by the cumulative effects of other deficiencies in the overlay (Nabar and Mendis 1997).

1.6.1 Causes of Cracking in Overlays

The main causes of cracking in overlays are plastic shrinkage, differential drying shrinkage, differential thermal stresses, reflective cracking from cracks in substrate, edge and corner curling stresses, and poor construction practices (ACI 224 1998, 2001). These causes are discussed below.

Plastic Shrinkage: Plastic shrinkage is "caused by excessive evaporation due to environmental conditions while the concrete is in its fresh or plastic state" (ACI 224 2001). Factors contributing to plastic shrinkage include conditions that combine to cause high rates of surface evaporation; examples of these conditions are air and concrete temperatures, relative humidity, and wind velocity. Generally, plastic shrinkage occurs within the first few hours of placement and tends to be unpredictable. Tensile stresses developing in the fresh concrete result in shallow cracks which vary in depth and width. Structurally, these cracks are seldom as bad as they appear; however, they do present the problem of durability and appearance of the overlay. The rapid drying out of the concrete is the primary cause of plastic shrinkage as the rate of evaporation exceeds the rate of bleeding.

Differential drying shrinkage: Differential drying shrinkage occurs between the material in the overlay and the substrate concrete. Since the existing concrete surface has previously completed its curing and shrinkage, when a new layer is added, the substrate concrete no longer can move with the freshly cast concrete. Therefore, the existing layer acts as a restraint which prevents the new concrete from being able to shrink normally. The combination of this type of restraint and shrinkage develops tensile stresses which results in cracking. These shrinkage cracks are more likely to increase or widen with time because much lower stresses than required for crack initiation are needed. Long-term observations by different investigations have determined that differential shrinkage is the most common cause of cracking in overlays (ACI 224 2001).

Differential thermal stresses: Differential thermal stresses typically occur one day to two or three weeks after casting. These types of stresses are usually caused by a different temperature in the fresh layer as compared to the existing substrate; they can also be caused or aggravated by different elastic properties and coefficients of thermal expansion. In general, aggregates with lower coefficients of thermal expansion should crack less and therefore are a key factor when selecting a mix. Other factors affecting thermal stresses include: reinforcement, stress raisers, and external and internal restraints. For an overlay, however, external restraint is unavoidable.

Reflective cracking: Reflective cracking is generally observed when cracks in the substrate are not properly identified and dealt with during the preparation for the overlay. These cracks extend from the existing substrate to the top of the overlay and eventually cause failure of the overlay. Edge and curling stresses can lead to delamination and other cracking problems. The main cause of delamination/debonding in the overlay is improper or inadequate surface preparation. Specifically for epoxy polymer overlays, any deviation from the correct ratio in the mix between the resin and the hardener in the epoxy binder can result in this mode of failure (Nabar and Mendis 1997).

Poor construction practices: Poor construction practices can include everything from inadequate preparation of the substrate to inferior mix control (for example, an excessive water to cement ratio) to improper curing procedures.

In addition to these general causes, specific problems occur in specific overlay types.

1.6.1.1 Fiber-Reinforced Concrete Overlays

The effect of fibrous concrete depends largely on field conditions in each situation. Significant long-term durability issues have been raised in question to glass fiber usage and partially bonded projects have demonstrated noticeable quantities of reflective cracking and edge curling.

1.6.1.2 Latex- and Epoxy-Modified Concrete Overlays

Latex- and epoxy-modified concrete overlays, also part of the group using portland cement, have exhibited distinctive cracking issues. A large number of bridge decks overlaid with latex-modified concrete have regularly revealed fine, random, shrinkage cracks (ACI 224 2001). The cause of these cracks can be credited at times to poor control in the construction process, but even when procedures are followed and well-managed, these cracks still appear. Usually during the first night after placement, unique conditions can cause thermal contraction of the overlay's surface while the existing concrete and bottom of the overlay does not have a similar experience. Part of the reason this cracking can occur is that the overlay has rigidity but has not yet realized its significant tensile strength.

1.6.1.3 Epoxy and Other Polymer Concrete Overlays

Polymer concrete overlays have been used frequently in the United States. The main causes of cracking PC overlays include water used in subsurface preparation, too high a moisture content in substrate concrete, use of thick placements, and use in hot weather. Also, polymers have significantly higher coefficients of thermal expansion than concrete. Therefore, changes in temperature create normal and shear stresses between the overlay and substrate's interface which in turn may produce cracking or delamination (ACI 224 2001).

1.6.2 Recommendations to Minimize Overlay Cracking

ACI Committee 224 provides recommendations to reduce the incidence of cracking as well as general guidelines for selecting and placing an overlay. If the existing concrete is relatively crack free, or if the planned overlay is thick and/or strong enough to withstand the extension of substrate cracks, then generally, the best approach is a well-bonded layer with matched joints. However, if the existing concrete is severely cracked and damaged or has the potential to later experience these problems, then a totally unbonded overlay with sufficient thickness is generally the best course of action.

Recommendations provided by ACI 224 (2001) for the mitigation of cracking in rigid concrete overlays are as follows:

1. The surface of the underlying concrete should be thoroughly prepared to ensure adequate bonding of the overlay. This can be accomplished by mechanical methods, such as shotblasting, scabbling, hand chipping, or sandblasting, and hydraulically by high-pressure waterblasting (hydrodemolition). Scarifying methods that impact the surface can cause cracking in the substrate that can result in delamination. Procedures for each project should be selected considering the condition of the concrete, the availability of equipment, and the environmental conditions. The end result should be a clean, sound concrete surface.
2. All equipment used for mixing, placing, and finishing should be designed for the type of overlay being used and should be accurately calibrated and in good working order. Both the contractor and inspecting personnel should be trained in the proper construction techniques of the particular overlay system.
3. Material quantities, including total water content, *w/cm*, and amount of polymer, should be closely monitored and recorded.
4. Traffic control should be evaluated for highway applications. The maintenance of traffic during reconstruction causes deflections, vibrations, or both in bridge decks. Consideration should be given to placing overlays when traffic is low, when vehicle speed is restricted or both.
5. Contraction joints in the deck should not be overlaid unless a joint or saw cut is immediately provided. Delayed saw cutting will usually result in a crack in the overlay over the joint and quite possibly, some debonding adjacent to the joint. The preferred method is to form the joint with a compressible material and place the overlay against it. After curing, the compressible material can be removed and replaced with the final joint material.

6. In new two-course construction of bridge decks, the overlay should be placed after removing the deck forms and shoring from the base concrete so that stresses caused by the weight of the overlay are carried by the underlying concrete. If placed before the forms are removed, the overlay will have to carry a portion of its own weight and can crack in negative moment regions.
7. Overlays should be placed only when the ambient weather conditions are favorable, as defined in ACI 308 or when appropriate actions are taken for hot-weather (ACI 305R) or cold-weather concreting (ACI 306R). Evaporations rates of about 1 $kg/m^3/h$ (0.2 $lb/ft^3/h$), as measured from a free water surface, can cause plastic shrinkage cracking that can increase the extent of cracking and increase the probability of delamination. Curing procedures, such as wet mats and fog spraying, can be required. For large construction projects, such as pavement overlays, the evaporation rate should be monitored to determine when more stringent curing procedures should be used.
8. Mechanical shear reinforcement is effective in reducing cracking in overlays placed during periods of high evaporation rates.

In addition to these recommendations, several recommendations are overlay type specific. These recommendations are listed below.

1.6.2.1 Fiber-reinforced concrete (FRC) Overlays

For fiber-reinforced concrete overlays, the success of the overlay depends largely on the field conditions in each situation (ACI 544.2R, ACI 544.3R; ACI 544.4R). Traditional approaches to FRC overlays have included partially bonded overlays, but it has been found through observations of many of these overlays that this is the least desirable approach. Partially bonded FRC overlays have shown clear amounts of reflective cracking and edge curling resulting in cracking of the overlays. Increasing the aspect ratio (ratio of fiber length to fiber diameter) or the volume fraction of fibers (ratio of volume of fibers to volume of concrete) can enhance the crack-arresting mechanism if fibers are uniformly distributed (ACI 224 2001).

1.6.2.2 Latex- and Epoxy-Modified Concrete Overlays

Cracking problems associated with latex- and epoxy-modified concrete overlays (LMC overlays) also require special considerations. As mentioned previously, on occasion, LMC overlays have had random pattern cracks and transverse cracks even when good construction practices are followed and the overlay is well designed. ACI recommends treating these cracks by brooming a penetrating high molecular weight methacrylate or low-viscosity epoxy or urethane on the surface after the curing and drying period, but before allowing traffic on the overlay. Also, the finishing and texturing for LMC overlays should be performed rapidly behind the placement operation and before the polymer in the latex begins to dry or coalesce at the surface (ACI 224 2001). This should minimize possible tearing, scarring and cracking. Latex- and epoxy-modified concrete overlays are discussed more thoroughly in ACI 548R and ACI 548.1R.

1.6.2.3 Epoxy and Other Polymer Concrete Overlays

For epoxy and other polymer concrete overlays, texture surface applications can include bridge decks. These types of overlays are ordinarily thin, do not use coarse aggregates, and can achieve excellent bonding with dry surfaces. For that reason, existing surface preparations should avoid using water and also, the substrate concrete's moisture content should be evaluated. According to ACI 224 (2001), a mat test should be performed and if moisture collects on the underside of the polyethylene sheet within the length of time needed to cure, then the concrete should be allowed to continue to dry. Thin PC overlays with low elastic modulus polymers should be used in order to reduce cracking. The reactions which harden materials in PC overlays are normally highly exothermic; therefore, they cannot be used in cases which need thick placements or in hot weather to avoid thermal stress problems.

1.7 Objective and Scope

The objective of this research project was to determine the factors affecting transverse and longitudinal bridge deck cracking in Indiana, as well as, to develop design recommendations that minimize or prevent these types of cracking in bridge decks. The research focused on the design and construction of new bridge decks. For bridge decks being rehabilitated with overlays, overlay cracking can also be of concern. Therefore, for completeness, recommendations to minimize this type of cracking are provided in Section 1.6.2. The research was divided into five phases and is presented in the following chapters as outlined below.

Phase 1 (Chapter 2): The first phase was a field evaluation to investigate the scope of the problem experienced in Indiana.
Phase 2 (Chapter 3): Using the information gathered from the first phase, the second phase instrumented a typical bridge structure to provide an understanding of the behavior of transverse cracks in a concrete bridge deck.
Phase 3 (Chapter 4): With the findings from the previous two phases, the third phase conducted a laboratory investigation to study the effects of shrinkage and restraint of a concrete deck and determine the contribution of stay-in-place steel forms to the formation of transverse cracking. Two models were constructed, instrumented, and monitored in the Purdue University, Karl H. Kettelhut Structural Engineering Laboratory.
Phase 4 (Chapter 5): The fourth phase investigated the effect of varying form type on shrinkage to determine whether the use of SIP or wood forms can provide advantages in the control of early-age bridge deck cracking. It had been established from the literature review that curling may increase the chances of early-age cracking. Because a SIP deck pan seals the bottom surface of a bridge deck, it may curl more than a bridge deck formed with wood forms. However, wood forms increase the surface-to-volume ratio of a bridge deck and can increase overall magnitude of shrinkage.
Phase 5 (Chapter 6): The fifth phase investigated the effect of reinforcing bar spacing and epoxy coating thickness on crack widths and spacing. Because restrained shrinkage cannot be eliminated in a bridge deck, cracking will occur. The spacing and width of these cracks is directly affected by the reinforcement spacing and thickness of the epoxy coating.

CHAPTER 2
FIELD INVESTIGATION

2.1 Introduction

The state of Indiana is divided into six regional transportation districts. A detailed field investigation was performed in two of these districts, Greenfield and Vincennes, to survey bridges which were either newly constructed or were known to have experienced deck cracked. Twenty bridge locations were inspected.

2.2 Field Investigation Procedure

The bridge field investigation was completed on two different days. Bridges in the Greenfield District were inspected on September 23, 1999, and bridges in the Vincennes District were inspected on March 23, 2000. The inspection process began by visually surveying the top surface of the bridge deck while walking the entire length of the bridge. Any type of cracking or deterioration was noted. Next, the inspection proceeded to the underside of the bridge. The superstructure type was identified and the bottom surface of the bridge deck was inspected. If cracks were visible in the bottom surface, the type and frequency were noted. Stay-in-place steel forms, however, prevented the identification of cracks on the bottom surface. The use of these forms was documented.

Photographs were generally taken of the bridge elevation, the superstructure, the top and bottom surfaces of the bridge deck, and any cracking that occurred on the top and bottom surfaces of the bridge deck. Crack widths and spacing were measured on bridges in the Vincennes District.

2.3 Inspection Results

The inspected bridges were divided into two categories – steel and concrete superstructures. Table 2.1 lists general information of the steel superstructure bridges while Table 2.2 lists general information of the concrete superstructure bridges. Detailed summaries with photographs of all the bridges inspected are available in Appendix A.

2.3.1 Steel Superstructure Bridges

Various types and degrees of cracking were discovered on 10 of the 11 bridges supported with steel superstructures. All bridges were continuous and all except Bridges 8, 9, and 10 incorporated composite action.

2.3.1.1 Transverse Cracking

Transverse cracking was observed on 9 of the 11 bridges inspected with a steel superstructure. Bridge 4 had no observed cracking and Bridge 6 had a latex-modified overlay on the top surface of the deck, which prevented the observation of surface cracking. Figure 2.1 shows the typical transverse cracking pattern. The transverse cracking occurred at fairly regular intervals, 3- to 10-ft apart, and was generally located in both the positive and negative moment regions of the bridge. The transverse cracks

were typically perpendicular to the girders, but were parallel to the skew of the end bents for Bridge 1.

Of the bridges inspected, 7 where known to have used stay-in-place steel forms and 6 of these bridges had transverse cracks. Figures 2.2 and 2.3 show the stay-in-place steel forms. The 2-in. thick stay-in-place steel forms are corrugated galvanized steel and are screwed to a 3-in. by 2-in. galvanized cold-rolled steel angle. The cold-rolled angle was welded directly to the top flange in the positive moment region and welded to a steel bar resting on the top of the flange in the negative moment region where welding is not permissible (Figure 2.4). Figure 2.5 shows a cross section of the bridge deck slab at a girder that incorporates the use of stay-in-place steel forms.

Figure 2.1: Transverse Cracking (Bridge 3)

Table 2.1: Steel Superstructure Bridges Inspected

Bridge Reference Number	INDOT Structure No.	Date Constructed	Date Rehabilitated (R), Widened (W), or Overlaid (O)	Date Inspected	Continuous	Composite	Skew Angle	Stay-in-Place Steel Forms	Cracking Type
1	I-65-118-4915C	1969	R 1996	9/23/99	Yes	Yes	20°	Yes	Longitudinal, Transverse
2	I-65-118-4838B NBL	1964	W 1996	9/23/99	Yes	Yes	17°	Yes	Transverse
3	I-65-119-4839B	1964	R 1997	9/23/99	Yes	Yes	-	Yes	Transverse
4	I-465-116-4500A SBL	1966	R 1999	9/23/99	Yes	Yes	7°	Yes	None
5	I-465-116-4501A SBL	1965	W 1999	9/23/99	Yes	Yes	3°	Yes	Transverse
6	I-69-40-2304C NBL and SBL	1963	O 1995	9/23/99	Yes	Yes	11°	Unknown	Map Cracking in Overlay
7	58-42-7288	1996	-	3/23/00	Yes	Yes	30°	Yes	Transverse
8	58-42-3241A	1939	W 1983	3/23/00	Yes	No	20°	No	Longitudinal, Transverse
9	54-28-2538	1982	-	3/23/00	Yes	No	27°	No	Transverse
10	(50)37-47-3416JC	1964	W 1988	3/23/00	Yes	No	-	No	Transverse
11	(50)37-47-6615	1984	-	3/23/00	Yes	Yes	-	Yes	Transverse

Table 2.2: Concrete Superstructure Bridges Inspected

Bridge Reference Number	INDOT Structure No.	Date Constructed	Date Rehabilitated (R), Widened (W), or Overlaid (O)	Date Inspected	Concrete Girder Type	Continuous	Skew Angle	Stay-in-Place Steel Forms	Cracking Type
12	I-70-82-5707B I-70-82-5707JB	1969	W 1986	9/23/99	Cast-in-Place	Yes	31°	No	Transverse Cracking in Widened Portion
13	I-465-111-4399C EBL and WBL	1999	-	9/23/99	Prestressed I-Beam	Yes	-	Yes	None
14	I-465-109-4402B	1999	-	9/23/99	Prestressed Box Girder	Yes	2°	No	Longitudinal, Transverse
15	I-69-31-4740D NBL and SBL	1963	R 1995	9/23/99	Prestressed I-Beam	Yes	-	Yes	None
16	I-69-40-4746JD I-69-40-4746B	1963	NBL O 1995 SBL O 1998	9/23/99	Cast-in-Place	Yes	11°	No	Map Cracking in Overlay
17	67-28-7701	1994	-	3/23/00	Prestressed I-Beam	Yes	20°	Yes	Longitudinal
18	231-28-2571	1994	-	3/23/00	Prestressed I-Beam and T-Beam	Yes	Varies	Yes	Longitudinal
19	54-47-6829	1987	-	3/23/00	Prestressed I-Beam	Yes	50°	No	Transverse
20	58-47-7178	1991	-	3/23/00	Prestressed Spread Box Girder	Yes	23°	Yes	Longitudinal Transverse parallel to skew

Figure 2.2: Steel I-Beam Superstructure with Stay-in-Place Forms (Bridge 3)

Figure 2.3: Steel Plate Girder Superstructure with Stay-in-Place Forms (Bridge 7)

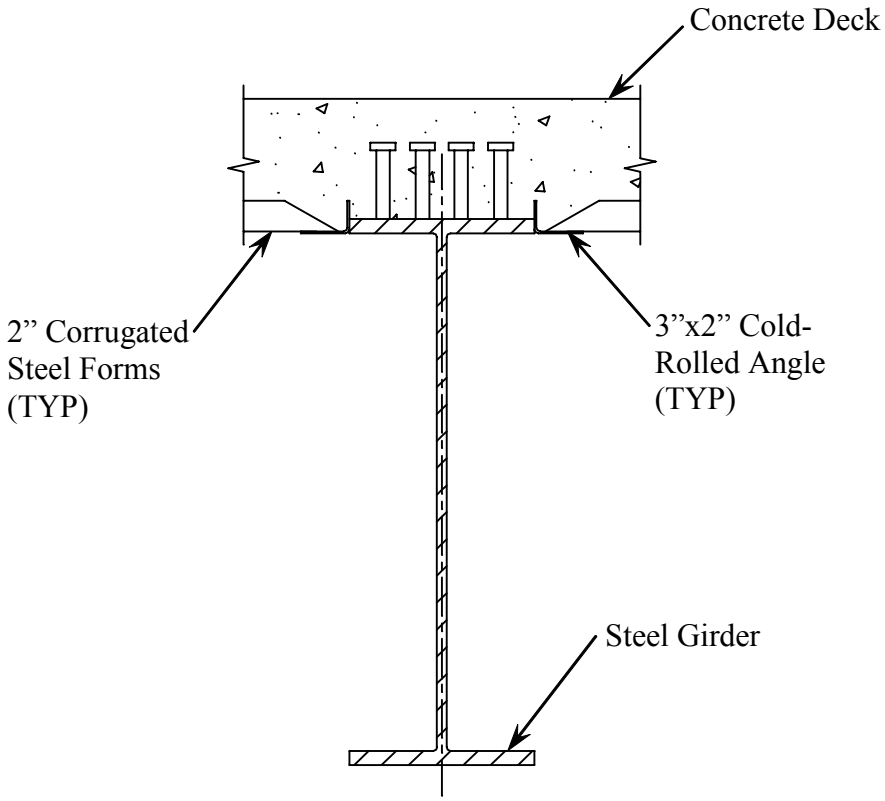

Figure 2.4: Steel Bar Detail to Support Angles in Negative Moment Region

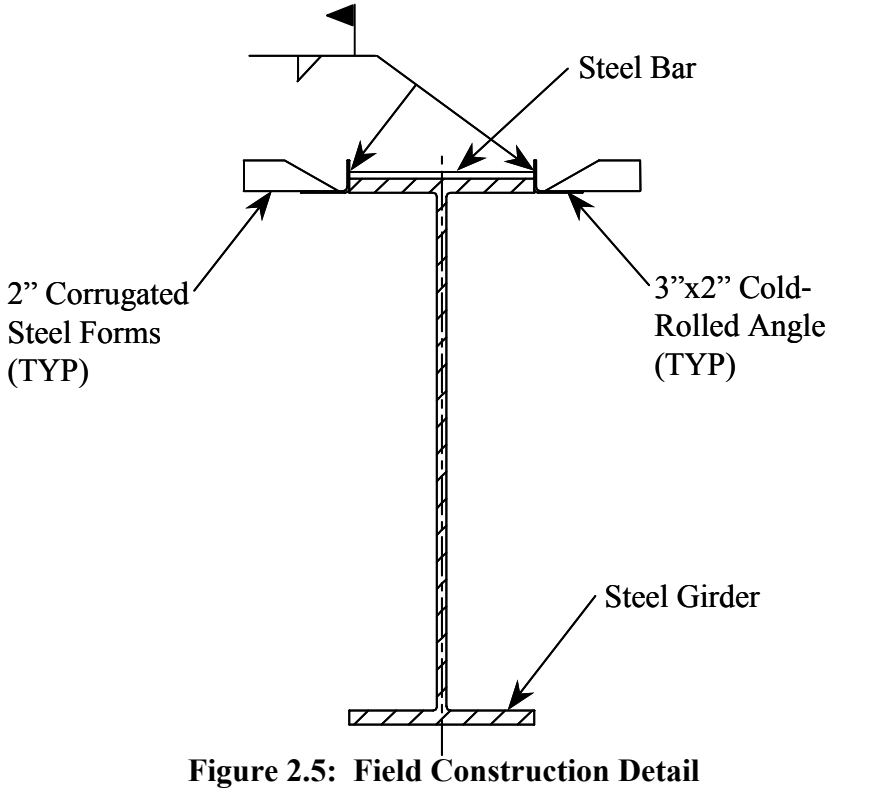

Figure 2.5: Field Construction Detail

2.3.1.2 Longitudinal Cracking

Longitudinal cracking was observed in Bridges 1 and 8 of the 11 bridges inspected with a steel superstructure. Figure 2.6 shows a longitudinal crack near the white lane edge line of Bridge 1. Figure 2.7 shows multiple longitudinal cracks running the entire length of Bridge 8. Bridge 1 incorporated composite action and was cast on stay-in-place steel forms. Bridge 8, however, did not incorporate composite action or stay-in-place steel forms.

2.3.1.3 Map Cracking

Map cracking was identified in Bridge 6. The cracking was in the approximately 2-in. thick latex-modified overlay placed on the top surface of the deck (Figure 2.8). This bridge was the only one containing an overlay. Map cracking was not identified in any of the other bridges with a steel superstructure.

Figure 2.6: Longitudinal Crack near White Lane Edge Line (Bridge 1)

Figure 2.7: Longitudinal Cracks (Bridge 8)

Figure 2.8: Map Cracking in Overlay (Bridge 6)

2.3.1.4 Other Concerns

During the inspection, concerns other than deck cracking were also noted. Bridge 4 had no observed cracking on the bridge deck; however, there were several loose rockers supporting the steel I-Beam girders as shown in Figure 2.9.

Figure 2.9: Unseated Rocker Support for Steel I-Beam Girder (Bridge 4)

2.3.2 Concrete Superstructure Bridges

Various types and degrees of cracking were discovered on 7 of the 9 bridges supported with concrete superstructures. Bridges 13 and 15 had no observed cracks when inspected. Bridges 11 and 16 were cast-in-place with the deck cast monolithically and continuously with the superstructure. The other 7 bridges were continuous with precast, prestressed concrete girders and incorporated composite action.

2.3.2.1 Transverse Cracking

For the bridges inspected with concrete superstructures, transverse cracking was observed on Bridges 12, 14, 19, and 20. Bridge 12 was a cast-in-place structure that was widened. Transverse cracks were noted in the widened portion of the bridge (Figure 2.10), but no cracks were observed in the original structure. The new construction was bonded directly to the old. It is probable that the original structure had already experienced the majority of its shrinkage and the new structure was restrained from shrinking freely. The restraint of this shrinkage likely resulted in the transverse cracks in the widened portion.

Bridge 14 was a precast, prestressed concrete box girder bridge that was under construction when inspected and not yet open to traffic. A few transverse cracks were noted in the negative moment region. Bridge 19 had a precast, prestressed concrete I-Beam superstructure with transverse cracking in the deck. The bridge did not contain stay-in-place steel forms which allowed the observation of the transverse cracks from the underside of the bridge (Figure 2.10). Bridge 20 had a precast, prestressed spread concrete box girder superstructure (Figure 2.11). A few transverse cracks parallel to the skew of the bridge were noted near the end bents. This bridge, as shown, also used stay-in-place steel forms.

Figure 2.10: Transverse Cracks (Bridge 19)

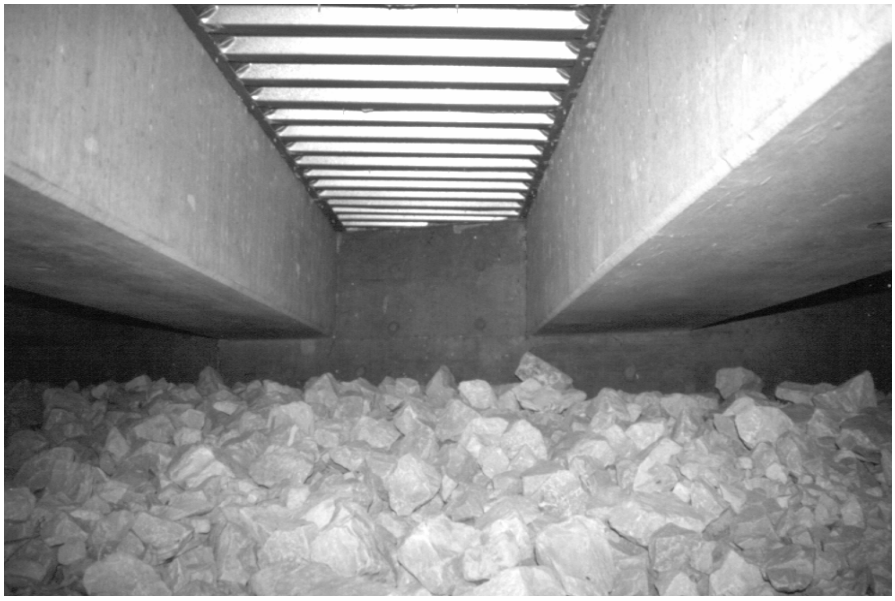

Figure 2.11: Precast Spread Box Girder Superstructure with Stay-in-Place Forms (Bridge 20)

2.3.2.2 Longitudinal Cracking

Of the 9 bridges inspected with a concrete superstructure, longitudinal cracking was observed in Bridges 14, 17, 18 and 20. Bridge 14 was a precast, prestressed concrete box girder bridge under construction when inspected and not yet open to traffic. Longitudinal cracks were observed the full length of the bridge and were assumed to be full depth (Figure 2.12). The longitudinal cracks in the deck were located above the edge of the box girders. The cracking was likely due to differences in height of adjacent box girders (Figure 2.13). The stepping of the boxes was used to adjust the slope of the deck for drainage.

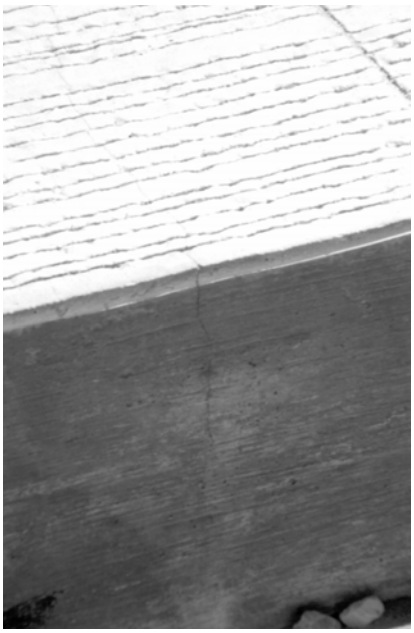

Figure 2.12: Full Depth Longitudinal Crack at end of Bridge 14

Figure 2.13: Elevation Difference in Box Girders (Bridge 14)

Bridge 17, a precast, prestressed concrete I-Beam superstructure bridge, had longitudinal cracks that were observed the full length of the bridge over both edges of the girders. The widths of the cracks were measured between 0.013 and 0.016 in. The bridge incorporated stay-in-place steel forms with a detail similar to Figure 2.5 (Figure 2.14).

Figure 2.14: Precast Concrete I-Beam Superstructure with Stay-in-Place Forms (Bridge 17)

Bridge 18 was a five span precast, prestressed bridge with 2 spans of I-beam girders and 3 spans of T-beam girders that incorporated stay-in-place steel forms. This bridge had longitudinal cracks that were observed over the entire length of the bridge. The cracks were located over both edges of the girders (Figure 2.15).

Figure 2.15: Longitudinal Cracks (Bridge 18)

Bridge 20 had a precast, prestressed spread concrete box girder superstructure (Figure 2.11) with longitudinal cracks the entire length of bridge over both edges of the girders. This bridge also used stay-in-place steel forms.

2.3.2.3 Map Cracking

Map cracking was identified on Bridge 16. The cracking was located in the approximately 2-in. thick latex-modified overlay placed on the top surface of the deck. Figure 2.16 illustrates the high concentration of this map cracking.

Figure 2.16: Map Cracking (Bridge 16)

2.4 Summary

Based on the survey of bridges, a few general trends were observed.

1. Bridge decks cast monolithically with a concrete superstructure had the fewest cracks. The only transverse cracking observed in bridges utilizing this construction method was in the widened portion of Bridge 12. As noted, this new construction was connected to the existing, which restrained shrinkage.
2. All overlays on bridge decks exhibited map cracking.
3. More transverse cracking was noted on steel girder bridges that incorporated composite action than those not incorporating composite action.
4. More transverse cracks were observed on bridges with a steel girder superstructure than bridges with a concrete superstructure.
5. More longitudinal cracking was observed on bridges with a concrete superstructure than bridges with a steel superstructure.
6. More transverse cracking was observed in bridges with a steel girder superstructure when stay-in-place steel forms were used versus removable plywood forms.
7. More longitudinal cracks were observed in bridges with precast, prestressed concrete girders when stay-in-place steel forms were used versus removable plywood forms.

As previously discussed, to accommodate the use of the 2-in. thick corrugated stay-in-place steel forms, a 3-in. by 2-in. galvanized cold-rolled steel angle was attached to the flange of the girders (Figure 2.5). The cold-rolled angle can either be welded directly to the top flange in the positive moment region or welded to a steel bar resting on the top of the flange in the negative moment region where welding is not permissible (Figure 2.4). The stay-in-place steel forms are typically attached to the angle and to each other using self-tapping screws. On the bridges inspected, the leg of the angle was typically turned upward into the deck. The leg of the angle included in the deck causes a discontinuity, which may cause a crack initiation location. This may explain some of the longitudinal cracks observed in the bridges surveyed.

CHAPTER 3
FIELD INSTRUMENTATION

3.1 Introduction

Based on review of the literature and the findings from the field investigation, a continuous steel superstructure bridge that incorporated composite action and stay-in-place steel forms was selected as an ideal structure for in-depth study. This type of bridge system was preferred because it was found to exhibit the most transverse cracking of any system and is a typical bridge type in Indiana. A list of bridges to be constructed or rehabilitated starting in the summer of 2000 was reviewed to locate a bridge fitting these criteria.

The northbound lane of Interstate 65 (I65) over State Road 25 (SR25) bridge (INDOT Bridge No. I-65-176-5543C) was selected. This bridge is a 150 ft, two-span, continuous, steel superstructure bridge, which integrates the use of composite action and stay-in-place steel forms (Figure 3.1). The bridge was originally constructed in 1969 with an overlay added in 1988. The new construction included a complete rehabilitation including deck replacement and structural modification. This bridge was designed and constructed to conform to the requirements in the *Standard Specifications for Highway* Bridges, 16th Edition (AASHTO 1996) and *INDOT Standard Specifications* (INDOT 1999). In addition, the integral end bents were designed in accordance to the *INDOT Bridge Design Memorandum #233* Revised (INDOT 1992). Plans for the I65 over SR25 bridge deck are available in Appendix B.

Figure 3.1: Elevation of I65 over SR 25 Bridge

3.2 Test Structure – Construction

The construction sequence during the rehabilitation will be described. First, the concrete deck was removed from the steel girders. Then the girders were elevated above the end bents and supported by temporary wood piles. The entire bridge was elevated to allow for more clearance underneath the bridge because the bridge had been struck by a truck and damaged. The original end bents were replaced with integral end bents, a new standard for Indiana starting in 1999. The end bents used the existing vertical shell piles, and additional H-piles were driven. The end bents and wing walls were formed, reinforced with epoxy-coated reinforcing steel, and cast. Because the elevation of the bridge was increased, pedestals had to be cast for each of the 7 steel girders on the center pier (Figure 3.2).

Figure 3.2: Pedestals on Center Pier to Raise Elevation

After the end bents and pedestals had cured, the steel girders were lowered slightly. The girders were then attached to the end bents (Figure 3.3) where they were simply supported on the pedestals. Sections of 3 girders that had been damaged were replaced. Next, the outside of the wing wall and the top portion of the abutment between the girders were formed; then, the deck itself was formed.

Stay-in-place steel forms were used to form the bottom of the slab between the girders. The 2-in. thick stay-in-place steel forms were corrugated galvanized steel and were screwed to a 3-in. by 2-in. galvanized cold-rolled steel angle. The cold-rolled angle was welded directly to the top flange in the positive moment region and welded to a steel bar resting on the top of the flange in the negative moment region where welding was not allowed (Figure 3.4). Figure 3.5 shows a cross section of the bridge deck slab at a girder. The 3-in. leg of the 3-in. by 2-in. cold-rolled angle was turned upward into the deck along all girders expect on portions of Girders 4 and 5. Figure 3.6 shows the portions of the girders where the angle was turned down.

Figure 3.3: Attachment of Steel Girder to End Bent

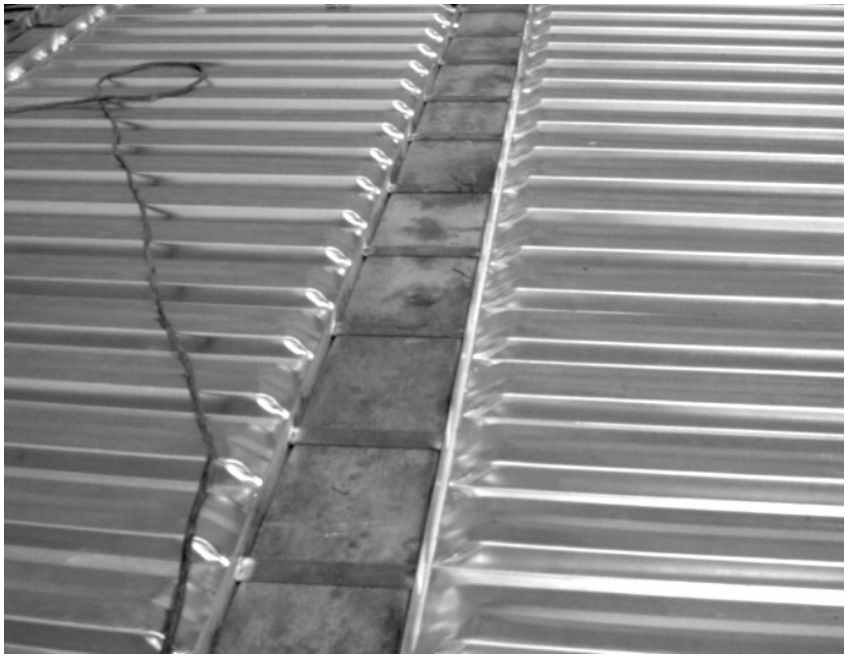

Figure 3.4: Bars Perpendicular to Girder to Support Angles

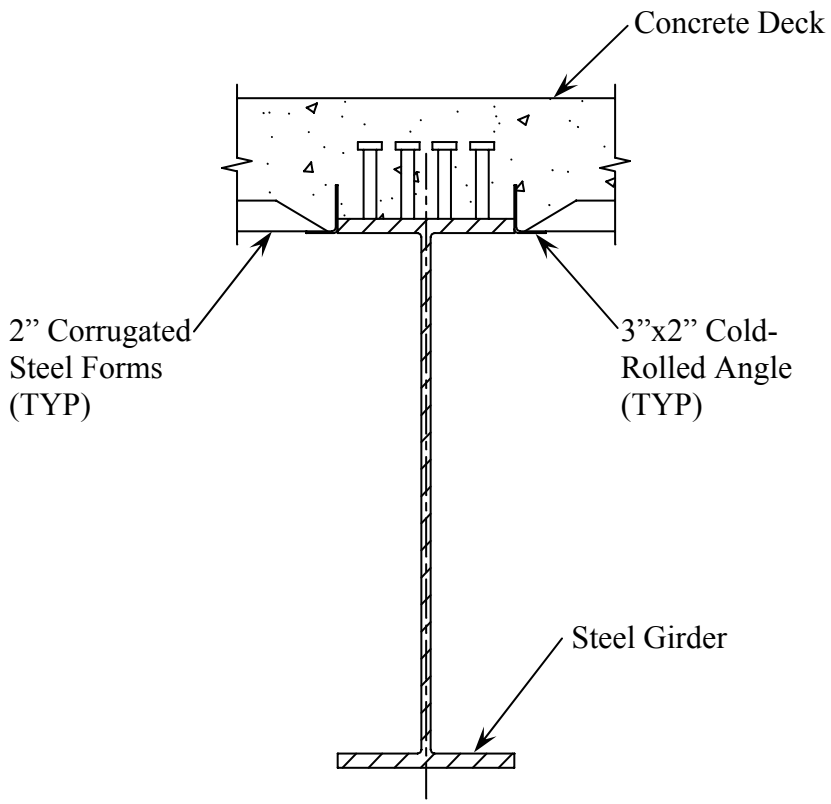

Figure 3.5: I65 over SR25 Construction Detail

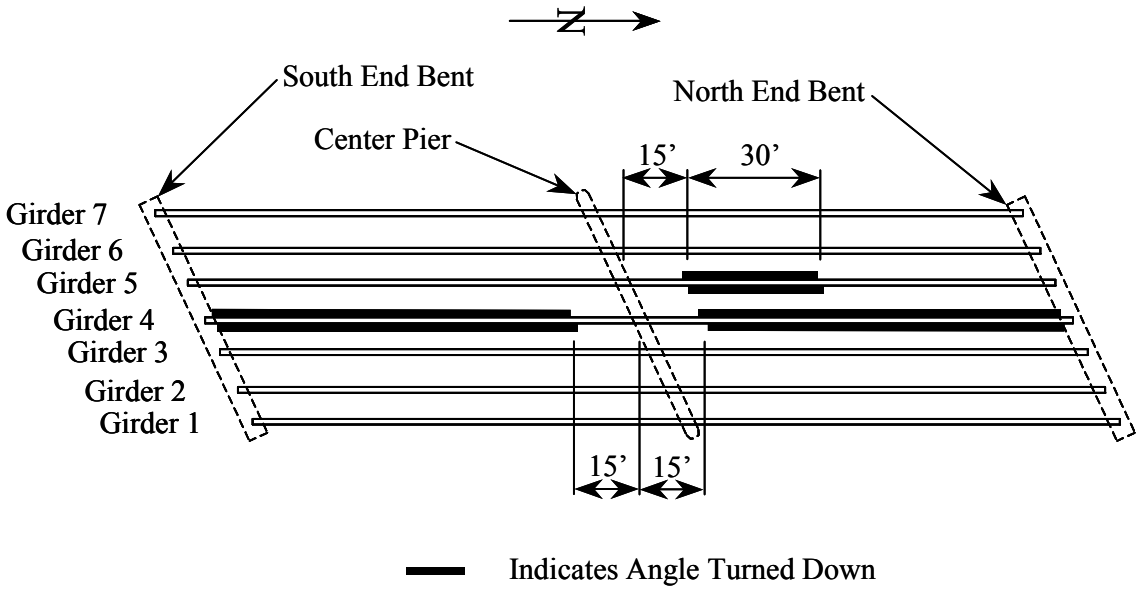

Figure 3.6: Girders with Angle Turned Down

After the stay-in-place forms were fastened, the outside coping line was formed. The coping line is the portion of the deck cantilevering beyond the outside girders where the barrier wall is cast. To form the coping line, standoffs were attached to the outside girders. Next, 4-in. by 4-in. joists were placed perpendicular to the standoffs to support the ¾-in. plywood (Figures 3.7 and 3.8). The side forms where then attached and braced off the coping line forms.

Figure 3.7: Standoffs Attached to Outside Girder

Figure 3.8: Coping Line Forms

After the bottom and side forms were secured, shear studs damaged from deck removal were replaced. The shear studs were 7/8-in. diameter by 5-in. tall. The spacing of the shear studs along the length of the girders varied from 9-in. to 24-in. Figure 3.9 shows the spacing of the shear studs over the width of flange of the girders. Shear studs were also added at the ends of the girders, in the negative moment region, and on the 3 replaced portions of the girders.

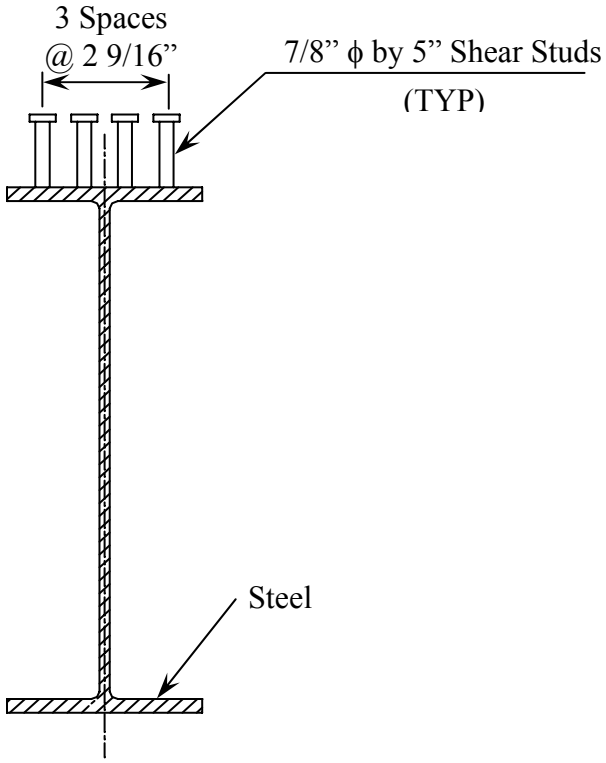

Figure 3.9: Shear Stud Spacing over Flange

Once the shear studs were installed, the epoxy-coated reinforcing steel was placed in the deck. The bottom cover was 1-in. and the top cover was 2.5-in. Figure 3.10 shows the actual reinforcement placed in the positive moment region of the deck. Figure 3.11 illustrates the size and layout of the reinforcing steel in the transverse and longitudinal directions in both the top and bottom mats of reinforcement.

Figure 3.10: Reinforcement in Positive Moment Region

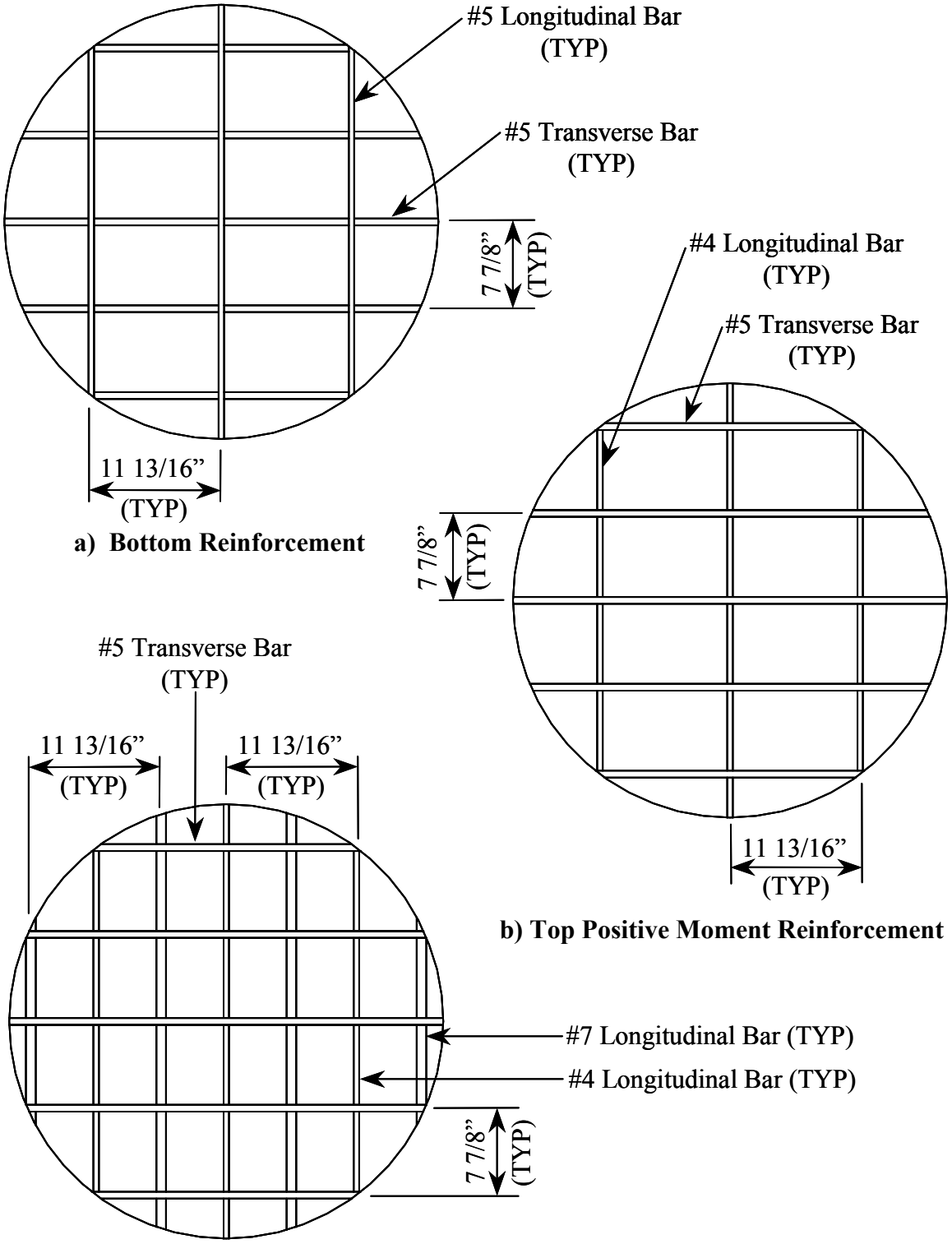

Figure 3.11: Deck Reinforcing Steel Size and Location

As the reinforcing steel was placed, the forms for the top portions of the wing walls and end abutments were completed and cast at the same time as the deck. Attaching the girders to the lower portion of the abutment and casting the girders in the upper potion of the abutment fixed the ends of the bridge from vertical movement and rotations. However, the bridge was only partially restrained from horizontal movement.

The deck was 7 7/8-in. thick and utilized an INDOT Class C concrete mix. The mix design and specifications are provided in Section 3.3.1. The placement of the deck began at 7:00 AM on August 15, 2000 at the south end of the bridge using a concrete pump (Figure 3.12). A mechanical screed was used to level and consolidate the concrete (Figure 3.13).

Figure 3.12: Concrete Placement on Deck with Concrete Pump

Figure 3.13: Mechanical Screeding of Deck

After the concrete began to set, wet burlene (burlap with a plastic backing) was placed on the deck starting at approximately 5:00 PM to wet cure the concrete. The burlene was rewetted the following day. On the 2nd day, rewetting was not required since it rained in the evening. No additional rewetting of the burlene was observed for the duration of the curing process. The burlene was removed on the morning of the 6th day. The deck was subsequently sandblasted and sealed the 9th day.

To complete the bridge construction, barrier walls were slip formed on the 10th day. The bridge was opened to traffic the 13th day, August 28, 2000 at 2:25 PM. Figure 3.14 illustrates the sequence of events between casting the deck and opening the bridge to traffic.

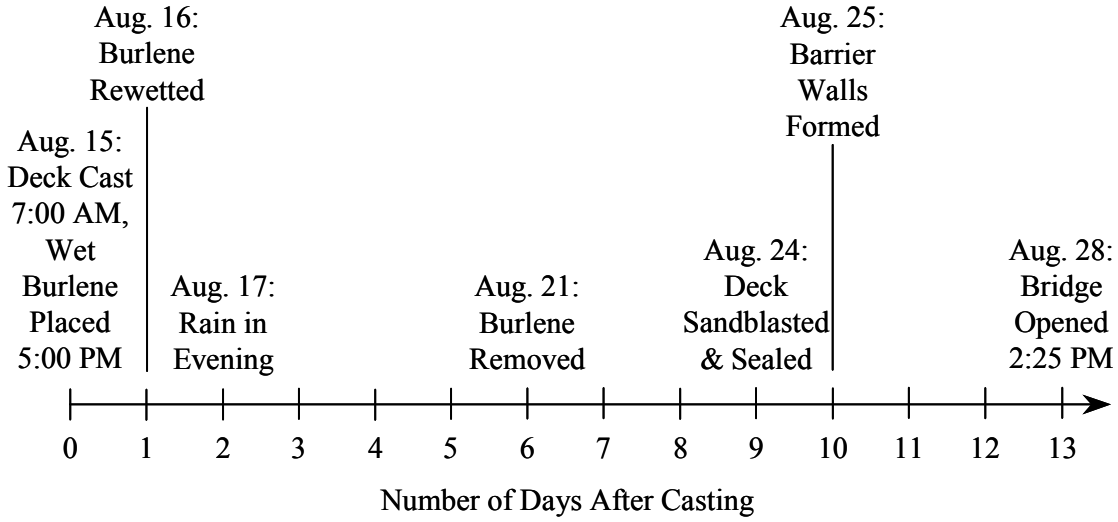

Figure 3.14: Time Line between Casting and Opening of Bridge

3.3 Materials

3.3.1 Concrete

The concrete was obtained from Irving Materials, Inc (IMI), a local ready mix supplier. An INDOT Class C concrete mix with design compressive strength of 4000 psi and a maximum aggregate size of ¾-in. was used for the bridge deck. The mix design and specifications for this concrete are provided in Table 3.1.

Table 3.1: INDOT Class C Mix Design

Material	Quantity	*Specifications/Suppliers*
Cement	659 lb/yd^3	ASTM C-150, Type I, Essroc Cement Co.
Ash	None	-
Micro-Silica	None	-
Sand	1220 lb/yd^3	ASTM C-33 & INDOT Specification #23 Sand from Vulcan Materials, Battleground, IN
Stone	1800 lb/yd^3	#8 Stone from US Aggregate, Delphi, IN
Water	292 lb/yd^3	-
Water Reducer	13.2 oz/yd^3	ASTM C-494, Water Reducer Type A Pozzolith 220N, Master Builders. Optional High Range Water Reducer Pozzolith 440N (plant added). Optional High Range Water Reducer (Super) Daracem 100 (plant added)
W/C	0.443	-
Air	5-8 %	ASTM C-260 Air Entrainment, Micro Air by Master Builders
Slump	4-in.	-

Standard 6-in. by 12-in. compressive cylinder samples were obtained at the time the deck was cast. The cylinders were wet cured on site for the same duration as the deck. The specimens were tested at the Karl H. Kettelhut Structural Engineering Laboratory at Purdue University at 7, 14, 21, 28, and 56 days with 3 specimens tested each day. The specimens were loaded at 60,000 lb per minute using a 600 kip testing machine. Figure 3.15 shows the strength gain curve for the concrete, which was obtained from the average of the 3 cylinders. As shown, the average 28-day compressive strength was 5800 psi.

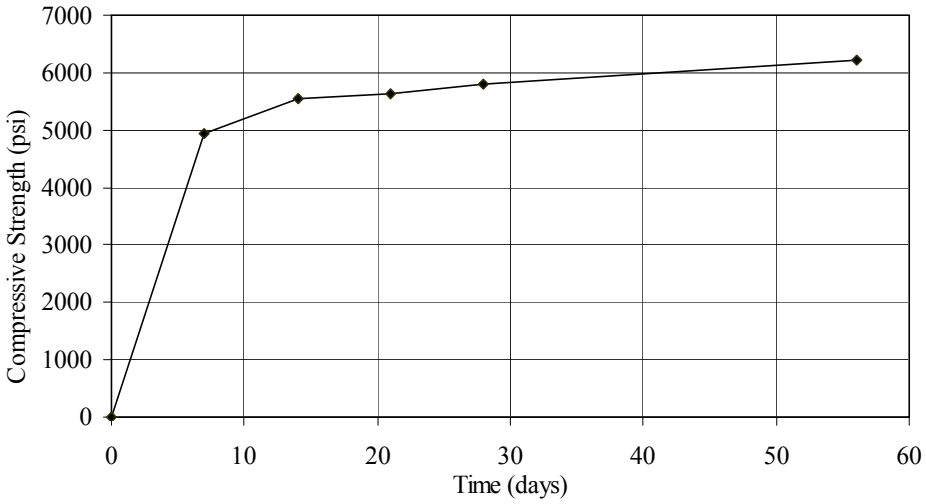

Figure 3.15: Strength Gain Curve for Concrete Compressive Cylinders

3.3.2 Reinforcing Steel

The deck reinforcement comprised 3 bar sizes: #4, #5, and #7. All reinforcing steel conformed to ASTM A615 Grade 60 and was epoxy-coated.

3.4 Instrumentation

3.4.1 Instrumentation Design

To study the effects of thermal and strain gradients on transverse and longitudinal cracking, strain gages and thermocouples were placed along the length of the bridge.

3.4.1.1 Strain Gages

As shown in Figure 3.16, strain gages were placed on the outside girders as well as the center girder to determine whether similar behavior existed at these locations. Strain gages were placed on the steel girders and on the reinforcing bars cast in the concrete deck to establish the strain gradient through the depth of the superstructure.

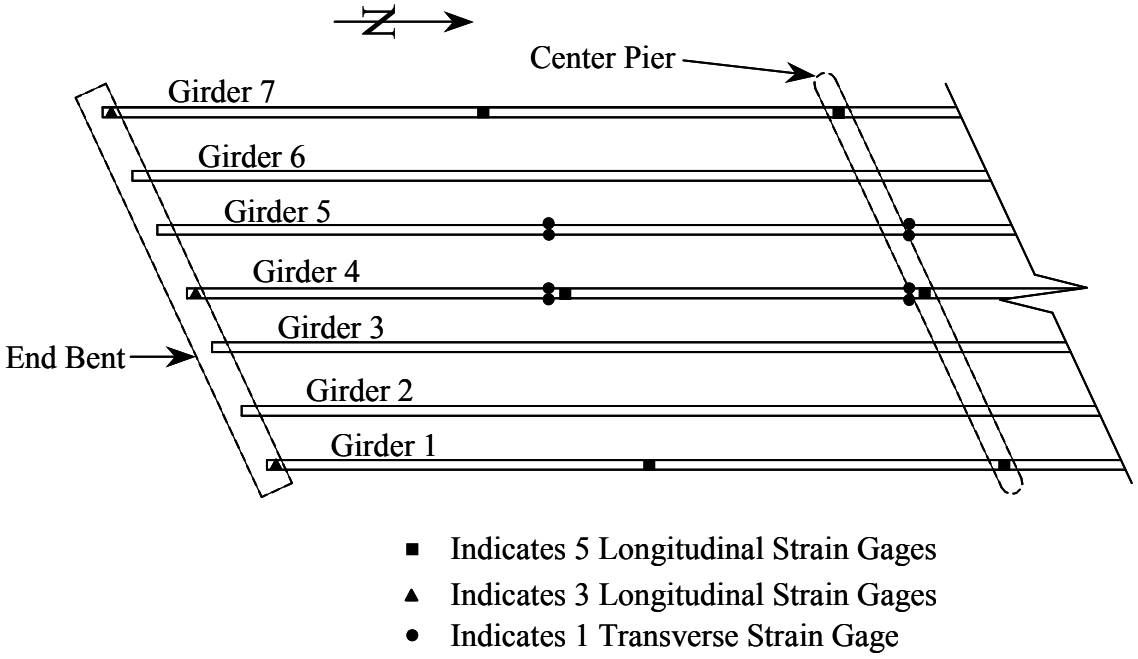

Figure 3.16: Plan View of Strain Gage Locations

As shown in Figure 3.17, strain gages on the steel girders were located at the bottom of the top flange, the center of the web, and the top of the bottom flange. At the south end of the bridge on Girders 1, 4, and 7, 3 strain gages were installed on each girder. At the other 6 locations, in addition to the girder gages, 2 additional gages were positioned on longitudinal reinforcing bars situated parallel to the girder at the top and bottom mats of deck reinforcement. All strain gages were oriented to measure strains in the longitudinal direction of the reinforcing bars and girders in order to investigate transverse cracking.

To investigate longitudinal cracking, strain gages were placed on transverse reinforcing bars positioned perpendicular to the girders. Transverse gages, as illustrated in Figure 3.16, were placed in the middle of the south span and over the center pier across Girders 4 and 5 at the bottom mat of deck reinforcement. The strain gages were placed directly over both edges of the flanges.

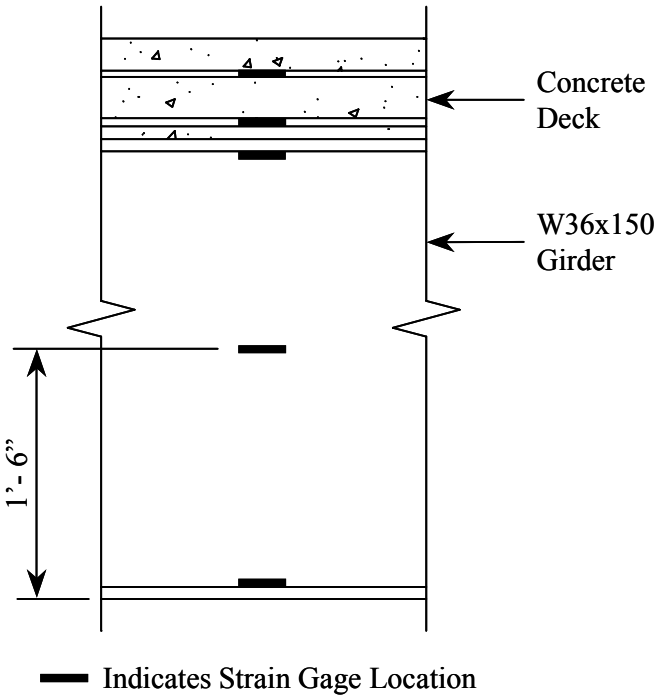

Figure 3.17: Elevation View of Strain Gage Locations

3.4.1.2 Thermocouples

Thermocouples were placed in the concrete deck and on the steel bridge girders. Figure 3.18 shows a plan view of the layout of the thermocouples. At each location shown, 4 thermocouples were installed through the section depth to determine the thermal gradient. As illustrated in Figure 3.19, 2 thermocouples were placed in the deck and 2 thermocouples were placed across the depth of the girders. The thermocouples in the deck were positioned at the same level as the top and bottom mats of reinforcing steel. The thermocouples on the steel girders were located on the bottom of the top flange and the top of the bottom flange. In addition to direct temperature readings of the structure, an ambient reading was recorded at the midspan of Girder 7. The ambient thermocouple was secured to the bottom flange of the girder restricting the end of the wire, where the temperature is read, from touching any portion of the structure.

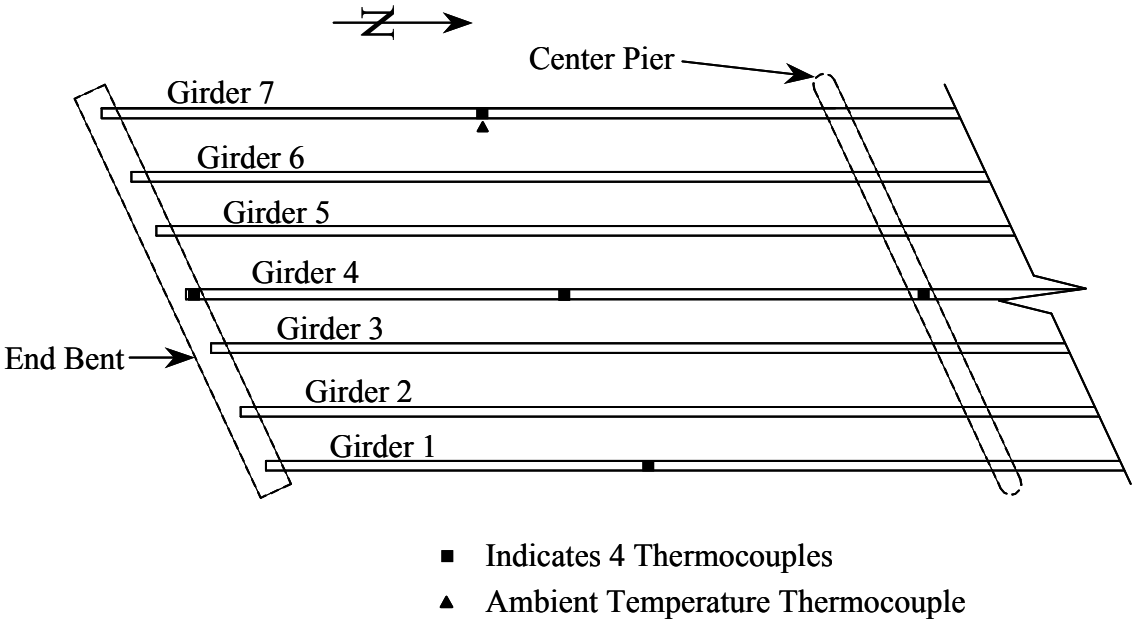

Figure 3.18: Plan View of Thermocouple Locations

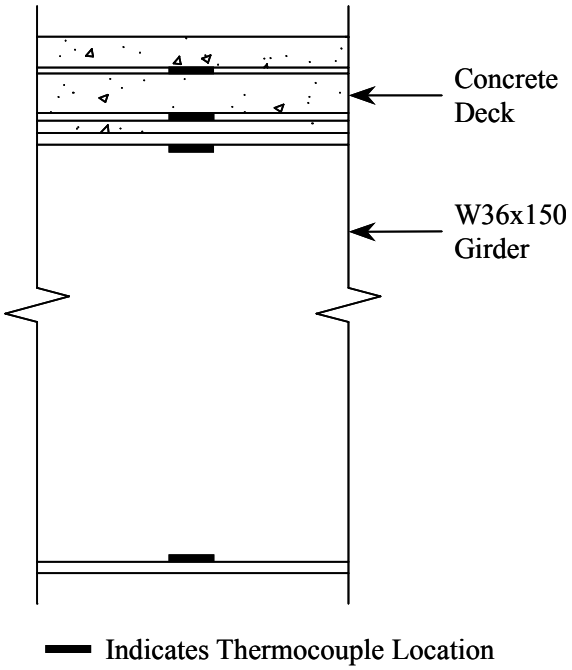

Figure 3.19: Elevation View of Thermocouple Locations

3.4.1.3 Instrument Identification

An identification system for the gages is presented below. This system assigns each gage a unique instrument identification as follows:

(Gage Type)-(Girder Number)-(Location)-(Depth)-(Orientation)-(Edge of Girder)

Gage Type:	Strain Gage (**S**)
	Thermocouple (**T**)
Girder Number:	See Figure 3.20
Location along Length:	See Figure 3.20
Depth through Section:	See Figure 3.21
Orientation:	Longitudinal with Girders (**L**)
	Transverse to Girders (**T**)
Edge of Girder:	East Edge of Girder (**E**)
	West Edge of Girder (**W**)

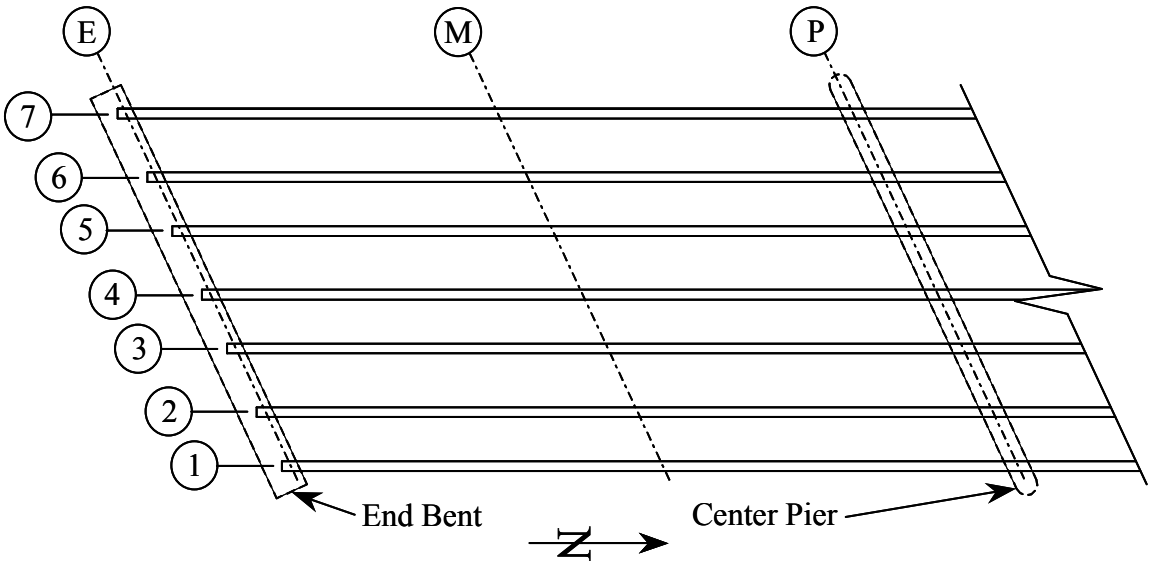

Figure 3.20: Plan View of Instrumentation Identification

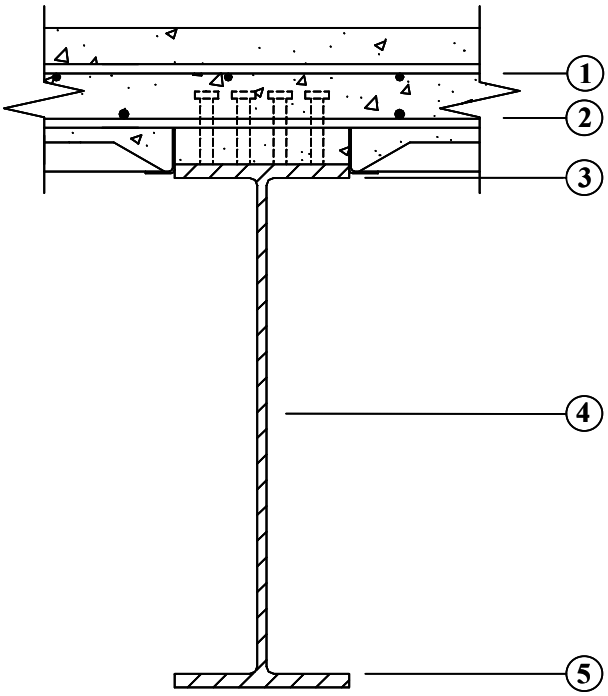

Figure 3.21: Elevation of Instrumentation Identification

3.4.2 Instrumentation Installation

The installation of the instrumentation was coordinated with work crews on site and placed as the construction progressed. Complete specifications for the instrumentation installed in this bridge are available in Appendix C.

3.4.2.1 Strain Gages

All strain gages on reinforcing bars were installed on "sister" bars to eliminate interference with the placement of the deck reinforcement. The strain gages for the deck were installed on #4 epoxy-coated reinforcing bars in the lab. For bars that were installed longitudinal to the girders, 1 strain gage was placed in the center of a 5-ft 9-in. long bar. This bar length was selected to provide adequate development on both sides of the gage. Then, these bars were tied directly over the bridge girders in the top and bottom mats of deck reinforcement as the reinforcing steel was placed. The 2 bars that were installed transverse to the girders were placed continuously across Girders 4 and 5 with 4 strain gages on each bar. These bars were 13-ft 3-in., to permit full development on both sides of the gages, and were tied to the bottom mat of deck reinforcement with the strain gages directly over the edges of the flanges. Figure 3.22 shows the transverse and longitudinal strain gages located over the center pier at Girder 4.

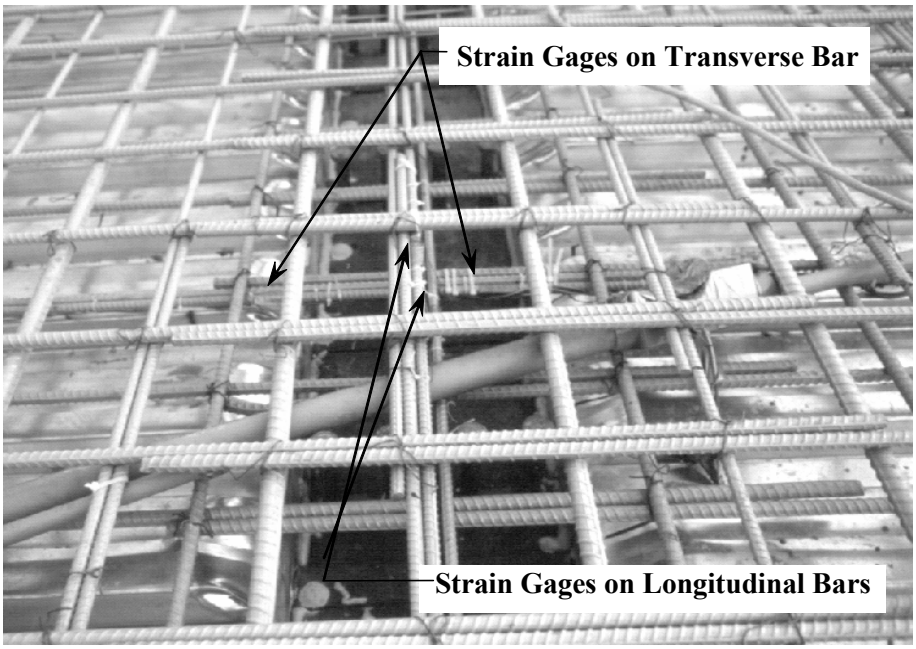

Figure 3.22: Strain Gages in Deck at Girder 4 over Center Pier

For strain gage installation on the #4 epoxy-coated reinforcing steel, a small portion of epoxy coating and approximately 3 lugs were removed (Figure 3.23(a)). After the epoxy coating where the gages were to be placed was removed, Micro-Measurements products were used to install and protect the strain gages.

Initially, the area was sprayed with CSM-1A degreaser to remove any oils on the surface. The area was then wet sanded with 400-grit silicon-carbon paper using Conditioner A. The surface was wiped clean with gauze and the process was repeated. The area was wiped clean again then washed with Neutralizer 5A using cotton swabs. The surface was cleaned with the neutralizer a minimum of 2 times with the surface being wiped with gauze between washings. The surface was washed until no particles were observed on the cotton swabs.

Once the surface was clean, the strain gage was taped to the surface using PCT-2A cellophane tape. The tape was then pulled back from one end exposing the back side of the strain gage. The gage was coated with M-Bond 200 Catalyst-C and allowed to dry 1 minute. Next, M-Bond 200 adhesive was applied to the surface and the strain gage was pressed into the adhesive for a minimum of 1 minute.

After the adhesive had cured, the cellophane tape was removed exposing the top side of the strain gage with the 2 soldering tabs. A short piece of 3 conductor, 26 AWG leadwire was attached to the strain gage. The ends of the wires and soldering tabs were coated with M-Flux and the black and white wires were soldered to one tab and the red wire was soldered to the other tab. The black and white wires, attached to the same soldering tab, were used to provide automatic temperature compensation for leadwire effects. This was especially important due to the long wire lengths required in the field installation. The connection was then cleaned with RSK Rosin Solvent to remove excess flux.

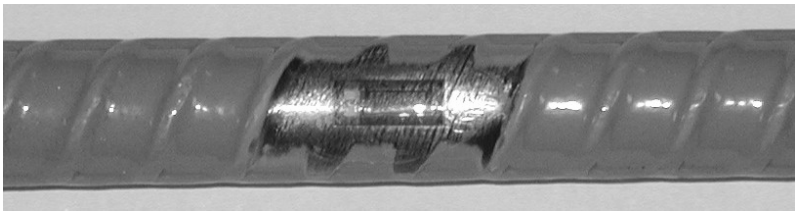

a) Strain Gage Adhered to Reinforcing Bar

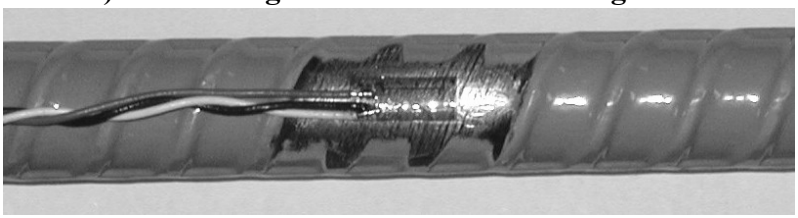

b) Leadwire Attached to Strain Gage

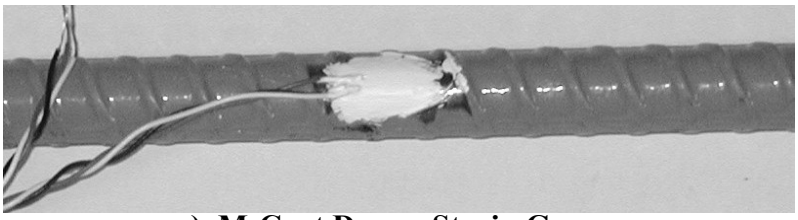

c) M-Coat D over Strain Gage

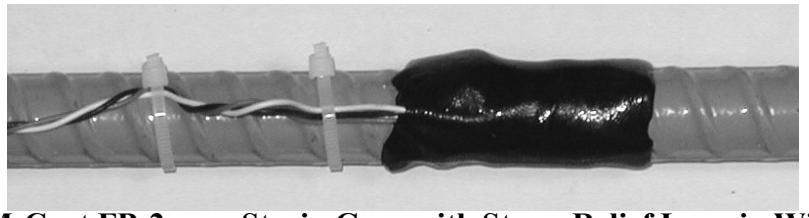

d) M-Coat FB-2 over Strain Gage with Stress Relief Loop in Wire

Figure 3.23: Strain Gage Installation and Protection

To provide protection for the gages, the following procedure was followed. Once the rosin solvent had evaporated, M-Coat D was applied over the strain gage and terminals. M-Coat D is an air-drying acrylic lacquer that waterproofs the strain gage. A second coat of M-Coat D was applied after the first coat cured for 15 minutes. After an additional 15 minutes, M-Coat FB-2 butyl rubber was placed over the M-Coat D. As a finally protector, M-Coat FN-2 neoprene rubber was taped over the strain gage area. The end of the leadwire closest to the strain gage was tied with a relief loop to the reinforcing steel or girder to protect the strain gage from being damaged if the leadwire was pulled. Figure 3.23 shows the progression of the strain gage installation and protection process on an epoxy-coated reinforcing bar.

For strain gages installed on the bridge girders, the paint was first removed to expose bare steel. Then, the installation and protection of the strain gages followed the same procedure as the reinforcing steel gages. Figure 3.24 shows the strain gage installation at the midspan of Girder 4 while Figure 3.25 shows the strain gages on Girder 7 over the center pier.

Figure 3.24: Strain Gage Installation on Girder

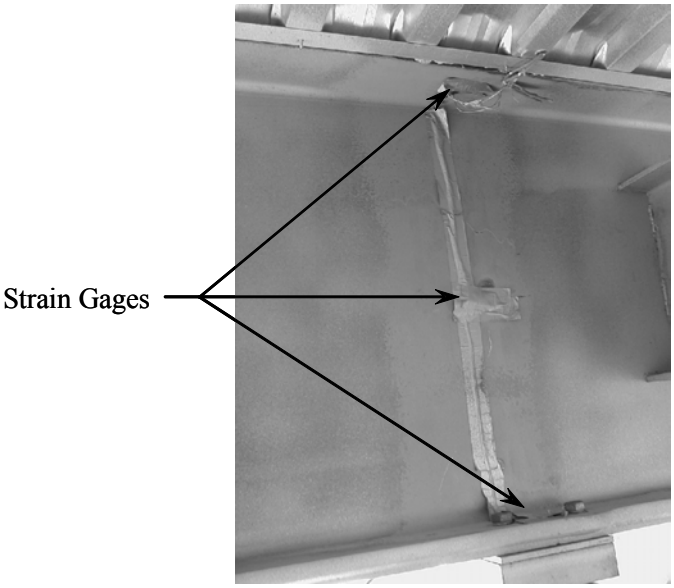

Figure 3.25: Strain Gages on Girder

3.4.2.2 Thermocouples

Thermocouple wire contains 2 wires with different material properties and reads temperature where these 2 wires touch each other. For the thermocouples placed on the bridge at the location where temperature readings were desired, the ends of the 2 wires were stripped, twisted together, and soldered. The deck thermocouples were protected with heat shrink-wrap and silicon caulking. Shrink-wrap was first placed over the soldered connection. Then, silicon caulking was placed on the shrink-wrap and a larger shrink-wrap was placed over the silicon. The deck thermocouples were then tied to the top and bottom mats of reinforcement. The girder thermocouples were glued directly to the girder using Micro-Measurements M-Bond 200 adhesive and only protected with multiple layers of tape.

3.4.2.3 Datalogger Systems

Datalogger systems were installed at each end of the bridge. The systems were first situated within 16-in. by 18-in. waterproof fiberglass enclosures (Figure 3.26). To further protect the datalogger systems, the enclosures were placed inside aluminum traffic controller M cabinets (Figure 3.27). Foundations with 4, ½-in. diameter by 12-in. anchor bolts were cast for the M cabinets at the time the lower portions of the end bents were cast. After the foundations cured, the cabinets were bolted to the foundations.

The datalogger systems were grounded using ½-in. diameter by 8-ft long copper grounding rods with 4 AWG solid copper wires connecting the ground rods to copper lugs on the fiberglass enclosures. The copper lugs were connected through the enclosures with 12 AWG stranded copper wires attached to the dataloggers.

Figure 3.26: Datalogger System in Fiberglass Enclosure

Figure 3.27: Datalogger System in M Cabinet

3.4.2.4 Conduit and Wiring

Schedule 40 electrical PVC conduits were placed in the deck to allow wires to be pulled from the datalogger systems to the strain gage and thermocouple locations (Figures 3.22 and 3.28). Conduits were placed through the end bents and data acquisition foundations prior to their casting. The conduits in the deck were placed between the 2 mats of reinforcing steel with the main conduit running in the coping line.

Figure 3.28: PVC Conduit between Mats of Steel in Deck

Belden 3-conductor shielded 24 AWG cable was pulled from the datalogger foundations to the location of each strain gage. Each cable was then spliced to the short piece of leadwire attached to the strain gage. Twisting and tinning each of the 3 individual conductors from the leadwire and the cable together made the splice. The 3 wire splices were protected with heat shrink-wrap and silicon caulking. Shrink-wrap was first placed over each individual wire splice. Silicon caulking was then placed on the shrink-wrap and a larger shrink-wrap was placed over all 3 splices and the silicon.

After all splices were made on the bridge, the ends of the wires at the datalogger foundations were pulled into the fiberglass enclosures and connected to the datalogger systems. The datalogger systems themselves were wired prior to installation of the fiberglass enclosures in the traffic controller cabinets. The power supplies were then connected to the datalogger systems.

3.4.3 Data Collection

The program for each datalogger was downloaded from a laptop computer prior to activation of each datalogger system. The dataloggers were programmed to record readings of all gages every 15 minutes. Both datalogger systems were started approximately 18 hours prior to deck casting. When the dataloggers were first activated, initial zero readings were recorded for all strain gages. Thermocouples record the actual temperature; therefore, zero readings were not required. Data from each datalogger system was periodically downloaded every 1-2 weeks.

3.5 Results

A summary of the data acquired from the dataloggers follows. In the plots of strain gages, positive values correspond with compressive strains.

3.5.1 Longitudinal Strain Gages

Of the 12 strain gages installed on longitudinal reinforcing bars, all longitudinal gages remained operational after construction except S-1-M-2-L. Following deck casting, the longitudinal gages indicated a gradual increase in compressive strain. On September 3, 2000 (19th day after casting) a sudden increase in compressive strain was noticed. All active longitudinal gages either went off scale or reached their highest strain value within 1 hour of each other except S-4-P-1-L. Figure 3.29 is representative of the 6 longitudinal gages located over the outside girders that reached their highest strain value, while Figure 3.30 is representative of the 4 longitudinal gages that went off scale, 3 of which were located over Girder 4. As shown in Figure 3.31, a steady rise in the compressive strain of S-4-P-1-L continued after September 3, 2000. It is interesting to note that this gage indicated very high strains on the day of casting, which may explain its erratic behavior.

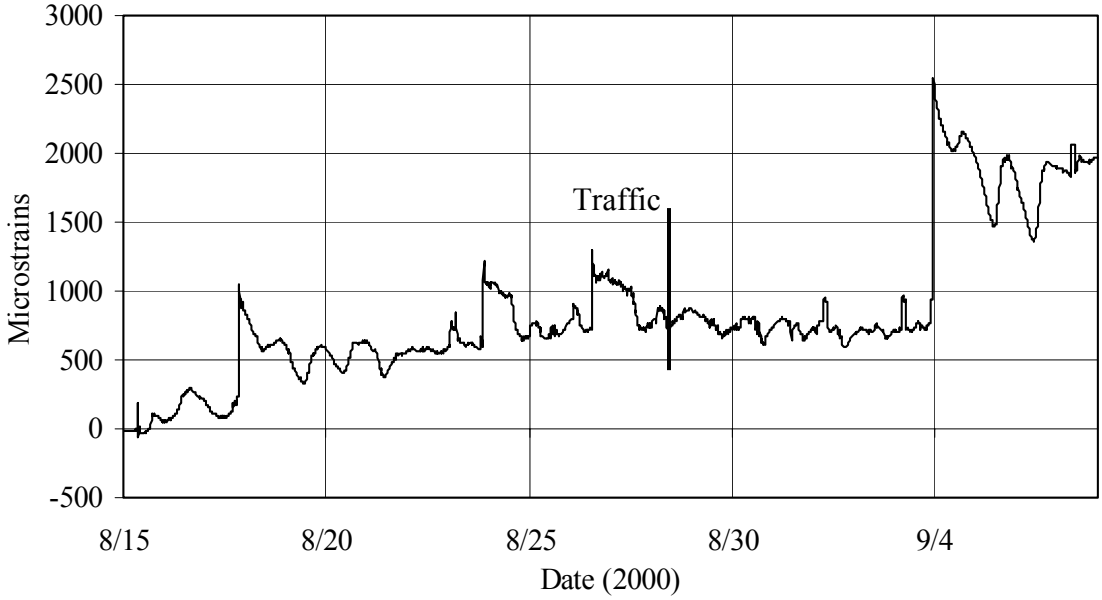

Figure 3.29: Longitudinal Reinforcement Strain (S-1-M-1-L)

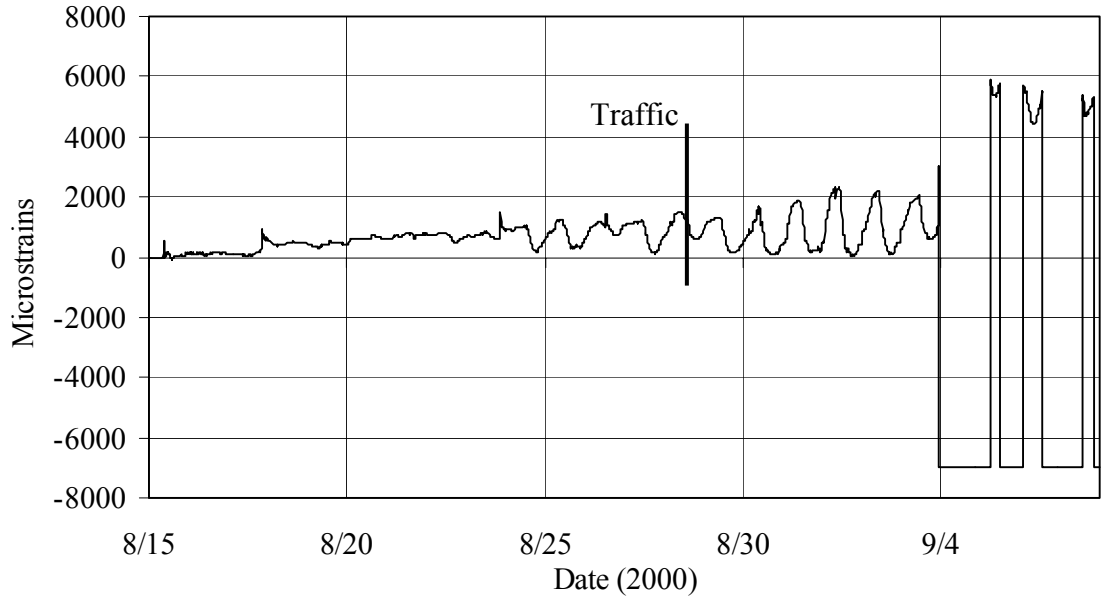

Figure 3.30: Longitudinal Reinforcement Strain (S-4-M-1-L)

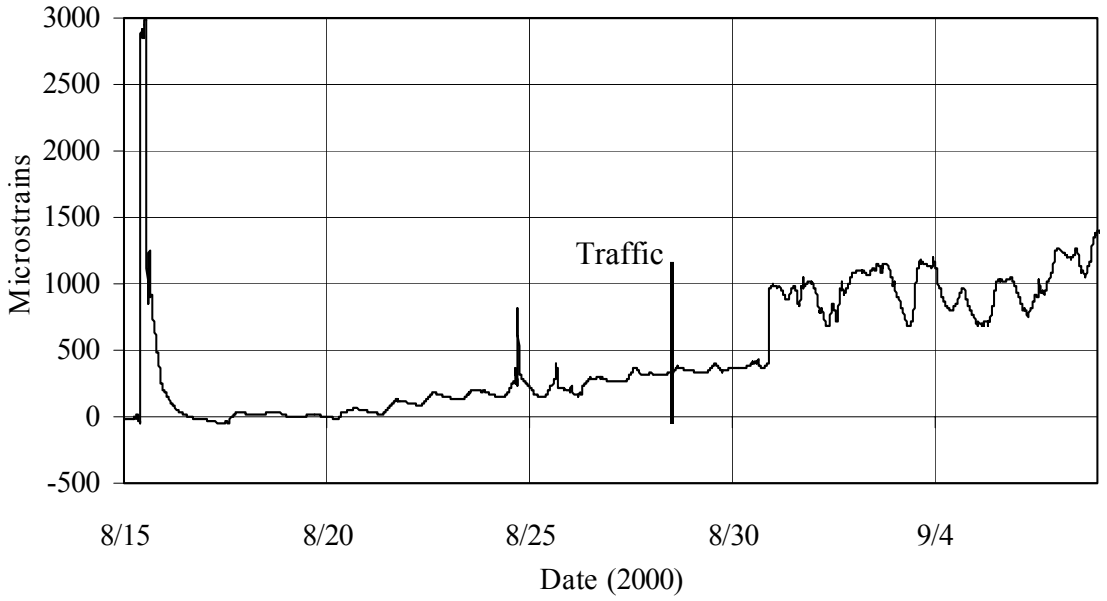

Figure 3.31: Longitudinal Reinforcement Strain (S-4-P-1-L)

3.5.2 Transverse Strain Gages

Of the 8 strain gages installed on transverse reinforcing bars, S-5-M-2-T-W was damaged prior to deck casting while during the deck casting S-4-P-2-T-W and S-5-P-2-T-E were damaged. Following deck casting, the remaining longitudinal gages indicated a gradual increase in compressive strain. The maximum strain and time to reach the maximum varied among these longitudinal gages. Figures 3.32 and 3.33 present the variation in the longitudinal gages.

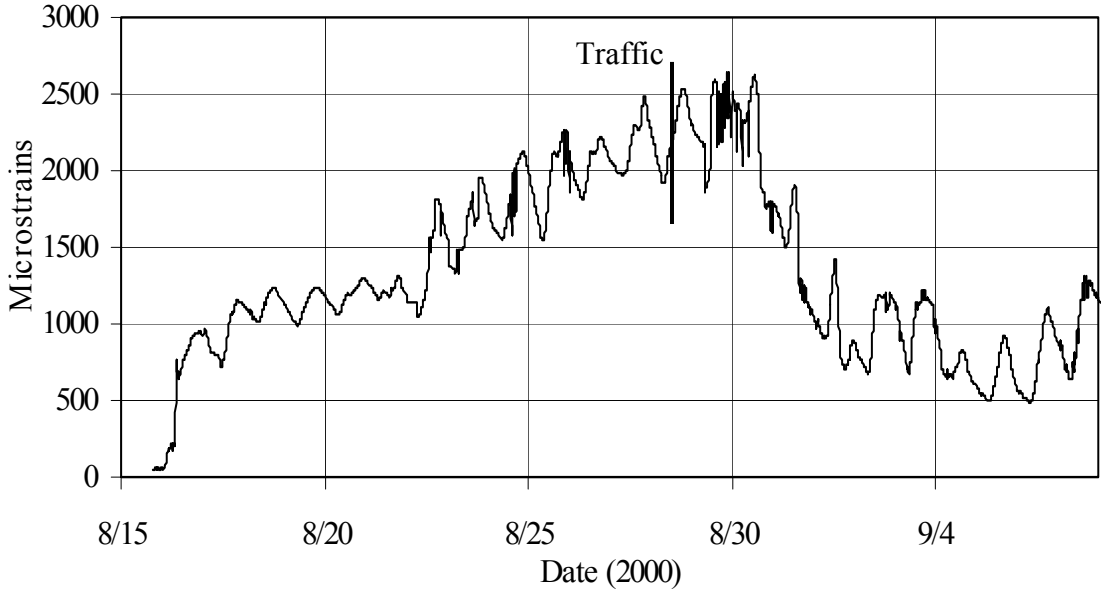

Figure 3.32: Transverse Reinforcement Strain (S-4-P-2-T-E)

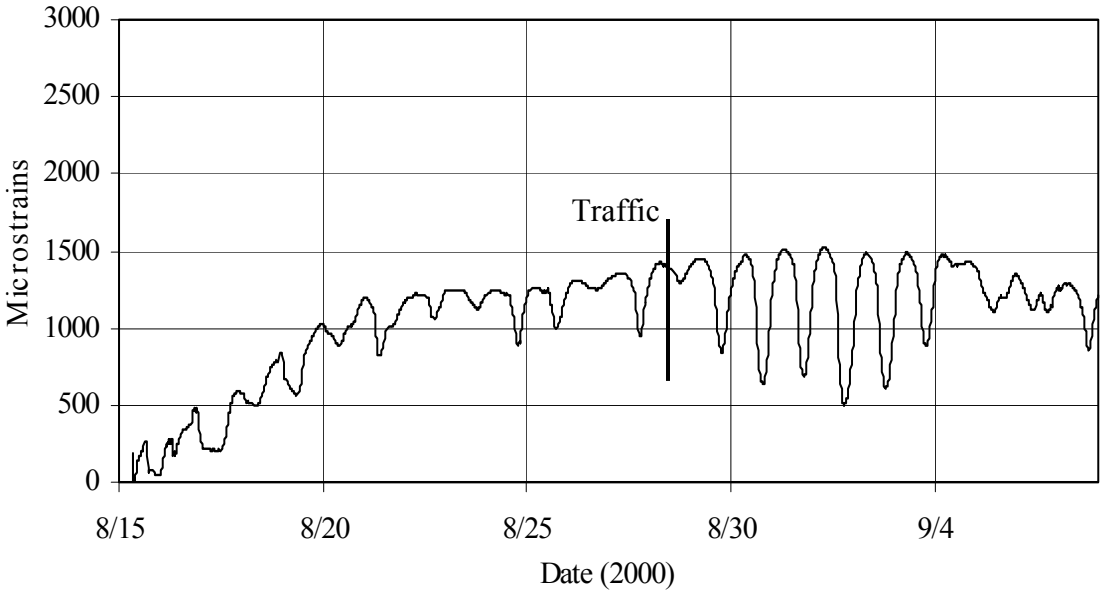

Figure 3.33: Transverse Reinforcement Strain (S-5-M-2-T-E)

3.5.3 Girder Strain Gages

After deck casting, all 27 girder gages remained operational. Following the heat of hydration period, the girder gages at the South End Bent demonstrated little strain. The gages at the middle of the south span indicated that the top flanges were in compression while the bottom flanges were in tension (positive moment). Over the

center pier, the girder gages indicated that the top flanges were in tension and the bottom flanges were in compression (negative moment). The strains over the center pier exceeded twice the strains as those at midspan. The difference in strains was expected because the negative moment over the center pier is approximately twice that of the positive moment at midspan. Figures 3.34, 3.35, and 3.36 exemplify the differences in compressive and tensile strains experienced in the top flange of Girder 4 at the south end abutment, midspan, and the center pier, respectively. These girder strains are consistent with generally expected behavior.

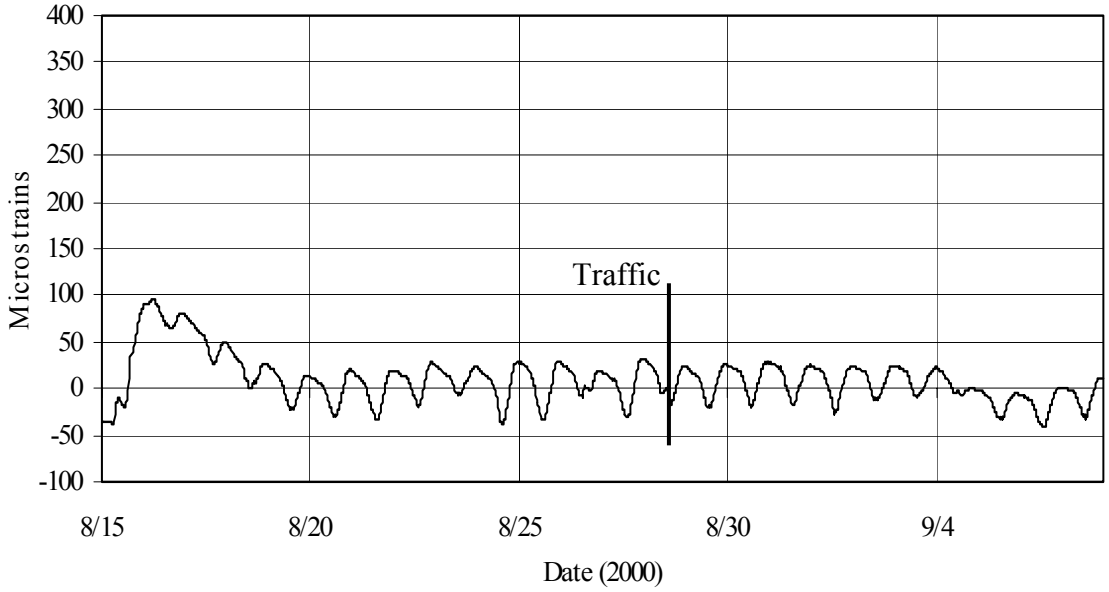

Figure 3.34: South End Girder Strain (S-4-E-3)

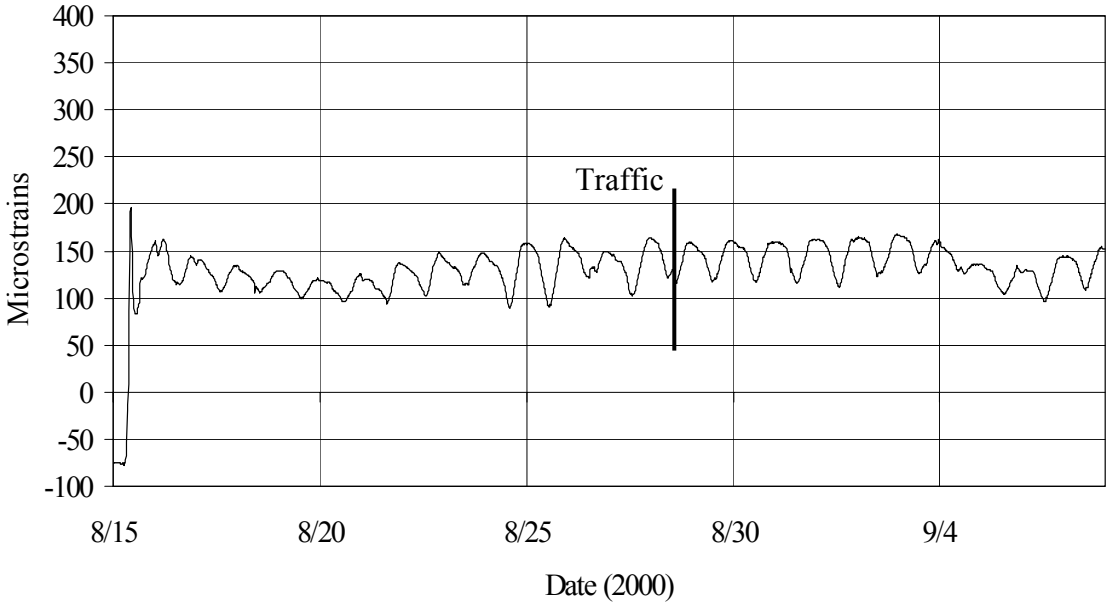

Figure 3.35: Midspan Girder Strain (S-4-M-3)

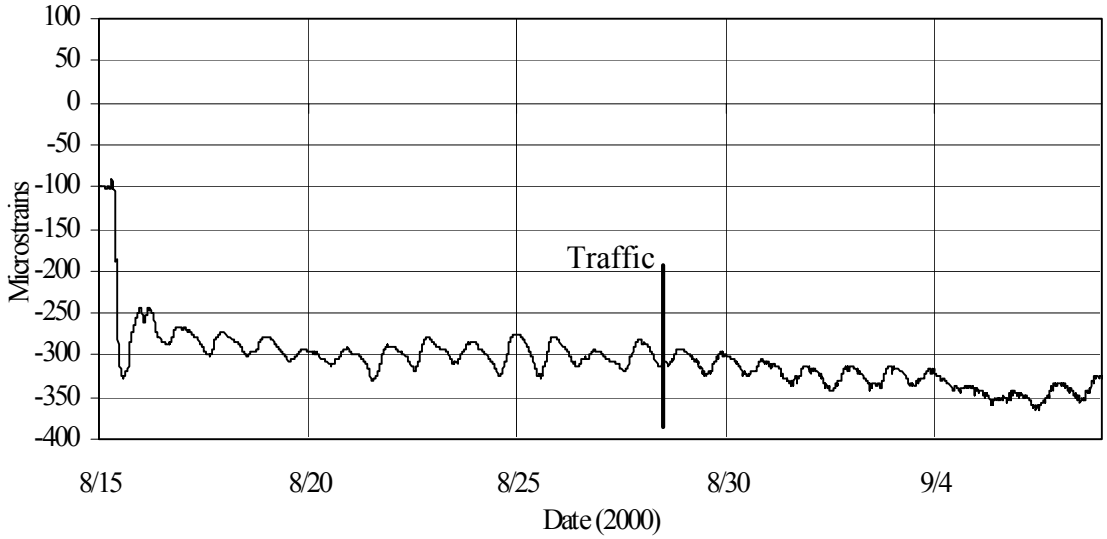

Figure 3.36: Center Pier Girder Strain (S-4-P-3)

3.5.4 Thermocouples

The ambient air temperature and the temperature of the deck were also investigated to identify significant differences in temperatures between the deck and the ambient temperature as well as the daily temperature ranges. Figure 3.37 presents the ambient air temperature, while Figure 3.38 presents the temperature of the deck at T-4-M-1.

In general after the curing process, it can be seen that the deck was always slightly warmer than the ambient air temperature. During both the day and night, the deck averaged approximately 8^{o} F warmer at its extremes.

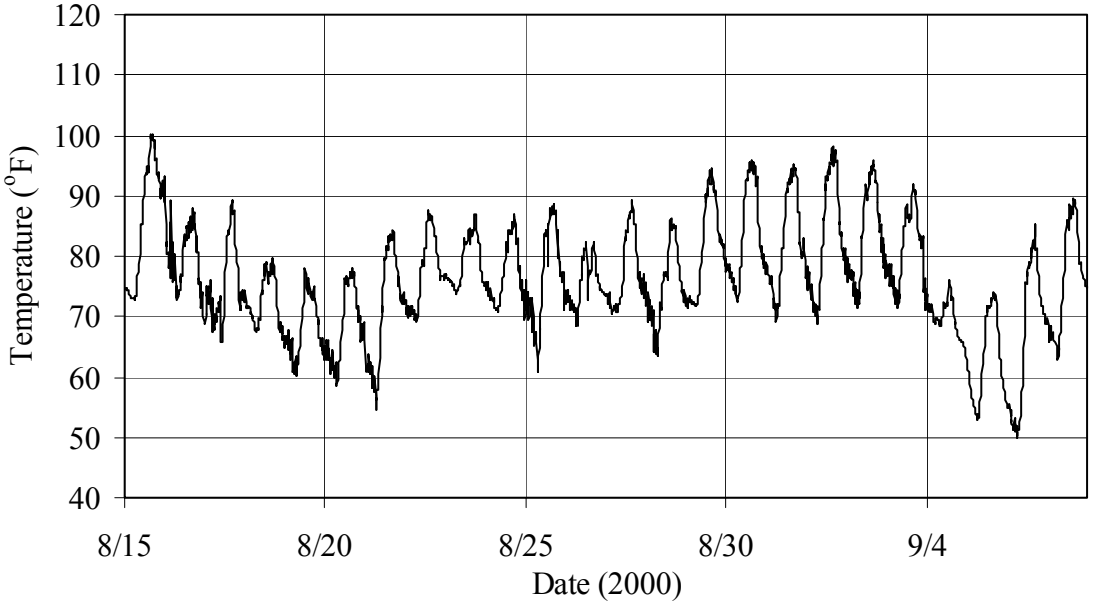

Figure 3.37: Ambient Air Temperature

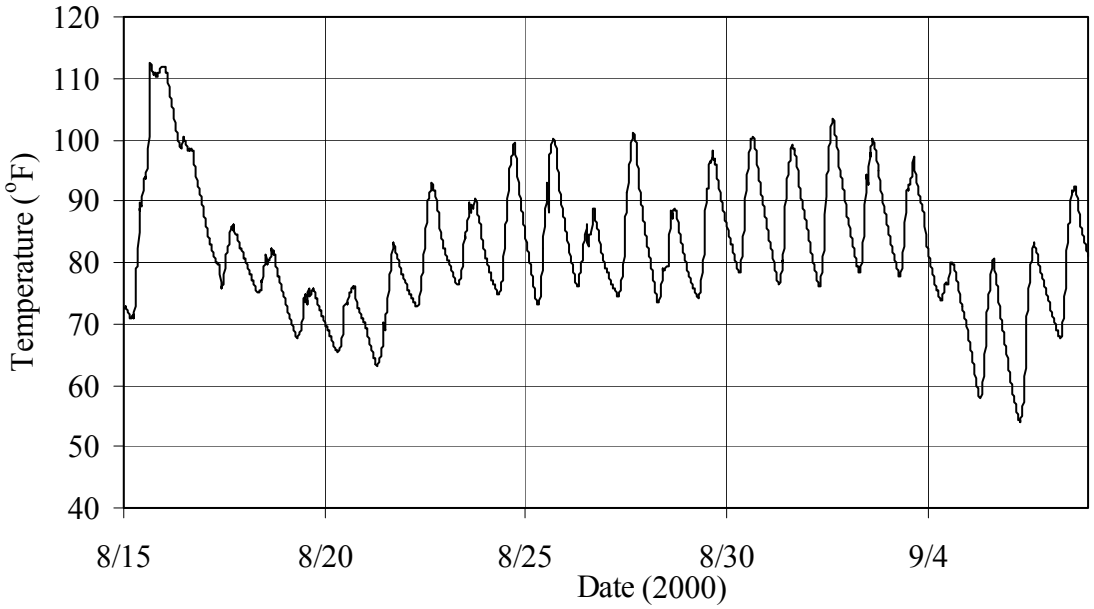

Figure 3.38: Deck Temperature (T-4-M-1)

3.6 Data Analysis

3.6.1 Transverse Cracking

Transverse cracking was investigated through the data obtained from strain gages placed on longitudinal reinforcing bars running parallel to the girders in the deck, strain gages attached to the steel girders, and the thermocouples.

A dramatic increase in strain was recorded in 10 of the 11 active longitudinal gages 19 days after casting (Figure 3.29 – 3.31). This sudden increase was observed with both data acquisition systems (half of the longitudinal gages were recorded with each system). In addition, an abrupt change was not noted in the girder strain gages (Figures 3.34 – 3.36) or the thermocouples on the 19th day after casting (Figures 3.37 and 3.38). Without variations in the girder gages and the thermocouples as well as the similar data recorded with 2 independent datalogger systems, the possibility of error in the datalogger systems was eliminated.

Figures 3.37 and 3.38 illustrate that the temperature due to the heat of hydration of the concrete in the deck exceeded the ambient temperature by a maximum of 31^{o} F at 2:15 AM on August 16, 2000. Following the period during the production of the heat of hydration, the deck was typically warmer then the ambient temperature both during the day and at night. The figures do not indicate any extreme temperature changes or major differences in temperature between the ambient temperature and the deck temperature.

Daily temperature differences induced strain in both the concrete deck and steel girders. As the temperature increased (Figures 3.37 and 3.38), the strain increased as shown in Figures 3.29 – 3.36. The daily strain increase in the steel girders fell within a range of 100 microstrains; however, the longitudinal strain gages in the deck varied daily as much as 2000 microstrains (Figure 3.30).

Maximum strain and temperature gradients were investigated for the first 19 days after casting at Girders 1, 4, and 7 at the midspan of the south span and at Girder 4 over the center pier. As shown in Figure 3.39, the maximum strain gradient between the top and bottom flanges of the girders was 698 microstrains over the center pier on Girder 4 on September 1, 2000 at 9:30 AM. As illustrated in Figure 3.40, the maximum temperature gradient between the top of the deck and the bottom of the girders was 41^{o} F at the midspan of Girder 7 on August 27, 2000 at 4:15 PM. Figure 3.41 shows that the maximum temperature gradient between the top and bottom of the girders was 40^{o} F at the midspan of Girder 7 on September 1, 2000 at 1:45 PM. In both temperature gradient cases, Girder 7 was warmer than the deck. Girder 7 is the outside girder on the west side of the bridge and was likely heated by solar radiation. For Figures 3.39 – 3.41, the corresponding temperature or strain gradient is also shown.

The AASHTO LRFD *Bridge Design Specifications*, 2nd edition specifies a maximum temperature gradient of 41^{o} F from the top of the deck to the bottom of the girder for a steel superstructure bridge with a concrete deck in Indiana (AASHTO 1998). However, the bottom of the steel girders is considered to remain at the ambient air temperature. The ASHTO LRFD specified temperature gradient is the same value as measured in the I65 over SR25 bridge, but the bottom of the girder was heated instead of the top of the deck.

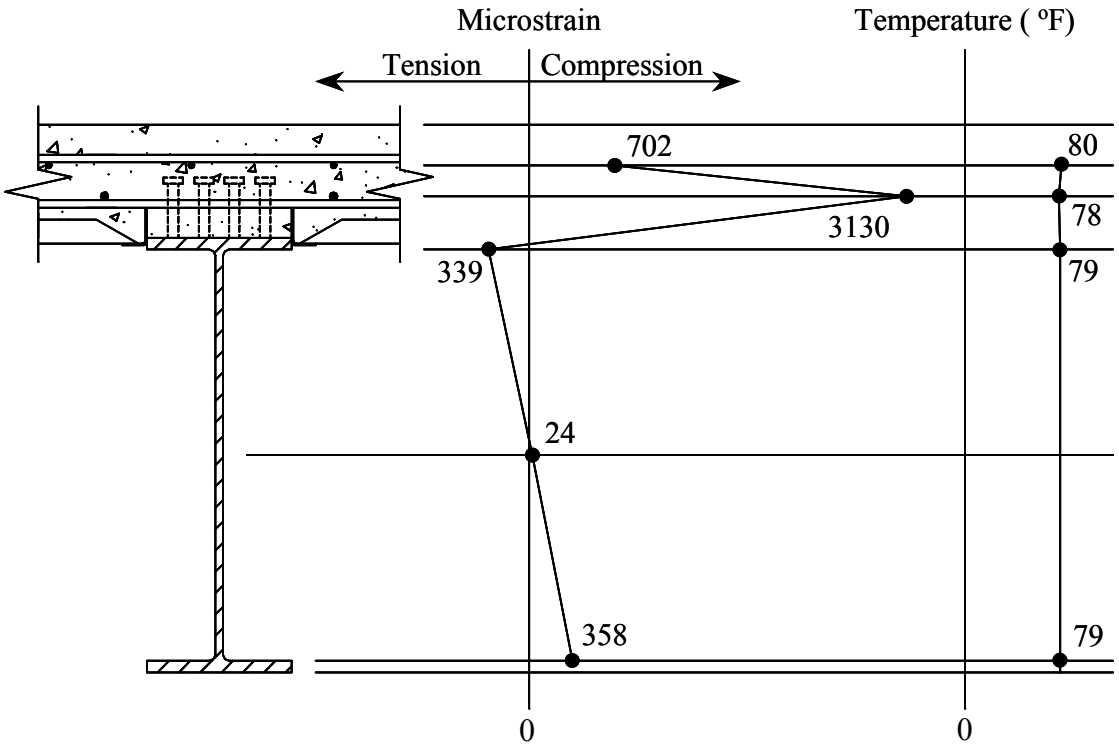

Figure 3.39: Maximum Girder Strain Gradient (Girder 4, Center Pier)

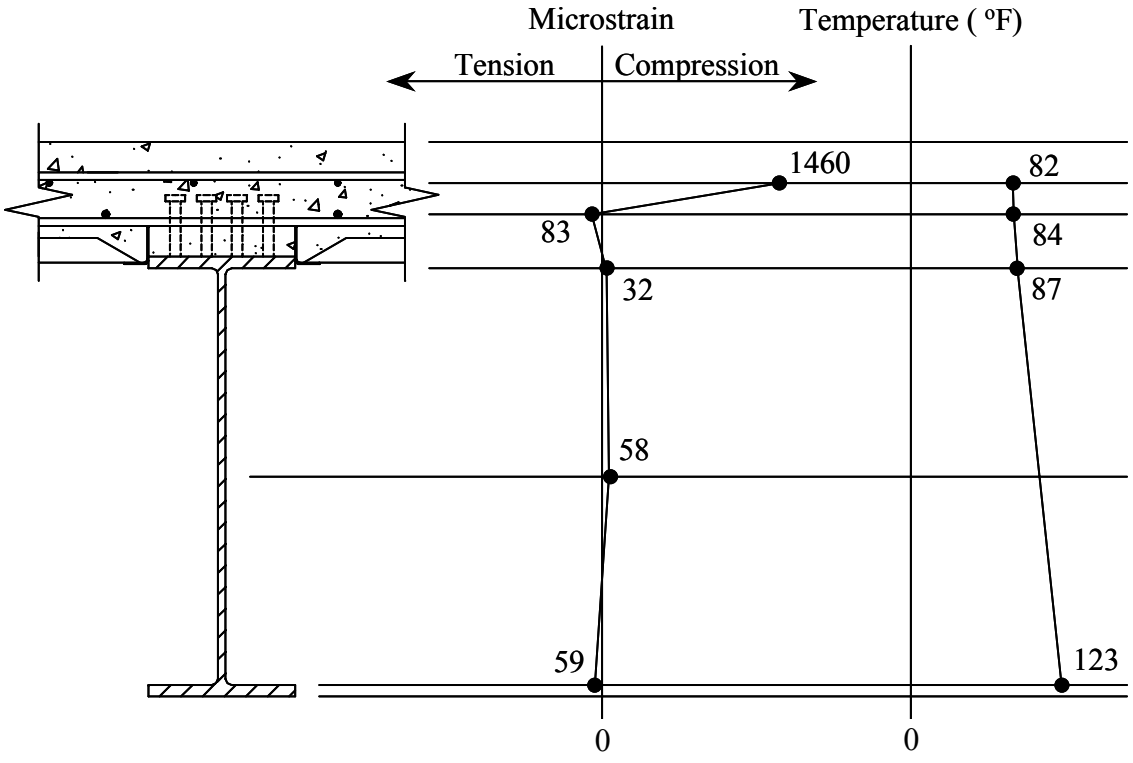

Figure 3.40: Maximum Thermal Gradient (Top of Deck/Bottom of Girder 7)

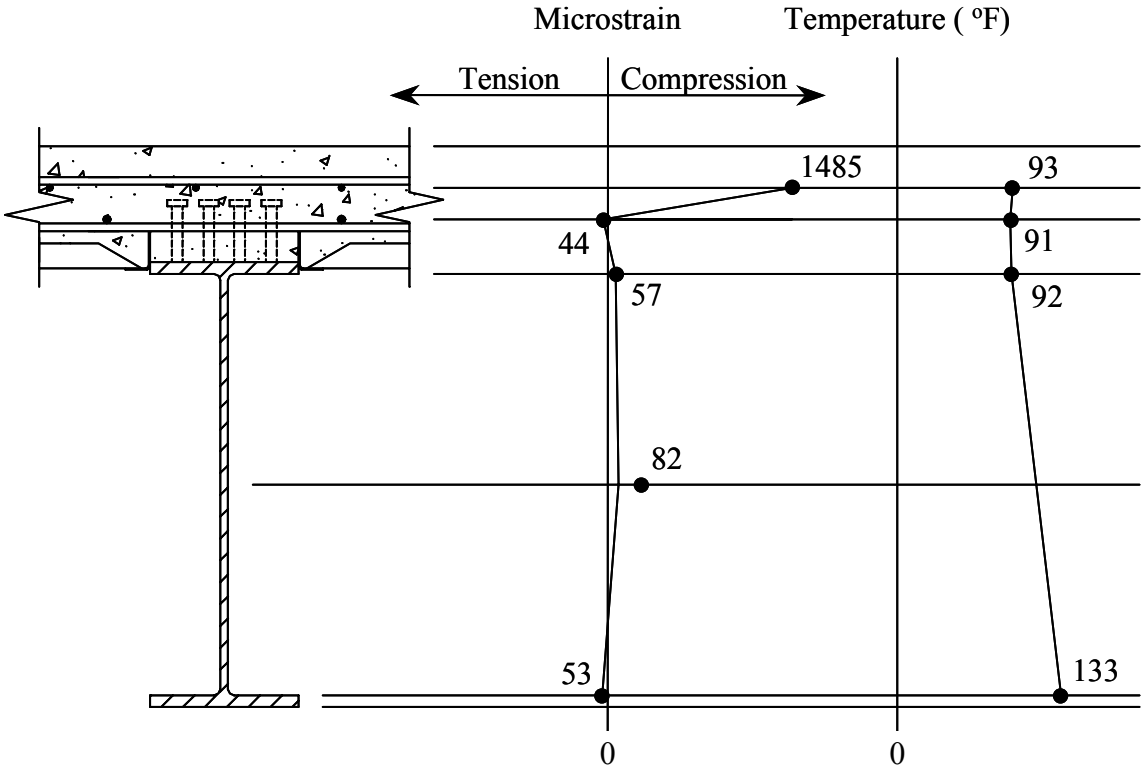

Figure 3.41: Maximum Thermal Gradient (Top/Bottom of Girder 7)

Traffic was allowed on the bridge beginning at 2:25 PM on August 28, 2000. Figures 3.30 and 3.33 illustrate an increase in the daily change in strain, but this change is not observed with the other gages shown.

The additional strain in the deck and girders over time was likely caused by the shrinkage of the concrete bridge deck. With 10 of the 11 active longitudinal strain gages in the deck recording a dramatic increase in compressive strain without a significant change in strain in the steel girders or temperature effects, it is highly probable that the bridge developed transverse cracks on September 3, 2000, 19 days after the deck was cast. The presence of these cracks could not be observed due to the sealing of the deck. An investigation of the bridge deck was performed on March 13, 2001, at which time, a transverse crack was observed directly over the center pier.

Once the deck cracked, the stress in the concrete was transferred to the reinforcing steel, which would account for the sudden increase in strain. The calculation of the transfer of strain from the concrete to the reinforcing steel is shown in Figure 3.42. By assuming a tensile strength in the concrete (f_t), the total force to produce cracking in a 1-ft strip of slab (F_t) was calculated. This force was equated to the force resisted by the reinforcing steel to determine the reinforcement stress produced (f_{cr}) and the resulting reinforcing strain (ε_{cr}).

Following this procedure, the strain transfer to the reinforcing steel after deck cracking was calculated to be 2800 microstrains if it is assumed that the steel remains in the elastic range. As shown in Figure 3.30, the sudden increase in strain 19 days after casting was measured to be approximately 2000 microstrains prior to going offscale and yielding the bar. The 6 longitudinal gages that did not go offscale (Figure 3.29) were located over the 2 outside girders in close proximity to the barrier walls. The barrier walls and barrier wall reinforcement possibly influenced the slightly lower strain measurements. This calculation procedure again illustrates that it is highly probable that the bridge developed transverse cracks 19 days after the deck was cast. The strain in the longitudinal bars then likely decreased over time due to redistribution of forces.

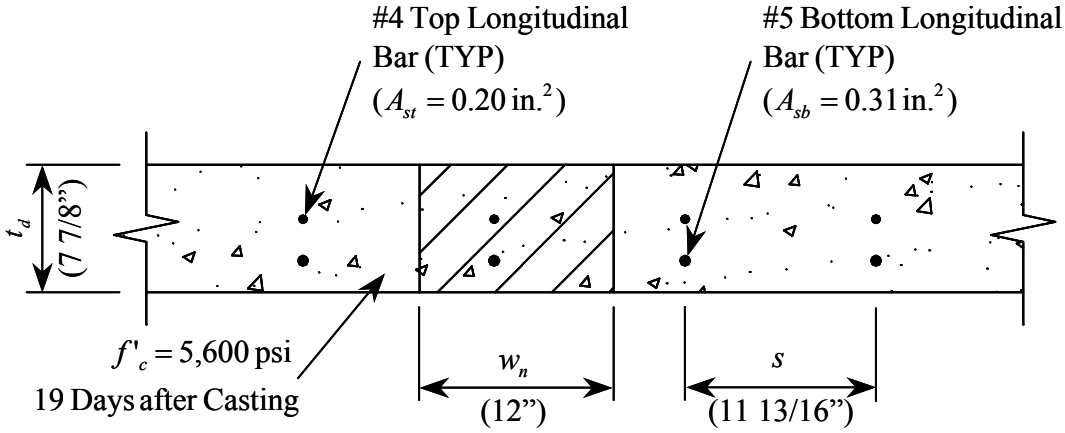

$$f_t = 6\sqrt{f'_c} \qquad \text{(Eqn. 3.1)}$$

$$f_t = 6\sqrt{5{,}600} = 449 \text{ psi}$$

$$F_t = f_t w_n t_d \qquad \text{(Eqn. 3.2)}$$

$$F_t = (449 \text{ psi})(12 \text{ - in.})(7\ 7/8 \text{ - in.}) = 42{,}430 \text{ lb}$$

$$A = \frac{A_{st} + A_{sb}}{s} * w_n \qquad \text{(Eqn. 3.3)}$$

$$A = \frac{0.20 \text{ in.}^2 + 0.31 \text{ in.}^2}{11\ 13/16 \text{ - in.}} * 12 \text{ - in.} = 0.52 \text{ in.}^2$$

$$f_{cr} = \frac{F_t}{A} \qquad \text{(Eqn. 3.4)}$$

$$f_{cr} = \frac{42{,}430 \text{ lb}}{0.52 \text{ in.}^2} = 81{,}600 \text{ psi}$$

$$\varepsilon_{cr} = \frac{f_{cr}}{E_s} \qquad \text{(Eqn. 3.5)}$$

$$\varepsilon_{cr} = \frac{81{,}600 \text{ psi}}{29{,}000{,}000 \text{ psi}} = 2{,}800 \text{ microstrains}$$

Figure 3.42: Calculation of Strain Transfer

Using the procedure presented in Figure 3.42 on the longitudinal reinforcement (#5 bars top and bottom @ 7 7/8-in. on center), the strain calculated would be 1500 microstrains. With the daily fluctuation in strain, yielding of the longitudinal bars would also be a possibility when the deck cracked. To control the crack widths in the concrete deck, the reinforcing steel should remain in the elastic region. Using #5 bars in the top and bottom mats of reinforcement spaced at a maximum of 6-in. (1200 microstrains at transfer) will likely minimize transverse crack widths.

3.6.2 Longitudinal Cracking

The presence of longitudinal cracks were investigated using data obtained from the 8 strain gages placed on transverse reinforcing bars running perpendicular to the girders in the deck and the thermocouples. The 2 instrumented transverse bars were resting directly on the cold-rolled angle in 3 of the 4 locations, which likely accounts for damage to 3 of the 8 transverse gages before or during deck casting. No correlation could be made between the remaining 5 transverse gages due to variations in strain readings. However, several longitudinal cracks were observed on the deck when it was sandblasted and sealed on August 24, 2000, 9 days after the casting.

CHAPTER 4
LABORATORY MODELS

4.1 Introduction

From the findings of the field investigation and field instrumentation, laboratory models were built to study the restraint and shrinkage in continuous steel superstructure bridges that incorporated composite action and stay-in-place steel forms. This type of bridge system was selected because it exhibited the most transverse cracking of any system and is a typical bridge for Indiana. Also, the I65 over SR25 bridge instrumented in the field instrumentation with similar construction developed transverse cracks 19 days after the deck was cast.

4.2 Model Design

The laboratory models consisted of two specimens. The models were full-scale sections taken from the positive moment region of the I65 over SR25 bridge. These models incorporated the identical epoxy-coated reinforcing bar size, bar spacing, girder flange width, shear stud size, girder spacing, and deck thickness. The only difference between the 2 specimens was the method used for forming the bottom of the deck. The first model was the as-built case, which used the same stay-in-place steel forms as the I65 over SR25 bridge. Figure 4.1 illustrates the stay-in-place steel forms used on both the I65 over SR25 bridge and the as-built model. The ends of these steel forms were factory tapered to complete the bottom formwork. The channels in the steel forms essentially create a shear key approximately every 8 ¾-in, which is likely to cause restraint in the bridge deck as the concrete experiences drying shrinkage. In addition, the 2-in. nearly vertical component of the steel forms may induce a crack initiation location.

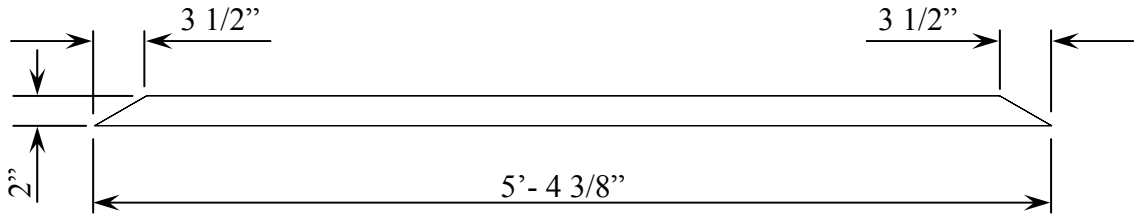

a) Profile of Stay-in-Place Steel Forms

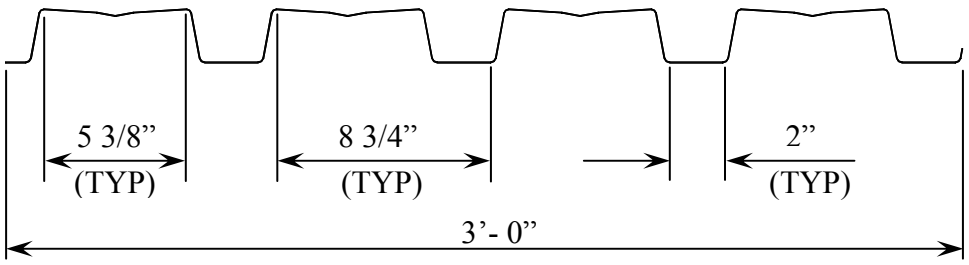

b) Cross Section of Stay-in-Place Steel Forms

Figure 4.1: Stay-in-Place Steel Forms

The second specimen was the free-shrinkage model. The free-shrinkage model used plywood forms with a similar profile, as shown in Figure 4.1(a), of the stay-in-place steel forms. To further minimize restraint, 2 layers of 10-mil Teflon sheets were placed on top of the plywood forms. The Teflon sheets permitted the concrete to shrink freely without restraint from the formwork.

Each model had a 9-ft by 9-ft slab cast on 2 steel girders. These dimensions were determined based on the girder spacing and size limitations in the lab. The spacing of the girders on the I65 over SR25 bridge was 78-in. on center. To fully develop the reinforcing steel between the 2 girders, a 9-in cantilevered section was added on the outside of each girder.

The smallest wide flange girder section with a 12-in. flange was used for these lab models. The 12-in. flange was desired because this dimension was the same width as the flange on the I65 over SR25 bridge. The smallest girder section was preferred because the lab specimens were only spanning 9-ft. It was desirable to select a section with a small moment of inertia, so that deflections could be measured on such a short span. These criteria resulted in a W12x65 girder.

Shear studs were placed on the girders with the same spacing across the flange and a similar spacing along the length of the girders. The stud spacing along the length of the I65 over SR25 bridge varied from 9-in. to 24-in.; therefore, a 12-in. spacing was selected for the lab models. Figure 4.2 shows the spacing of the 7/8-in. diameter by 5-in. tall shear studs.

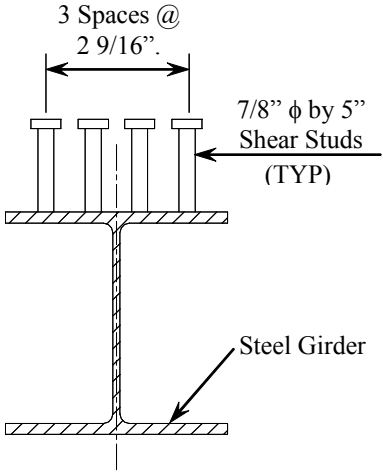

a) Shear Stud Spacing over Flange

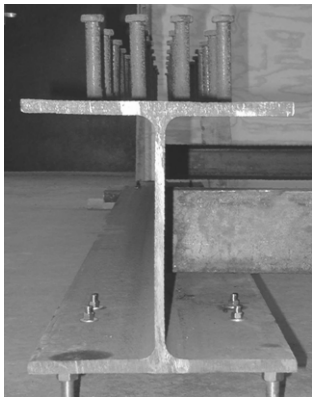

b) Actual Shear Stud Spacing

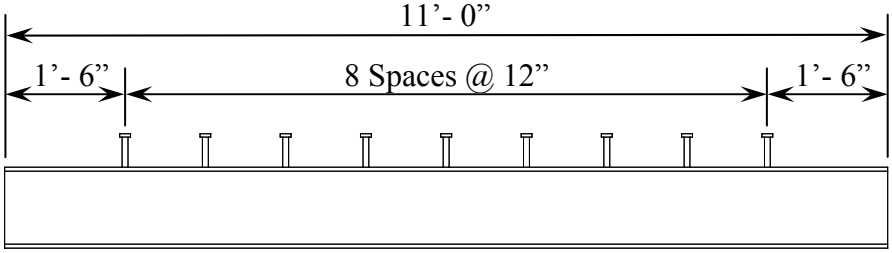

c) Shear Stud Spacing over Length of Girder

Figure 4.2: Shear Stud Spacing

Diaphragms were also used in the lab models. Diaphragms are required during bridge construction to reduce the lateral braced length, to resist overturning moments of the girders, and to maintain the girder spacing. Figure 4.3 illustrates the steel diaphragm (C5x6.7) and the support locations for the lab models.

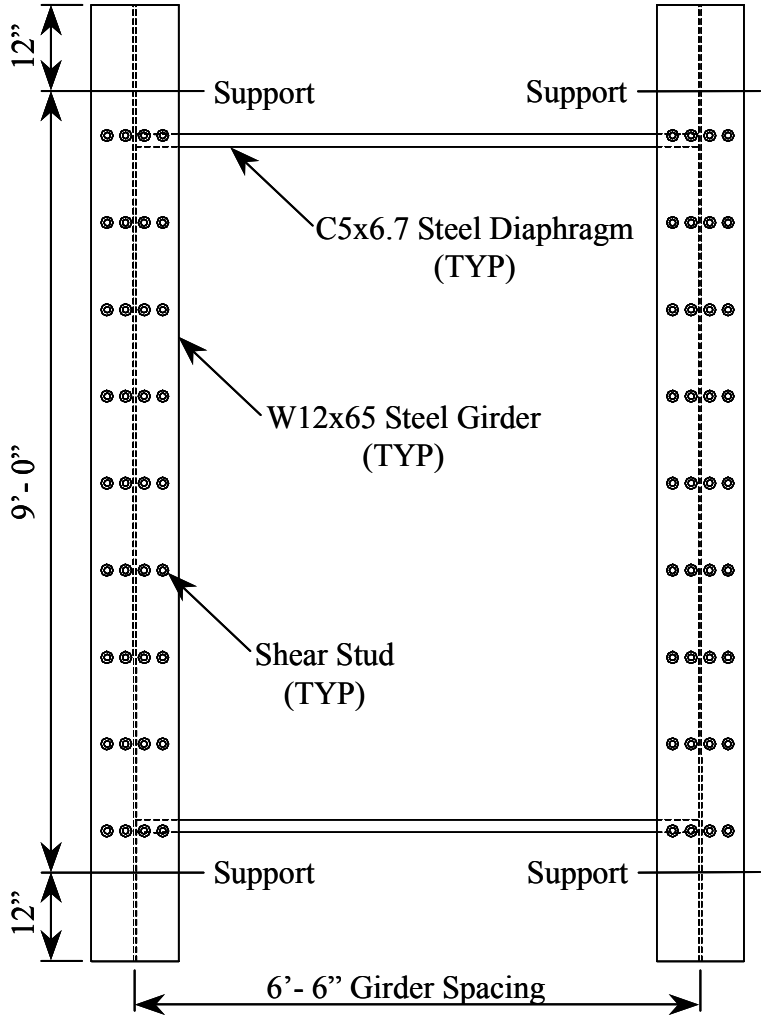

Figure 4.3: Diaphragm and Support Locations for Lab Models

4.3 Model Construction Sequence

The two models were constructed simultaneously in the lab. Identical materials were used in each model with the exception of the bottom forming materials.

4.3.1 Steel Girders

A local fabricator constructed the girder and shear stud assemblies. The girders were 11-ft long to permit formwork and supports to be attached near the ends of the girders (Figure 4.2c). Once received, the girder assemblies were stored outside for approximately 1 week to permit a light surface rust to form. The surface rust generates better bonding between the steel and the concrete and is similar to field conditions.

The girder assemblies were then moved inside the lab. The assemblies were spaced 78-in. apart on center and leveled. Then, the C5x6.7 steel diaphragms were welded to the webs between the steel girders near the supports (Figure 4.3).

4.3.2 Supports

Once the diaphragms were welded, the girders were set on supports. The bases of the supports were short sections of a wide flange beam. Steel plates, with rounded grooves along the centerline of the top surface, were bolted to each support and the girders. The steel plates bolted to the girders were spaced 12-in. from each end of the girder to the centerline of the plates. Round steel bars were placed in the grooves of the steel plates to form pinned connections between the supports and the steel girders. Figure 4.4 shows this pinned connection.

After the girders were set on the supports, the tops of the steel girders were leveled using a surveyor's automatic level. The elevation of the girders was adjusted by shimming the supports. Hydrostone was then poured under the supports to fix the elevation and location.

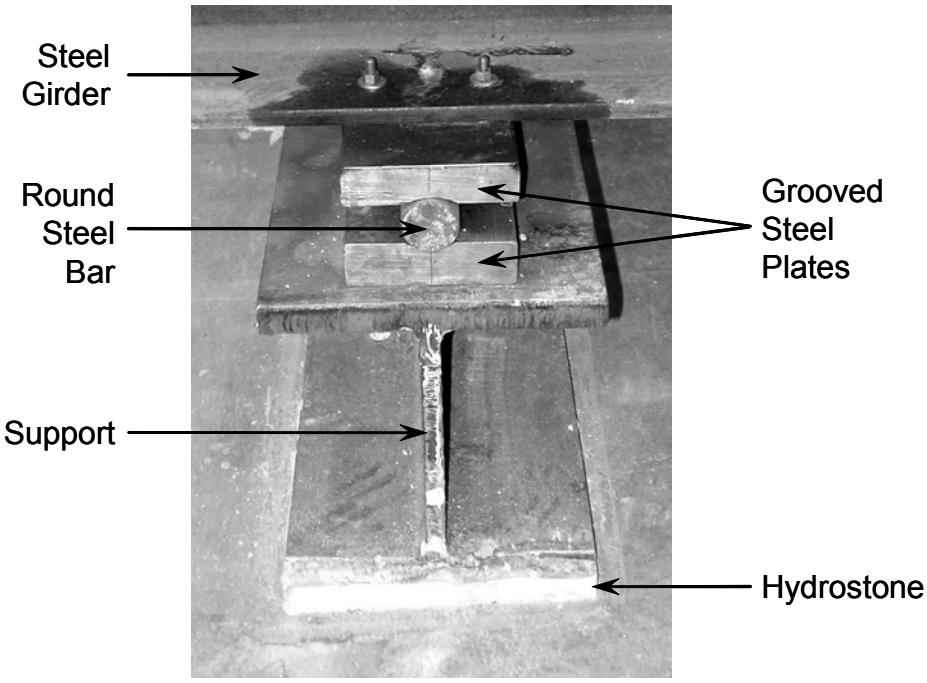

Figure 4.4: Pinned Connection between Steel Girder and Support

4.3.3 As-Built Model Formwork

Stay-in-place steel forms and 3-in. by 2-in. galvanized cold-rolled steel angles from the I65 over SR25 bridge were used to form the bottom of the slab. The bottom formwork covered the area between the girders and the two 9-in. cantilevered sections on the outside of the girders. Figure 4.5 illustrates the cross-section of the as-built model.

The cold-rolled angle was welded directly to the top flange with the 2-in. leg of the angles turned down (Figure 4.6). The absence of the leg into the deck eliminated the possible stress concentration point. Then, end forms were bolted to the ends of the girders, 9-ft apart. These end forms were constructed with ¾-in. plywood and reinforced with 2-in. by 4-in. lumber. Next, the 2-in. thick stay-in-place steel forms shown in Figure 4.1, were screwed to the cold-rolled steel angle using self-tapping screws.

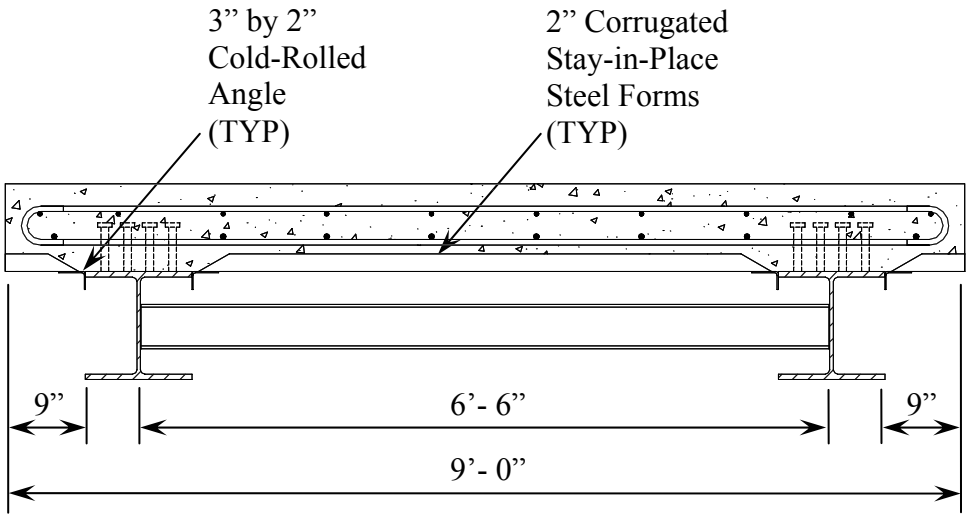

Figure 4.5: Cross Section of As-Built Model

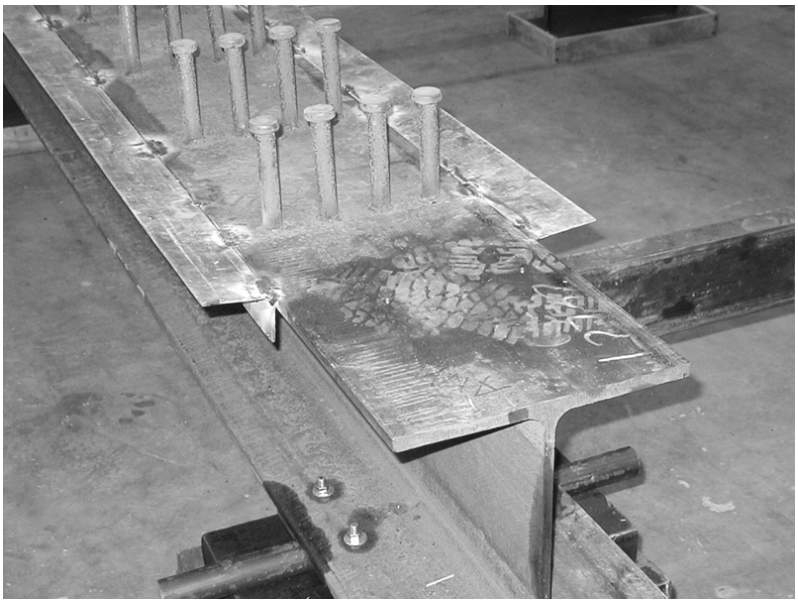

Figure 4.6: Cold-Rolled Angles Welded to Top Flange of Girder

The cantilevered sections of the stay-in-place steel forms were supported from the top of the bottom flange of the girders (Figure 4.7). Kickers were cut to fit into the joint formed between the web and flange of the girder and notched where the kickers intersected the steel forms. The kickers were made using 2-in. by 4-in. lumber. Holes were then drilled through the bottom channel of the steel forms where the kickers were placed. Next, the steel forms were screwed to the kickers through these holes.

The kickers also supported the ¾-in. plywood side form, which was placed and screwed to the vertical component of the notch in the kickers at the stay-in-place steel form location. The side forms were additionally reinforced with ¾-in. plywood screwed to the kickers. Figure 4.8 shows the completed formwork for the as-built model.

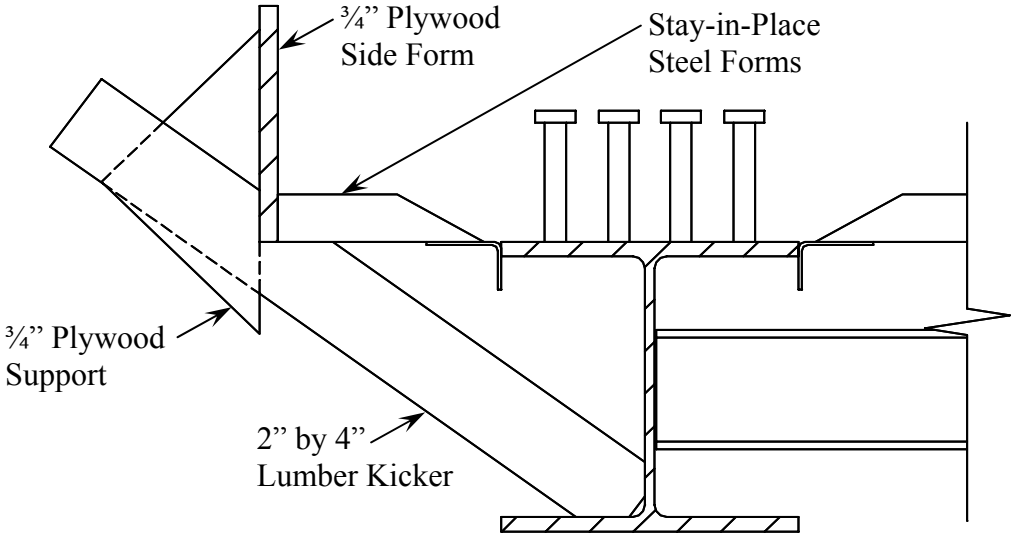

Figure 4.7: Kickers for Cantilevered Section of As-Built Model

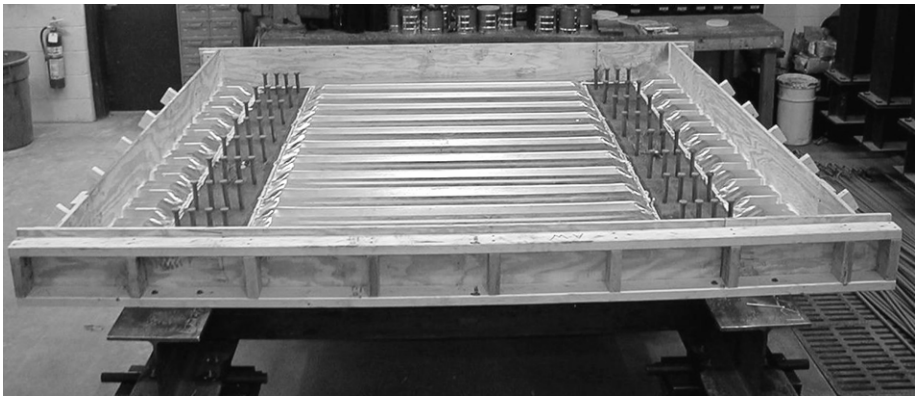

Figure 4.8: Completed Formwork for As-Built Model

4.3.4 Free-Shrinkage Model Formwork

The free-shrinkage model used plywood to form the bottom of the slab. As in the as-built model, the bottom formwork covered the area between the girders and the two 9-in. cantilevered sections on the outside of the girders. Figure 4.9 illustrates the cross-section of the free-shrinkage model.

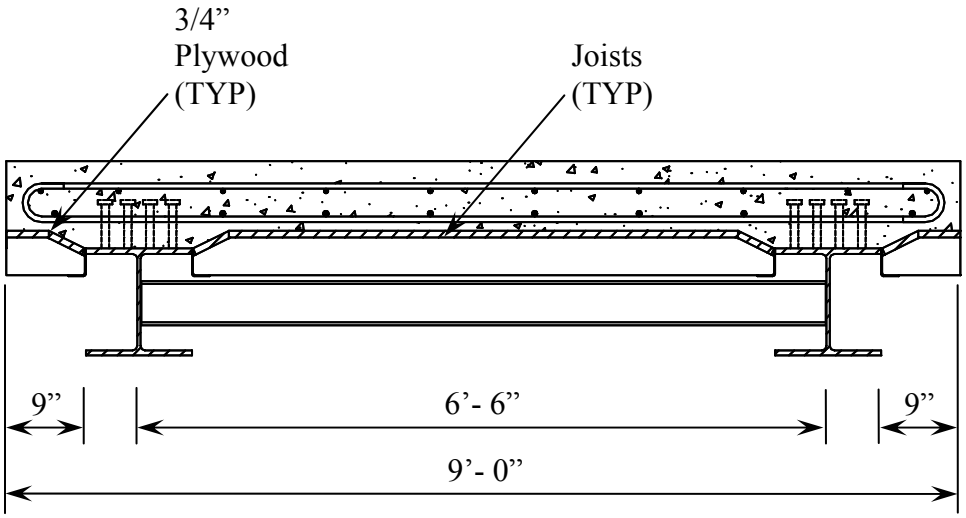

Figure 4.9: Cross Section of Free-Shrinkage Model

A similar moment of inertia for the two models was preferred for comparison of the two models. Therefore, the profile of the stay-in-place steel forms was duplicated with the plywood forms. Joists were placed between the girders and in the cantilevered sections to support the plywood forms.

To support the joists and plywood, short angle clips were welded to the girders as shown in Figure 4.10. The angle clips were cut from the 3-in. by 2-in. cold-rolled angle. Then, a hole was drilled in the 2-in. leg of the angle. The 3-in. leg of the clips was welded flush to the top of the girder every 12-in with the 2-in. leg turned away from the girder.

Once the clips were welded, end forms were bolted to the ends of the girders, 9-ft apart. These end forms were constructed with ¾-in. plywood and reinforced with 2-in. by 4-in. nominal material. Next, the joists were attached to the clips.

To obtain a profile similar to the stay-in-place steel forms, 2-in. by 6-in. lumber was ripped to 4 ¼-in. Then, an angle was cut on both ends of the joists running between the girders and on one end of joists in the cantilevered section. These joists were then screwed to the clips through the drilled holes. Figures 4.11 and 4.12 show the joists attached to the clips as well as the angles cut on the ends of the joists.

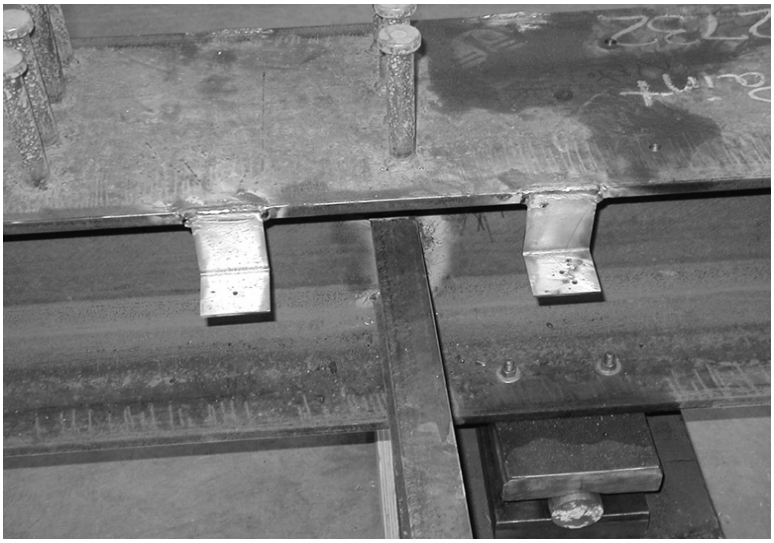

Figure 4.10: Clips Welded to Top Flange of Girder

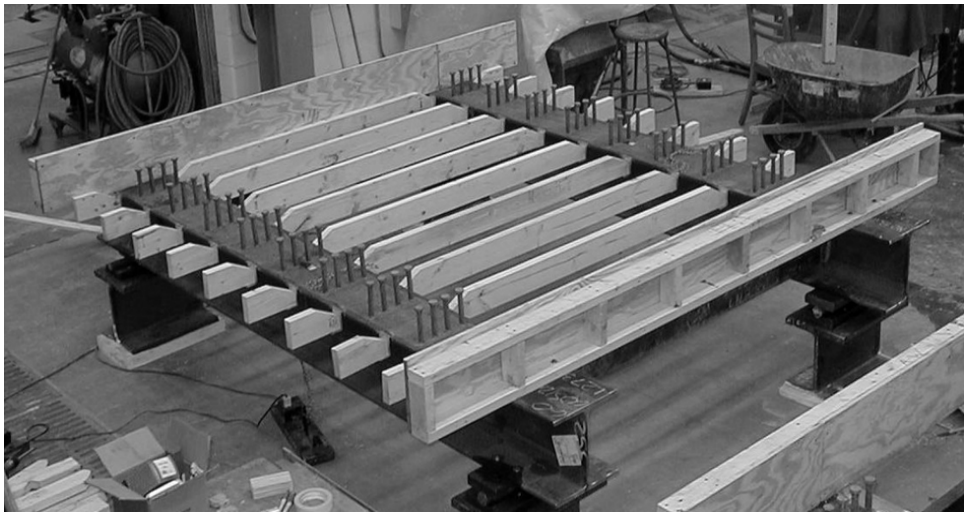

Figure 4.11: Joists Attached to Clips in Free-Shrinkage Model

Figure 4.12: Angle on Ends of Joists in Free-Shrinkage Model

The cantilevered sections were supported from the top of the bottom flange of the girders in the same manner as the as-built model. Kickers were cut to fit into the joint formed between the web and flange of the girder and notched were the kickers intersected the plywood forms (Figure 4.13). The kickers were made using 2-in. by 4-in. lumber. First, ¾-in. plywood was screwed to the top of the joist in the cantilevered section. Next, the kickers were placed on one side of the joists and screwed together.

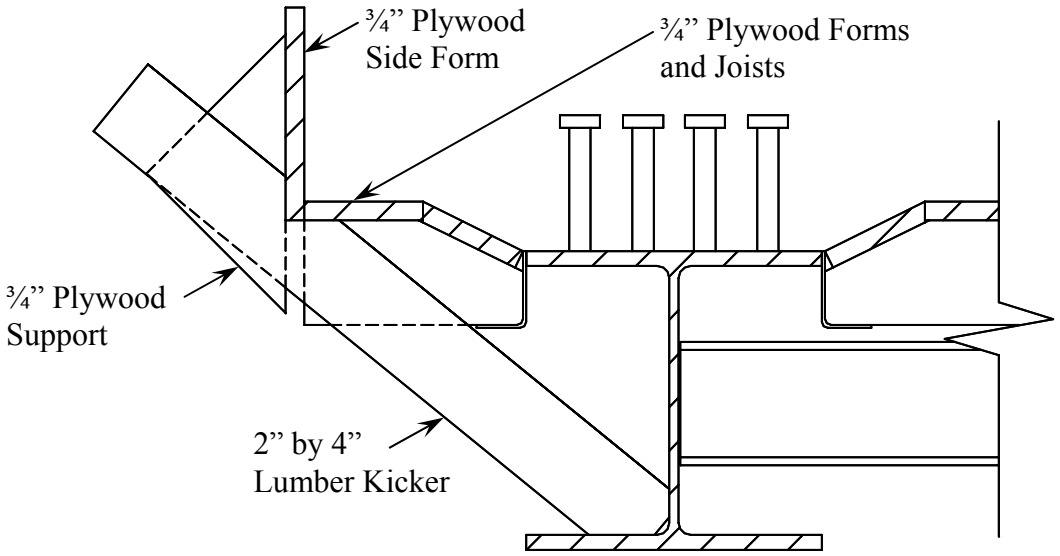

Figure 4.13: Kickers for Cantilevered Section of Free-Shrinkage Model

The kickers also supported the ¾-in. plywood side form, which was placed and screwed to the vertical component of the notch in the kickers at the plywood form location. The side forms were additionally reinforced with ¾-in. plywood screwed to the kickers. Figures 4.14 and 4.15 show the completed formwork for the free shrinkage-model.

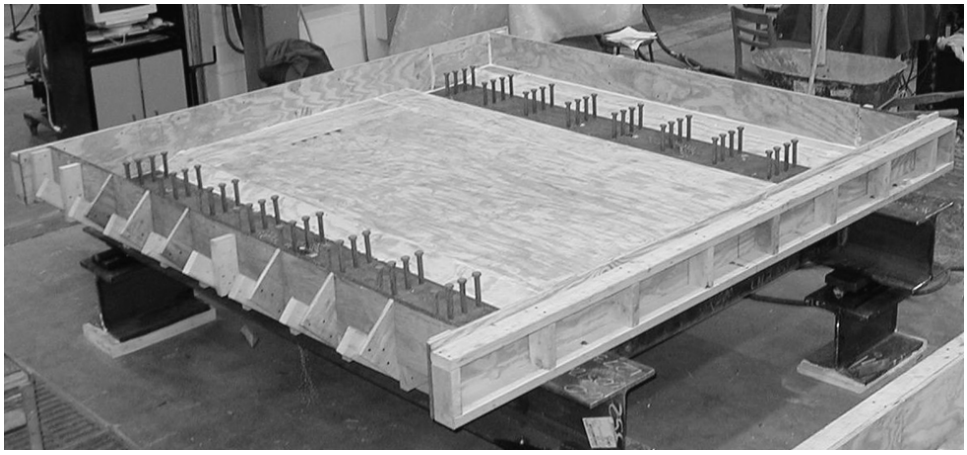

Figure 4.14: Completed Formwork for Free-Shrinkage Model

Figure 4.15: Fabricated Profile for Free-Shrinkage Model

Once the formwork was completed, Teflon sheets were placed on top of the plywood. The Teflon sheets permitted the concrete to shrink freely without restraint across with formwork. Figure 4.16 shows the Teflon sheets covering the plywood in the free-shrinkage model.

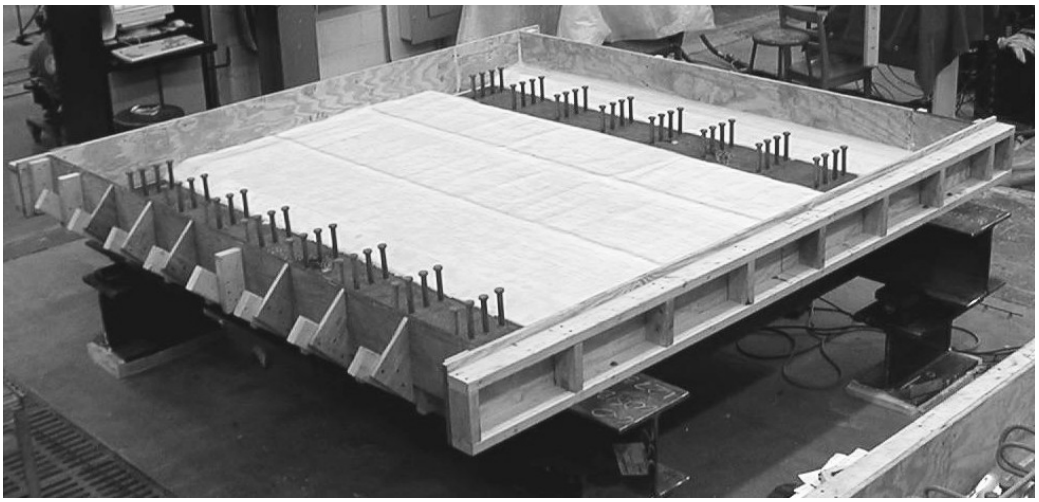

Figure 4.16: Teflon Sheeting on Plywood of Free-Shrinkage Model

4.3.5 Reinforcing Steel

Once the formwork was completed, the epoxy-coated reinforcing steel was placed. The same size, spacing, and clear cover were used in the models as in the positive moment region in the I65 over SR25 bridge. The bottom cover was 1-in. and the top cover was 2.5-in. Bottom and top transverse reinforcement and bottom longitudinal reinforcement were #5 bars. Top longitudinal reinforcement was #4 bars. Figure 4.17

illustrates the layout for the bottom layer of reinforcing steel while Figure 4.18 illustrates the layout for the top layer of reinforcing steel.

To provide a shorter development length, 180° standard hooks were used at the ends of the reinforcing steel. The reinforcing steel bars were 105-in. out-to-out. Figure 4.19 shows the epoxy-coated reinforcement as placed in the as-built model.

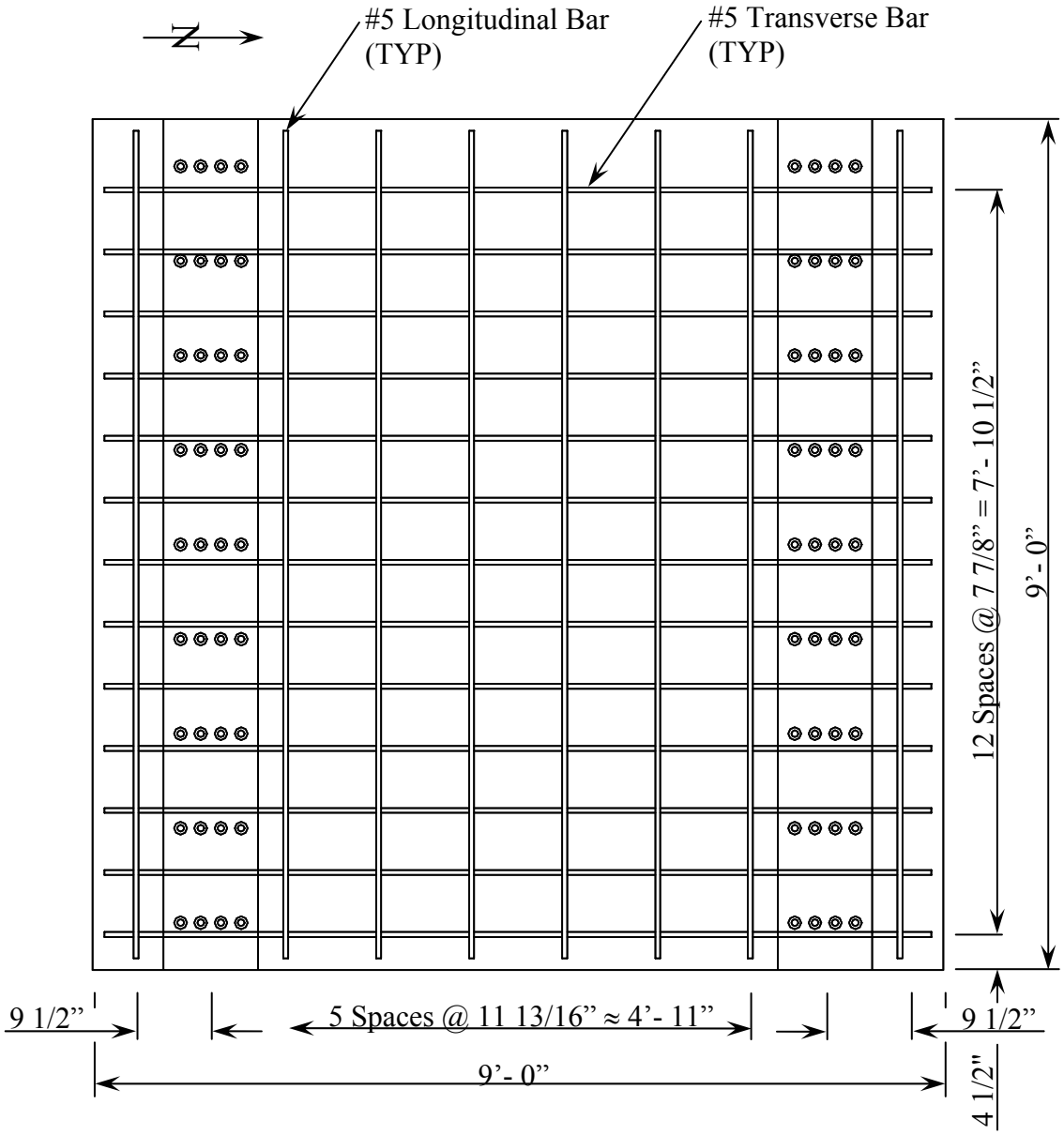

Notes:

#5 Epoxy-Coated Transverse Bars w/ 180° Standard Hooks on Each End

#5 Epoxy-Coated Longitudinal Bars w/ 180° Standard Hooks on Each End

Figure 4.17: Layout of Bottom Mat of Reinforcing Steel

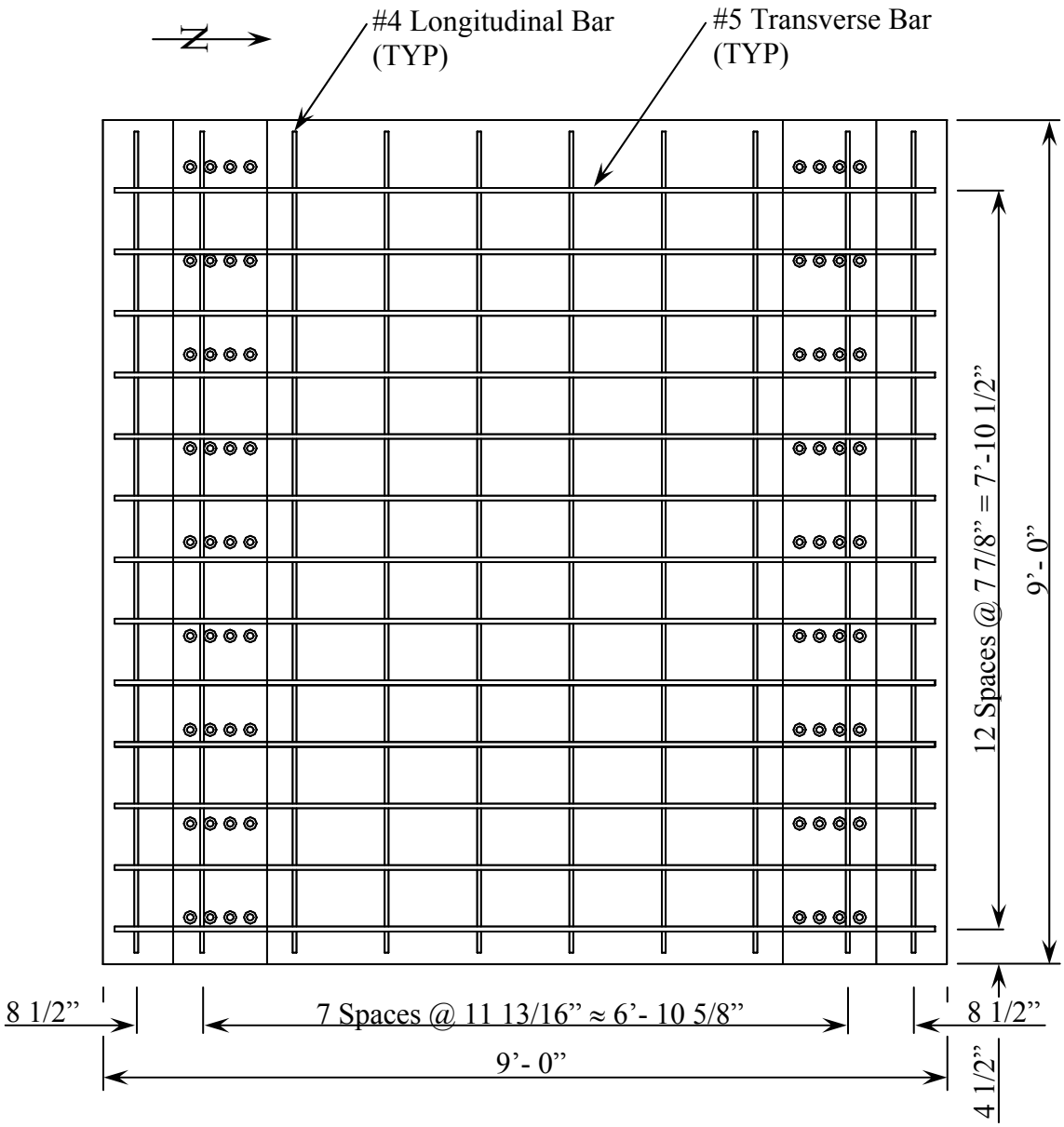

Notes:

#5 Epoxy-Coated Transverse Bars w/ 180° Standard Hooks on Each End

#4 Epoxy-Coated Longitudinal Bars w/ 180° Standard Hooks on Each End

Figure 4.18: Layout of Top Mat of Reinforcing Steel

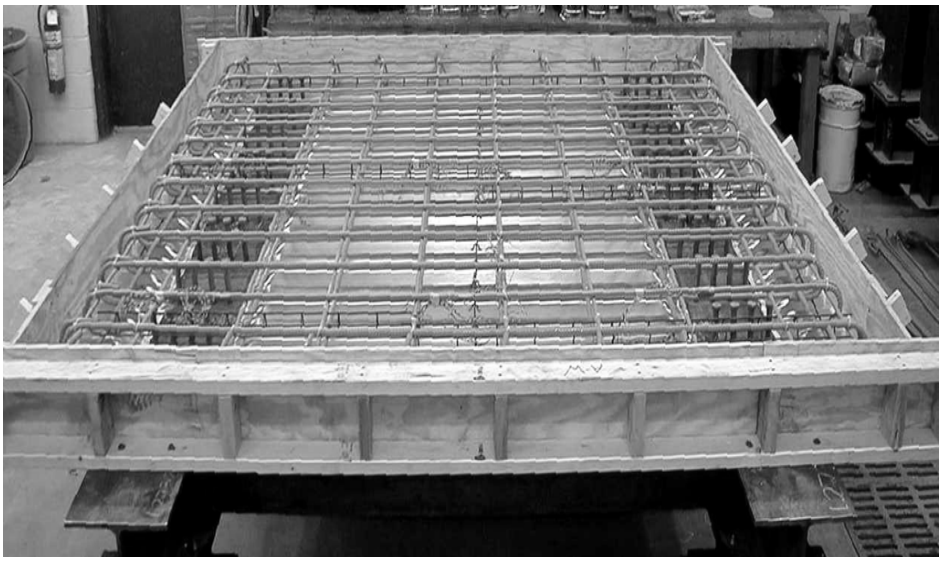

Figure 4.19: As-Built Model with Reinforcement

4.3.6 Deck Casting

The deck thickness and concrete mix were the same as the I65 over SR25 bridge. The deck was 7 7/8-in. thick and utilized an INDOT Class C mix. The mix design and specifications are provided in Section 4.4.1. The casting of the models began at 9:20 AM and were finished at 10:15 AM on Monday, February 26, 2001. The concrete in the models was vibrated and hand screeded. The surfaces of the models were finished using a magnesium bull float. Figure 4.20 shows the bull floating of the free-shrinkage model and the concrete vibrating of the as-built model.

Figure 4.20: Bull Floating the Free-Shrinkage Model and Vibrating the Concrete in the As-Built Model

Immediately after the initial concrete set, wet burlap and plastic were placed on the 2 specimens at 1:00 PM. The burlap was rewetted the following three days. The burlap was removed on March 2, 2001 at 8:15 AM, the 4th day after casting to conform to the minimum requirements of the *INDOT Standard Specifications* (INDOT 1999).

4.4 Materials

4.4.1 Concrete

The same concrete mix design and supplier were used for the laboratory models as for the I65 over SR25 bridge. An INDOT Class C concrete mix with design compressive strength of 4000 psi and a maximum aggregate size of ¾-in. concrete was obtained from Irving Materials, Inc. The mix design and specifications for this concrete are provided in Table 3.1.

Standard 6-in. by 12-in. cylinder samples were obtained at the time the models were cast. The cylinders were wet cured in the lab for the same duration as the deck. The specimens were tested at 3, 7, 14, and 21 days with 3 specimens tested on each day. The compressive cylinders were loaded at 60,000 lb per minute using a 600 kip testing machine. Figure 4.21 shows the strength gain curve for the concrete, which was obtained from the average of the 3 cylinders. As shown, the average 21-day compressive strength was 5700 psi.

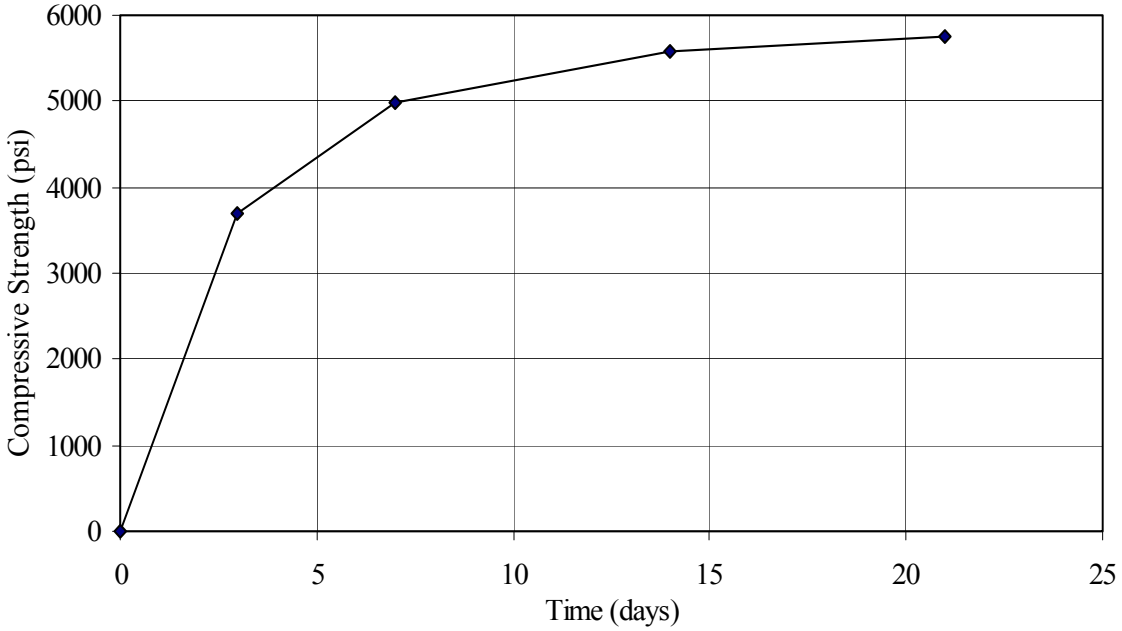

Figure 4.21: Strength Gain Curve for Concrete Compressive Cylinders

In addition to compressive cylinders, split cylinder tests were performed on the 6-in. by 12-in. cylinder samples. The split cylinders were loaded at 17,000 lb per minute using the same 600 kip testing machine. Figure 4.22 shows the split cylinder tensile strength gain curve for the concrete, which was obtained from the average of the 3 cylinders. As shown, the average 21-day tensile strength was 530 psi.

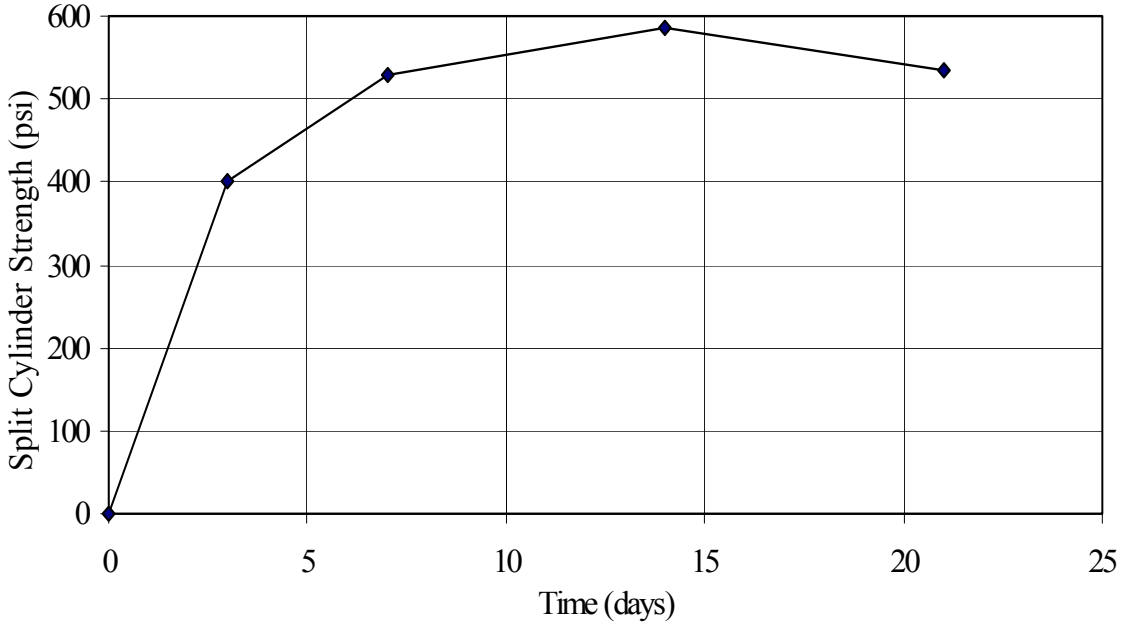

Figure 4.22: Strength Gain Curve for Split Cylinder Tests

4.4.2 Reinforcing Steel

The deck reinforcement comprised 2 bar sizes: #4 and #5. All reinforcing steel conformed to ASTM A615 Grade 60 and was epoxy-coated.

4.4.3 Girder Steel

The steel girders (W12x65) conformed to ASTM A572 Grade 50.

4.5 Instrumentation

4.5.1 Instrumentation Design

The instrumentation layout was designed to investigate transverse cracking induced by thermal gradients through the depth of the models, the shrinkage of the deck, and the restraint of this shrinkage. Strain gages, thermocouples, and LVDT's were placed along the width and length of the models. The gage layout was identical in both models with the exception of 4 additional strain gages placed on the stay-in-place steel forms on the as-built model.

4.5.1.1 Strain Gages

Strain gages were placed on the 2 girders and on the longitudinal reinforcing bars parallel to the girders to establish the strain gradient through the depth of the models. Figure 4.23 shows the location of the strain gages located on the girders, Figure 4.24 illustrates the location of the strain gages in the bottom layer of reinforcement, and Figure 4.25 illustrates the location of the strain gages in the top layer of reinforcement.

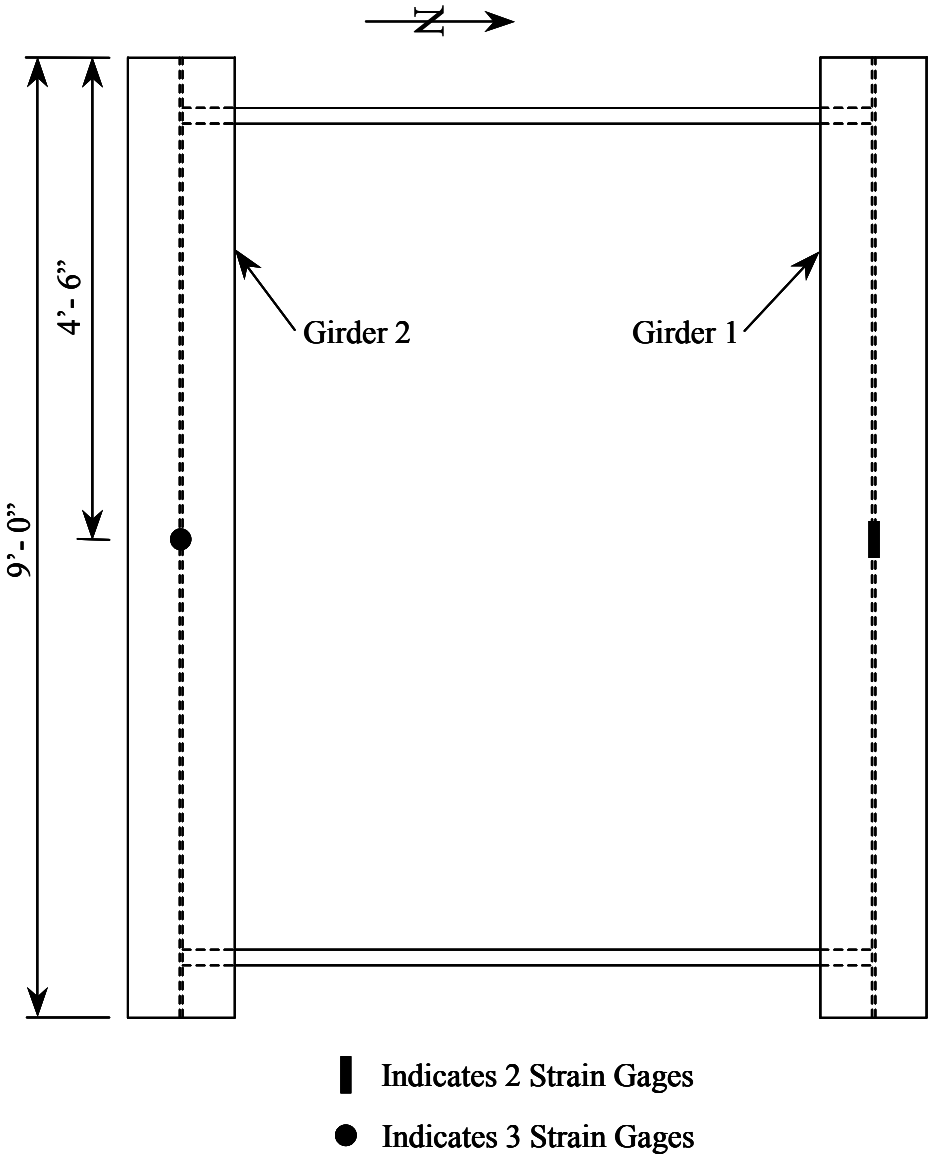

Figure 4.23: Girder Strain Gage Locations

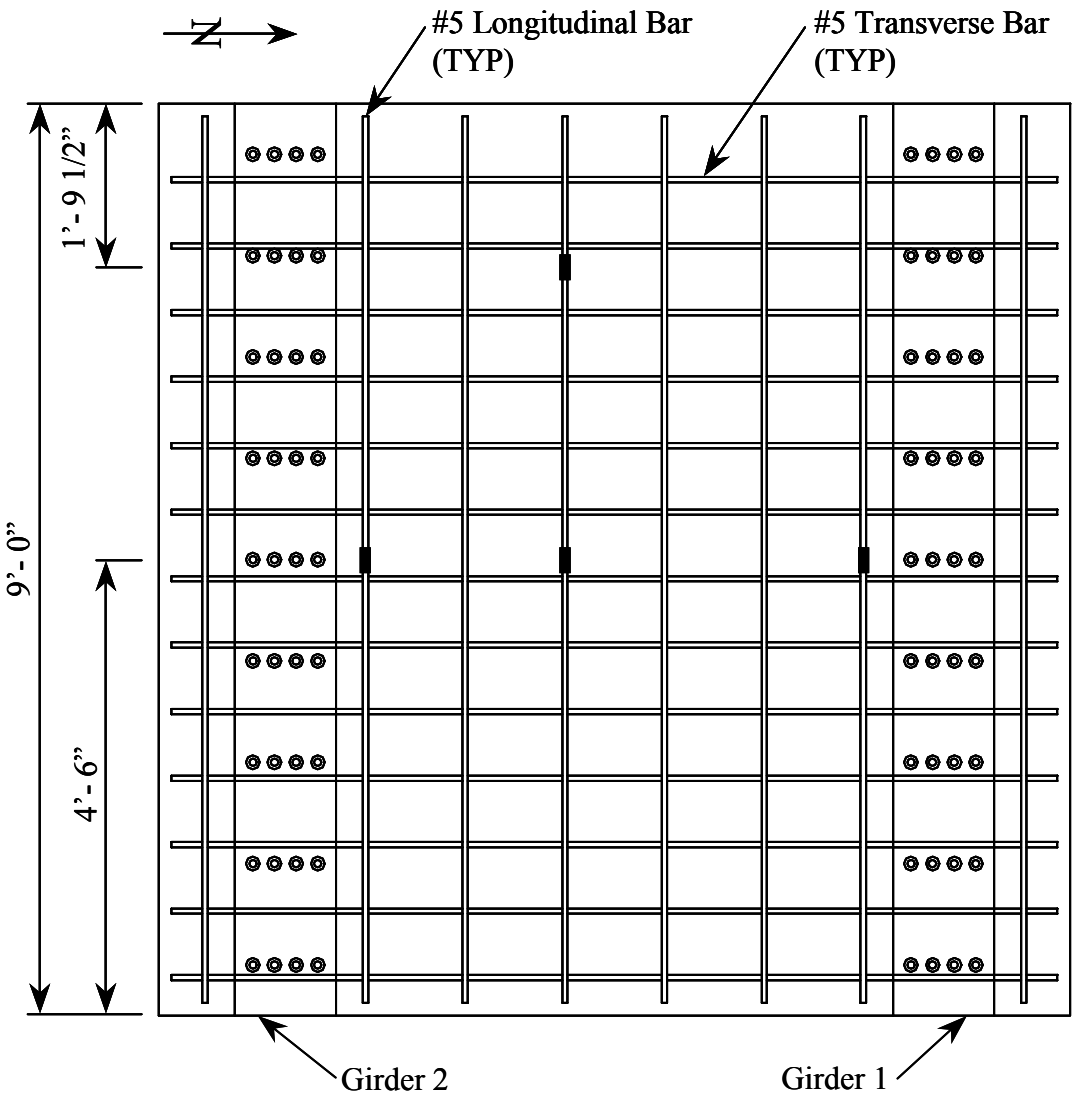

Figure 4.24: Strain Gages in Bottom Reinforcing Mat

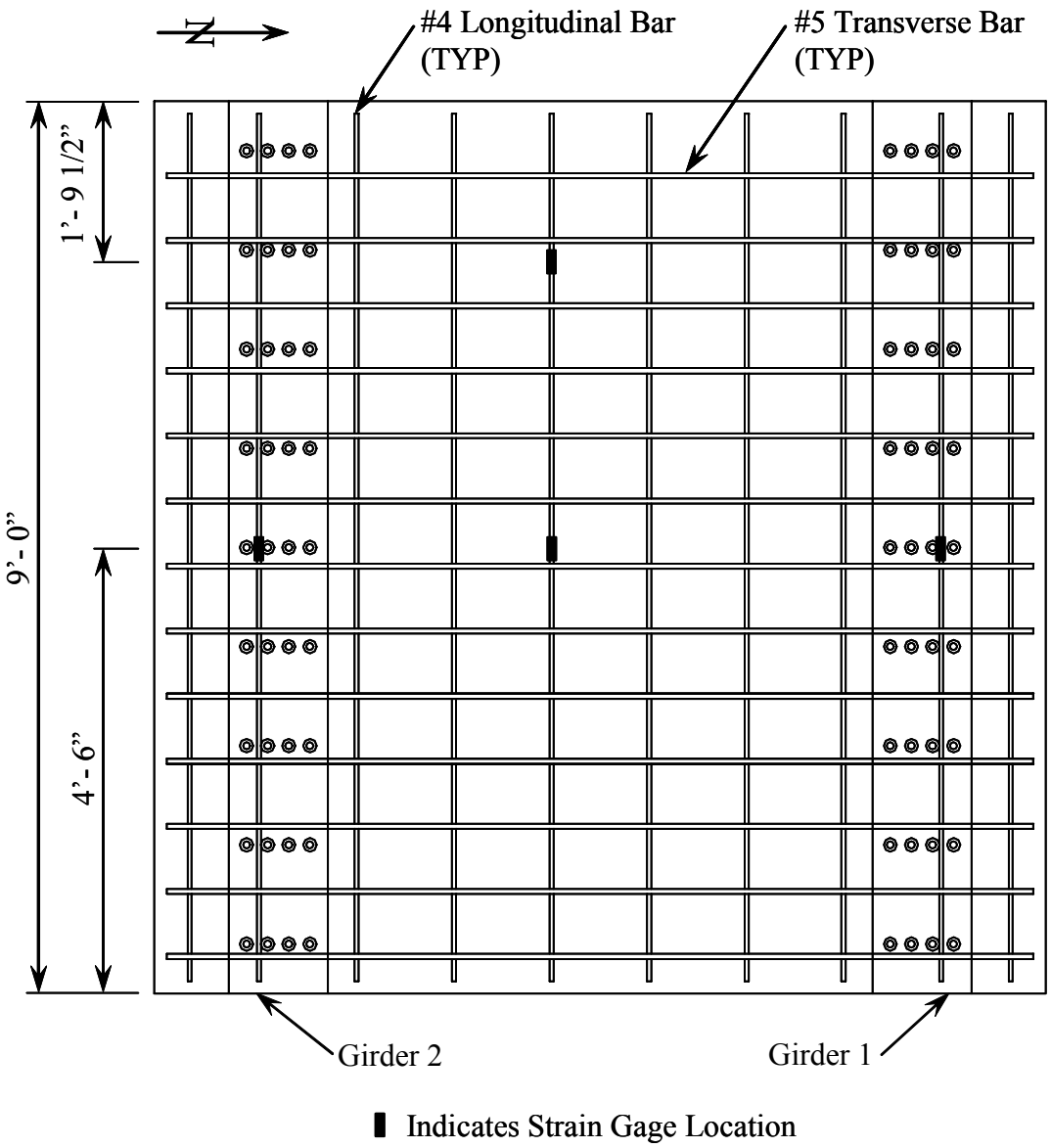

Figure 4.25: Strain Gages in Top Reinforcing Mat

Strain gages on Girder 1 were located on the top of the top flange and on the bottom of the bottom flange (Figure 4.26). On Girder 2 in addition to the top and bottom flange gages, a strain gage was installed at the middle of the web (Figure 4.27). The strain gages on longitudinal reinforcing bars were placed at the midspan near Girders 1 and 2. In addition, gages were installed near the center of the slab at midspan and at 1-ft 9 ½-in. from the west end of the models (Figures 4.24 and 4.25). All strain gages were oriented to measure strain along the longitudinal direction of the reinforcing bars and girders.

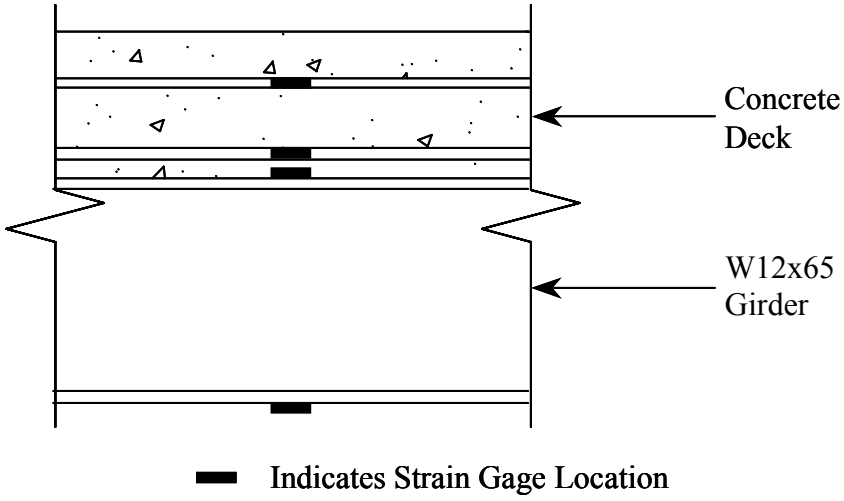

Figure 4.26: Elevation View of Strain Gages at Girder 1

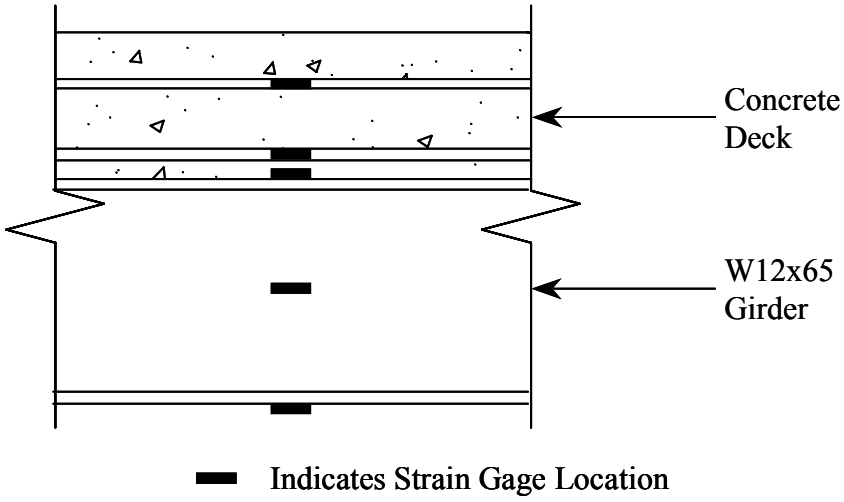

Figure 4.27: Elevation View of Strain Gages at Girder 2

Strain gages were also placed on the stay-in-place steel forms at the center of the deck on the as-built model to investigate restraint caused by the corrugations. As shown in Figure 4.28, 2 strain gages were placed on the top channel and 2 gages were placed on the bottom channel. On each of the 2 channels, one strain gage was installed transverse to the girders while one was installed longitudinal to the girders.

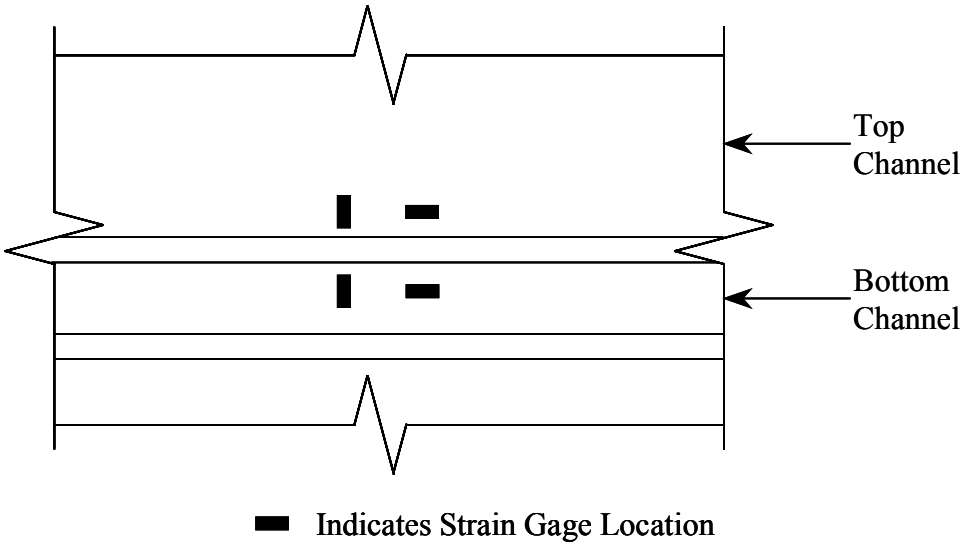

Figure 4.28: Strain Gages on Stay-in-Place Steel Forms

4.5.1.2 Thermocouples

Thermocouples were placed in the concrete deck and on the steel girders. Figure 4.29 shows a plan view of the layout of the thermocouples. At the location shown, 4 thermocouples were installed through the section depth to obtain the thermal gradient. As illustrated in Figure 4.30, 2 thermocouples were placed in the deck and 2 thermocouples were placed on the girder. Thermocouples in the deck were positioned at the same level as the top and bottom mats of reinforcing steel. The thermocouples on the girders were located at the top of the top flange and the bottom of the bottom flange. In addition to direct temperature readings of the models, an ambient reading was recorded at the midspan of Girder 2 on the as-built model. The ambient thermocouple was secured to the bottom flange of the girder restricting the end of the wire, where the temperature is read, from touching any portion of the structure.

4.5.1.3 LVDT's

A variety of 1-in. and 2-in. LVDT's were used to measure the deflections of the deck models. The LVDT's were calibrated using an Instron Extensiometer High Magnitude Calibrator that was graduated to ten-thousandths (0.0001) of an inch. The calibration values were required to convert voltage outputs to deflections using the data acquisition system.

Figure 4.31 illustrates the layout of the LVDT's. LVDT's were placed at the midspan of the girders and at the center of the slab. The LVDT's located at the supports were used to detect support settlement.

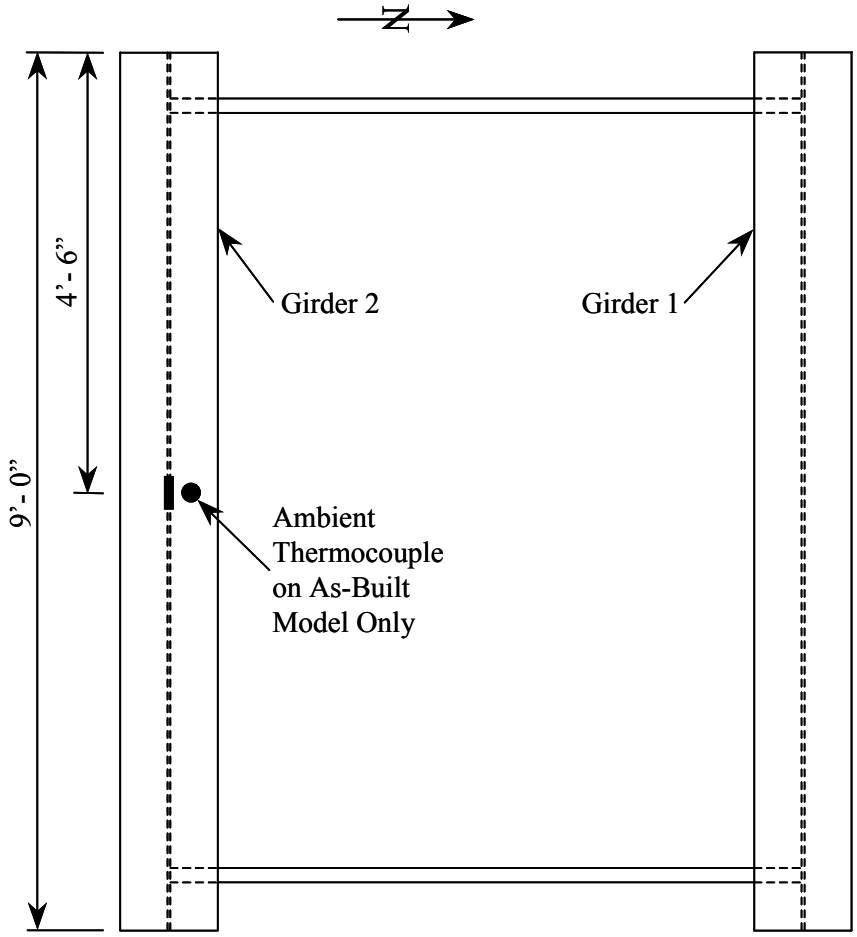

Figure 4.29: Thermocouple Layout

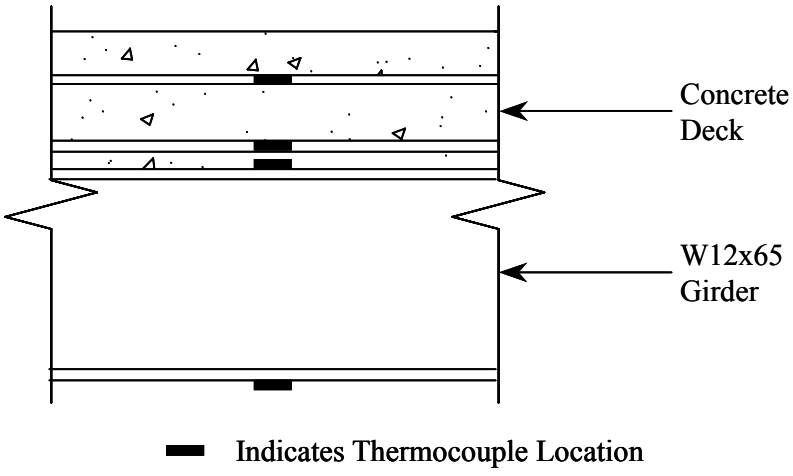

Figure 4.30: Elevation of Thermocouples

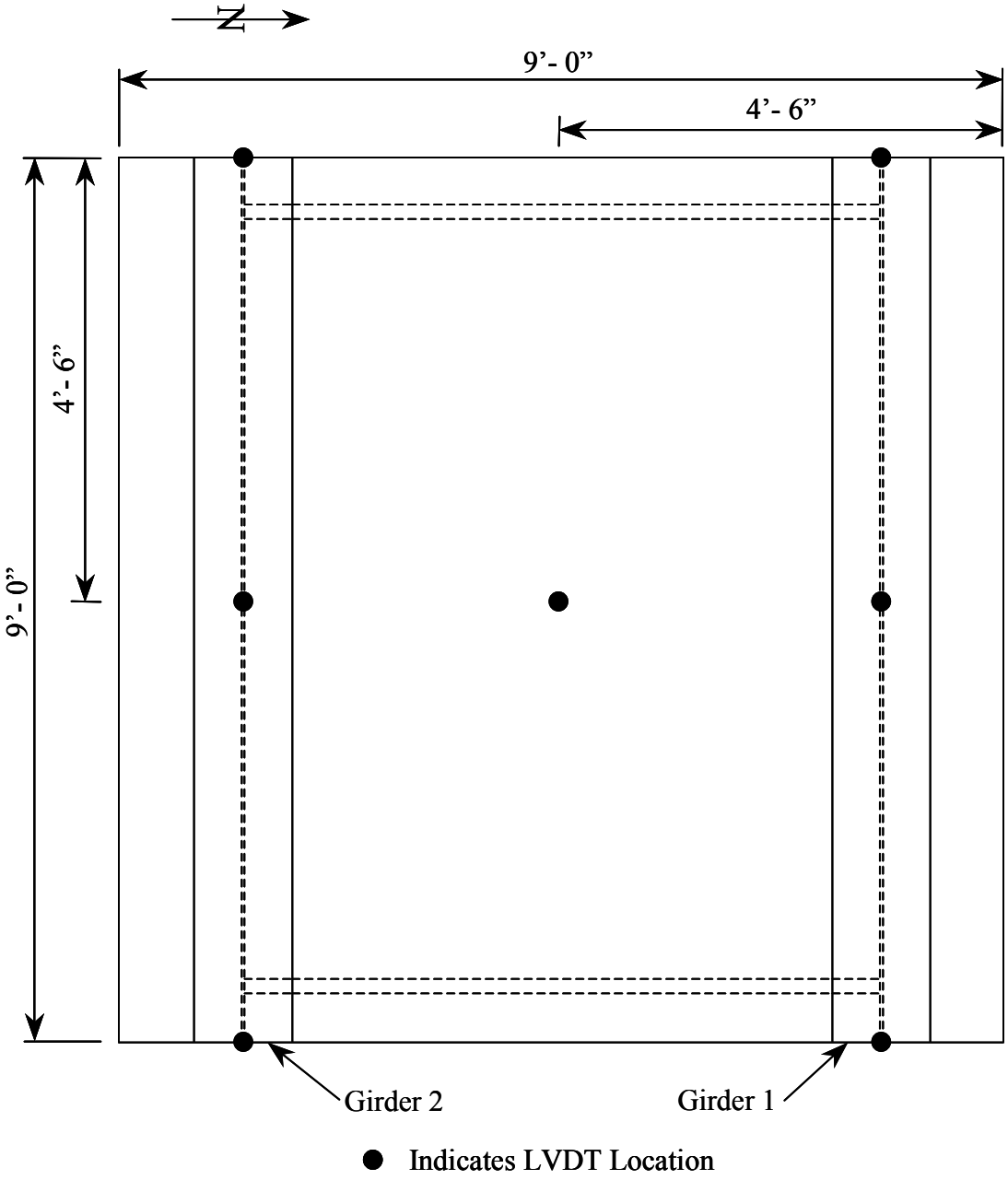

Figure 4.31: LVDT Layout

4.5.1.4 Instrument Identification

An identification system for gages is presented below. This system assigns each gage a unique instrument identification as follows:

(Model)-(Gage Type)-(North/South)-(East/West)-(Depth)-(Orientation)

Model:	As-Built (**A**)
	Free-Shrinkage (**F**)
Gage Type:	Strain Gage (**S**)
	Thermocouple (**T**)
	LVDT (**L**)
North/South Location:	See Figure 4.33
East/West Location:	See Figure 4.33
Depth through Section:	See Figure 4.32
Orientation:	Transverse to Girder (**T**)
	Longitudinal with Girder (**L**)

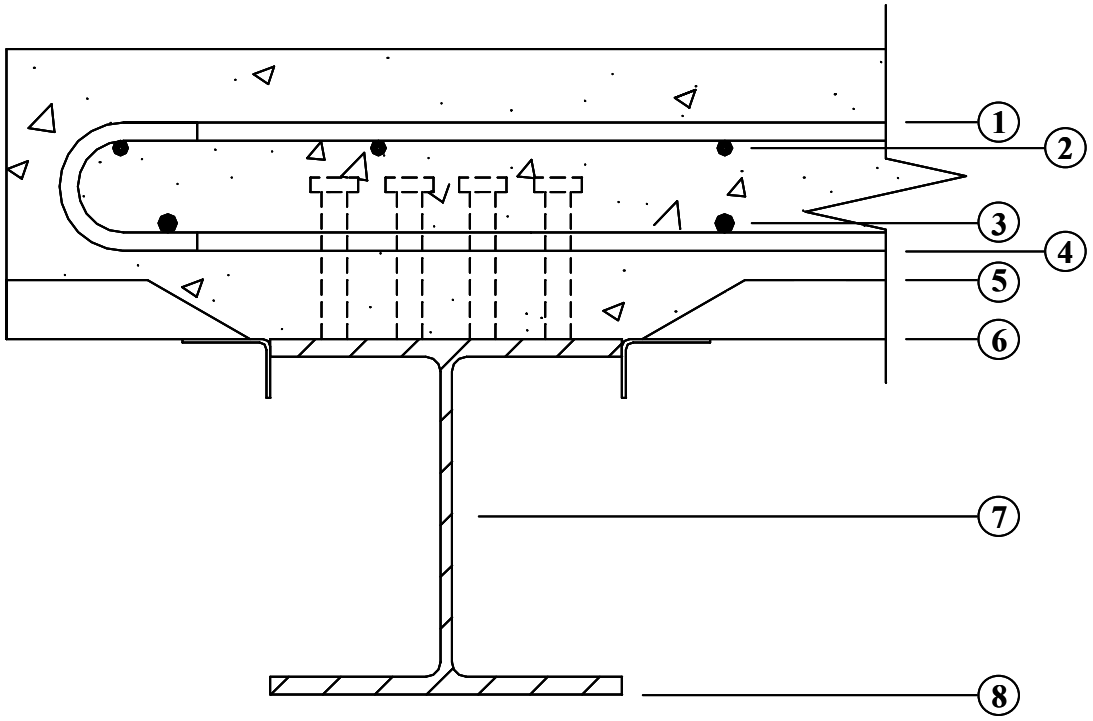

Figure 4.32: Depth through Section Identification

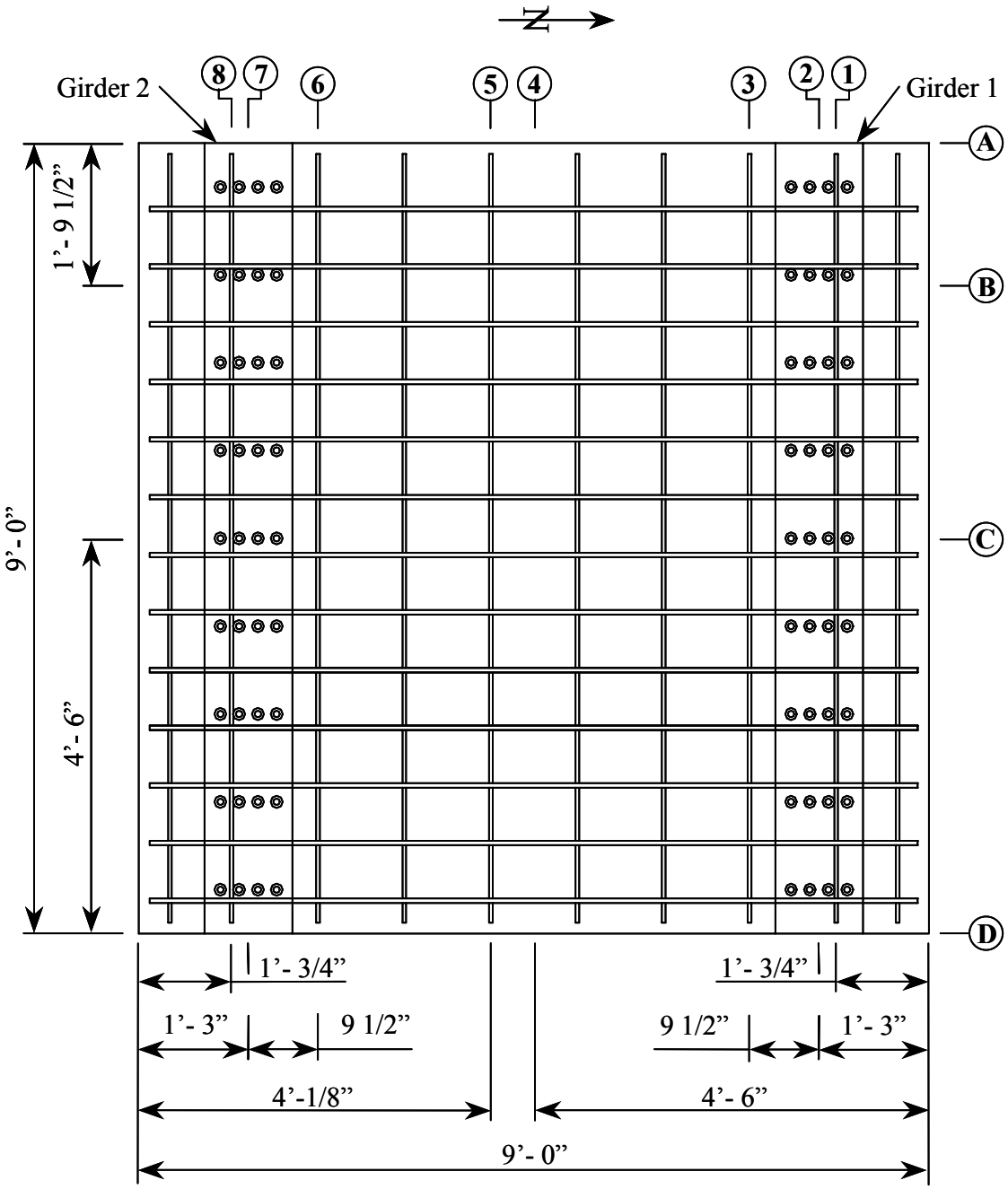

Figure 4.33: North/South and East/West Identification

4.5.2 Instrumentation Installation

The installation procedure for all gages is presented below. Complete specifications for the strain gages and thermocouples are available in Appendix C.

4.5.2.1 Strain Gages

The strain gages cast in the deck were installed directly on the steel reinforcing bars prior to the installation of the reinforcement. The installation and protection of the strain gages on the reinforcing steel followed the same procedure as outlined in Section 3.4.2.1 with one exception. For the laboratory models, the FN-2 neoprene rubber was not used because more caution was exercised to protect the gages when casting these models as opposed to the field casting.

To provide protection for the leadwires, the wires were pulled through holes drilled through the bottom forms. On the as-built model, rubber grommets were placed around the hole. Then, each leadwire to be cast in the deck was placed inside ¼-in. plastic tubes. The tubing was installed to prevent loss of reinforcement strain data by fracture of the wires after the deck cracked. Figure 4.34 illustrates the longitudinal strain gages and the tubing used to protect the leadwires over Girder 2 in the free-shrinkage model.

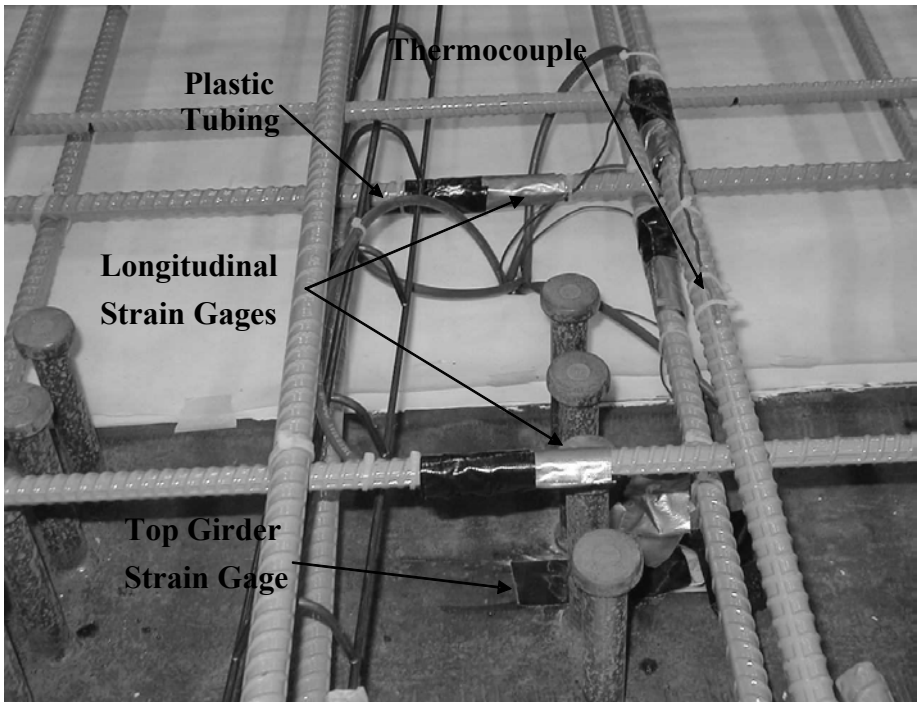

Figure 4.34: Instrumentation Locations

The strain gages installed on the steel girders were installed and protected using the same procedure outlined in Section 3.4.2.1 with the same exception as noted for the longitudinal strain gages. Figures 4.34 and 4.35 show the strain gage installed on the top of the girder flange between the center shear studs.

The strain gages installed on the stay-in-place steel forms were also installed and protected using the same procedure outlined in Section 3.4.2.1 for the steel girders with the same exception as noted for the longitudinal strain gages. These steel form gages were installed on the bottom side of the stay-in-place steel forms prior to being screwed to the cold-rolled angle. Figure 4.36 illustrates the 4 strain gages installed on the steel form.

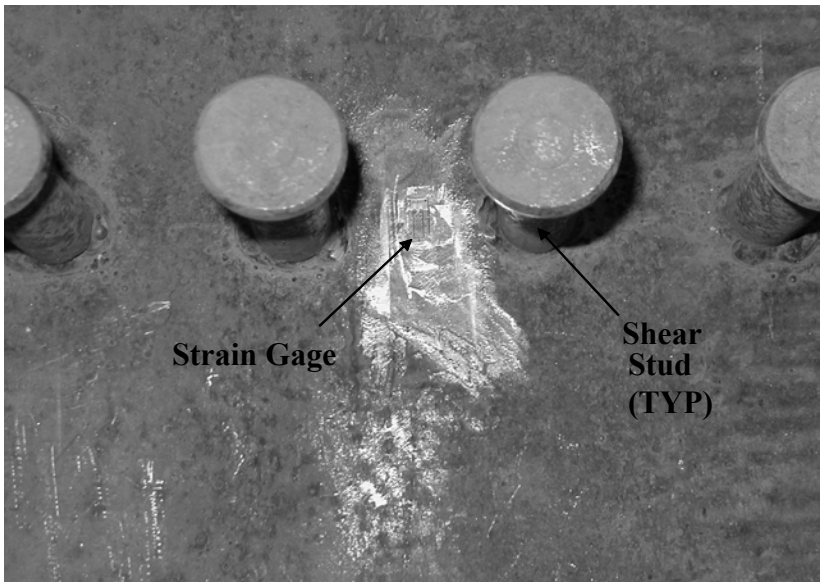

Figure 4.35: Strain Gage on Top of Girder (F-S-7-C-6)

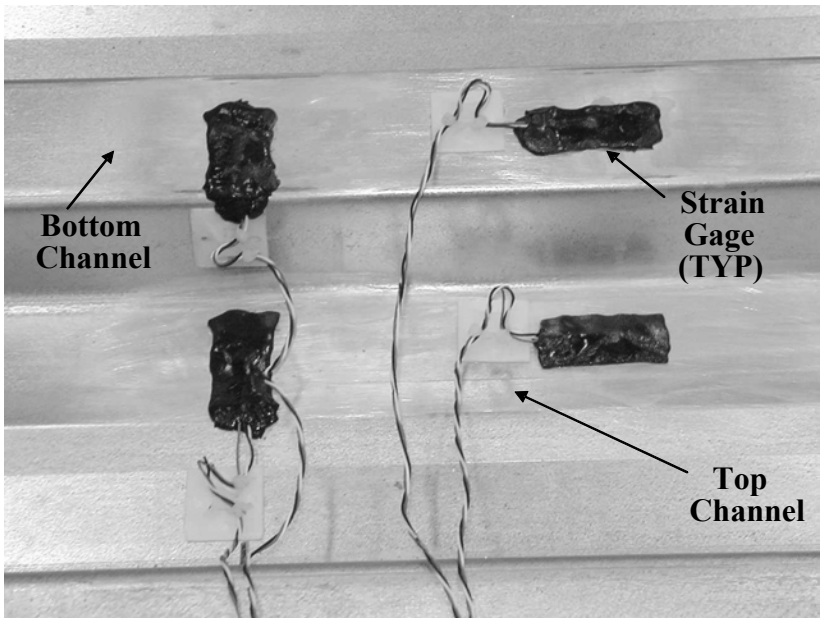

Figure 4.36: Stay-in-Place Steel Form Strain Gages

4.5.2.2 Thermocouples

The thermocouples on the deck models were installed and protected using the same procedure outlined in Section 3.4.2.2. Figures 4.34 and 4.37 show the thermocouples installed in the deck of the free-shrinkage model.

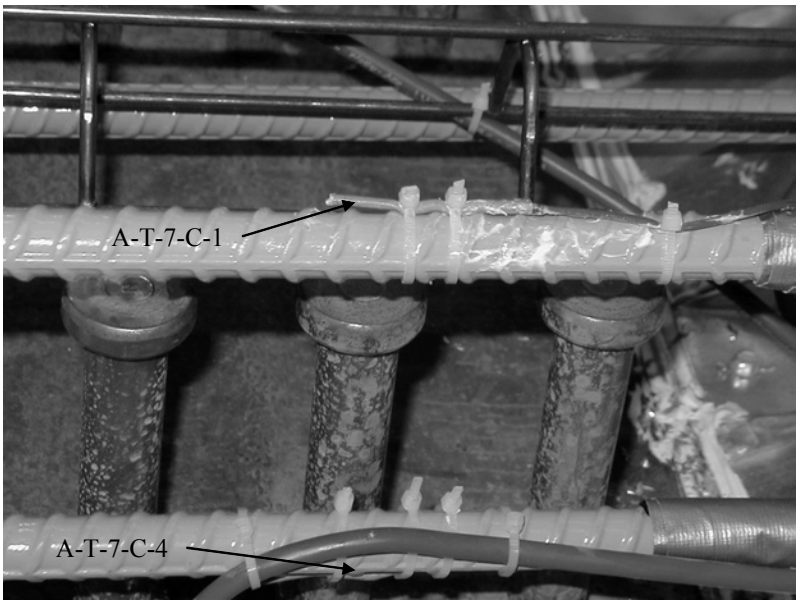

Figure 4.37: Thermocouples in Deck

4.5.2.3 LVDT's

To record deflections with LVDT's, threaded rods were connected to the cores of the LVDT's and then attached to the models. For the LVDT's located at midspan of the girders, a small aluminum angle was epoxied to the bottom flange of the girder. A small hole was drilled in the end of the angle and the threaded rod was positioned through this hole and fixed in place with nuts. The LVDT's were held in place with LVDT stands and the bases of the stands were hydrostoned to the floor. Figure 4.38 shows the LVDT at the midspan of Girder 1 of the free-shrinkage model.

The LVDT's located over the supports were attached in a similar manner as those at the midspan. Small pieces of the cold-rolled angle were cut and small holes were drilled near the end. The angles were epoxied to the web of the girder over the supports. The threaded rods were positioned through this hole and fixed in place with nuts. The LVDT's were held in place with stands and hydrostoned to the floor. Figure 4.39 shows the LVDT over the support at the west end of Girder 1 of the free-shrinkage model.

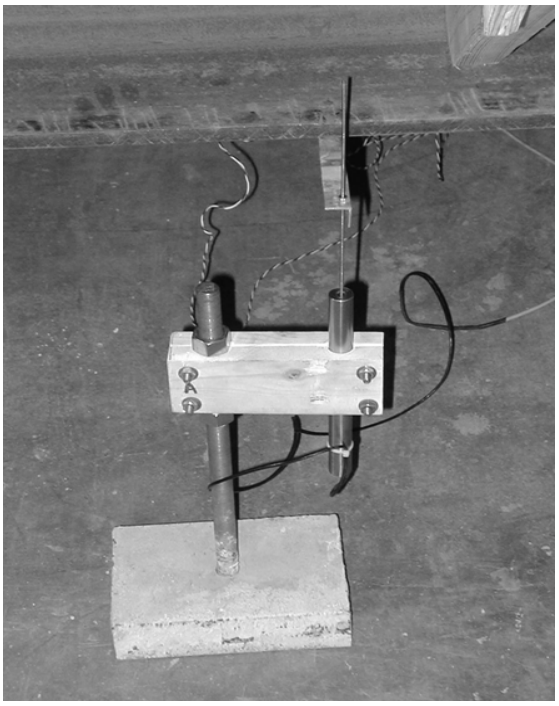

Figure 4.38: LVDT at Midspan (F-L-2-C)

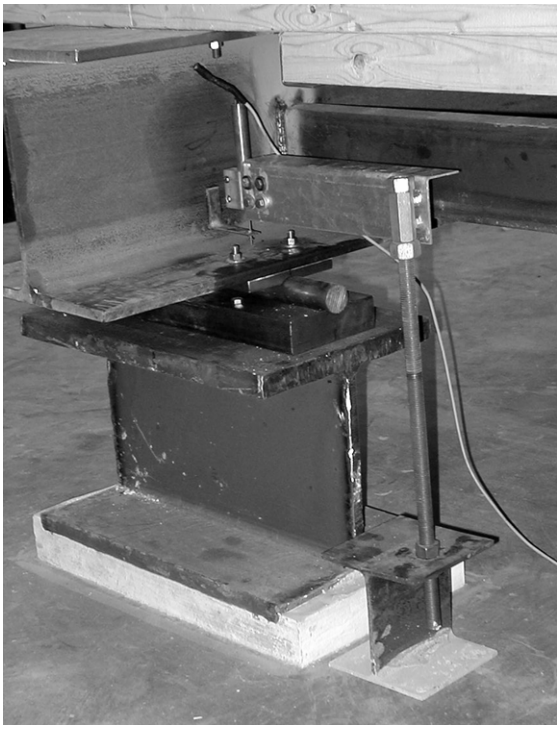

Figure 4.39: LVDT over Support (F-L-2-A)

The LVDT's placed in the center of the slabs required plates to be cast into the concrete to record the deflections of the bottom of the deck instead of the formwork in the event that the deck and formwork separated. First, small holes were drilled in the center of the forms. Then, 2 ½-in. by 2 ½-in thin steel plates, with 4 small screws for additional bonding, were centered over each hole. The edges of the plates were taped to the formwork to prevent concrete from getting under the plates. The threaded rods were then epoxied to the bottom side of the plates through the holes. The LVDT's were held in place with stands and hydrostoned to the floor. Figure 4.40 shows the steel plate installed on top of the stay-in-place forms in the as-built model.

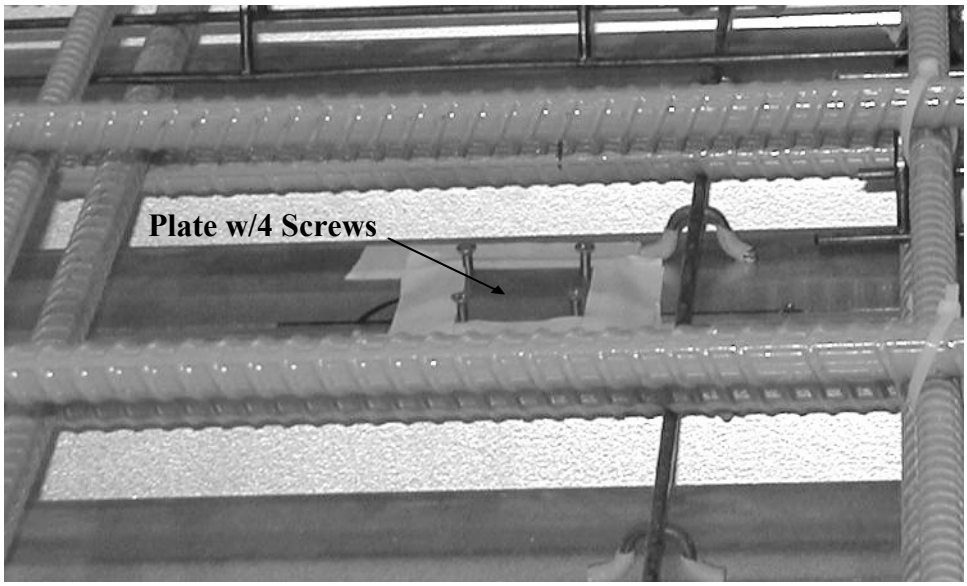

Figure 4.40: Steel Bonding Plate in As-Built Model

4.5.3 Data Collection

To monitor the strain gages, thermocouples, and LVDT's, a data acquisition system was required. A Measurements Group System 5000 data acquisition system in conjunction with a desktop computer was used. The program for the data acquisition system was programmed to record readings every 15 minutes. The system was activated 3 days prior to casting the models to check for gage drift or any other gage errors. When the system was first activated, initial zero readings were recorded for all strain gages and LVDT's. Thermocouples record the actual temperature; therefore, zero readings were not required. The data acquisition system was stopped daily to download the data and restart the computer.

4.6 Results

A summary of the data acquired during the course of testing is presented. In the plots of strain gages, positive values correspond with tensile strains. In the graphs of the LVDT's, negative values indicate a downward movement. Figure 4.41 illustrates the sequence of events between casting the models and removing the wet burlap.

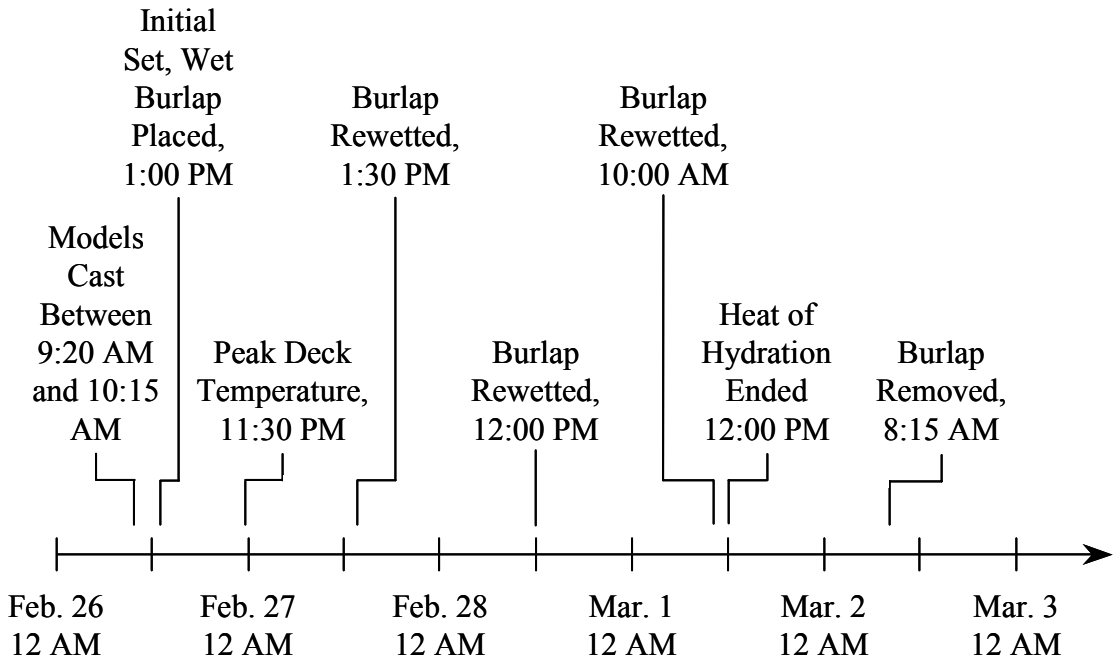

Figure 4.41: Time Line between Casting and Burlap Removal

4.6.1 Thermocouples

The ambient air temperature of the lab and both models were monitored to investigate temperature differences throughout the cross sections of the models. Figure 4.42 presents the ambient lab temperature, while Figure 4.43 illustrates the temperature at the top of the deck in the as-built model. In Figure 4.42, the 3 sudden decreases in temperature were due to the temporary opening of the overhead door permitting the lab to cool. As shown in Figures 4.42 and 4.43 after the heat of hydration period, the deck models were generally a few degrees warmer than the ambient lab temperature.

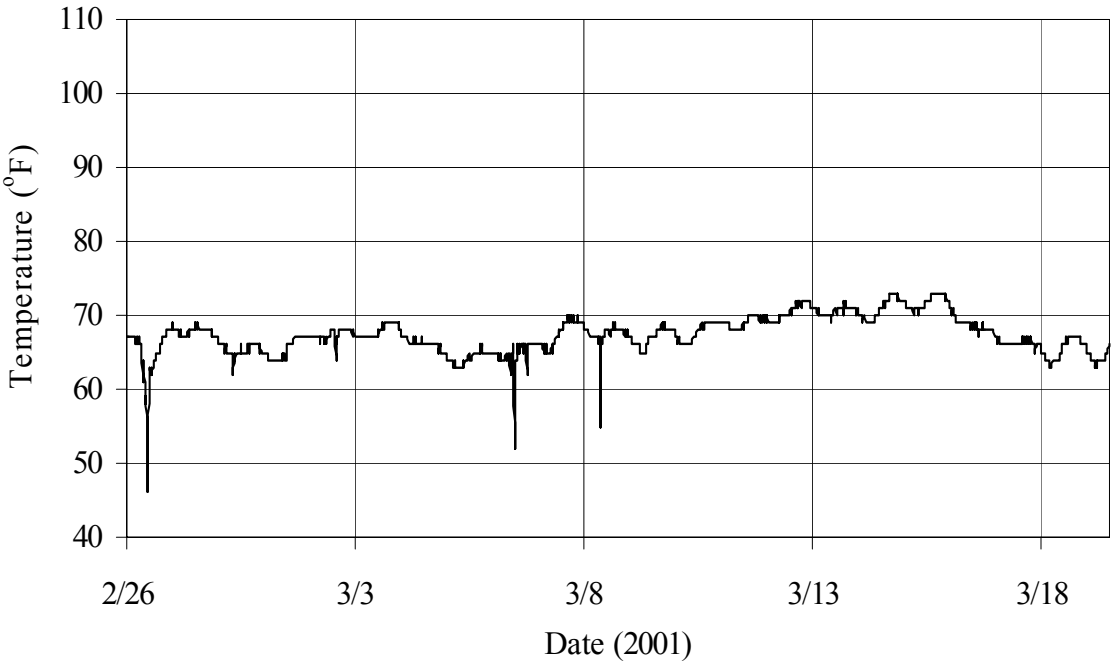

Figure 4.42: Ambient Air Temperature

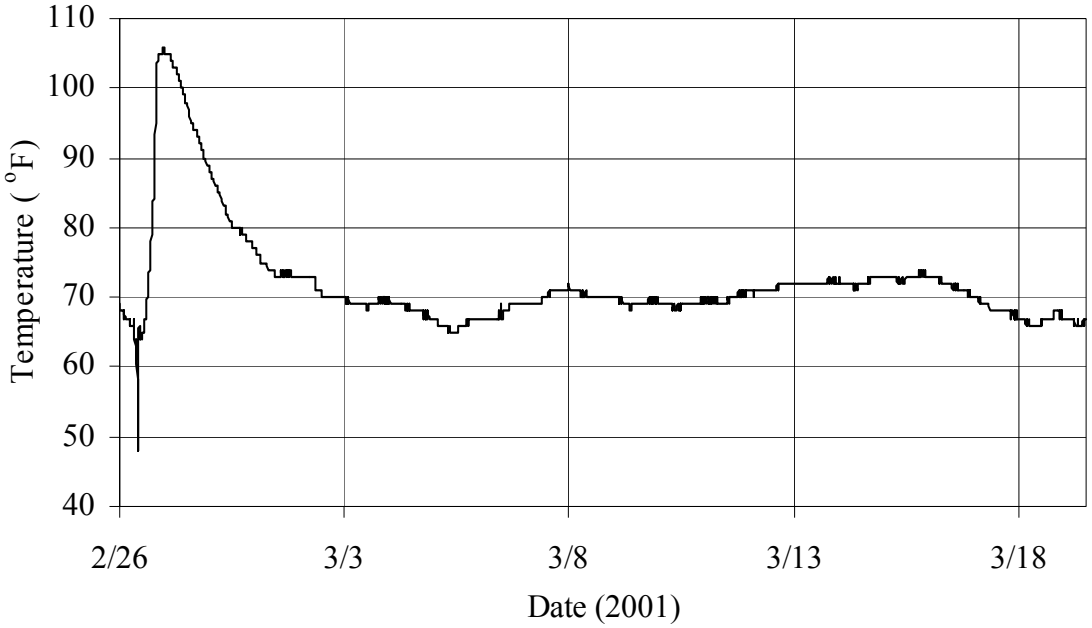

Figure 4.43: Deck Temperature (A-T-7-C-1)

4.6.2 Top Longitudinal Strain Gages

Of the 8 strain gages installed on longitudinal reinforcing bars in the top mat of reinforcement, 7 remained operational after construction. Prior to casting, the channel on the data acquisition system for A-S-5-C-2 was not functioning properly. Figures 4.44 and 4.45 illustrate the strains in the top longitudinal reinforcing bars in the as-built and free-shrinkage models, respectively.

All active gages indicated an increase in compressive strain as the models were cast. The strain then slightly decreased until shortly after the initial set, at which time a rapid increase in compressive strain occurred. The compressive strain increased as the deck temperature rose, and declined as the temperature decreased. The reduction in compressive strain continued until the wet burlap was removed. As moisture was lost from the top surfaces, compressive strain increased in the top longitudinal reinforcing steel in both models.

4.6.3 Bottom Longitudinal Strain Gages

All 8 strain gages installed on longitudinal reinforcing bars in the bottom mat of reinforcement were functioning after casting. Figures 4.46 and 4.47 present the strains in the bottom longitudinal reinforcing bars in the as-built and free-shrinkage models, respectively.

All 8 gages indicated a tensile strain as the models were cast. The compressive strain increased sharply shortly after the initial set and continued to rise until the maximum deck temperature was reached. A decline in compressive strain then began and tensile strain was experienced until the wet burlap was removed. As moisture was lost from the top surfaces, compressive strain increased in the bottom longitudinal reinforcing steel in both models.

4.6.4 Girder Strain Gages

All 10 strain gages installed on the steel girders remained functional after casting. The girder gages on the bottom flanges (Figures 4.48 and 4.49) indicated tensile strains while the girder gages on the top flanges (Figures 4.50 and 4.51) indicated compressive strains as expected for positive moment. After the heat of hydration period, the strain gages on the webs of the girders (Figures 4.52 and 4.53) showed virtually zero strain. As shown in Figures 4.48 – 4.52 the compressive strain in the top flanges was slightly higher in magnitude than the tensile strain in the bottom flanges shortly after the burlap was removed.

The bottom flanges of the girders (Figures 4.48 and 4.49) experienced tensile strain as the models were cast. The tensile strain increased suddenly as the heat of hydration of the concrete began and continued until the peak concrete temperature was obtained. The tensile strain then gradually decreased until the wet burlap was removed, after which time the tensile strain rose steadily.

The top flanges of the girders (Figures 4.50 and 4.51) exhibited compressive strain as the models were cast, then decreased after the initial concrete set. As the heat of hydration temperature rose, the compressive strain sharply increased until the maximum deck temperature was reached. Once the deck temperature began to cool, the compressive strain decreased slightly. Upon removal of the burlap, the compressive strain steadily increased.

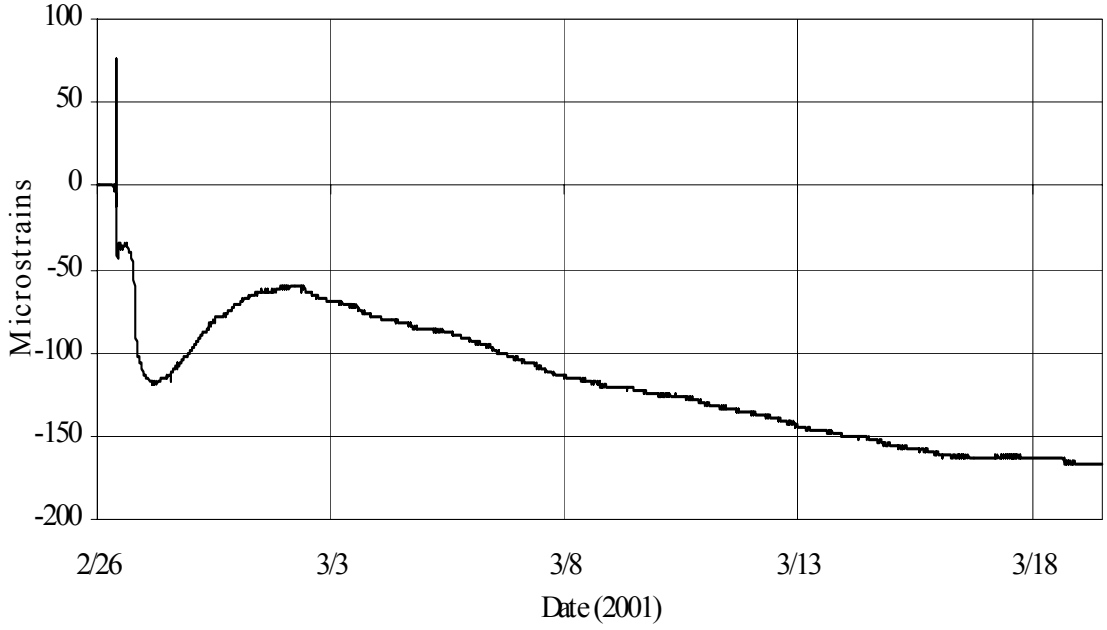

Figure 4.44: As- Built Top Reinforcing Steel Strain (A-S-5-B-2)

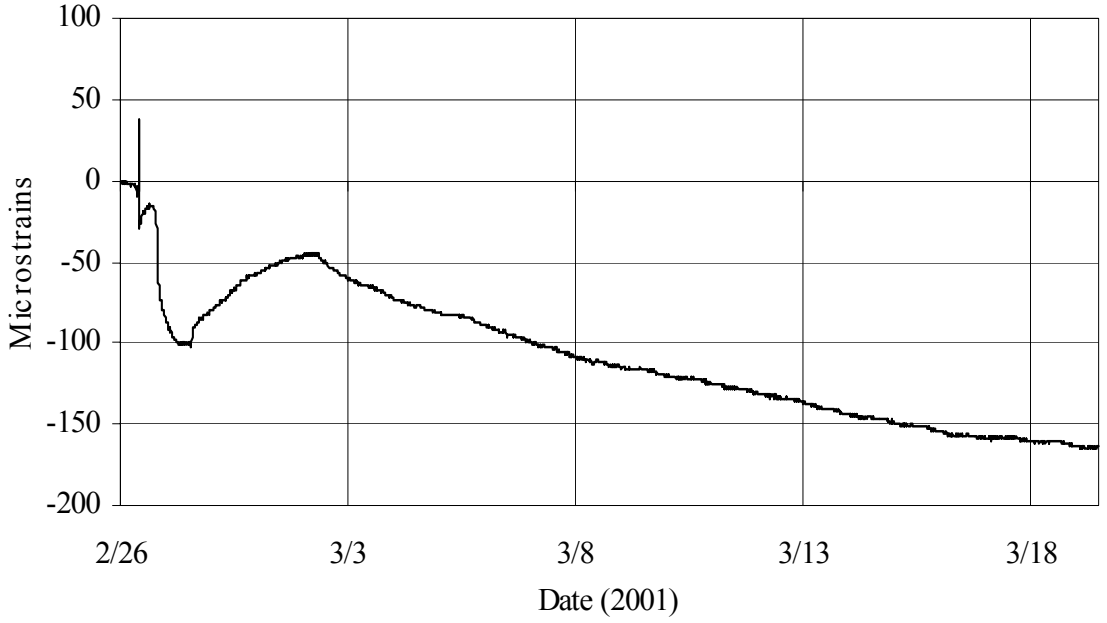

Figure 4.45: Free-Shrinkage Top Reinforcing Steel Strain (F-S-5-B-2)

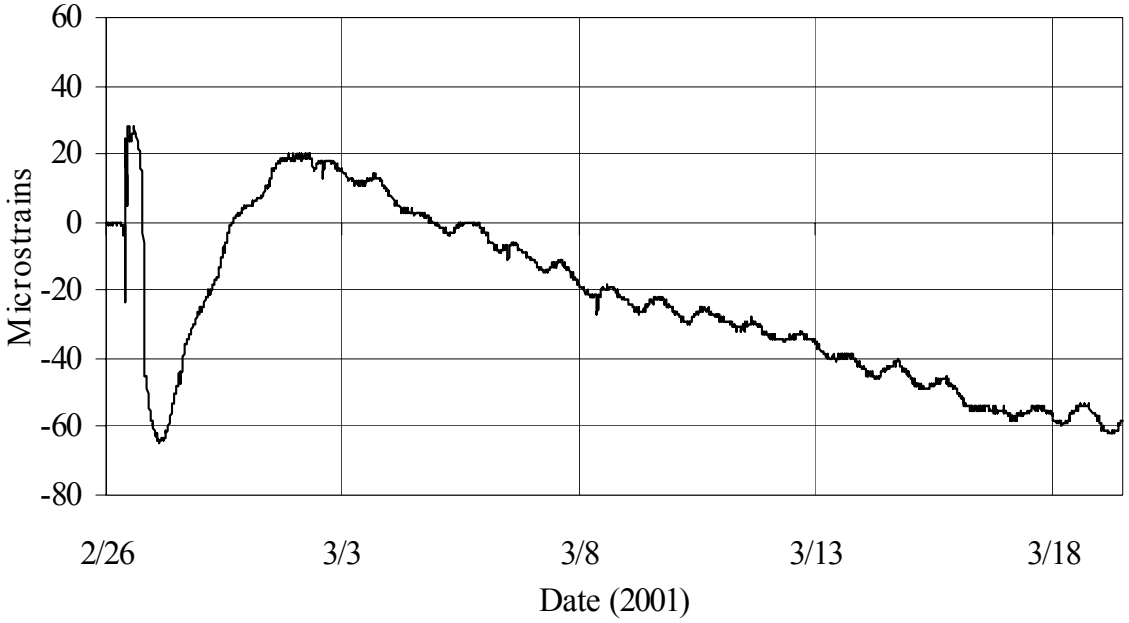

Figure 4.46: As-Built Bottom Reinforcing Steel Strain (A-S-6-C-3)

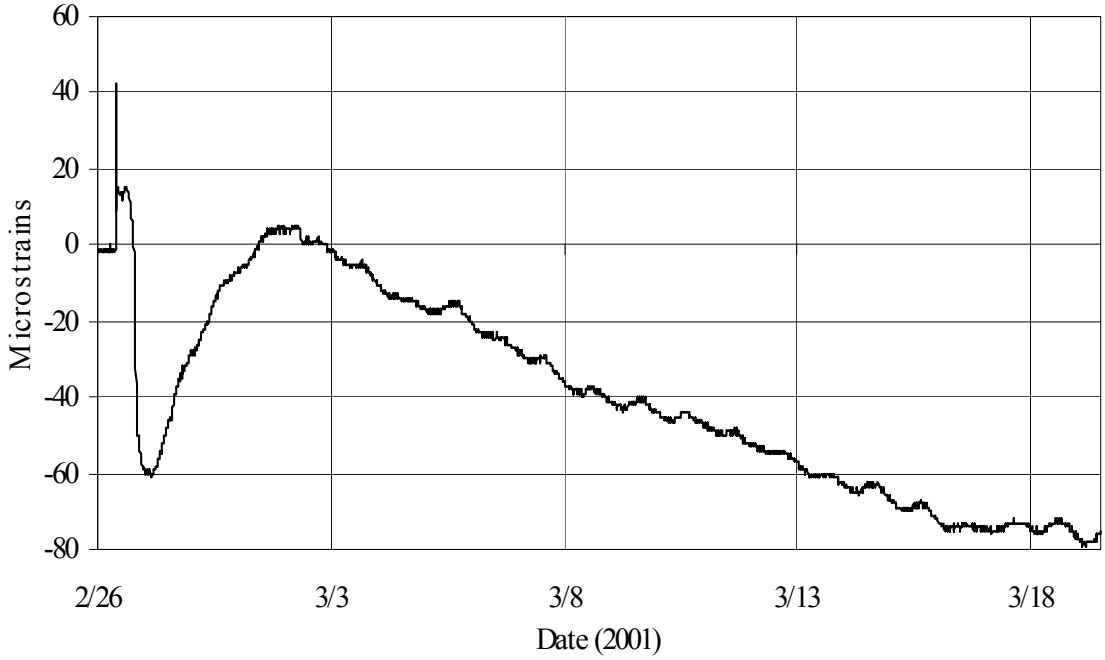

Figure 4.47: Free-Shrinkage Bottom Reinforcing Steel Strain (F-S-6-C-3)

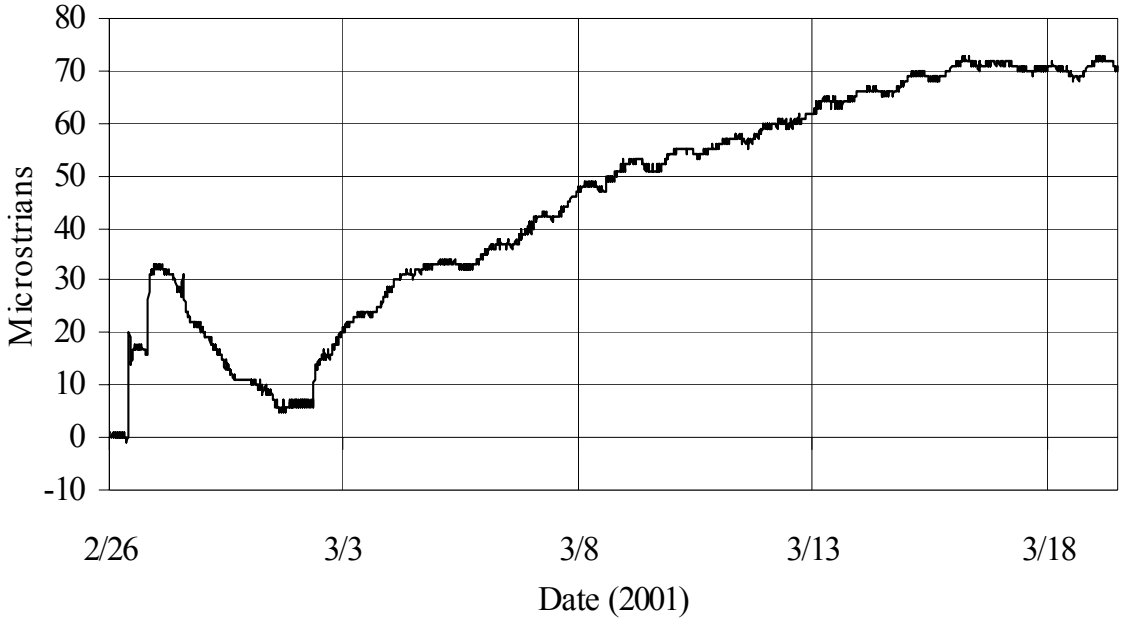

Figure 4.48: As-Built Steel Girder Strain, Bottom Flange (A-S-7-C-8)

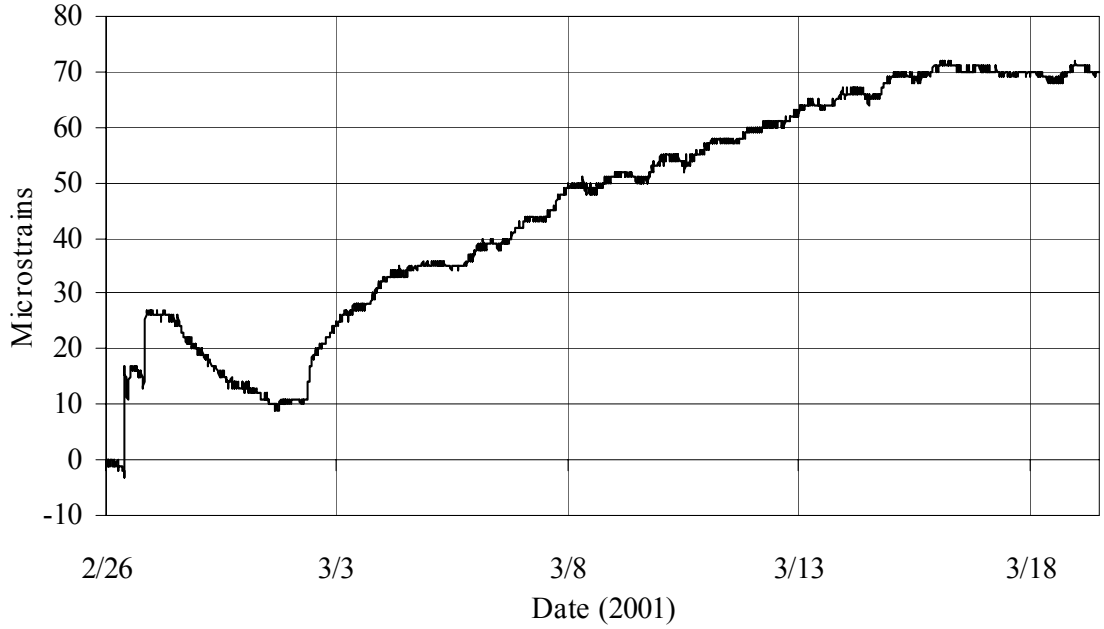

Figure 4.49: Free-Shrinkage Steel Girder Strain, Bottom Flange (F-S-7-C-8)

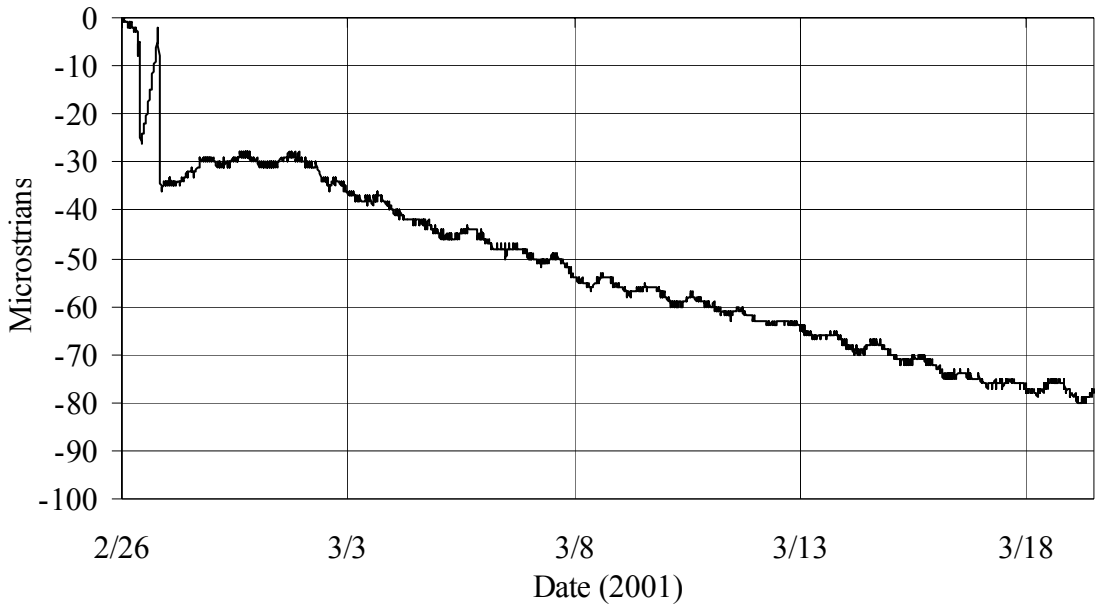

Figure 4.50: As-Built Steel Girder Strain, Top Flange (A-S-7-C-6)

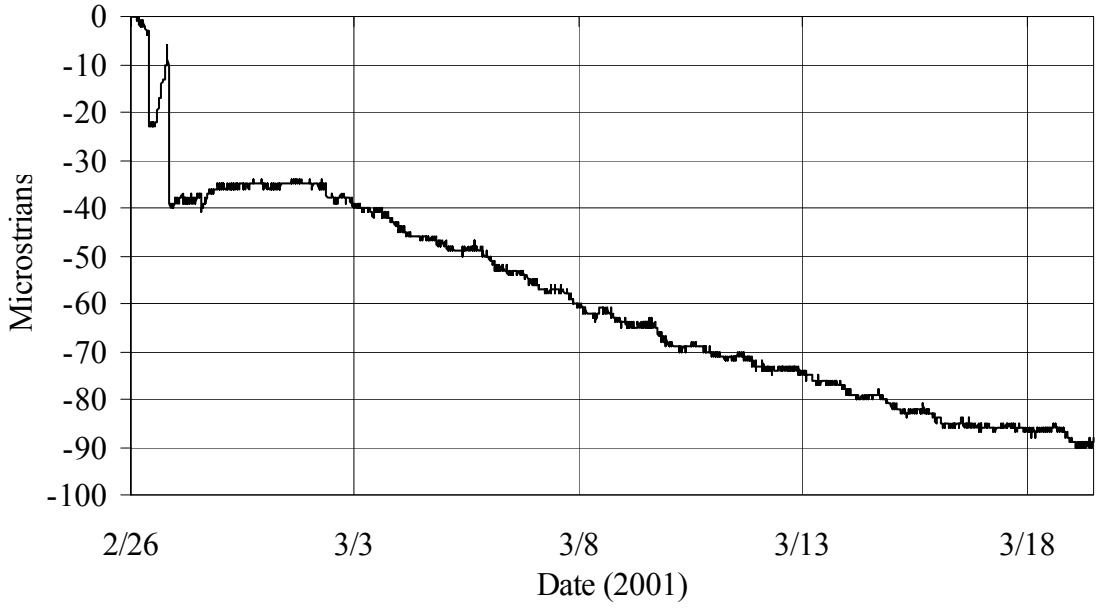

Figure 4.51: Free-Shrinkage Steel Girder Strain, Top Flange (F-S-7-C-6)

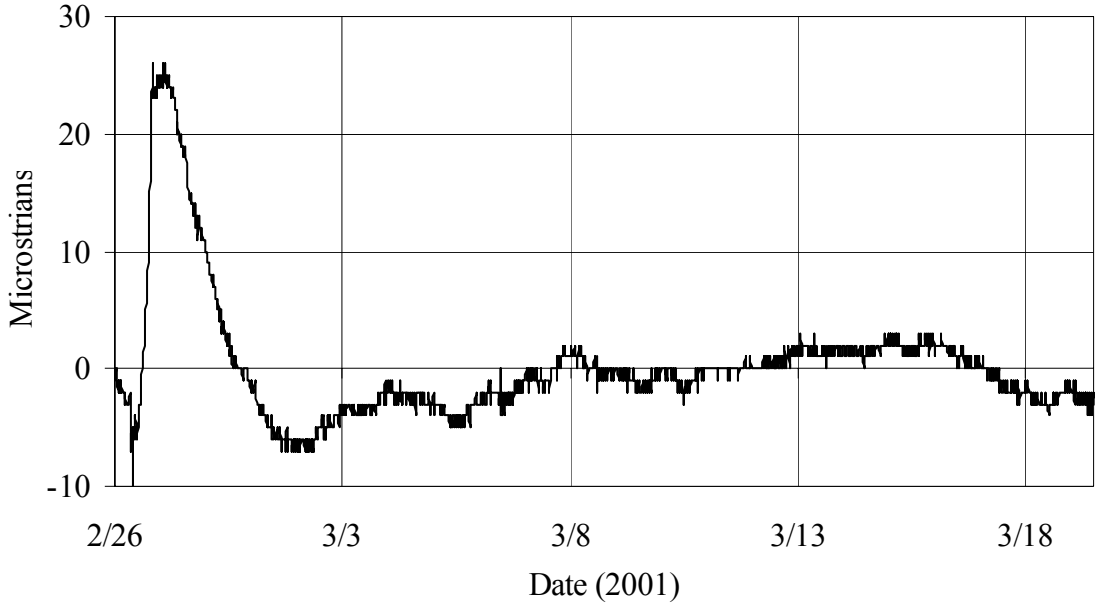

Figure 4.52: As-Built Steel Girder Strain, Center of Web (A-S-7-C-7)

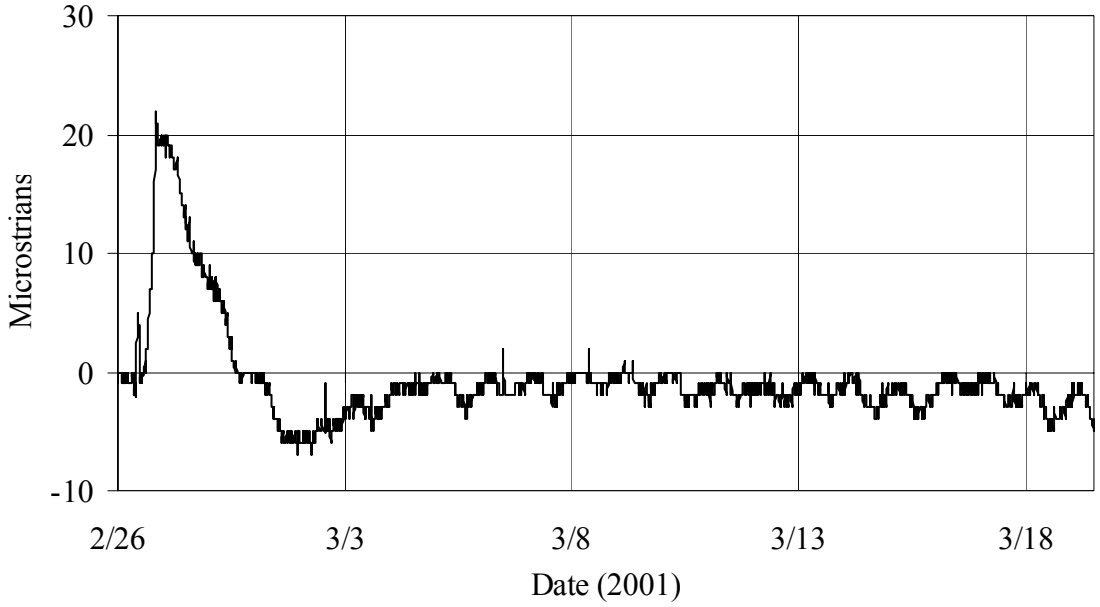

Figure 4.53: Free-Shrinkage Steel Girder Strain, Center of Web (F-S-7-C-7)

4.6.5 Stay-in-Place Steel Form Gages

All 4 strain gages installed on stay-in-place steel forms on the as-built model remained operational after casting. Figures 4.54 and 4.55 show the strain gages transverse to the girders on the top and bottom channels, respectively. Figures 4.56 and 4.57 present the strain gages longitudinal with the girders on the top and bottom channels, respectively. All 4 strain gages showed an instantaneous strain as the concrete was placed on the stay-in-place steel forms.

Figure 4.54 illustrates a slight decrease in compressive strain until soon after the initial set. The strain then steadily increased until the maximum deck temperature was reached and decreased as the deck temperature declined. Once the burlap was removed, the compressive strain again gradually decreased.

Figure 4.55 demonstrates a gradual decrease in tensile strain until the burlap was removed. As the surface moisture was lost, the tensile strain steadily increased.

Figures 4.56 and 4.57 present a slight rise in tensile strain until shortly after the initial set. The strain then decreased as the deck temperature rose and began to increase as the temperature fell. Once the burlap was removed, the tensile strain gradually decreased.

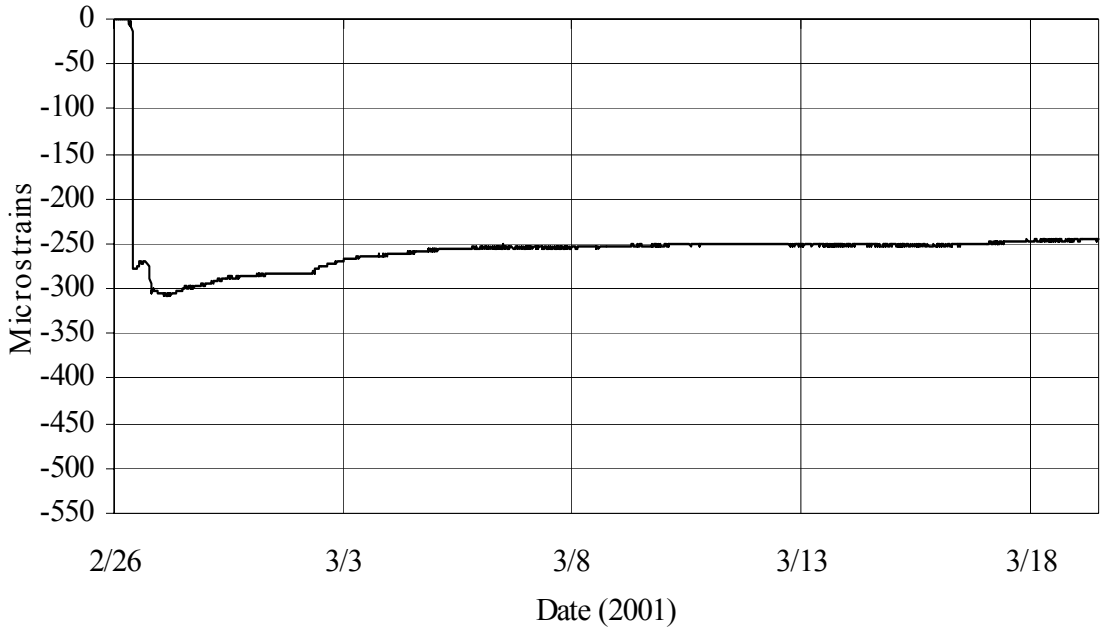

Figure 4.54: Top Channel, Transverse Stay-in-Place Steel Form Strain, (A-S-4-C-5-T)

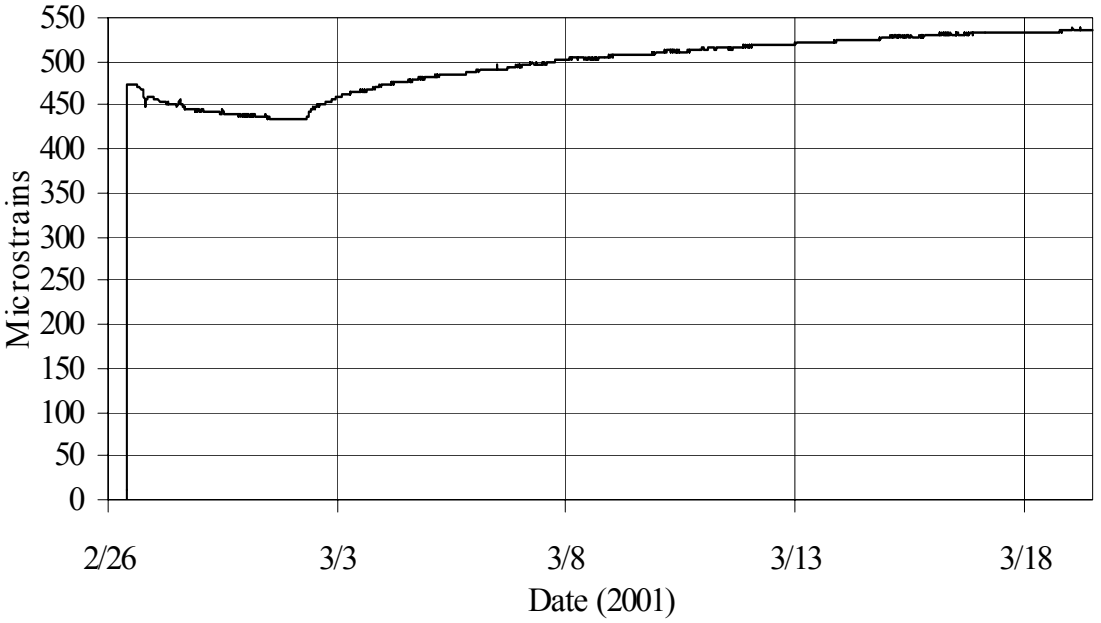

Figure 4.55: Bottom Channel, Transverse Stay-in-Place Steel Form Strain, (A-S-4-C-6-T)

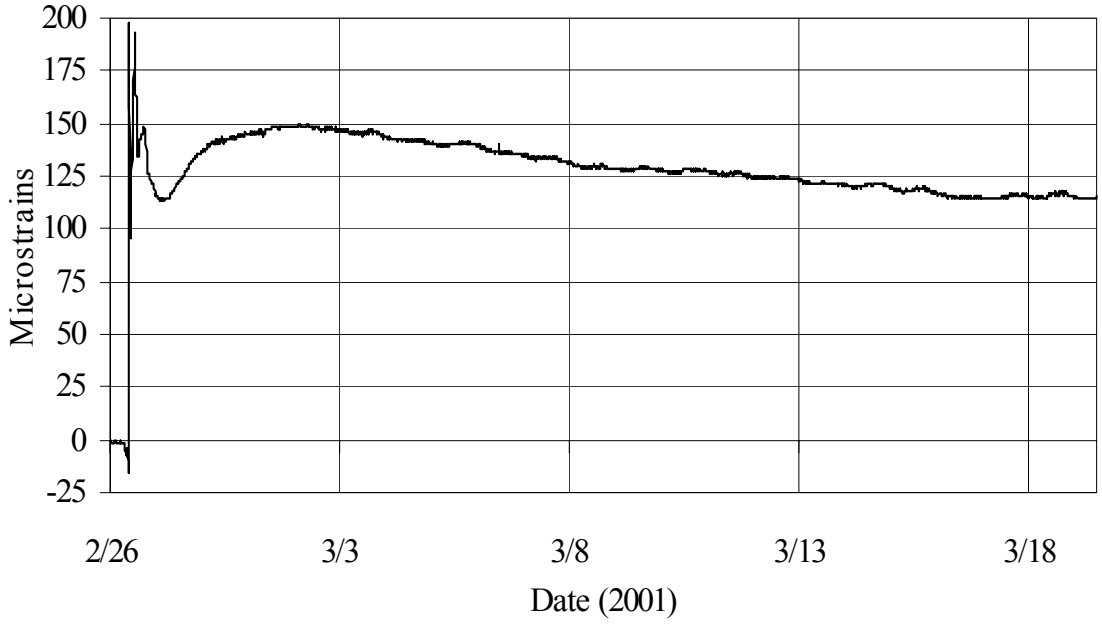

Figure 4.56: Top Channel, Longitudinal Stay-in-Place Steel Form Strain, (A-S-4-C-5-L)

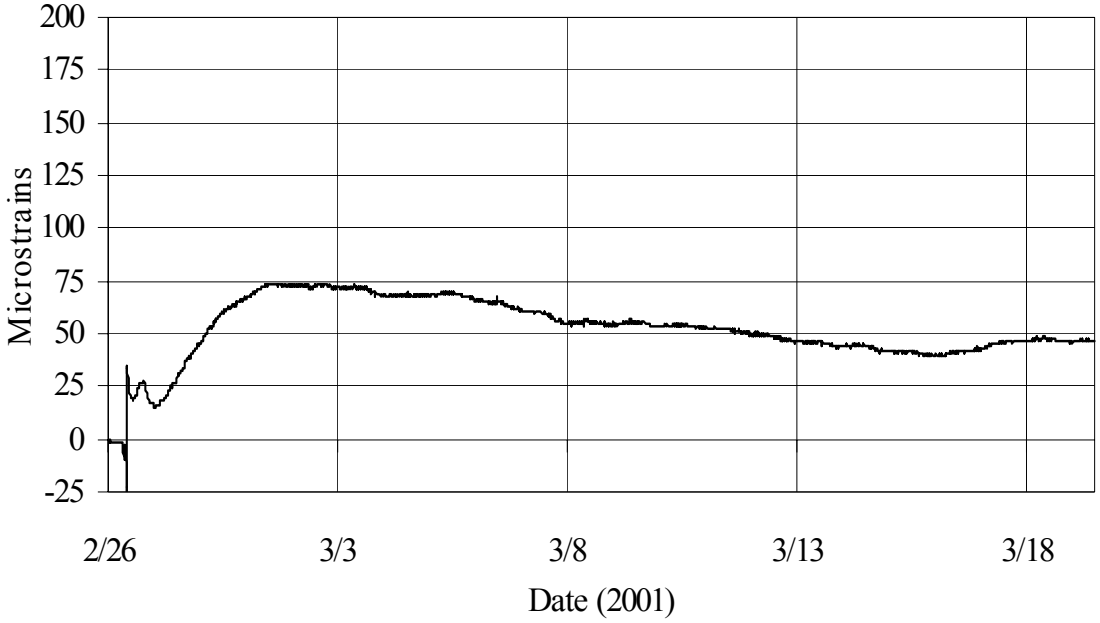

Figure 4.57: Bottom Channel, Longitudinal Stay-in-Place Steel Form Strain, (A-S-4-C-6-L)

4.6.6 LVDT's

All LVDT's at midspan showed an instantaneous downward deflection as the concrete was placed in the models. Figures 4.58 and 4.59 illustrate the downward movement of the center of the deck for the as-built and free-shrinkage models, respectively. Figures 4.60 and 4.61 present the downward movement of the girders at midspan of the as-built and free-shrinkage models, respectively. The graphs present the raw data as well as the data corrected for support settlement.

All curves illustrate downward deflections until soon after the initial set. Then, the models exhibited a decrease until the maximum deck temperature was obtained. The deflections then gradually increased as the deck temperature fell until the burlap was removed. As the surfaces of the models experienced moisture loss and drying shrinkage, the rate of deflections increased.

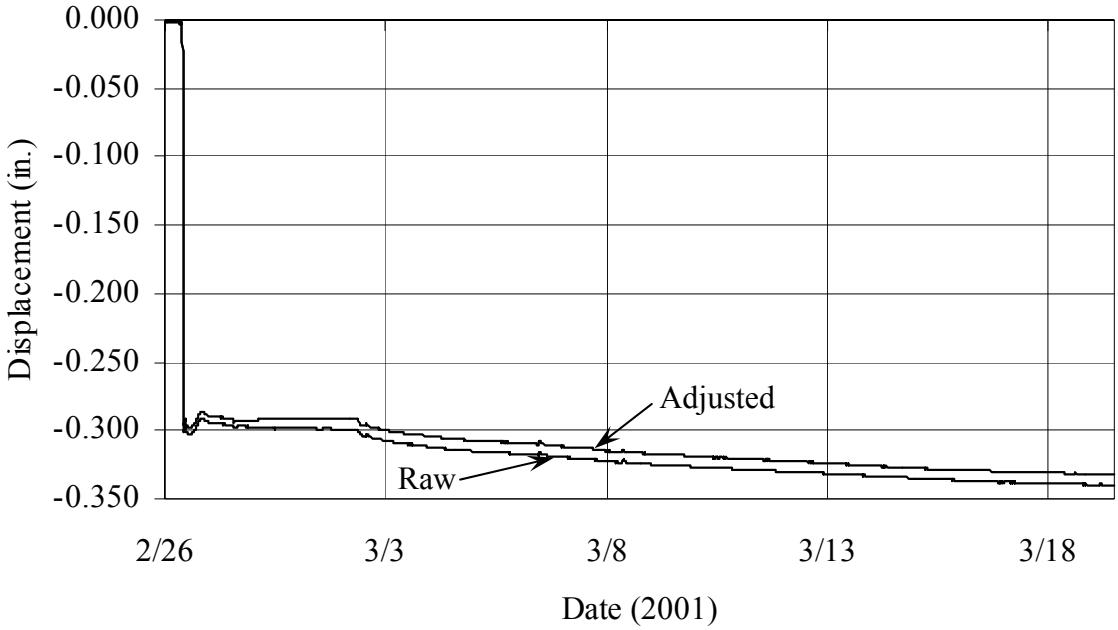

Figure 4.58: As-Built LVDT Center of Deck Displacement (A-L-4-C)

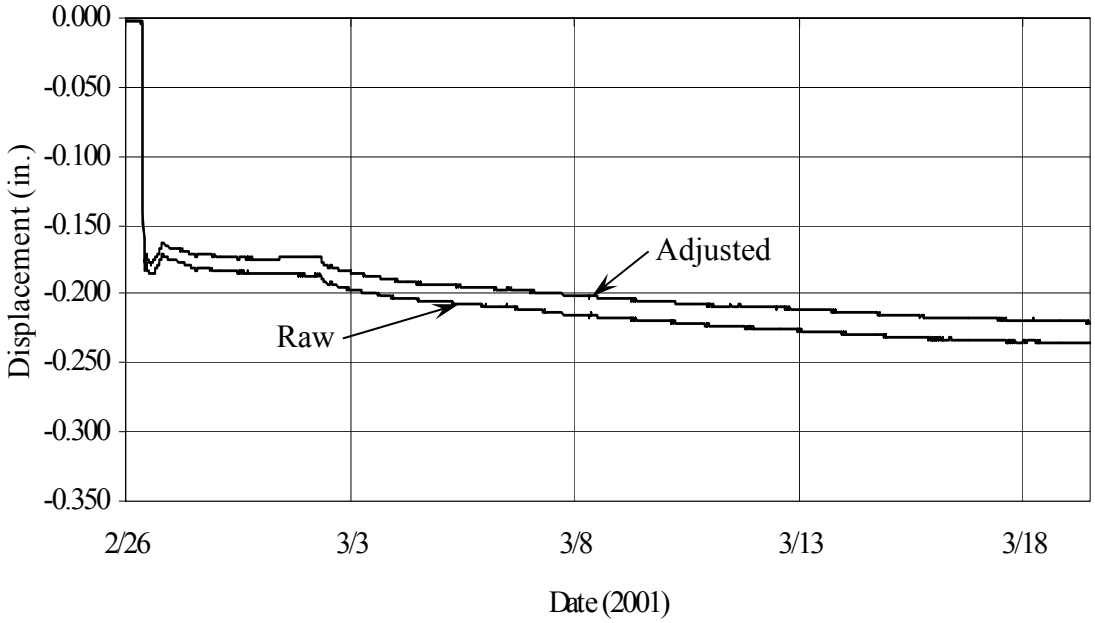

Figure 4.59: Free-Shrinkage LVDT Center of Deck Displacement (F-L-4-C)

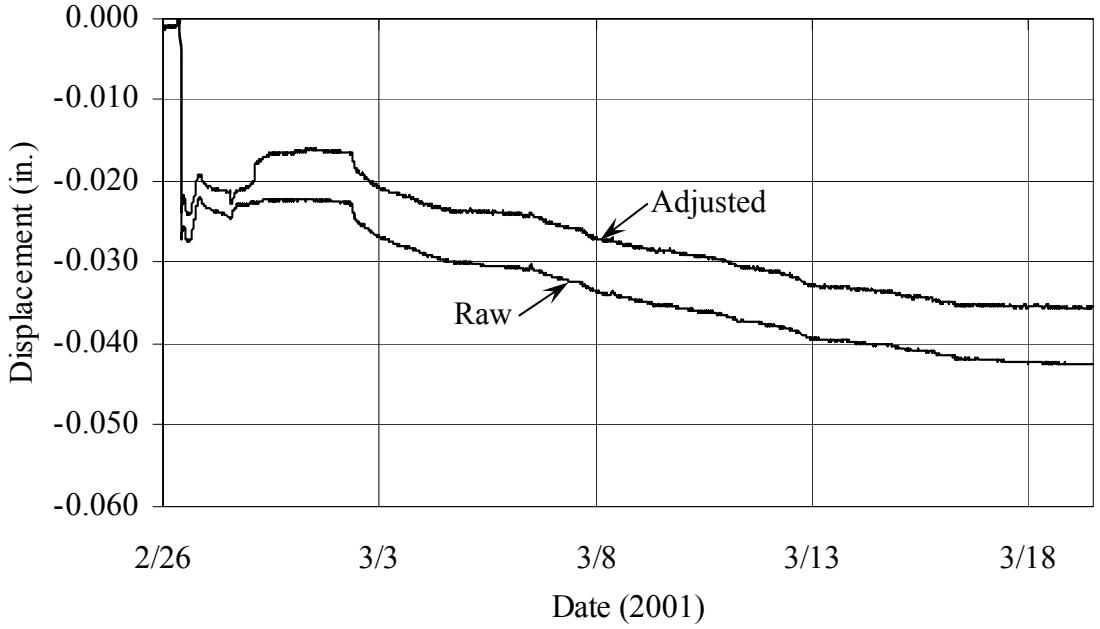

Figure 4.60: As-Built LVDT Girder 2 Displacement (A-L-7-C)

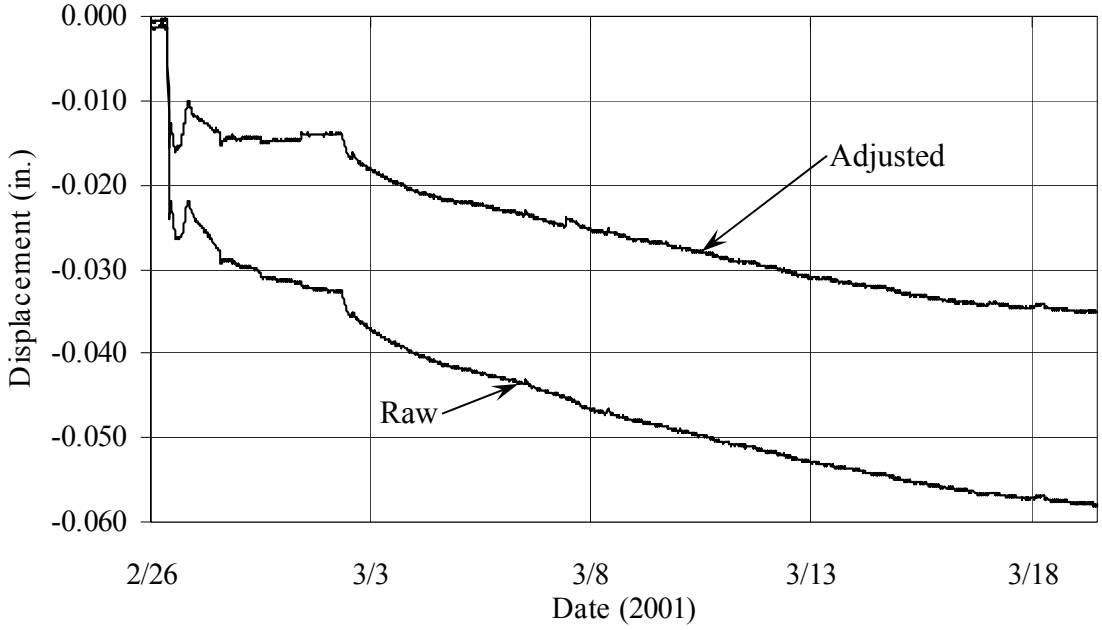

Figure 4.61: Free-Shrinkage LVDT Girder 2 Displacement (F-L-7-C)

4.7 Data Analysis

The temperature variations between the lab and models (Figures 4.42 and 4.43) initially induced fluctuations in the strains (Figures 4.44 – 4.57) and deflections (Figures 4.58 – 4.61). For the strain gages, the tensile strains increased slightly after casting. As the concrete began to set, the compressive strains escalated until the heat of hydration generated an increase in the concrete temperature. During the rise in the heat of hydration temperature, the tensile strains increased except in A-S-4-C-6-T (Figure 4.55). As shown in Figure 4.46, the maximum rise in tensile strain during this period was roughly 85 microstrains.

Once the wet burlap was removed, the moisture at the concrete surface evaporated. As the concrete experienced moisture loss and drying shrinkage, the compressive strains in the longitudinal reinforcing steel (Figures 4.44 – 4.47) and the top flanges of the girder increased (Figures 4.50 and 4.51), while the tensile strains increased in the bottom flanges of the girders (Figures 4.48 and 4.49).

For the strain gages on the stay-in-place steel form placed longitudinal to the girders (Figures 4.56 and 4.57), the tensile strains decreased once the burlap was removed. As the concrete experienced drying shrinkage, the channels were likely compressed, resulting in a decrease in the tensile strain in the forms.

For the stay-in-place steel form strain gages placed transverse to the girders (Figures 4.54 and 4.55), the tensile strains increased once the burlap was removed. The concrete was presumed to be bonded to the stay-in-place steel forms and to be restrained along the girders by the shear studs. As the concrete encountered drying shrinkage, it is likely that the concrete was shrinking from the center of the slab toward the shear studs. The shrinkage of the concrete resulted in an increase in the tensile strain in the stay-in-place steel forms.

Maximum strain gradients were investigated at the midspan of Girder 2 for both models. As shown in Figure 4.62, the maximum strain gradient between the top and bottom flanges of the girders was 161 microstrains on the free-shrinkage model on March 18, 2001 at 11:50 PM. At this time, the strain gradient in the as-built model was similar and was recorded as 153 microstrains.

Maximum temperature gradients were also investigated at the midspan of Girder 2 for both models. The maximum temperature gradient between the top of the deck and the bottom of the girders was 32^{o} F, which occurred various times the evening of casting (February 26, 2001) on both models between the hours of 8:00 PM to 9:00 PM. The maximum temperature gradient between the top and bottom of the girders was 22^{o} F on the as-built model, which was measured on numerous occasions the same day between the hours of 8:00 PM to 11:15 PM. The maximum thermal gradient for both thermal cases, which occurred during the heat of hydration period, is illustrated in Figure 4.63 for the as-built model at 8:00 PM on February 26, 2001. For Figures 4.62 and 4.63, the corresponding temperature or strain gradient is also shown.

For the LVDT's, the deflections initially increased slightly until the heat of hydration generated an increase in the concrete temperature. During the heat of hydration period, the deflections decreased as the temperature of the models increased and increased as the temperature decreased. The model deflection responses were due to the temperature gradient between the top and bottom flanges of the girders (Figure 4.63). The concrete heated the top flange of the girder, whereas through convection, the bottom

flange was only slightly warmer than the ambient lab temperature. As the temperature gradient increased, the deflections decreased due to the upward cambering of the girders.

The expected displacement of the steel girders was modeled with SAP 2000 using plane elements to define the sections. The upward movement of the girders due to a 40^{o} F rise in the concrete deck temperature was calculated to be 0.015-in., for concrete with a compressive strength of 600 psi after 11 hours (Figure 4.21). As shown in Figures 4.60 and 4.61, the measured displacement due to the temperature rise was 0.005-in., 11 hours after the models were cast. The difference in the calculated value and the experimental value is likely due to the thermal gradient through the depth of the models as shown in Figure 4.63, which was not modeled.

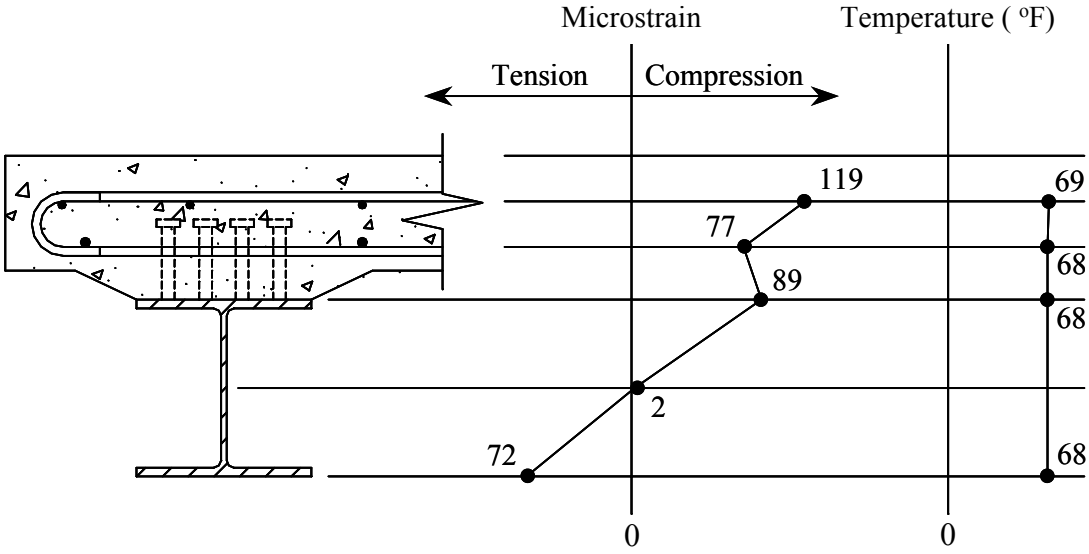

Figure 4.62: Maximum Girder Strain Gradient, Free-Shrinkage Model

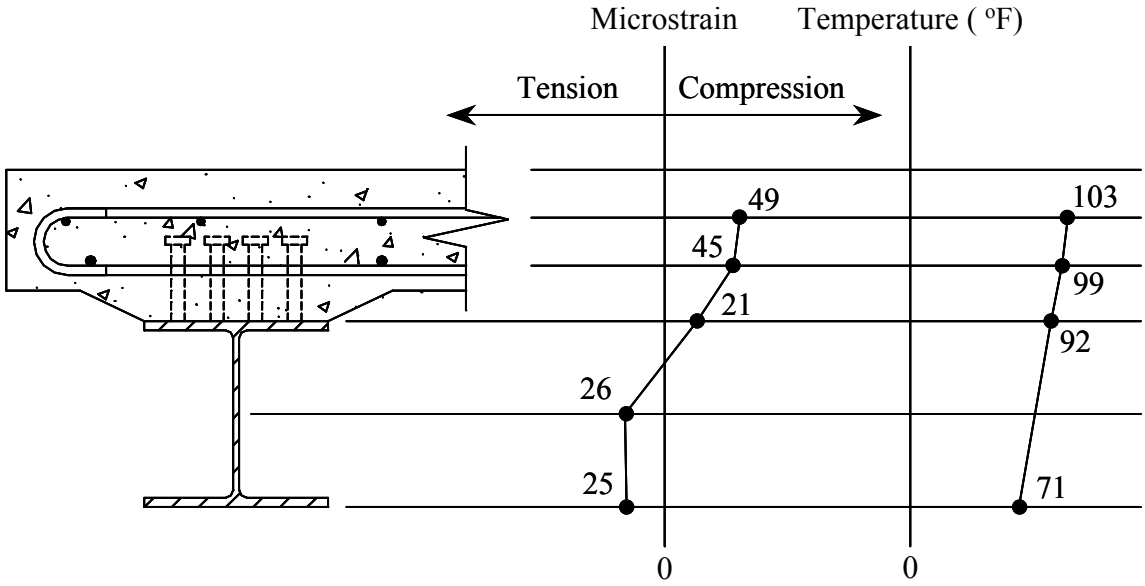

Figure 4.63: Maximum Thermal Gradient, As-Built Model

Based on the strain gage analysis and expected behavior, the compressive strains in the deck increased as the concrete underwent drying shrinkage. The compression in the deck increased the deflections of the models. The downward displacement was calculated to be 0.009-in. due to a concrete shrinkage of 100 microstrains and 0.040-in. for shrinkage of 500 microstrains. As shown in Figures 4.60 and 4.61, the measured deflections for the centerline of the girders between the end of the heat of hydration period and 21 days after casting were 0.020-in. The increase in compressive strains after the heat of hydration period in the top and bottom longitudinal reinforcing steel strain gages, illustrated in Figures 4.44 – 4.47, was approximately 100 microstrains. It is likely that the strain in the concrete due to shrinkage was between 100 and 500 microstrains.

4.8 Long Term Performance

The deck models were monitored under shrinkage loads for approximately three months. Because the primary goal of the experiment was to determine how the shape and stiffness of the formwork affected early-age cracking, the wood formwork was covered with two layers of teflon sheets to minimize restraint. After adequate data had been collected to analyze the effect of the shape and stiffness of the SIP forms, the wood forms were removed to examine if the shrinkage rate would increase. Approximately two months after the concrete had been cast; the effect of removing the wood formwork was immediately obvious. Figure 4.64 displays data collected from longitudinal reinforcing bars (parallel to the girders) located in the deck models. The time at which the wood forms were removed is labeled on the graph.

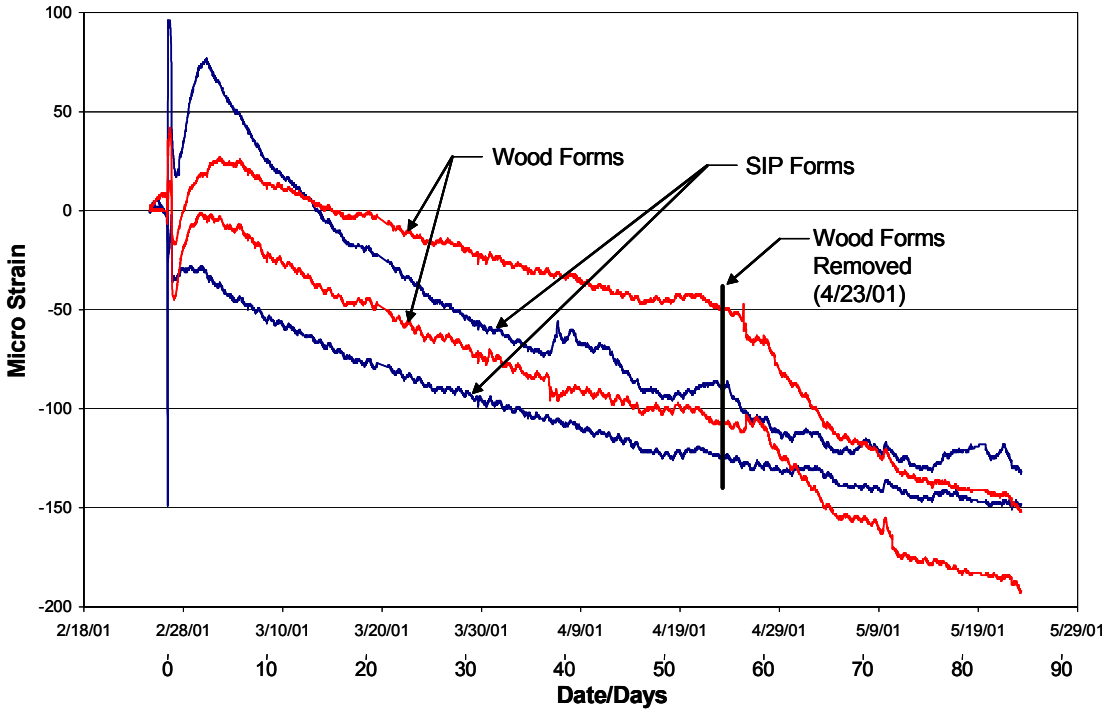

Figure 4.64: Reinforcing Bar Strain Gage Data Collected From Deck Models

From the strain data collected from the reinforcing bars, it appears that removing the wood forms increase the rate of shrinkage. Because the SIP deck pans were not removed (SIP forms are not removed in actual construction), the shrinkage rate in this specimen continued to decrease.

CHAPTER 5
LABORATORY SHRINKAGE MODELS

5.1 Introduction

To provide an improved understanding of the influence that formwork type has on early age cracking of concrete bridge decks, ten deck models were designed, constructed, and tested in the Kettelhut Structural Engineering Laboratory. It was established from the previous restrained shrinkage experiment (Section 1.2) that the use of wood formwork, as opposed to stay-in-place (SIP) forms, may have considerable influence on the amount of total shrinkage and the distribution of shrinkage through the depth of a bridge deck. This investigation was designed to determine the effect of form type on shrinkage during the first month of a bridge decks' life.

5.2 Specimen Design

5.2.1 Specimen Sizes

The deck models were designed to represent a cut section from a typical concrete bridge deck built in Indiana. Each model needed to be large enough to provide adequate shrinkage so comparisons could be made between each deck model. Because of laboratory space limitations and the shape of the manufactured SIP deck pan, each of the specimens was designed with a longitudinal length of 4'-4". Shrinkage strains could then be measured in this direction (Figures 5.1 and 5.2).

The width (2'-9 ½") of each deck model was selected to be large enough to represent adequately the effect of both the deck pan and reinforcement within a bridge deck. In addition, this width was sufficient to minimize any effects of moisture loss from the sides of the specimens.

Nine of the ten deck model's depths were designed at 7-7/8 in. (not including the deck pan's depth). This dimension was used to directly correlate with the SR25 over I65 concrete bridge deck discussed in Chapter 3 (Figure 5.3), which was designed using AASHTO's Standard Specifications for Highway Bridges 16th Edition (1996). One additional deck model was designed with an 8-7/8 in. thickness to evaluate the effect of slab thickness on the measured shrinkage strains. Specimen dimensions are shown in Figures 5.1 and 5.2.

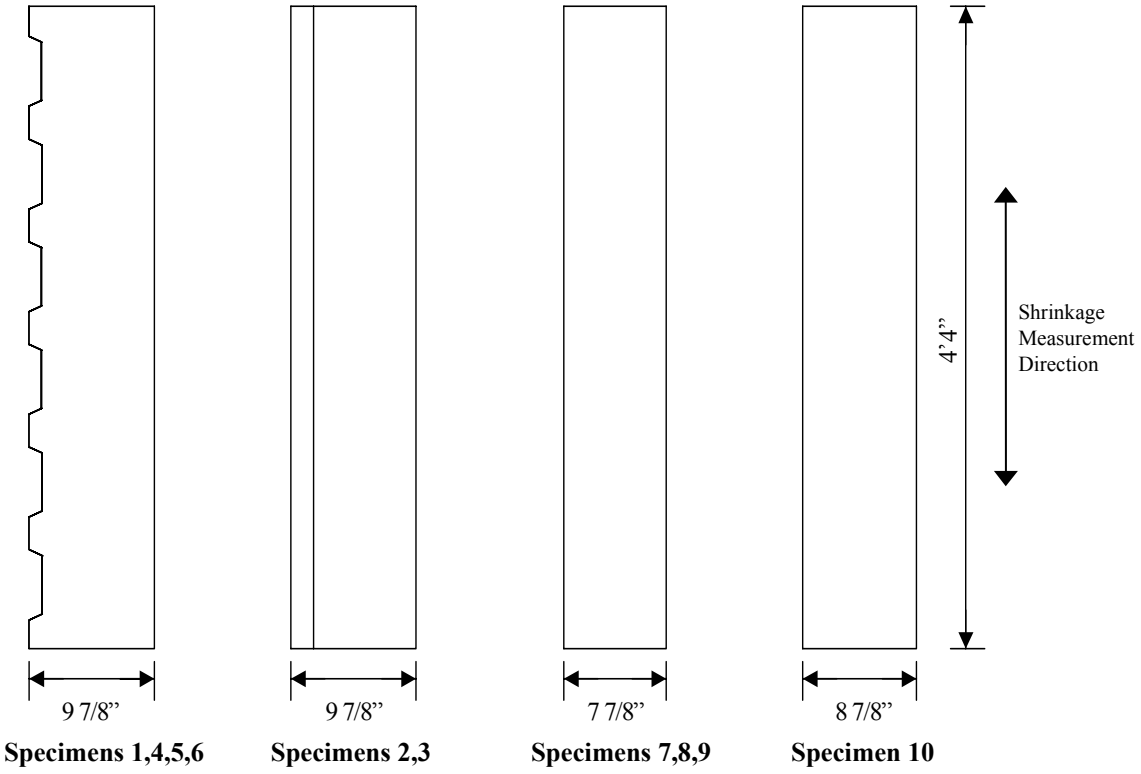

Figure 5.1: Deck Model Elevations

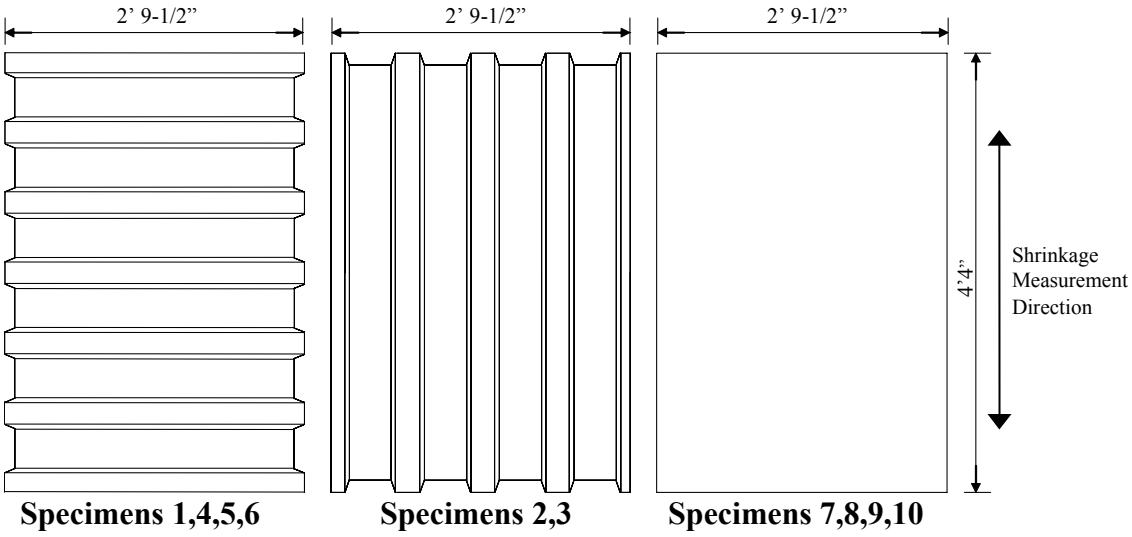

Figure 5.2: Plan View of Deck Models

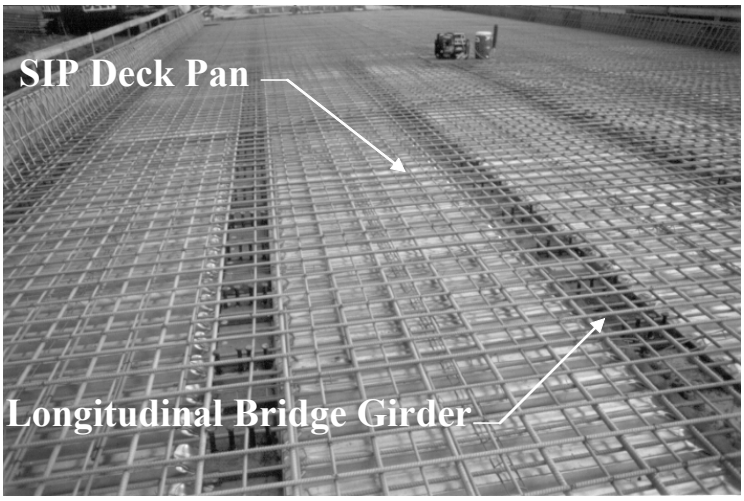

Figure 5.3: SIP Deck Pans Placed Between Girders (I65 over SR25)

5.2.2 Specimen Variables

To determine the effect of form type on shrinkage and early-age deck cracking, the ten deck models were designed differently. Each model was designed to vary in form shape, form type, and form orientation. Also, two of the deck specimens included reinforcement. Table 5.1 presents the characteristics of each of the ten different laboratory models.

Table 5.1: Characteristics of Shrinkage Specimens

Specimen	Form shape	Form Type	Deck Pan Orientation	Sealed	Rebar	Width (in)
1	Deck Pan	Metal Pan	Transverse	Yes	Yes	9 7/8*
2	Deck Pan	Metal Pan	Longitudinal	Yes	No	9 7/8*
3	Deck Pan	Wood	Longitudinal	Yes	No	9 7/8*
4	Deck Pan	Wood	Transverse	Yes	No	9 7/8*
5	Deck Pan	Metal Pan	Transverse	Yes	No	9 7/8*
6	Deck Pan	Wood	Transverse	No	No	9 7/8*
7	Flat	Wood	-	No	Yes	7 7/8
8	Flat	Wood	-	Yes	No	7 7/8
9	Flat	Wood	-	No	No	7 7/8
10	Flat	Wood	-	No	No	8 7/8

* Thickness includes the depth of the deck pan

5.2.2.1 Form Shape

To determine the effect of form type on early age shrinkage, two different types of formwork were used for the experimental program. As described in Chapter 1, concrete bridge decks can be formed with removable wood forms or SIP steel corrugated deck pans.

A bridge deck built with wood forms is flat on the bottom surface (Specimens 7-10). On the other hand, if SIP forms are used (Specimens 1,2,5), the bottom side of the slab will conform to the corrugated shape of the deck pan (Figure 5.4).

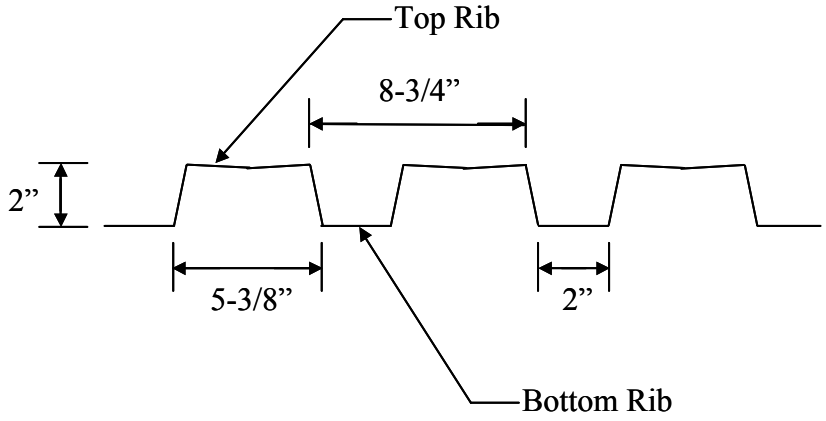

Figure 5.4: Cross Section of Stay-in-Place Steel Form

Because of geometric differences between the wood and SIP form, their shape may affect how a bridge deck shrinks and its susceptibility to early age cracking. A SIP deck pan will increase the depth of the slab in places due to the corrugated shape. This shape may induce bending and behave differently than a bridge deck built with wood forms. In addition, the vertical section of the deck pan’s metal ribs may induce a stress concentration leading to a crack initiation location.

5.2.2.2 Form Orientation

The orientation of a wood form will not affect how a bridge deck shrinks, but the orientation of a SIP deck pan may. Because a deck pan is designed to span in the transverse direction of the bridge span (Figure 5.3), its bending resistance is much larger when the pan ribs are parallel to that direction. Therefore, if shrinkage induces bending in a bridge deck, a SIP will create more restraint in the transverse direction of the bridge than the longitudinal direction (Figure 5.5). As a result, form orientation may affect shrinkage and early-age-cracking.

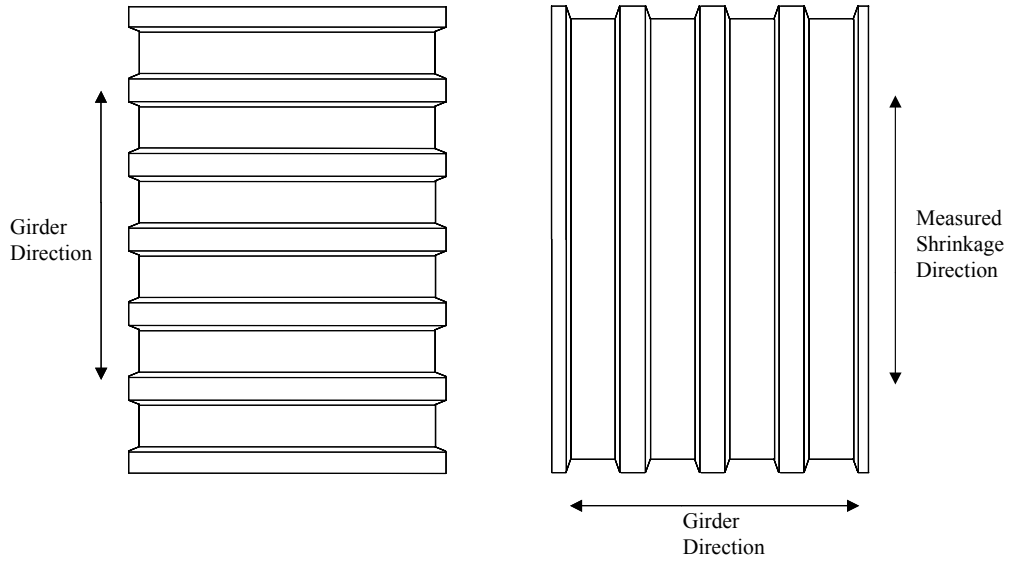

(a) Transverse Orientation **(b) Longitudinal Orientation**

Figure 5.5: Plan View of a Deck Pan

From the previous literature review and field evaluation, transverse cracking was observed to be more frequent and detrimental to the lifespan of a bridge deck. Consequently, of the six deck models built in the shape of deck pan, four were designed in the transverse orientation to investigate shrinkage in the direction of the bridge span while two were designed in the longitudinal orientation to investigate shrinkage transverse to the bridge span.

5.2.2.3 Form Type

The two different form types may have a major effect on shrinkage. Therefore, to determine the effect of form type on shrinkage and curling, three specimens were built using SIP forms (Specimens 1,2,5), and three others (Specimens 7,8,9) were designed with flat wood forms.

Because a SIP form is not removed from a bridge deck, the surface-to-volume ratio of a bridge constructed with this type of formwork is substantially reduced when compared to a wood formed bridge. Wood forms are usually removed within days after casting. The reduced surface-to-volume of the SIP formed bridge will slow and decrease the amount of drying shrinkage from the bottom surface of a bridge deck (NCHRP 380 1996). The non-uniform shrinkage causes internal compressive and tensile stresses as well as curling of the bridge deck. Internal restraint is also produced in a bridge deck built with wood forms, but because the formwork is removed, the surface-to-volume ratio is much larger and will result in more shrinkage. However, this shrinkage will be more uniform; consequently, the deck will not curl as much as when a SIP form is used.

5.2.2.4 Sealing

As described previously, the sealing effect of a SIP deck pan may play an important role in the early-age cracking of bridge decks. To determine the effect of sealing on shrinkage and curling, Specimens 3, 4, and 8 were designed using the shape of a deck pan or a wood form. In addition, these specimens were sealed. The objective of this design was to produce a non-uniform shrinkage profile without the resistance of a SIP. Therefore, the effect of the stiffness of a metal deck pan can be isolated, and the sealing effect can be directly investigated.

5.2.2.5 Reinforcement

Reinforcement is typically placed in a bridge deck for structural resistance as well as to provide shrinkage and temperature reinforcement. To determine the effect of this reinforcement on the overall shrinkage, two deck models (Specimen 1 and 7) were designed to include two mats of longitudinal reinforcement. The bottom mat of reinforcement was designed with #5 epoxy coated bars and the top mat was designed with #4 epoxy coated bars (Figure 5.6 and 5.7). To accommodate a representative amount of reinforcement, the widths of the deck models were designed to accommodate three rows of longitudinal reinforcement with adequate side cover (≈ 4.9 in.). The spacing and top and bottom cover dimensions of the reinforcement were consistent with the I65 over SR25 bridge deck. The bottom and top cover were 1 in. and 2.5 in., respectively. Transverse reinforcement was omitted since it should not affect the amount of shrinkage or curling in the direction being considered.

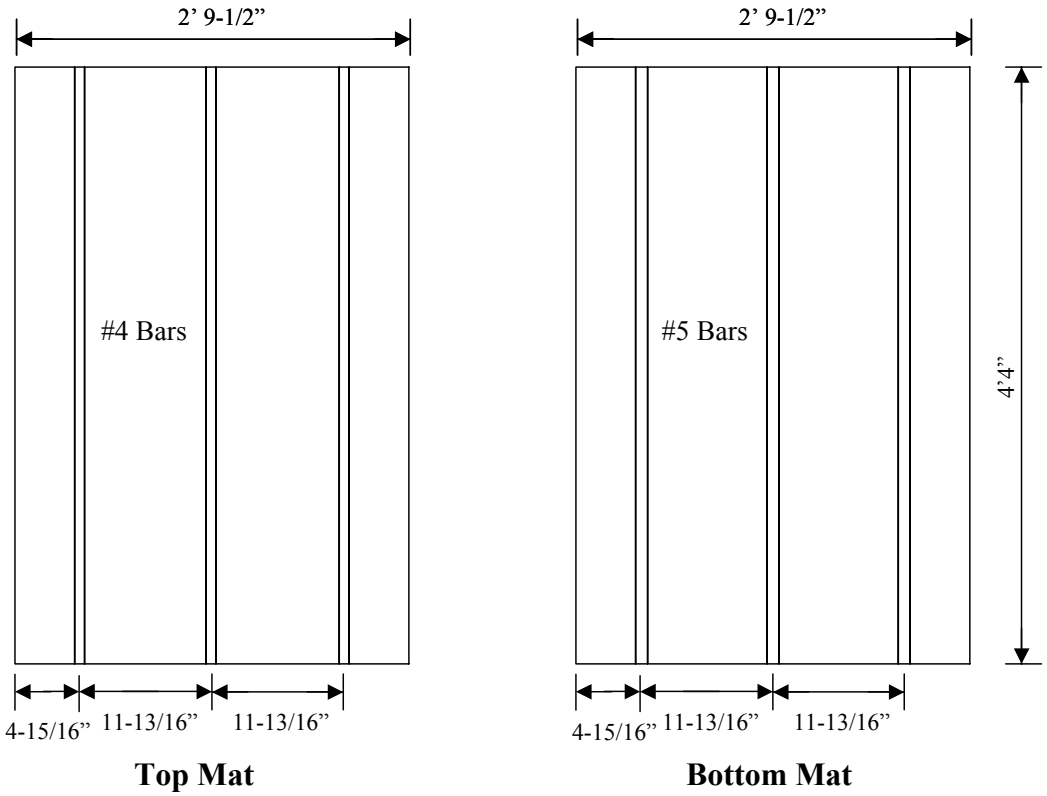

Figure 5.6: Plan View of Specimens 1 and 7 Reinforcement

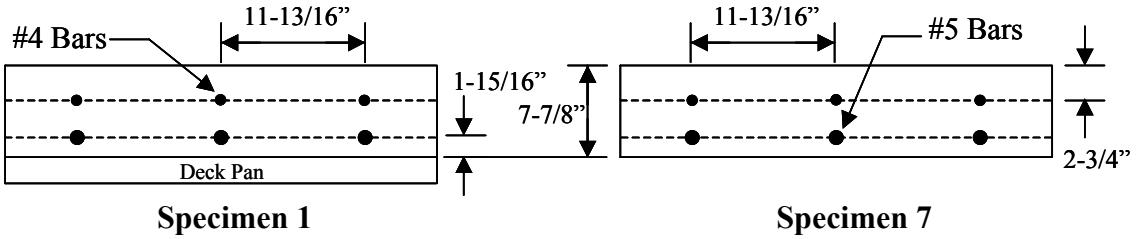

Figure 5.7: Cross Section View of the Reinforcement of Specimens 1 and 7

5.2.2.6 Thickness

The thickness dimensions chosen for the laboratory models were selected to directly compare with INDOT design recommendations and the I65 over SR25 bridge deck. The concrete slab depth for I65 over SR25 was designated in metric units, which in turn resulted in an unusual depth of 7-7/8 in. when converted to U.S. customary units. Since forming technique is not specified on the plans, the deck pans are not accounted in design. Therefore, for SIP corrugated deck pans, the depth of the pan is not included within the total depth of the concrete deck. Specimens 1-6 are labeled at a depth of 9-7/8 in. (7-7/8 in. + 2 in. deck pan) to easily determine the differences between each of the specimens.

In addition to the nine specimens designed using 7-7/8 in. depth, Specimen 10 was designed 1.0 in. thicker than the wood formed specimens (Figure 5.2). This deck model was used to investigate the effect of slab depth on shrinkage.

5.3 Materials

5.3.1 Concrete

To represent a bridge deck constructed in Indiana, INDOT Class C concrete was used for the experimental program. This mix is the same as that used in the bridge deck for I65 over SR25 and was supplied from the same local ready-mix producer (Irving Materials Inc. (IMI)) that also constructed the bridge. The mix included a maximum aggregate size of ¾” (crushed stone) and a water-to-cement ratio of 0.34. Specific mix proportions are provided in Table 5.2.

To construct the ten deck models, 5 yd^3 of concrete were ordered. Once the concrete had arrived, additional water was added to the mix to increase workability. The addition of the extra water (3 gallons) increased the slump from 4 to 6.25 in. (Table 5.3). This additional water is included in the quantities presented in Table 5.2.

Table 5.2: Mix Design (INDOT Class C Concrete)

Material	Quantity Per Yard	Total Quantity	Specifications/Suppliers
Cement	658 lb/yd^3	3290 lbs	ASTM C-150, Type I, Essroc Cement Co
Sand	1280 lb/yd^3	6400 lbs	ASTM C-33 & INDOT Specification #23 Sand from Vulcan Materials, Battleground, IN
Stone/ Gravel	1836 lb/yd^3	9180 lbs	#8 Stone from US aggregate, Delphi, IN
Water	27.6 gallon/yd^3	138 gallons	-
Water Reducer	13 oz/yd^3	65 oz	ASTM C-494, Water Reducer Type A Pozzolith 220N, Master Builders.
Air	8 oz/yd^3	40 oz	ASTM C-260 Air Entrainment, Micro Air by Master Builders
Ash	None	None	-
Micro-Silica	None	None	-

Table 5.3: Additional Concrete Mix Information

W/C	0.34
Slump	6.75 in
Air Temperature at Arrival	75 ^{o}F
Relative Humidity at Arrival	58 %
Amount of Concrete Ordered	5 yd^3

Both compression and modulus of elasticity tests were performed on 6 in. by 12 in. cylinders after casting. A 600-kip Forney compression testing machine was used to perform the compression tests according to ASTM-C39 96. The strength gain curve resulting from these tests is shown in Figure 5.8. The 28-day compression strength was 4,780 psi.

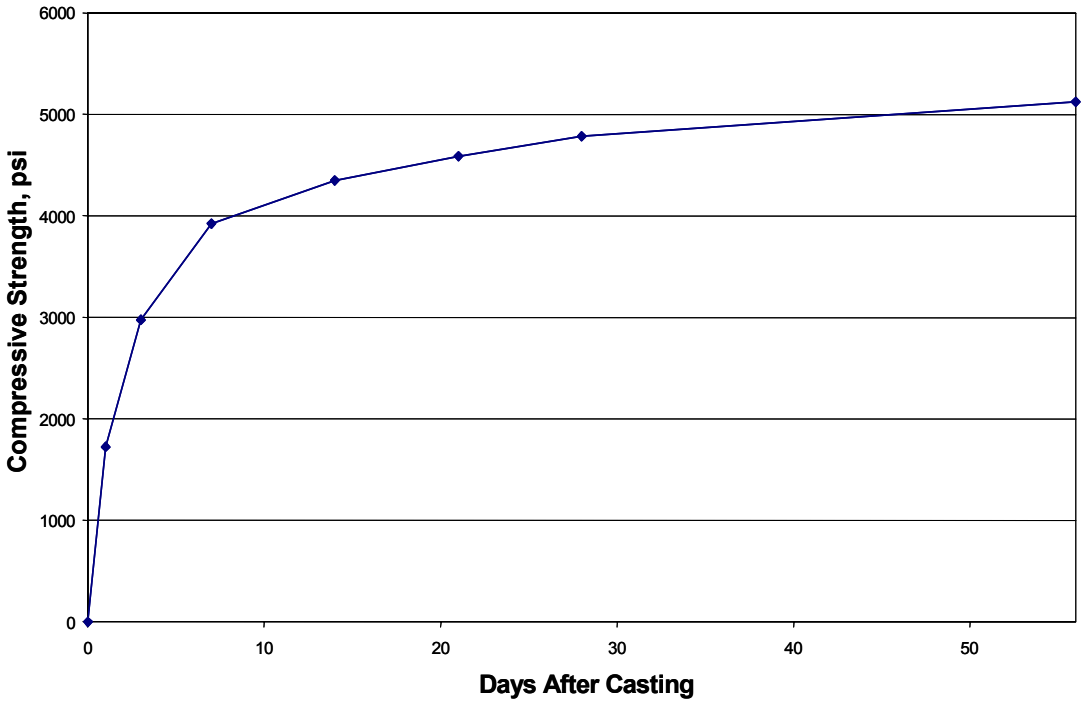

Figure 5.8: Concrete Compressive Strength

Modulus of elasticity tests were performed on a 120-kip Baldwin universal testing machine (Figure 5.9). The testing procedure followed ASTM-C469. The modulus of elasticity measurements were determined using the secant stiffness at 45% of the concrete cylinders compressive strength that were tested on the same day. Figure 5.10 presents the increase in the modulus of elasticity over time. The 28-day modulus of elasticity was approximately 3,750 ksi which correlates well with the common relationship of modulus of elasticity to compressive strength, $57{,}000\sqrt{f_c'}$ (ACI 318-99, AASHTO 16ed.).

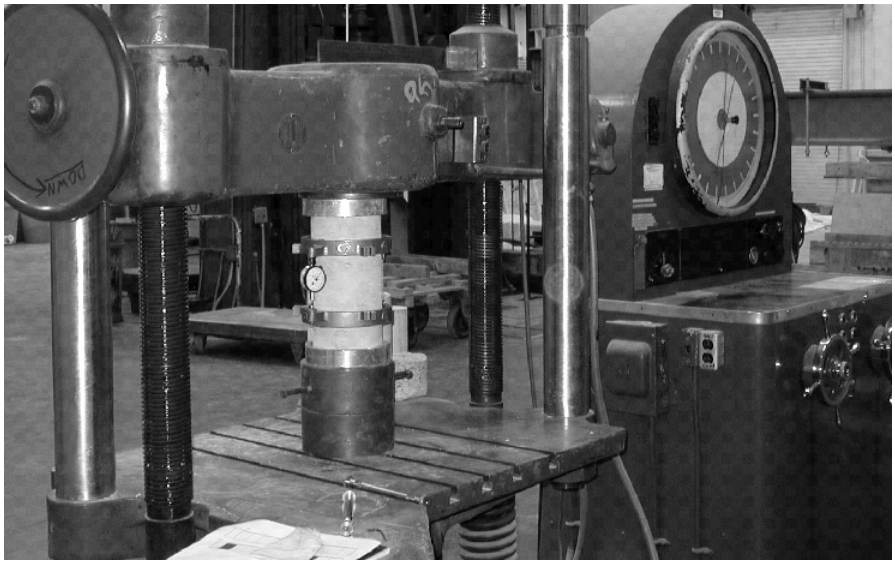

Figure 5.9: Modulus of Elasticity Testing

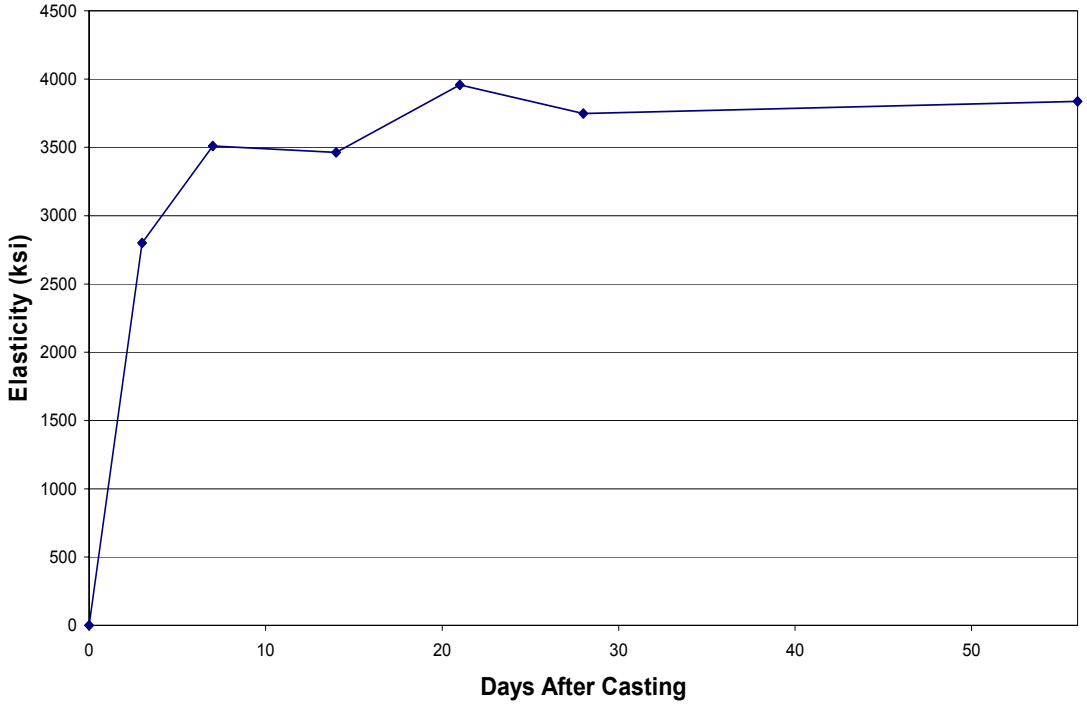

Figure 5.10: Modulus of Elasticity vs. Time

5.3.2 Reinforcing Steel

Both #4 and #5 epoxy coated reinforcing bars were used in the specimens. All bars were of the same specified tensile strength (ASTM A615, Grade 60). Tensile tests were performed on three #4 and #5 bars using a 120-kip Baldwin universal testing machine. A representative stress-strain curve is shown Figure 5.11. The #4 reinforcing bars yielded at an average of 76 ksi, and the #5 reinforcing bars yielded at an average of 73 ksi.

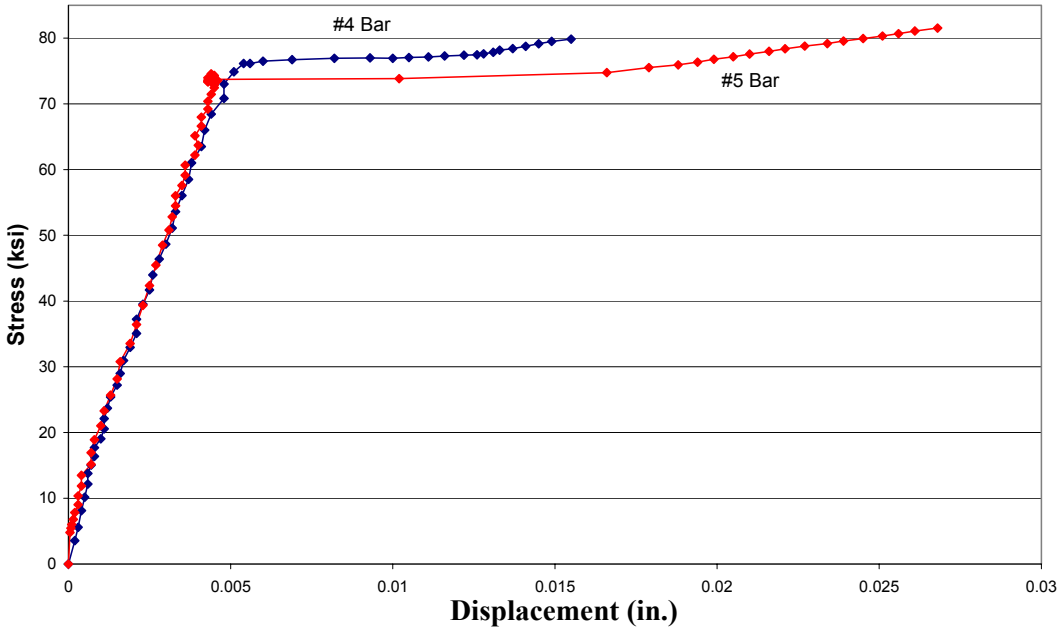

Figure 5.11: Reinforcement Tensile Test (#4 and #5 Bars)

5.3.3 Stay-in-Place Steel Deck Forms

The deck pans used for this experiment were obtained directly from the jobsite during the construction of the I65 over SR25 bridge deck. This type of SIP deck pan is common for bridge deck construction throughout the state. The deck pans were 0.042 in. thick steel that were galvanized for corrosion protection. Before the deck pans were cut to the specified specimen dimensions, they had a width of 36 in. and a length of 64.5 in. Figure 5.4 shows the cross sectional dimensions of the deck pans used for the experimental program.

5.4 Model Construction

5.4.1 Specimen Formwork

The deck formwork was built in two sections. One section contained Specimens 1-6 (Group 1) and the other, Specimens 7-10 (Group 2). Because Specimens 1-6 were designed with the same thickness, their formwork was convenient to group together. Both sets of formwork are shown in Figures 5.12 and 5.13.

All formwork was built with Grade B-B, ¾ in. plyform, reinforced with 2 in. by 4 in. construction lumber. Once the base and walls of the formwork were completed, Specimens 1, 2 and 6 were fitted with deck pans. To form the base of Specimens 3-5, ¾-in. plywood and 2 in. by 4 in. lumber was used to create the deck pan profile (Figures 5.14). All forms were caulked to limit leakage during casting.

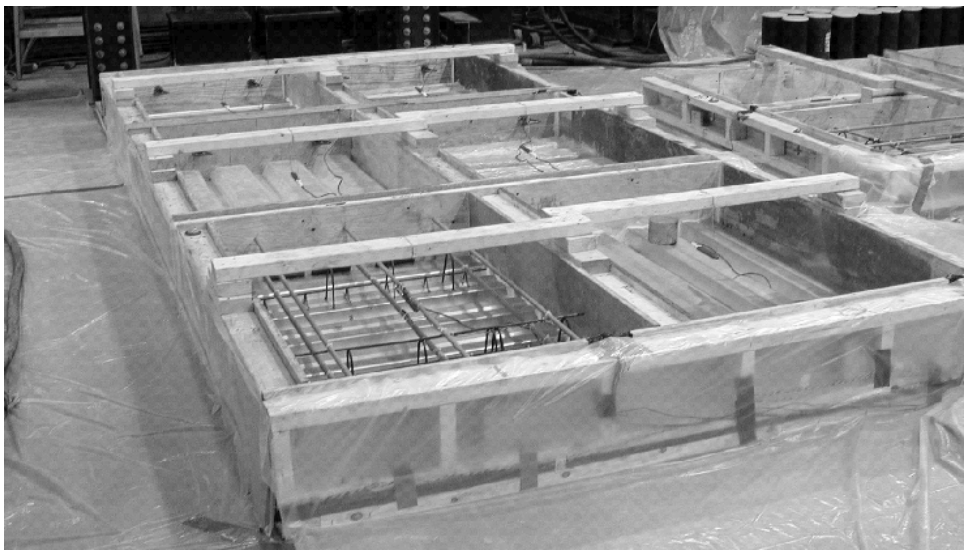

Figure 5.12: Formwork for Specimens 1-6

Figure 5.13: Formwork for Specimens 7-10

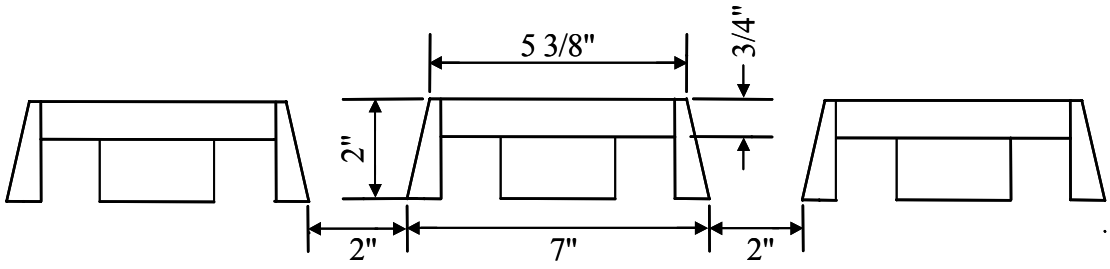

Figure 5.14: Constructed Cross Sectional View of the Deck Pan's Shape

Once all of the reinforcing bars were instrumented, the longitudinal bars were set in the forms (Specimens 1 and 7). Chairs were used to ensure proper top (2.5 in.) and bottom (1 in.) cover for each reinforcing bar. The bars were then tied to the chairs to minimize movement during concrete placement (Figure 5.15).

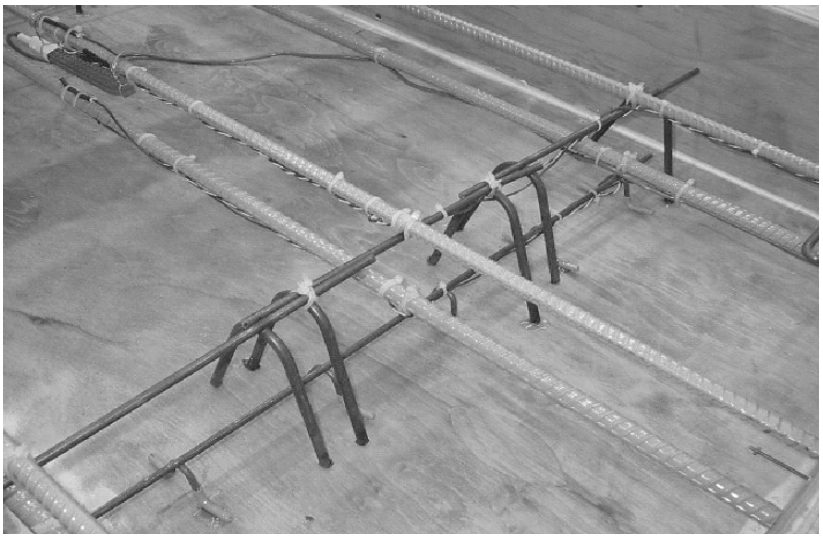

Figure 5.15: Epoxy Coated #4 and #5 Reinforcement in Specimen 7

Also included within each form were two ¾ in. concrete single flared coil inserts (Figure 5.16). Each insert had a tensile capacity of 7,500 lbs. The inserts were equally spaced (11 in. from specimen centerline) at the top edge of each specimen. The inserts allowed the deck models to be easily moved from the casting formwork to the testing setup after curing.

Finally, all formwork for both the specimens and concrete test cylinders were covered with form oil to ensure easy removal after curing.

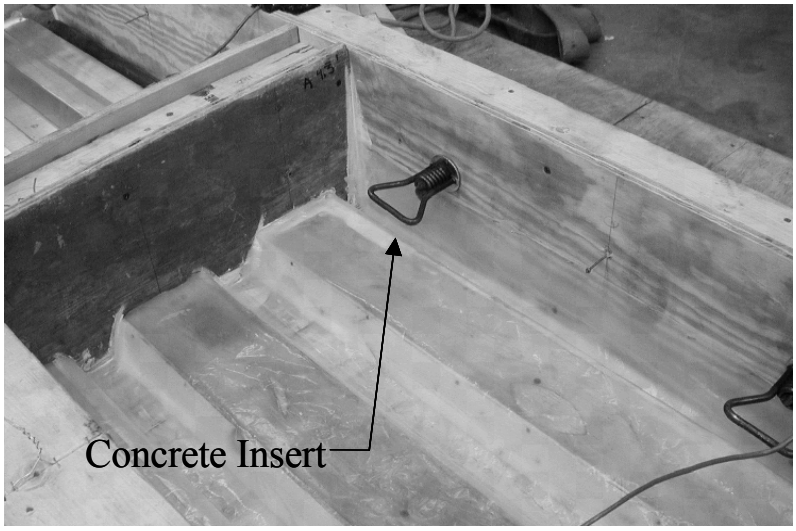

Figure 5.16: Formwork (Specimen 4)

5.4.2 Testing Frame

To accurately measure the amount of free shrinkage and curling of the deck models, the specimens were designed to be positioned vertically. This position allowed more accurate measurements of curling and provided negligible friction. Due to the weight of each deck model (a maximum stress of 4 psi), a small amount of creep was estimated (0.2 με), but was considered insignificant relative to the estimated shrinkage. Because of the difficulties in pouring the deck models in the vertical position, the specimens were cast in a flat position and then moved into the testing setup after curing.

The testing frame had two primary functions. It was used to prevent the deck models from tipping over or moving during testing and to secure the testing instrumentation. The testing frame was built in two sections (Figures 5.17 and 5.18). Both were completely constructed with 2 in. by 4 in. lumber. The testing frame was designed tall enough (4 ft) to ensure that the specimens could not tip over. Space was provided (2-½ ft) between each deck model to provide access to the instrumentation. The testing frame was also designed so that it did not touch the deck models except at the base of each specimen to eliminate friction and provide unrestrained shrinkage.

Figure 5.17: Testing Frame Before Placement of Specimens and Instrumentation

Figure 5.18: Testing Frame After Placement of Specimens and Instrumentation

5.5 Instrumentation Design and Installation

To monitor the shrinkage and curling of the deck models, five different types of instrumentation were implemented. Strain gages measured strains on both the reinforcing bars and the deck pans. Concrete strain gages were placed in each specimen to monitor internal strains. Linear voltage displacement transducers (LVDTs) were used to measure the displacement from the top of each specimen while Whittemore points were used to measure changes in displacement (strains) at the faces of each specimen. Thermocouples measured both internal and external temperatures of the deck models, and a hydrometer measured the relative humidity during testing. By applying the instrumentation at different locations through the specimen depth, it was possible to measure the strain distribution.

*5.5.1 Strain Gage*s

Micro Measurement strain gages were used for the experiment program. Four strain gages were applied to reinforcing bars, two in Specimen 1 and two in Specimen 7. All gages were orientated to measure strain parallel to the direction of the #4 and #5 reinforcing bars. Each gage was located in the middle of the length and width of the deck model (Figure 5.19 and 5.20). The strain gages were applied on the middle row of reinforcement in the event that additional drying shrinkage occurred near the sides of the model. Details of the strain gages are shown in Table 5.4. The strain gage installation procedure can be found in Appendix D.

Table 5.4: Strain Gage Details

Model Number	CEA-06-250UN-350
Gage Length	¼ ”
Resistance	350.0 Ω
Gage Factor	2.100
Excitation Voltage	3 V

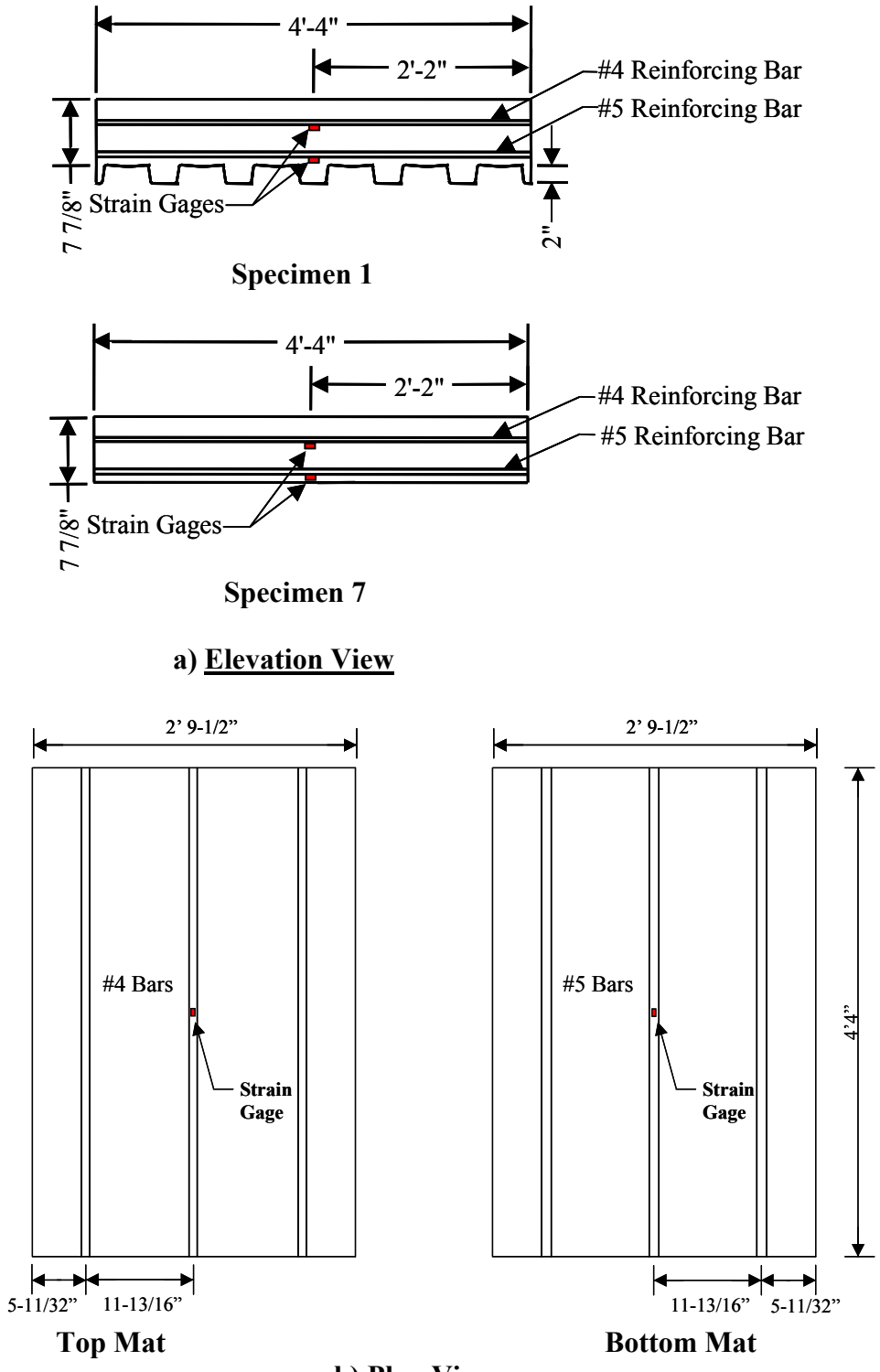

Figure 5.19: Reinforcement Strain Gage Locations (Specimen 1 and 7)

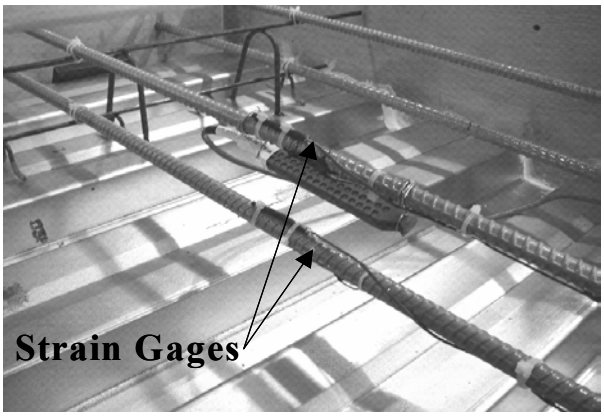

Figure 5.20: Strain Gages on the Bottom Side of the Reinforcing Bar

Six gages were applied to the bottom of the three deck models designed with deck pans (Specimens 1, 2, and 5). The strain gages on Specimens 1 and 5 were orientated to measure strain perpendicular to the ribs of the pan, but parallel to the length of the specimen. The strain gage on Specimen 2 was orientated parallel to both its deck pan and the length of the deck model. Of the two strain gages applied to each of the deck pans, one was placed on a top rib and the other on the bottom rib. Each gage was placed as close to the middle of the deck pan as possible (Figure 5.21).

Finally, one strain gage was used as a control gage. It was attached to a #5 epoxy coated reinforcing bar and orientated parallel to its length. This gage was monitored as all other gages, but was not exposed to any physical strains. The gage was used to measure the resolution of the strain gages, determine the level of noise produced by temperature changes, and determine if the measurements drifted.

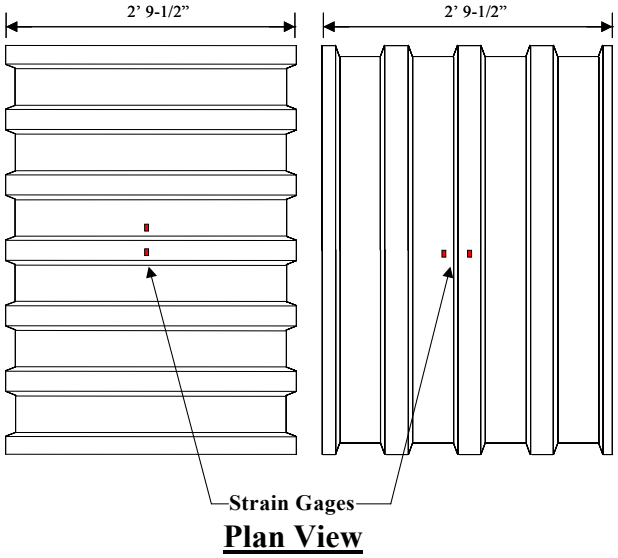

Figure 5.21: Deck Pan Strain Gage Locations

5.5.2 Internal Strain Gages

To measure internal concrete strains, 4 in. Micro Measurement concrete strain gages were installed in each of the deck models. Details for these gages are shown in Table 5.5. To obtain representative average strain values, the concrete strain gages were located at the center of the deck models (Figure 5.22). To position these gages correctly, wire was attached to the front and back of each gage and hung into position from either the top mat of reinforcement for Specimens 1 and 7 (Figure 5.22) or from a 2 in. by 4 in. piece of lumber running across the width of each deck model (Figures 5.13).

Table 5.5: Concrete Strain Gage Details

Model Number	EGP-5-350
Gage Length	4 ”
Resistance	350.0 Ω
Gage Factor	2.06
Excitation Voltage	3 V

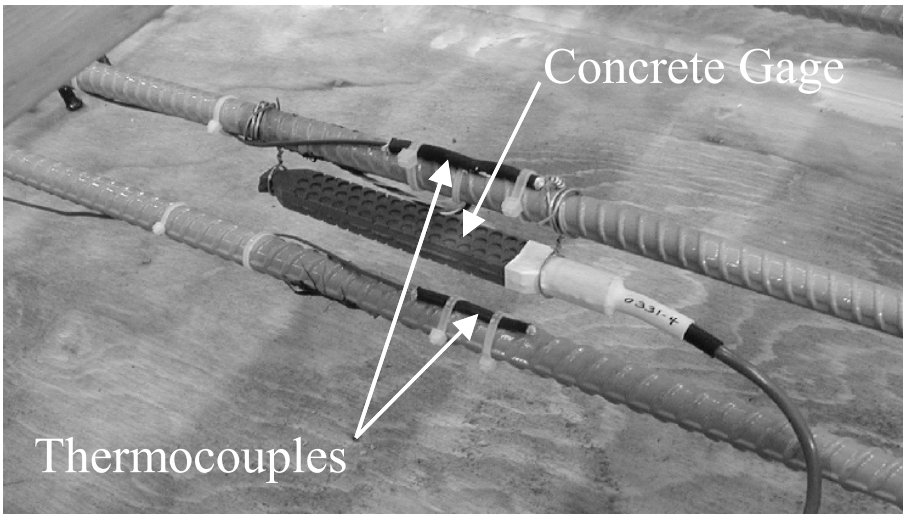

Figure 5.22: Location of Internal Concrete Gage and Thermocouples (Specimen 7)

5.5.3 LVDTs

Linear voltage displacement transducers (LVDTs) were used to monitor the displacement caused by shrinkage at the mid-depth of the deck models. Before the concrete was cast, threaded rods were installed through the formwork at a depth of approximately 4 in. (Figure 5.16). The threaded rods were located directly in the center of the width and height of the top end of each deck model so that the total magnitude of shrinkage from each specimen could be compared (Figure 5.23).

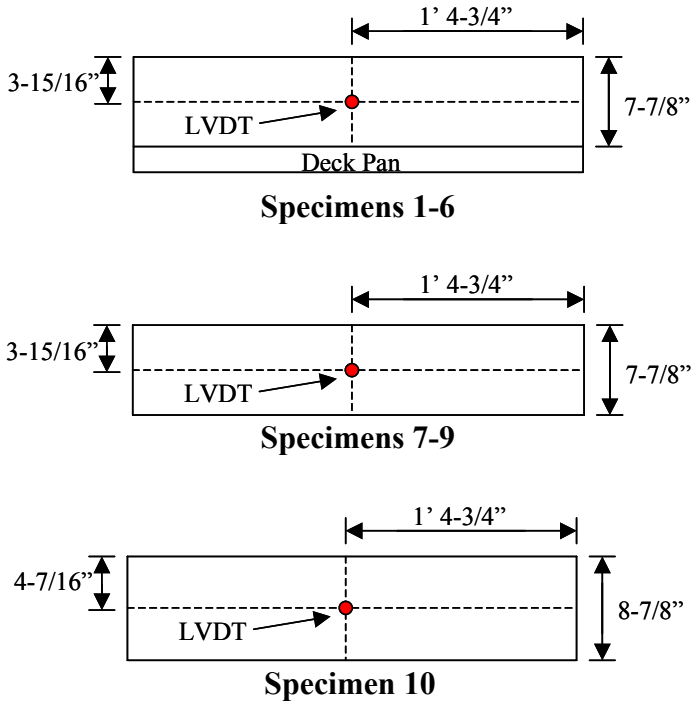

Figure 5.23: LVDT Locations Plan View

After the concrete was cast and the deck models cured, the specimens were lifted into the testing frame. The LVDT stands were installed and each threaded rod and screw-on-core were aligned with the LVDTs (Figure 5.24). To hold the LVDTs above the height of the deck models, stands were made with two 5-foot aluminum D-channels and a short metal angle to span across the thickness of each specimen. The LVDT stands were sturdy, but had a different value of thermal expansion ($\approx 13 \times 10^{-6}$ /^{o}F) from the concrete ($\approx 5.5 \times 10^{-6}$ /^{o}F) (Beer and Johnston 1992). With substantial ambient temperature changes, the LVDT stands can expand or contract more than the concrete deck models. However, due to the limited temperature changes expected inside the laboratory, additional displacement resulting from temperature changes was not considered a major factor.

Each LVDT was excited with 30 Volts and had an accuracy of 0.001 in. This accuracy was considered acceptable for the estimated shrinkage displacement of 0.02 in. Prior to testing, each LVDT was calibrated to ensure accurate results.

Once the LVDTs were aligned with each specimen, they were zeroed. Data acquisition began approximately 36 hours after the concrete had been cast.

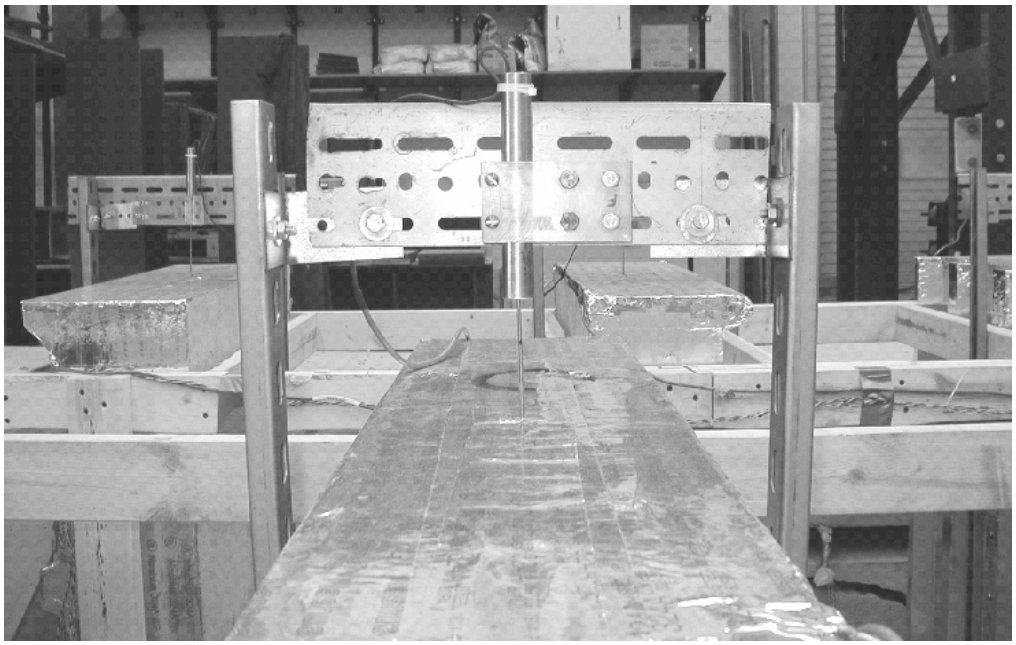

Figure 5.24: LVDT Location

5.5.4 Whittemore Gages

Application of Whittemore points on each deck model provided the capability of measuring shrinkage displacements on both faces of the specimens. Curling can be most easily determined by the difference in strain readings between the points located on the top face compared to those located on the bottom face of each specimen. The Whittemore points were placed on each face of all deck models except where the transverse deck pan shape restricted their placement. The Whittemore points were located in a vertical column 2 in. from centerline of the width (Figure 5.25). The points were located off-center to ensure the LVDT stands would not be disturbed while measurements were taken. Each column of Whittemore points consisted of seven points spaced at 5 in. The distance between each point was monitored daily with a Whittemore strain gage which can be read with an accuracy of 0.0001 in.

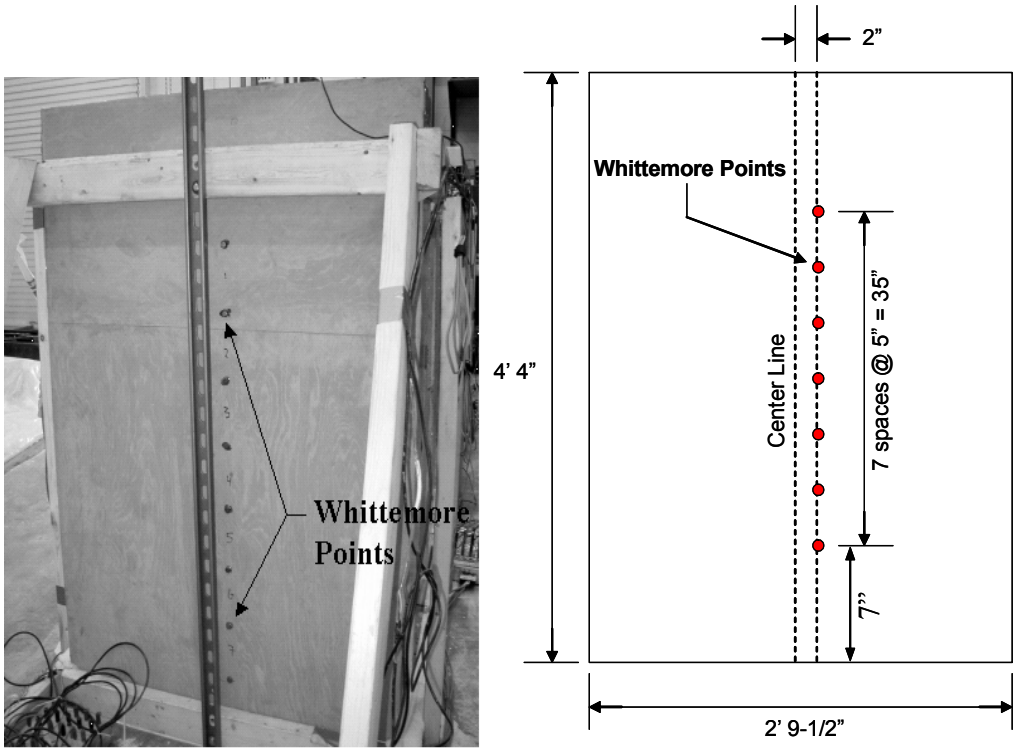

Figure 5.25: Spacing and Location of Whittemore Points

5.5.5 Thermocouples

Five thermocouples were used for the experimental program. Four of these gages were installed in the deck models, and one was used to monitor the ambient temperature in the laboratory. The concrete and air temperatures are important for several reasons. First, the high temperatures reached in the specimens during hydration may be directly related to residual stresses in a concrete bridge deck (NCHRP 380 1996). While the concrete is still in its plastic stage, internal temperatures can dramatically increase, significantly expanding the concrete, supporting girders, and deck pan. By the time the deck starts to cools, the concrete has increased in both strength and stiffness. Because the concrete at this time can resist strain, shrinkage of the girders and concrete during cooling can induce significant tensile and compressive stresses within the deck and girders. Therefore, higher hydration temperatures will lead to larger stresses, which could increase the possibility of early age concrete deck cracking.

Ambient temperature changes can also have considerable effects on stresses within a bridge deck. Because of the different thermal expansion rates between a steel girder ($\approx 6.5 \times 10^{-6}$ /^{o}F) and its composite concrete deck ($\approx 5.5 \times 10^{-6}$ /^{o}F), daily and yearly temperature cycles can induce added stresses and strains (Beer and Johnston 1992). Because this experimental program does not include composite girders with the deck models, the ambient thermocouple gages were not used for this purpose. The ambient temperature gages were used to monitor the difference in temperature between internal hydration and ambient temperature, to determine the effect of temperature variance on shrinkage, and to determine the measured displacements unrelated to shrinkage (i.e. differential expansion rates between LVDT stands and the concrete).

The two specimens including thermocouples were Specimens 1 and 7. These deck models were used because they had reinforcement on which the thermocouples could be attached. The gages were attached to the top of the #4 and #5 reinforcing bars in the middle section of the two specimens (Figures 5.22 and 5.26). This arrangement provides a good representation of the maximum temperature reached during hydration and a distribution through the depth of the deck models.

Two-wire, Type J, Micro Measurement gages were used to monitor temperatures. The two wires were stripped, twisted together, and tinned at the desired location of temperature monitoring. These wires were then protected by a coating of silicon followed by shrink-wrapping the twisted end of the wire.

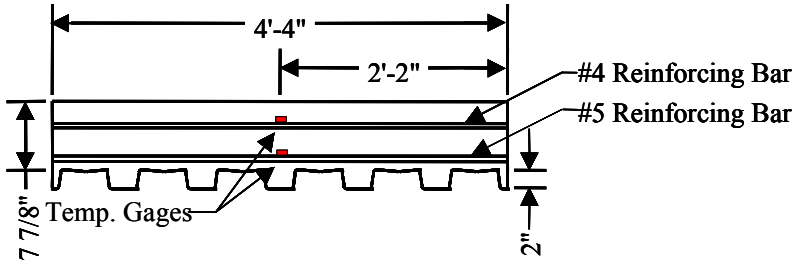

Specimen 1

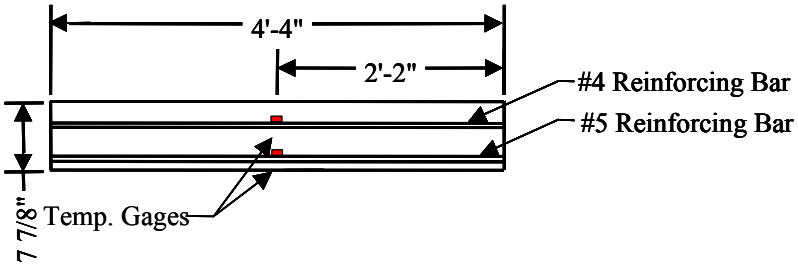

Specimen 7

Figure 5.26: Location of Thermocouples (Specimens 1 and 7)

5.5.6 Relative Humidity Gage

During casting and throughout the monitored shrinkage period, the relative humidity was monitored with a Fisher Scientific Hygrometer (Model 11-661-19). Relative humidity is important because of its direct relationship with shrinkage. An increased relative humidity will allow less water to evaporate from a concrete specimen. As the relative humidity decreases, the drying shrinkage rate will increase. Chapter 1 provides additional information on the importance of the relative humidity to concrete curing and shrinkage.

5.6 Casting and Curing

The deck specimens were cast in a flat position simulating actual deck placement. All specimens were cast on July 31, 2001. After the concrete had been placed into the forms, the specimens were screeded and finished with trowels (Figure 5.27). The specimens were then allowed to set for two and half hours before wet burlap and plastic were used to cover the exposed top surfaces of the deck models.

Figure 5.27: Deck Model Finishing

Because much of the overall shrinkage of concrete occurs within the first days after casting, the experiential program was designed with only one day of wet curing to simulate a worst case scenario. This curing schedule was also used so that the specimens could be moved to the test setup to begin monitoring of shrinkage. The short curing time may exaggerate the amount of drying shrinkage to each deck model, but the magnitude of the difference between specimens should remain constant. Wet curing consisted of covering the deck models and test cylinders with saturated burlap and plastic (Figures 5.28 and 5.29). The burlap was saturated periodically to ensure that the surface of the deck models remained moist at all times. Table 5.6 shows the time line of events for the placement and curing of the deck models.

Table 5.6: Time Line For Placement and Curing of Specimens

Task	Time	Day
Arrival of Concrete	10:35 AM	31-Jul
Start Concrete placement	10:55 AM	31-Jul
Finish Concrete Placement	11:25 AM	31-Jul
Finishing Operation Complete	12:20 PM	31-Jul
Placement of Burlap and Plastic	2:50 PM	31-Jul
First Wetting of Burlap	2:55 PM	31-Jul
Second Wetting of Burlap	9:25 PM	31-Jul
Third Wetting of Burlap	8:25 AM	1-Aug
Removal of Plastic and Burlap	12:05 PM	1-Aug

Figure 5.28: Deck Models Covered with Burlap and Plastic

Figure 5.29: Wetting of Burlap

5.7 Testing Setup and Procedure

After the deck specimens were cured for 24 hours, the burlap and plastic were removed. Before the specimens were removed from their forms, Whittemore points were epoxied to the top faces of all specimens, and three concrete cylinders were tested to ensure that the specimens would not crack under their own weight when lifted. After completing these steps, the specimens were removed from their forms (Figure 5.30). A time line of events is presented in Table 5.7.

Table 5.7: Time Line For Transferring Specimens

Task	Time	Day
24 Hours of Curing Completed	12:00 PM	1-Aug
Removal of Plastic and Burlap	12:05 PM	1-Aug
Concrete Compressive Test Strength Completed	12:20 PM	1-Aug
Whittemore Point Application Completed	1:50 PM	1-Aug
First Deck Model (Specimen #10) Installed	2:35 PM	1-Aug
Last Deck Model (Specimen #1) Installed	11:35 PM	1-Aug
LVDT Data Acquisition Begun	12:35 AM	2-Aug

Figure 5.30: Transferring Deck Models to the Testing Frame

Each specimen, after being removed, was turned over so that Whittemore points could be applied on their bottom face (there were no points applied to the bottom face of models with a transverse deck model shape, Specimens 1, 4, 5, and 6). At this time, the sides and tops (when standing on one end) of all the specimens were covered with 3 in. wide aluminum tape. The tape was used to minimize the amount of moisture loss from the models and replicate a cut section from a bridge deck. Deck models that were designed as "sealed" (Specimens 3, 4, and 8) were also covered with the same aluminum tape on their bottom face (Figure 5.31).

Figure 5.31: Aluminum Tape Applied to Specimen 3

Once the aluminum tape and Whittemore points were completely applied to the specimens, the deck models were installed in the testing frame and hydrostoned to the floor. Hydrostone was used to provide a uniform bearing surface and to secure the specimens. Once in place, the LVDTs and their stands were installed.

Figure 5.32: Installing Deck Models Into Test Frame

Data was collected using a Micro Measurements 5100 series data acquisition system. This system accepted input from the strain gages, concrete gages, LVDTs, and thermocouples. The timeline for data acquisition is shown in Table 5.8. Data acquisition of all the strain gages, concrete gages, and thermocouples began approximately one hour before the concrete was poured. Data was acquired continuously at 15-minute intervals. After the specimens were installed in the testing setup, the LVDTs were installed and zeroed. Subsequently, data acquisition of the LVDTs began recording continuously in 15-minute intervals. In addition, data from the humidity gage was manually recorded twice a day during the monitoring period. The specimens were tested for 78 days. However, the first month (28 days) of data was of primary interest since early age cracks typically occur during this time frame.

Table 5.8: Time Line of Event For Data Acquisition

TASK	TIME	DAY
Data Acquisition of Strain Gages and Thermocouples Started	9:35 AM	31-Jul
Start Concrete Placement	10:55 AM	31-Jul
Finish Concrete Placement	11:20 AM	31-Jul
Finished installation of LVDT Stands	12:15 AM	1-Aug
LVDTs Calibrated and Data Acquisition Started	12:35 AM	1-Aug

5.8 Results

5.8.1 General Behavior

Figure 5.33 presents measurements from a typical internal temperature gage and the ambient temperature gage over the first six days of testing. Hydration temperatures reached approximately 115^{o} F ($\approx 40^{o}$ F above ambient) in each specimen monitored The thermocouples in Specimen 1 and 7 showed an increase in concrete temperature for approximately 12 hours.

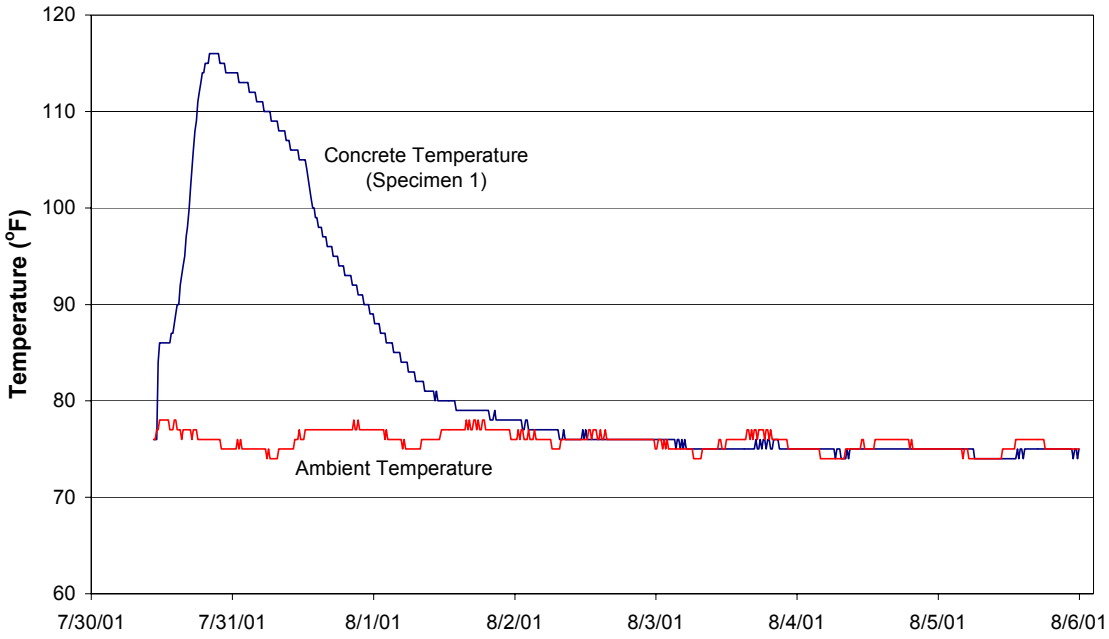

Figure 5.33: Hydration temperatures (Specimen 1)

The strain gage readings also reflect the influence of the heat of hydration. The strain induced on the deck pan, internal concrete strain gage, and reinforcing bars are plotted in Figure 5.34 to shown the effect of hydration temperature on Specimen 1. As the hydration temperature increased, the internal strain gages measured increasing strain (tension). The strain gages located on the bottom side of the deck pans also were affected by the temperature changes, but not of the same magnitude as the internal strain gages. After the peak hydration temperature had been reached, the strain gage measurements started to decrease in strain (compression). The strain gages did not respond immediately to the temperature change, but within two hours, each reflected that the concrete had started to cool.

Without directly reading the internal temperature gages, it was not possible to determine when the internal temperatures of the specimens reach ambient levels from the strain gage data. The rate of decreasing strain did not level off after the specimens had completely cooled.

Within approximately 72 hours after casting, internal concrete temperatures returned to the ambient temperature and remained equivalent for the remainder of the testing period. Only slight day to night temperature changes were observed after the original hydration temperature. The maximum and minimum recorded ambient temperatures within the laboratory were 78^{o} F and 64^{o} F, respectively (Figure 5.35).

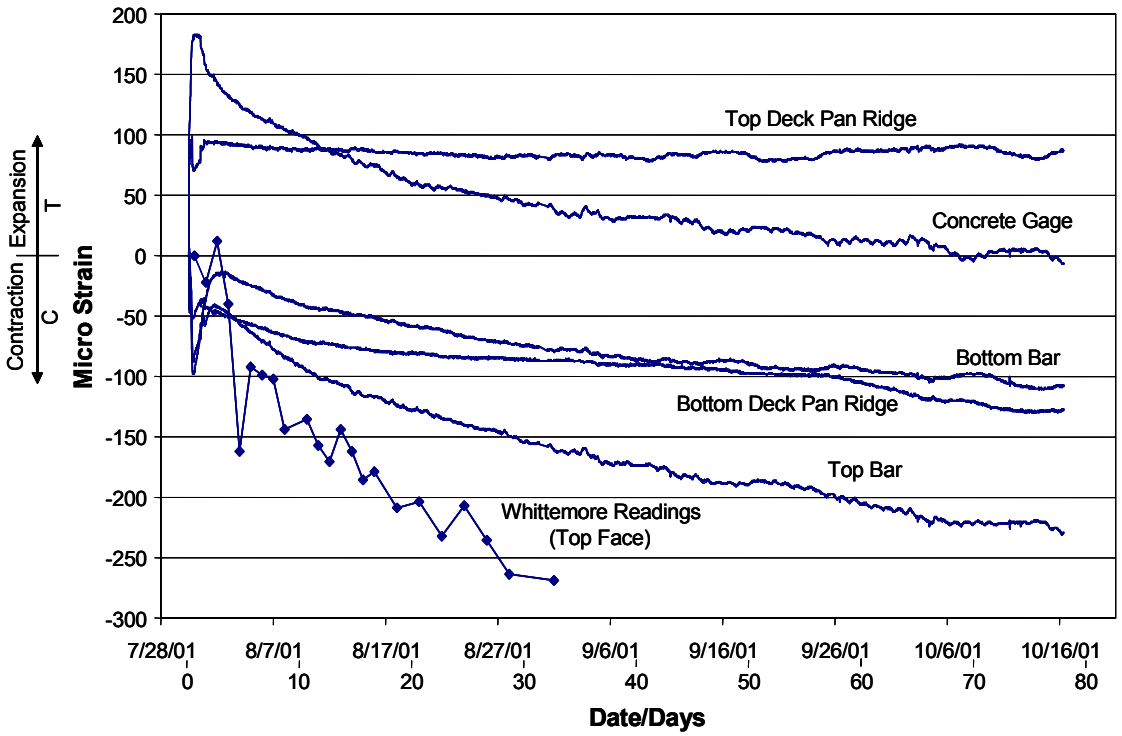

Figure 5.34: Shrinkage Measurements (Specimen 1)

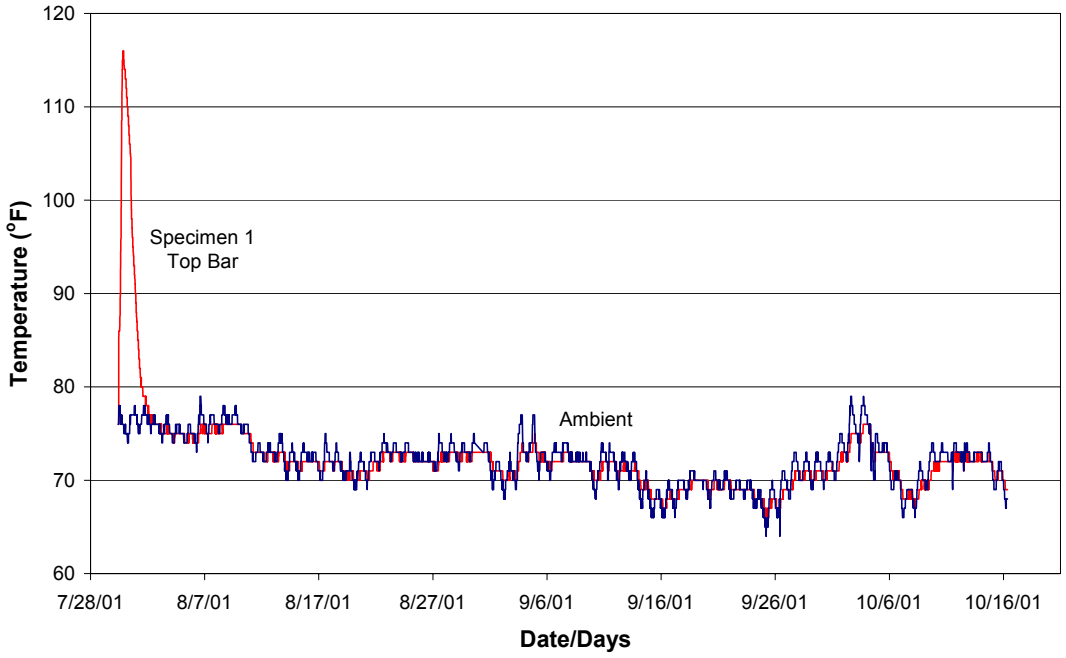

Figure 5.35: Concrete and Ambient Temperature Readings

The increase in strain due to hydration temperatures (based on concrete gage readings) varied between each specimen, but all were within the same range (≈150-250με). Before the specimens reached ambient temperatures, the decrease in strain also

varied (≈25-100με). Figures 5.36 and 3.37 display the data collected for the complete testing period from the internal concrete gages and LVDTs. The data from each specimen is labeled by its number designation. The concrete gage located within Specimen 10 was lost during casting and therefore is not shown.

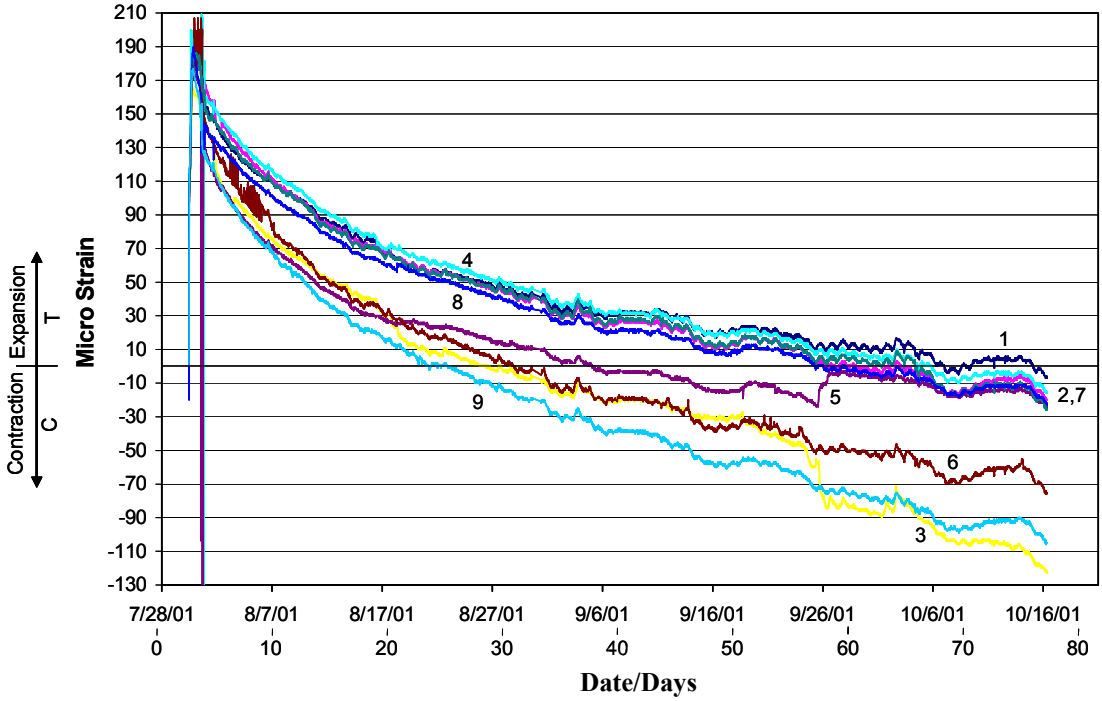

Figure 5.36: Data Collected by the Concrete Strain Gages

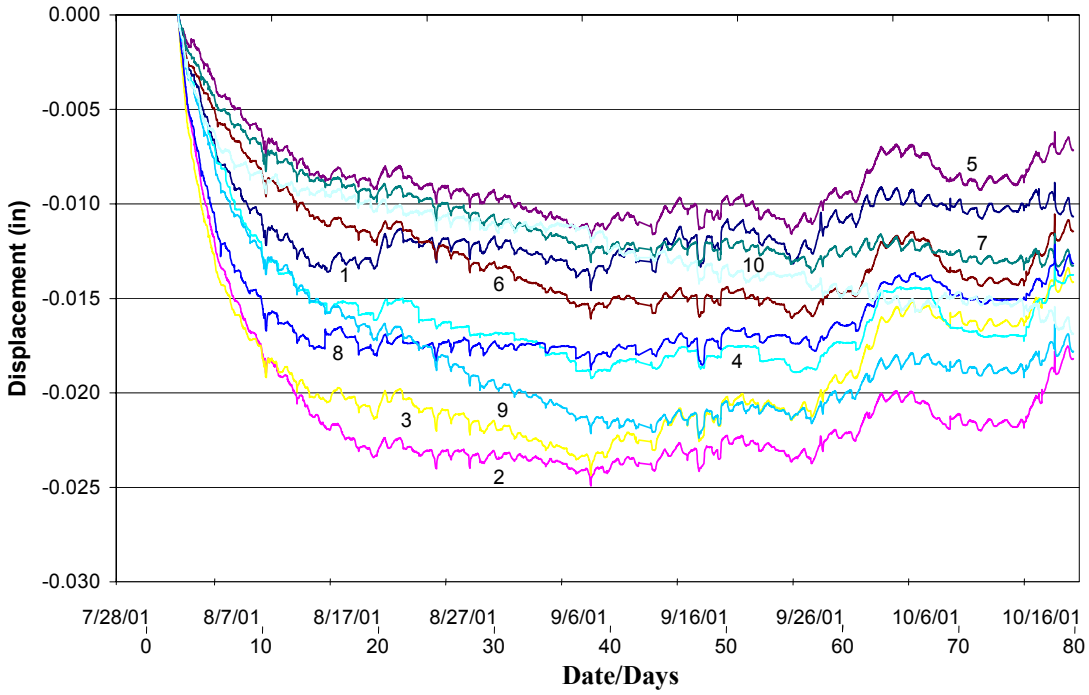

Figure 5.37: Data Collected by the LVDTs

Once the ambient and internal concrete temperatures were similar, both internal strain gage data and external Whittemore point readings indicated that the specimens were shrinking. During testing the difference between each of the specimens could be examined by comparing the slopes of the strain data. The data suggested that differences could be determined between form type and sealing effect. The strain gage data from the specimens containing reinforcement also indicates differences in comparison to those specimens without reinforcement. Differential displacements (on each specimen face) measured daily from Whittemore points indicated that some specimens started to curl immediately after the hydration temperatures had reached equilibrium with the ambient temperature. The curling increased throughout the testing period, as shown by the difference in surface strains in Figure 5.38.

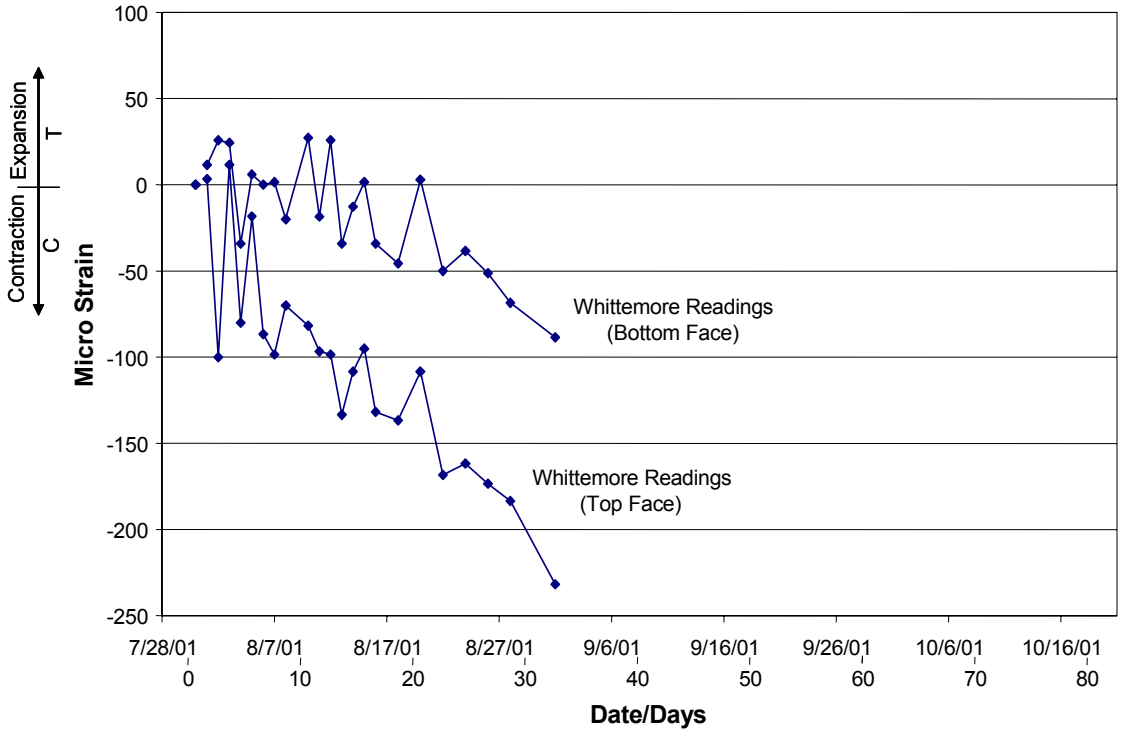

Figure 5.38: Whittemore Readings (Specimen 10)

At no point during testing did the specimens (according to the strain gage readings) stop shrinking; however, the rate of shrinkage declined over time (Figure 5.36). The LVDT data, plotted in Figure 5.37, suggests that soon after a month of testing, the specimens stopped shrinking. However, as noted above, the strain gage data does not suggest that shrinkage stopped. The test was terminated approximately 2 months after the specimens were cast. All data collected from each specimen is available in Appendix E.

5.8.2 Relative Humidity

As discussed in Chapter 1, the relative humidity can affect curing, concrete strength gain, early-age shrinkage, and cracking. Therefore, a hydrometer gage was used to monitor the relative humidity. As shown in Figure 5.39, the relative humidity did not vary significantly. On average, the humidity remained at approximately 60 %.

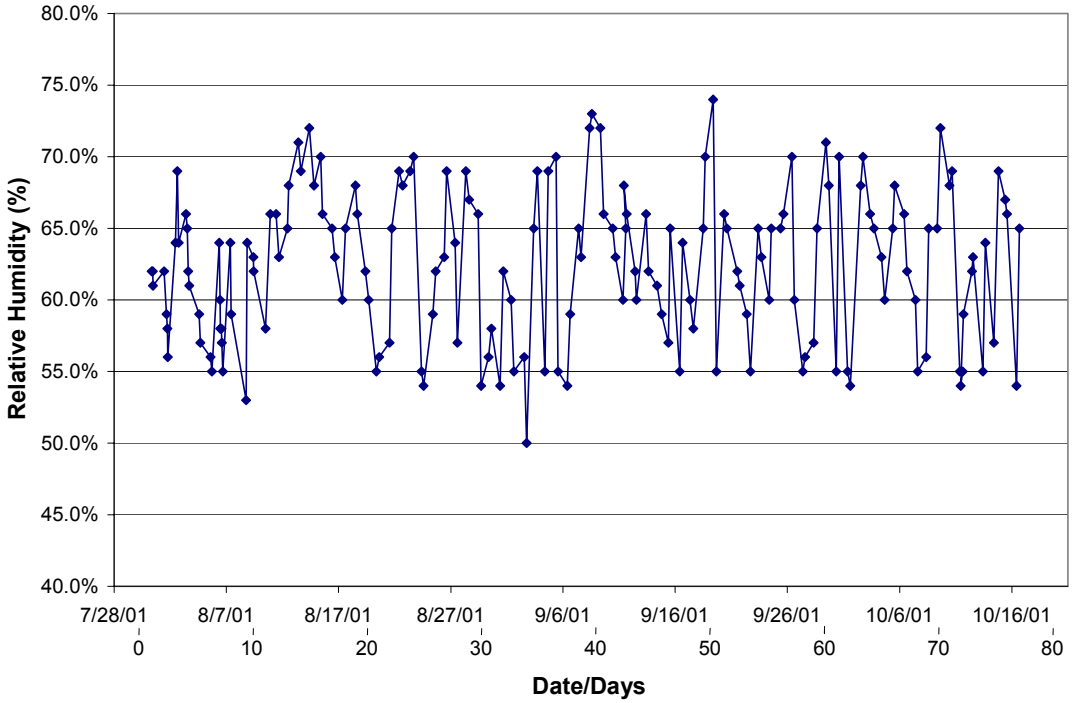

Figure 5.39: Relative Humidity During Testing

5.8.3 Control Gage

During the data acquisition period, one strain gage was used to monitor the effect of temperature on strain readings and to monitor the stability of the readings during the testing period. The gage was placed on a #5 reinforcing bar next to the test specimens. As shown in Figure 5.40, the strain gage was very stable during testing. The length of testing did not affect the results of this gage indicating that strain readings can be assumed with an accuracy of +/- 5 microstrains.

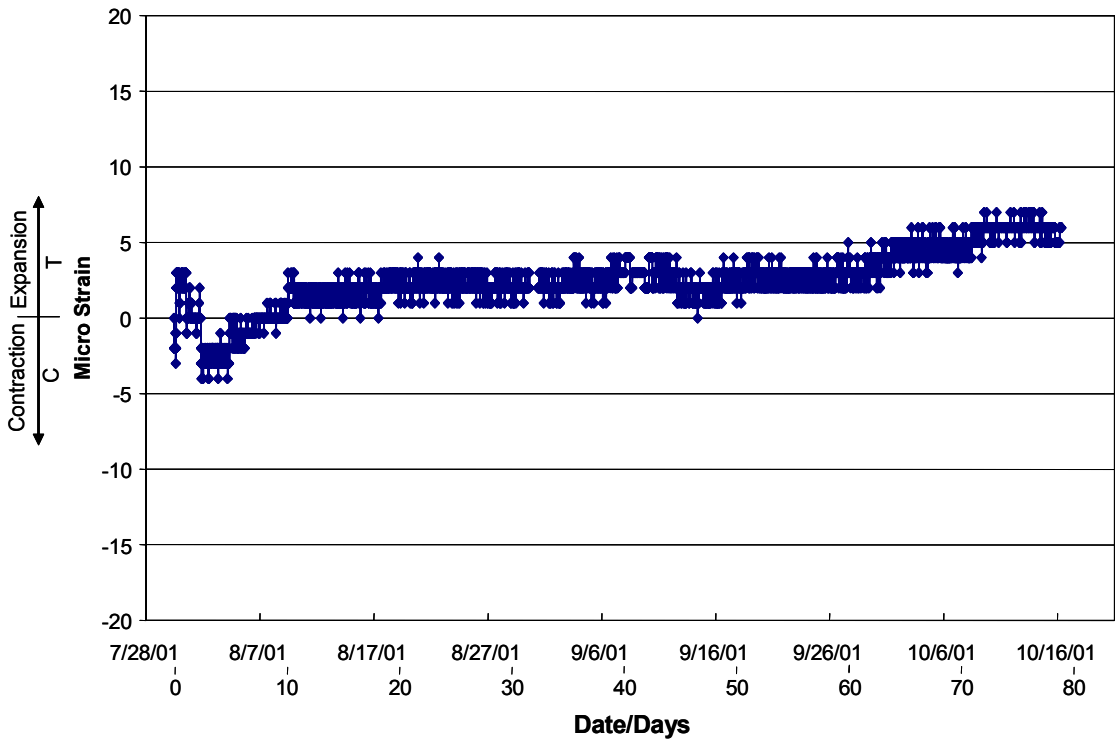

Figure 5.40: Data Collected From the Control Gage

5.9 Strain Profiles

To visualize the measured strain data, the strain distribution of each specimen is plotted in Figure 5.41. The data shown is for the first month (28 days) of monitoring starting immediately after the hydration temperatures had peaked (July 30, 10:00 PM). Analysis of the specimens will compare data collected during the first month to directly correlate with early-age cracking. Strains at the surfaces were obtained from the Whittemore data while internal strains were recorded directly from the strain gages. Since the reinforcement strain gages were placed on the bottom of each bar, the data obtained was plotted at that location and not at the center of the bar.

During casting, the internal concrete strain gage in Specimen 10 was lost, and consequently, the only available data to create the strain profile was from the Whittemore gage. These two data points have been plotted in Figure 5.41; however the strain data was not adequate to define the strain profile. Also, only two data points were available from Specimen 6.

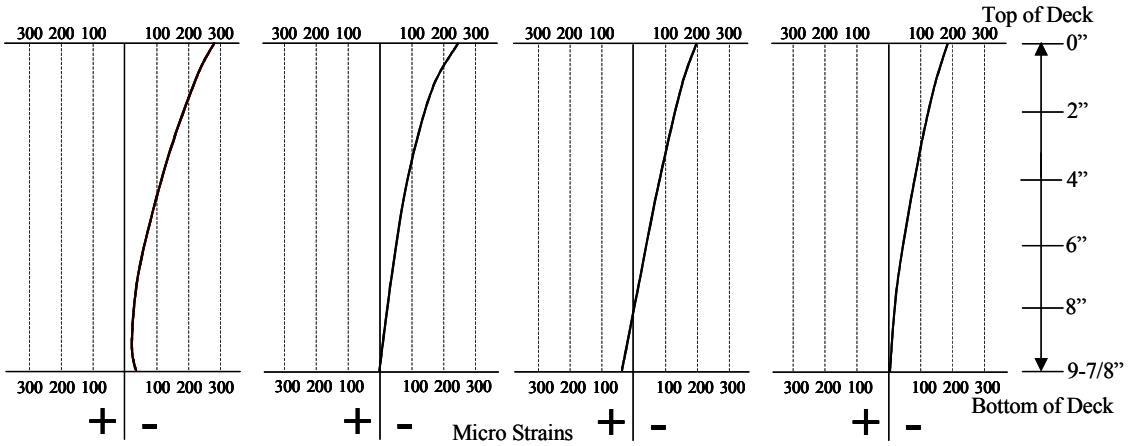

Figure 5.41a: Strain Profiles of Deck Models After One Month of Testing (Specimens 1-4)

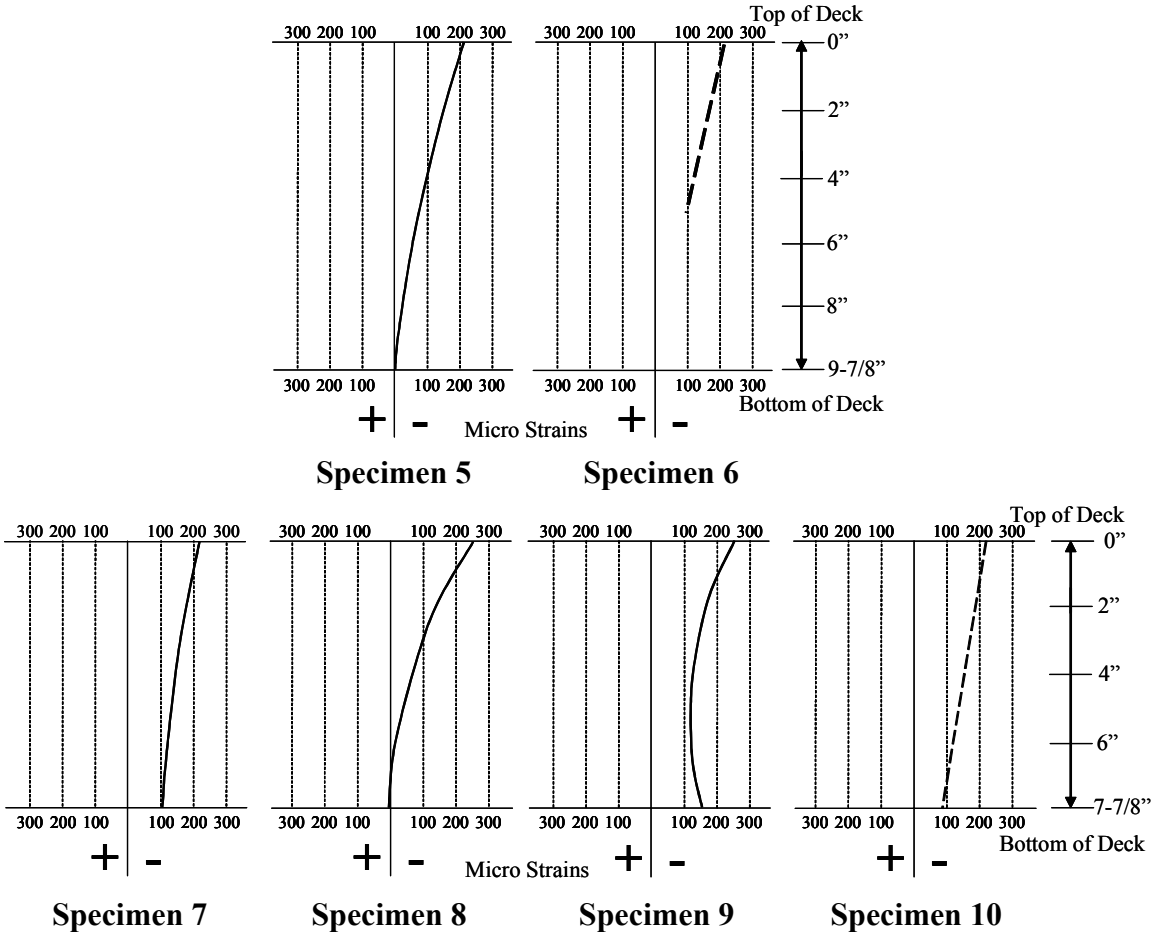

Figure 5.41b: Strain Profiles of Deck Models After One Month of Testing (Specimens 5-10)

In most cases, the data from the instrumentation indicated a strain profile that was nonlinear. Cracking was not observed on the surfaces of the specimens so compatibility was assumed to exist across the section depth.

In general, a larger change in displacement (converted into strain) was measured on the top surfaces of the specimens than on the bottom surface. The largest top and bottom surface magnitude strains were -280 με (Specimen 1) and -144 με (Specimen 9) respectively. The smallest top and bottom surface magnitude strains were -178 με (Specimen 4) and 5 με (Specimen 8) respectively. From the data collected from each specimen, the curvature magnitudes were calculated for each specimen. The curvature was determined based on a linear regression of the measured data points (Table 5.9).

Table 5.9: Curvature of Specimens

Specimen	Curvature (μ/in)
1	24.2
2	24.7
3	23.5
4	18.1
5	22.3
6	22.0
7	15.2
8	31.4
9	13.0
10	17.8

The magnitude of curvature provides an estimation of the curling experienced by each specimen. The largest curvature value was calculated from Specimen 8, which was designed with flat wood forms and sealed on the bottom surface. The smallest curvature values were calculated from Specimen 7, which was designed with flat wood forms and reinforcement.

5.10 Data Analysis

5.10.1 Effect of Deck Pan Stiffness

5.10.1.1 Transverse Orientation

The results from Specimens 4 and 5 were compared to determine how the stiffness of the deck pan in the transverse direction (ribs perpendicular to the direction of shrinkage) affected the shrinkage strain profiles. Specimen 4 was built in the shape of a transverse deck pan and was sealed, but did not have a deck pan. Specimen 5 was built with a transverse deck pan; therefore, it was exactly the same as Specimen 4 but included the stiffness of the pan. Neither of the specimens was reinforced.

Results from the concrete strain gages (Figure 5.42) show that Specimen 4 and 5 resulted in approximately the same amount of strain after one month. The difference in strain was approximately 5με, a 4% difference.

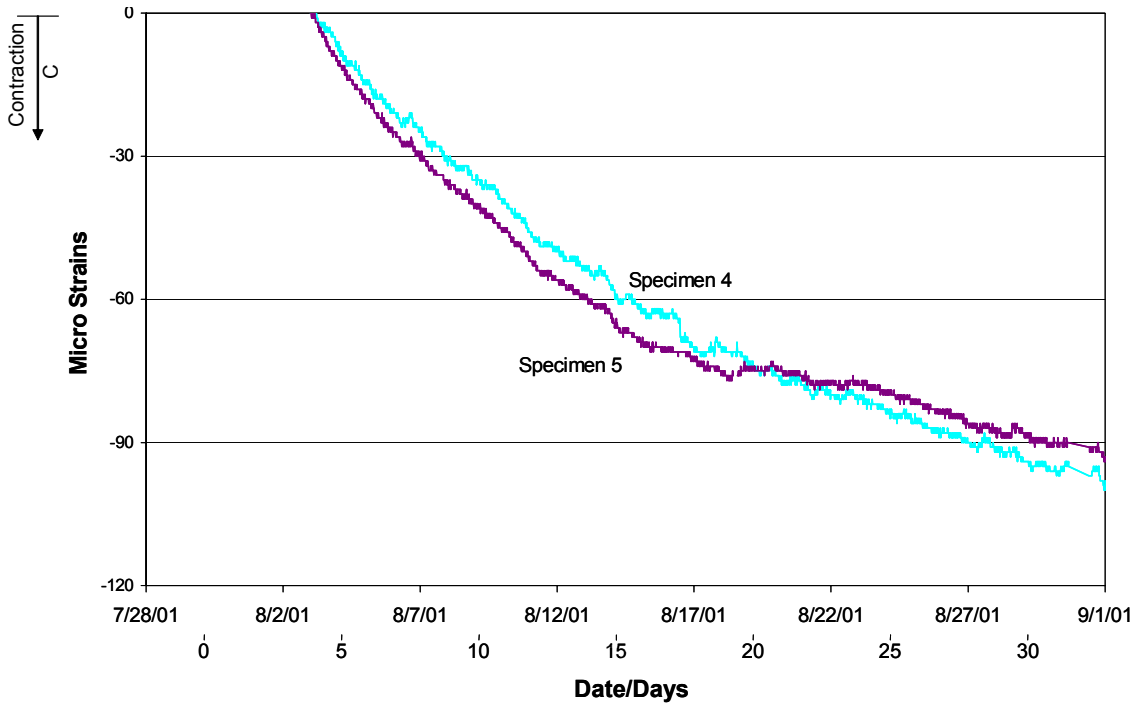

Figure 5.42: Internal Strain Gage Data (Specimens 4 and 5)

The data was also examined to determine if the stiffness of the deck pan affected the magnitude of curvature between Specimens 4 and 5. The difference in curvature was not significant (Figure 5.41 and Table 5.9). Therefore, the data suggests that the stiffness of the deck pan had little effect on the final strain profile of the deck specimens. Because a deck pan is only designed to span between girders in its longitudinal direction, bending resistance about its longitudinal axis is not necessary and consequently did not provide significant shrinkage resistance. The results also imply that the aluminum tape, acting as a sealant, worked sufficiently for Specimen 4. It must be noted that the above conclusions assume that the deck pan was adequately bonded to the concrete, which is reasonable.

5.10.1.2 Longitudinal Orientation

Specimens 2 and 3 were compared to determine the effect of the stiffness of the deck pan in the longitudinal direction (ribs parallel to the direction of shrinkage). Specimen 2 was built with a deck pan orientated in the longitudinal direction while Specimen 3 was built in the shape of a longitudinal deck pan and sealed, but without the deck pan's stiffness. Because a deck pan is designed to span in one direction only (transverse to the bridge girders), its moment of inertia is largest in that direction. Therefore, the effect of the deck pan should be more significant in the longitudinal direction.

By comparing the concrete strain gage data, it can be seen that Specimen 3 resulted in 15 με (≈ 11%) greater than Specimen 2 during the first month of shrinkage (Figure 5.43). This difference is more than twice that found when comparing the effect of stiffness from the deck pan in the transverse direction (Specimen 5). Therefore, the data suggests that the deck pan's stiffness has more effect when aligned in the longitudinal direction. However, it must be noted that this variation is small and is fairly insignificant.

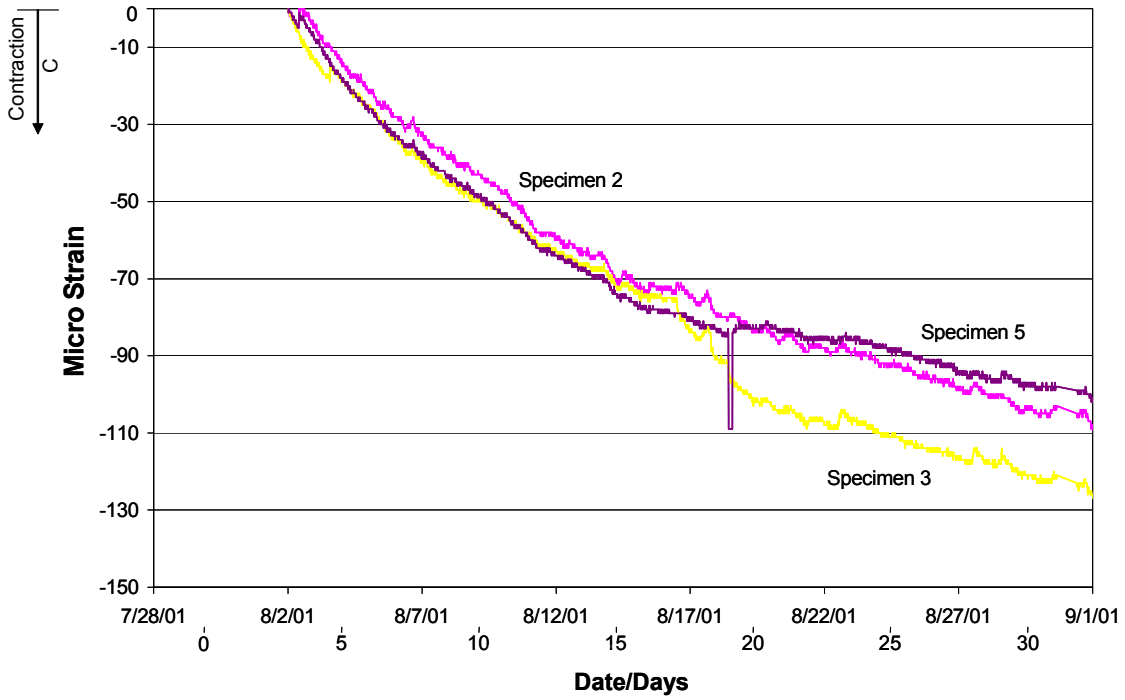

Figure 5.43: Internal Strain Gage Data (Specimens 2, 3 and 5)

The effect of the stiffness of the deck pan on curling can also be examined by comparing Specimens 2 and 3. A variation in curvature between these specimens can be noted, but these differences are relatively small (Table 5.9). More significantly, the strain from Specimen 2, at its bottom surface, was practically zero after one month of shrinkage (Figure 5.41). However, this was not the case for Specimen 3. The strain profile for this specimen shows that the strain at the bottom surface of the slab was positive. This result provides evidence that the aluminum tape sufficiently sealed Specimen 3 and confirms that very little shrinkage occurred at this location during the first month of concrete decks' life. These results also indicate that the deck pan's stiffness in Specimen 2 must have resisted the small amount of tension found in Specimen 3.

5.10.2 Sealing Effect of a Deck Pan

To determine the effect that a SIP deck pan has on the total shrinkage and curling of a concrete bridge deck, the results of Specimens 5 and 6 were compared. Specimen 5 was built with a transverse deck pan, while Specimen 6 was built in the shape of a transverse deck pan but not sealed. The difference in curling between each specimen was determined using the curvature found from the strain profile (Table 5.9).

The curvature of Specimen 5 (with deck pan) was found to increase by ≈1% when compared to Specimen 6. The stiffness of the deck pan in the transverse direction may cause a discrepancy when comparing the results, but the data presented previously in Section 5.10.1 suggests that it had a minor effect on the total shrinkage and curling of each specimen.

Even though the curvature of Specimen 5 was slightly larger than that measured in Specimen 6, the total magnitude of shrinkage was larger for Specimen 6. This can be seen from the internal concrete strain gage data plotted in Figure 5.44. After one month of shrinkage, the concrete gages in Specimen 6 picked up an additional 30 με when compared to Specimen 5 (≈ 23% more strain).

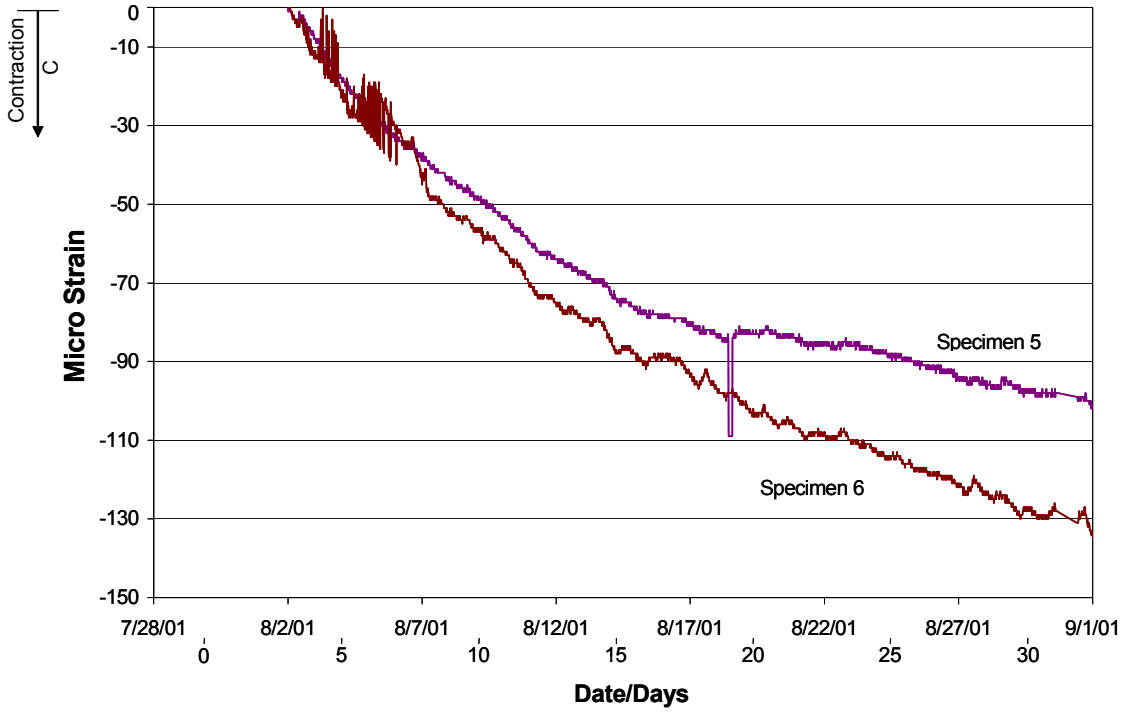

Figure 5.44: Internal Strain Gage Data (Specimens 5 and 6)

A concrete specimen with a larger surface-to-volume ratio (under similar environmental conditions) will shrink more quickly and to a greater extent than one with a smaller surface-to-volume ratio. The increased surface area will allow more water to escape from the specimen at a faster rate. In the case of these two specimens, the surface-to-volume ratios of Specimens 5 and 6 are 0.104 and 0.254 respectively (144% increase). The increase in this ratio is more than twice the difference because of the ribbed shape of the deck pan. Following this rationale, it would then be assumed that Specimen 6 would shrink more (as it did), and therefore be more susceptible to early-age cracking.

The magnitude of shrinkage, however, may not directly correlate with the amount of transverse cracking in a bridge deck. Because the bottom side of Specimen 5 was sealed it curled slightly more than Specimen 6 (1% greater). The increase in curling will produce larger negative moments on the top surface of a bridge deck and can increase the probability of cracking.

Specimens 1 and 7 were also used to investigate the sealing effect of the deck pan. Specimen 1 and 7 were built exactly the same, while Specimen 1 was built with a deck pan and Specimen 7 was built with flat wood forms. Both were reinforced with steel and both contained more instrumentation that provided additional strain data through the depth. The strain recorded in both the bottom and top bars in Specimen 7 were very similar (Figure 5.45). After the initial hydration period, the strain in the top and bottom bars of Specimen 7 increased approximately 180 and 160 με, respectively, in compression. At the same time, Specimen 1 picked up 120 and 55 με in the top and bottom bars, respectively.

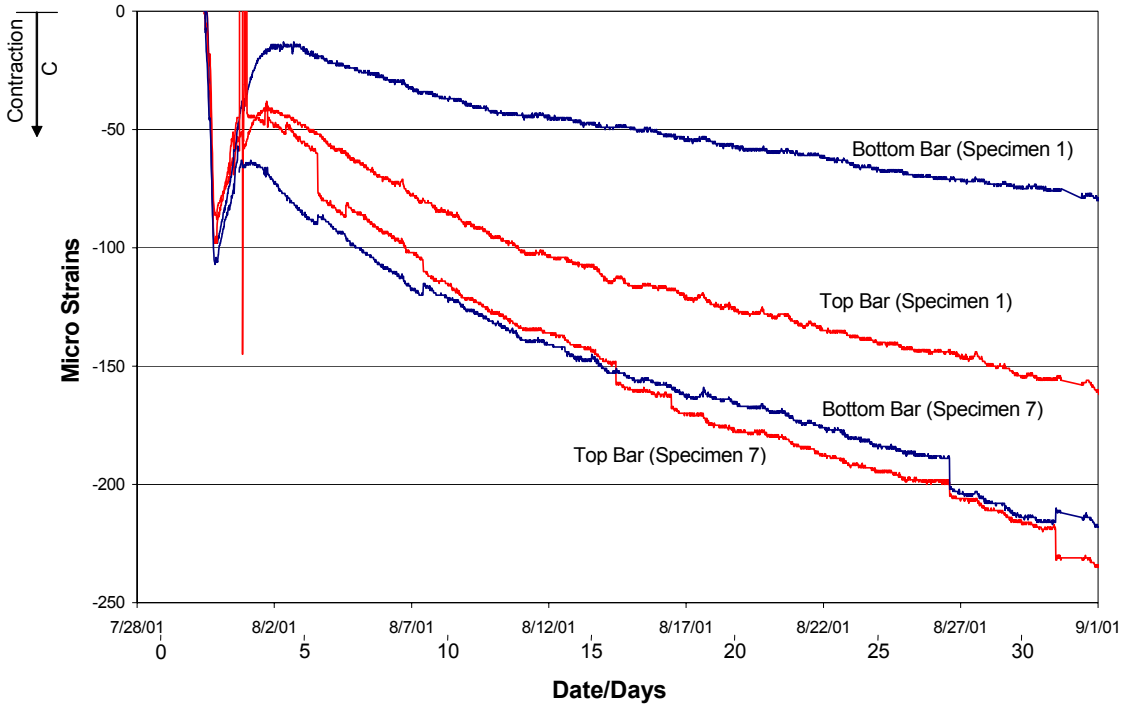

Figure 5.45: Reinforcement Strain Gage Data (Specimens 1 and 7)

Because the concrete on the bottom surface of Specimen 1 did not shrink as much as on the top surface, the difference in strain measurements from the top and bottom mat of steel increased substantially when compared against the data found from Specimen 7. The strain profile through the depth of Specimen 1 shows an increase of over 50% in curvature when compared with the data from Specimen 7 (Table 5.9).

As before, the specimen with the larger surface-to-volume ratio (Specimen 7) shrank more during the testing period. In fact, both reinforcing bars in Specimen 7 resulted in larger strain magnitudes than found in Specimen 1. Therefore, even though Specimen 1 curled more than Specimen 7, it is difficult to determine which form type would be more susceptible to early age cracking, one that induces less shrinkage or one that results in less curling.

5.10.3 Effect of Reinforcement

Specimens 1 and 7 were the only specimens that contained reinforcing bars. The reinforcement layout was identical to the I65 over SR25 bridge deck as previously discussed in Chapter 3. Specimen 1 was constructed with a deck pan (in the transverse direction) while Specimen 7 was constructed using flat wood forms. The depth of each the specimen (not including the depth of the deck form) were both approximately 8 in.

The most obvious effect the reinforcement had on the two specimens can be seen from the internal concrete gage data located directly in the center of each specimen. Of the ten deck models, both Specimens 1 and 7 had the second and third least (2 με difference) amount of final strain (Figure 5.46). Because these two specimens had the largest axial and bending resistance of all ten specimens, the concrete strain gage data appears accurate.

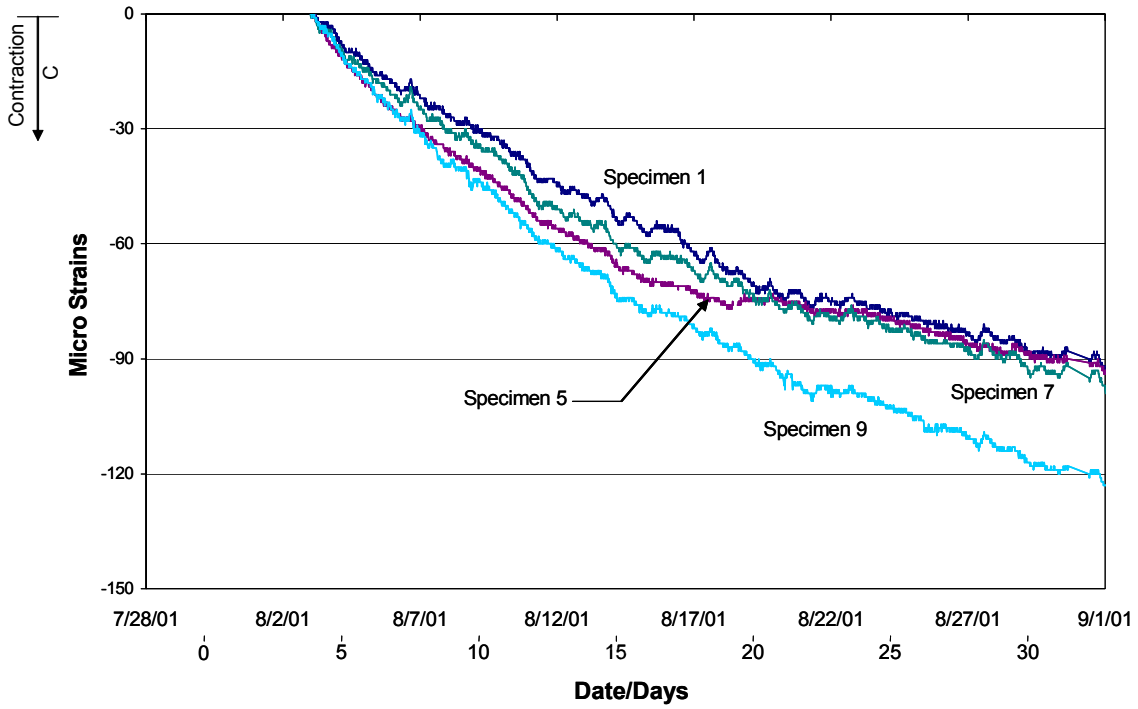

Figure 5.46: Internal Strain Gage Data (Specimens 1, 5, 7 and 9)

To further understand the effect of the reinforcement on the decks, Specimen 5 was designed the same as Specimen 1 but without reinforcement and Specimen 9 was designed the same as Specimen 7 but also without reinforcement. The unreinforced specimens developed more shrinkage strain from the concrete gages than from the reinforced specimens (Figure 5.46). An additional 6 με was measured from Specimen 5. Also, an additional 24 με was measured from Specimen 9. Specimen 9 ultimately resulted in the largest strain of all specimens at the location of the concrete gage. It seems from the data presented in Figure 5.46 that reinforcement plays more of a role in a specimen built with wood forms than one which is built with SIP deck pan forms. This may be because the specimens constructed with wood forms shrank more than those constructed with SIP forms. Also, the SIP forms can act as reinforcement.

Another implication the reinforcement had on the specimens was the overall curvature of the deck models, which can be seen by comparing the deck models constructed with and without reinforcement (Specimen 1 versus 5 and 7 versus 9). Figure 5.47 presents the strain profiles of Specimens 1, 5, 7 and 9 after one month of shrinkage.

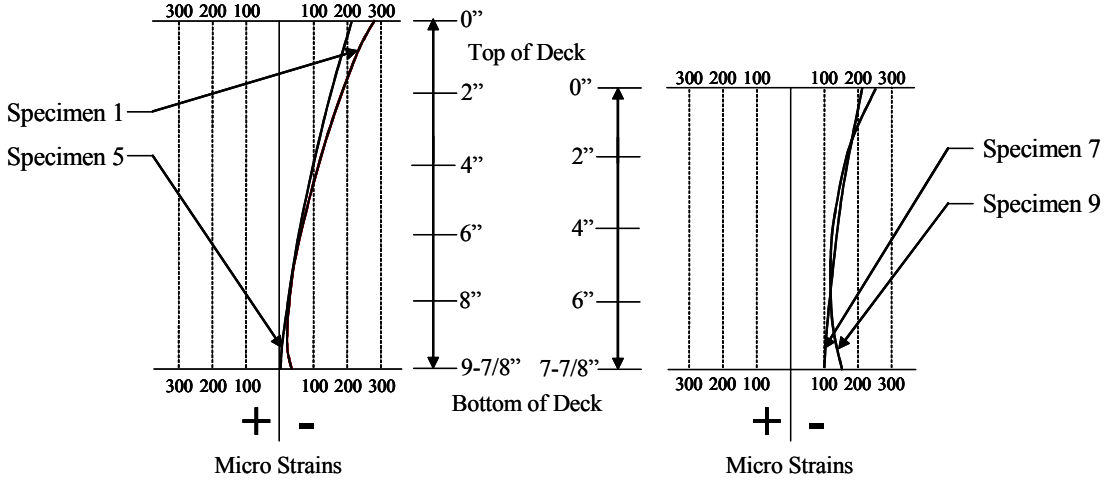

Figure 5.47: Strain Profiles of Specimens 1, 5, 7 and 9

Reinforcement can cause a concrete deck to curl because of its non-symmetric stiffness. In the case of the deck models, the top and bottom cover varied (2.5 in top and 1.5 in bottom) and each mat of reinforcing bars was of different size (#4 top and #5 bottom). The deck model with reinforcement (Specimen 1) had a curvature approximately 8% more than the model without reinforcement (Specimen 5). The difference in curvature between Specimen 7 and 9 (15% difference) was much more dramatic (most likely because Specimen 9 had no reason to curl). Therefore, the increase in curling measured in Specimen 7 likely occurred because of the non-symmetric stiffness of the reinforcement. It should be noted that the total curvature of Specimens 7 and 9 were both substantially smaller than that of Specimens 1 and 5.

5.10.4 Effect of Slab Thickness

Specimen 10 was designed one inch thicker that Specimen 9 to investigate the effect of shrinkage with an increased bridge deck thickness. Because the concrete strain gage for Specimen 10 was lost during the pouring sequence, the Whittemore measurements were the only data available to compare the two specimens. On both faces of the specimens less displacement/strain was measured from the thicker specimen (Figure 5.48). On average, the surfaces of Specimen 10 produced 16% less strain than Specimen 9. Overall, measured surface displacements were expected to be lower from the thicker specimen due to the increased depth required for moisture migration.

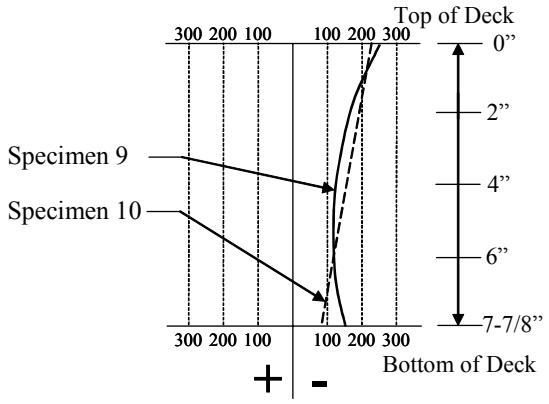

Figure 5.48: Strain Profiles of Specimens 9 and 10

5.10.5 Effect of Temperature Due to Form Type

Specimens 1 and 7 were the only specimens that contained thermocouples. Each of these specimens had two gages located on the top sides of the two mats of reinforcement, directly in the center of each deck model. In each case, the measured temperature during the heat of hydration was approximately the same for each specimen on both the bottom and top mat of reinforcement (Figure 5.35). The temperatures at all times were within 4^{o} F of each other. The peak temperatures from each gage ranged from 114 to 117^{o} F approximately 12 hours after the initial pour. At the same time the ambient temperature was approximately 75^{o} F. Twenty-four hours after casting, all thermocouples reached ambient temperature. Following the heat of hydration period, the temperature of the specimens followed the ambient temperature very closely as shown. Therefore, form type did not have any effect on the heat of hydration or later thermal response under laboratory testing conditions.

CHAPTER 6
REINFORCED CONCRETE SLAB MODELS

6.1 Introduction

To further investigate design methods aimed at reducing the detrimental effects of cracking in concrete bridge decks due to early-age-shrinkage, ten slab specimens were designed, constructed, and tested in the Kettelhut Structural Engineering Laboratory. This experimental study was designed to identify how transverse cracking, caused by early-aged shrinkage, is affected in concrete bridge decks by varying the distribution of the longitudinal reinforcement and the thickness of the epoxy coating.

6.2 Specimen Design

6.2.1 Specimen Sizes

Ten bridge deck specimens were designed to represent a full scale cut section from a bridge deck. Because tensile stresses created from shrinkage in a bridge deck are difficult to simulate in the laboratory, it was decided to develop tensile stresses by loading the test specimens. Since the main objective of the experimental program was to determine how different types of reinforcement affect the spacing and width of cracks, the tensile stresses at the location of the reinforcement were of primary interest. Therefore, by using a loading system that creates a constant moment region (shear is zero), it is possible to induce tensile stresses at the location of the reinforcement similar to tensile stresses found in a bridge deck caused by shrinkage. Figure 6.1 displays a simplified comparison between the stress distribution caused by bending and shrinkage. As shown, the strain distribution does not simulate the actual strain distribution caused by shrinkage. This test, however, does permit relative comparison of test variables involved in deck cracking. In addition, crack widths at the top of the slab should be consistent with actual deck performance since strains at the level of the reinforcement are approximately of the same magnitude for equal reinforcement stress levels.

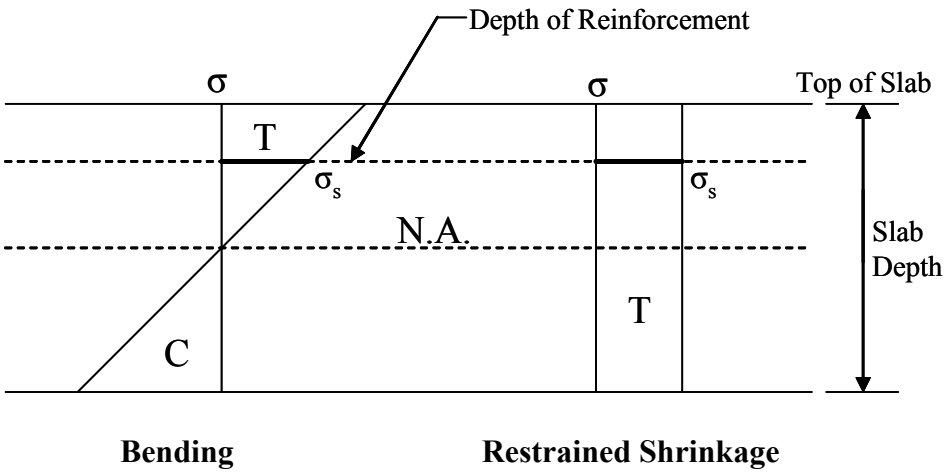

Figure 6.1: Stress Distribution of the Slab

The loading system shown in Figure 6.2 was selected. Due to the arrangement of the laboratory strong floor anchor points, an 8 ft constant moment region was selected. This length provides adequate distance for cracks to develop and to determine the differences caused by the variation of each slab model. The total length of the slab specimens was designed at 15'-6". This length provided a 2 ft moment arm (on each side of the constant moment region) that was adequate to both crack the specimens and yield the reinforcement.

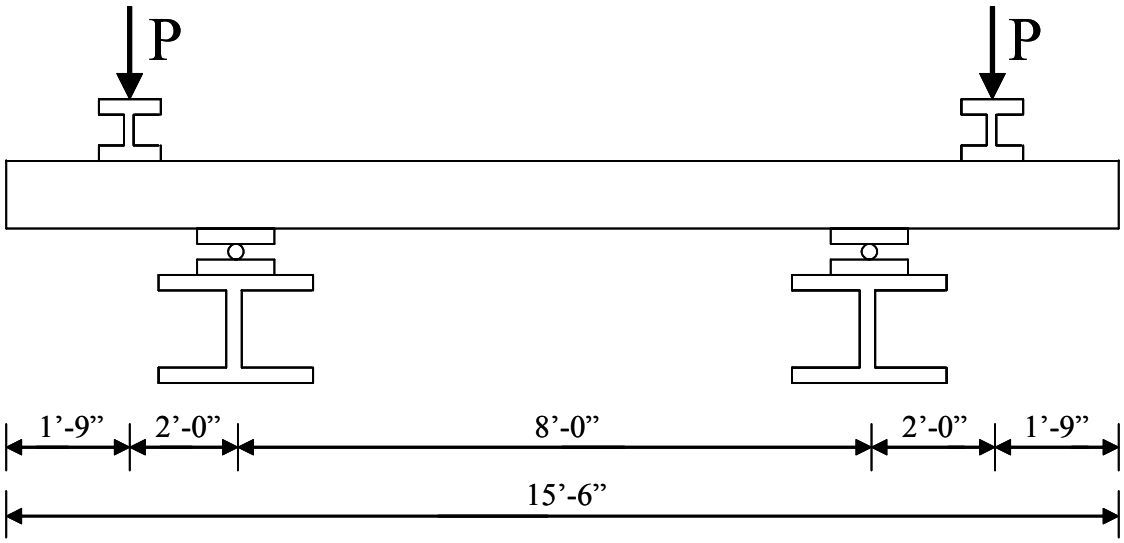

Figure 6.2: Four-Point Loading Testing Apparatus

To easily measure crack widths during the testing procedure, the slab specimens were designed to produce tension on the top surface. This method allowed cracks to be located on the top surface so that crack measurements would not be required under the specimens.

The specimen width of 36 in. was chosen to provide adequate space to investigate various reinforcement layouts. Specimen cross-sectional dimensions are presented in Figure 6.3. A depth of 8 in. was provided to be consistent with typical deck design as well as with the previous research phase.

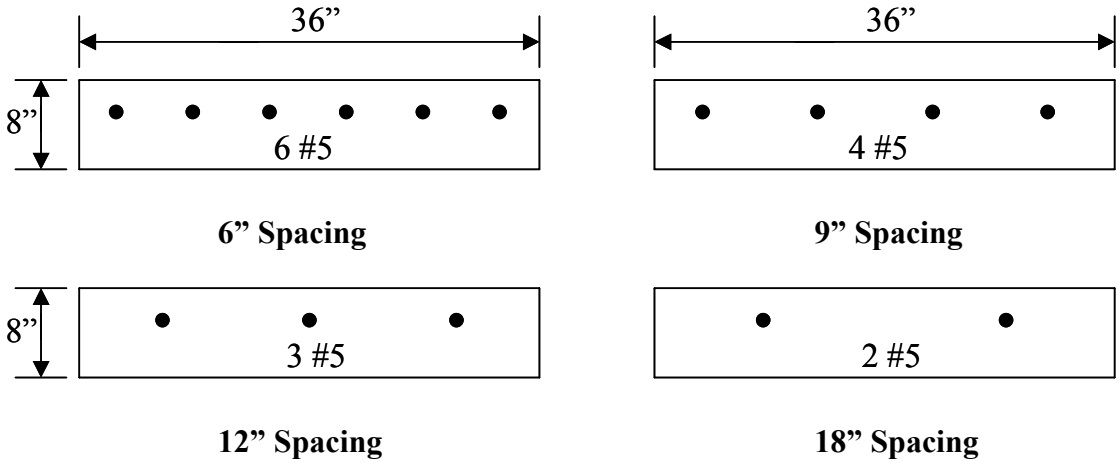

Figure 6.3: Specimen Cross-Sectional Dimensions

6.2.2 Specimen Variables

The primary variables evaluated in the study were the spacing of the reinforcement and the epoxy coating thickness. Complete details of all specimens are provided in Table 6.1. Specimens are identified by the initial of the reinforcement type (Black or Epoxy) followed by the thickness of the epoxy coating in mils, if applicable, followed by the spacing of the reinforcement in inches.

Table 6.1: Slab Specimen Details

Specimen	Spacing of Reinforcement (in.)	Epoxy Coating Thickness (mils)
B-6	6	0
B-9	9	0
B-12	12	0
B-18	18	0
E12-6	6	12
E12-9	9	12
E12-12	12	12
E12-18	18	12
E6-9	9	6
E18-9	9	18

6.2.2.1 Spacing

The I65 over SR25 bridge was designed (longitudinal direction) with a bottom mat of #5 reinforcing bars and a top mat of #4 bars both spaced at 11-13/16 in. on-center. To simulate this deck design, two deck models were designed with reinforcement spaced at 12 in. Since reinforcement spacing is known to affect crack spacing, three other spacings were investigated: 6 in., 9 in. and 18 in. These spacings were selected since they are multiples of each other. The maximum spacing of 18 in. was selected since this spacing represents the maximum allowed by code (ACI 318-99, AASHTO 1996, AASHTO 1998). In addition, INDOT is currently considering the use of this wider spacing for bridge decks. All specimens were designed using #5 reinforcing bars since these are the maximum size typically used in a bridge deck. Specimen cross section dimensions are shown in Figure 6.3.

Since it is known that crack spacings and widths are directly related to reinforcement spacing (Gergely and Lutz 1968), the reinforcement was spaced so that the side cover of the exterior bars was the same distance as half the clear spacing (Figure 6.3).

6.2.2.2 Epoxy Coating

To investigate the effect of epoxy coating on crack widths and spacing, the specimens were designed with varying reinforcement epoxy thickness. INDOT specifies that bridge deck reinforcement must conform to ASTM-A775-97. This specification requires that reinforcement must be covered with an epoxy ranging in thickness from 5 to 12 mils. Even though an 18-mil epoxy is not presently accepted by ASTM-A775, there is currently a recommendation to increase this limit to 18 mils to increase the durability of the coating during construction. Therefore the coating thicknesses included in the test series were 6 mil, 12 mil, and 18 mil so that a range of coating thickness could be evaluated. In addition, bars not coated with epoxy (black bars) were included for comparison purposes.

6.3 Materials

6.3.1 Concrete

To represent bridge deck construction in Indiana, INDOT Class C concrete was used for the experimental program. This mix is the same used for the I65 over SR25 bridge deck and for the previous shrinkage experiment. Due to limited lab space, two casting sequences were used to construct the ten slab specimens. Both batches of concrete came from the same local ready-mix producer, Irving Materials Inc. (IMI). Table 6.2 indicates the specimens that were included in the first and second casting series.

Table 6.2: Specimens Included in Each Casting Series

Casting Series I	Casting Series II
B-9	E6-9
B-12	E12-18
E12-9	E12-6
E12-12	B-18
E18-9	B-6

The mix was specified to have a maximum aggregate size of ¾" and a water-to-cement ratio of 0.34. Specific mix proportions can be found in Table 6.3. The slump of the each mix was measured upon arrival of the concrete (Table 6.4 and Figure 6.4). Three gallons of water were added to the concrete mix (increasing the w/c ratio slightly) for Casting Series II to improve workability.

Table 6.3: Mix Design (INDOT Class C Concrete)

Material	Quantity Per Yard	Specifications/Suppliers
Cement	658 lb/yd^3	ASTM C-150, Type I, Essroc Cement Co
Sand	1280 lb/yd^3	ASTM C-33 & INDOT Specification #23 Sand from Vulcan Materials, Battleground, IN
Stone/Gravel	1836 lb/yd^3	#8 Stone from US aggregate, Delphi, IN
Water	27.6 gallon/yd^3	Before Adding Water at the Kettelhut Laboratory
Water Reducer	13 oz/yd^3	ASTM C-494, Water Reducer Type A Pozzolith 220N, Master Builders.
Air	8 oz/yd^3	ASTM C-260 Air Entrainment, Micro Air by Master Builders
Ash	None	-
Micro-Silica	None	-

Table 6.4: Additional Concrete Mix Information

	Casting Series I	Casting Series II
W/C	0.34	0.34*
Slump	5.25 in.	5.75 in.*
Air Temperature at Arrival	52^o F	35^o F
Relative Humidity at Arrival	61 %	51 %
Amount of Concrete Ordered	7.5 yd^3	7.5 yd^3

* After adding water to the mix at the Kettelhut Laboratory

Figure 6.4: Slump Test (Series II)

Compression strength tests were performed on 6 in. by 12 in. cylinders. A 600-kip Forney compression testing machine was used to perform these tests. The concrete strength gain curves for both batches of concrete (Series I and II) used in the experimental program are shown in Figure 6.5. Series I had a 28-day compressive strength of 6,100 psi while Series II achieved a compressive strength of 6,690 psi. In general, the strength gain curves for both series are essentially identical.

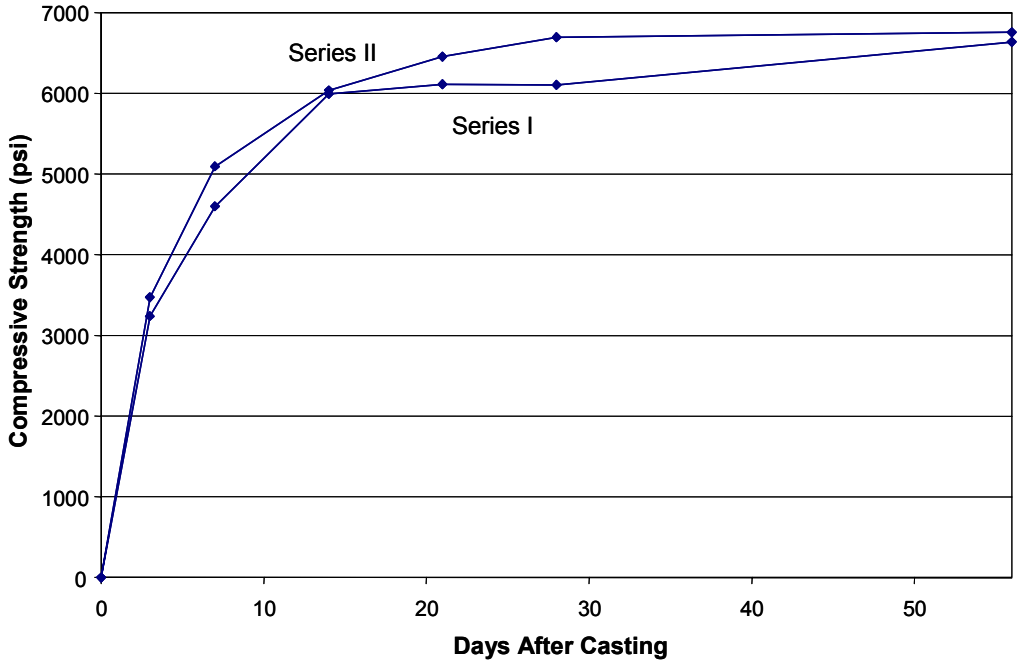

Figure 6.5: Concrete Compression Strength Gain

Immediately after the testing of each of the ten slab specimens, three concrete cylinders, from the same cast, were tested for compressive strength. Each slab model was allowed to dry for at least 28 days. Table 6.5 lists the results from the cylinder tests. As shown, the compressive strengths varied only slightly.

Table 6.5 Concrete Cylinder Compressive Test Results

Slab Test	Date	Days After Casting	Average Compressive Strength (psi)
B-9	1/14/02	45	6440
B-12	1/17/02	48	6449
E12-9	01/19/02	50	6731
E12-12	01/21/02	52	6634
E18-9	01/26/02	57	6666
E6-9	02/07/02	28	6692
E12-18	02/09/02	30	6790
E12-6	02/11/02	32	6778
B-18	02/13/02	34	6875
B-6	02/15/02	36	6765
Average	-	-	6682
Standard Deviation	-	-	135

6.3.2 Reinforcing Steel

The reinforcing bars used in the experimental program were ASTM A615 Grade 60 #5 bars. The epoxy coated and black reinforcing bars were obtained from different heats of steel. A tensile test was performed on three #5 black bars and three #5 epoxy bars using a 160 kip Baldwin universal testing machine. The stress-strain relationships are presented in Figure 6.6. The black bars yielded at approximately 21 kips (68 ksi), and the epoxy-coated bars yielded at 23 kips (74 ksi).

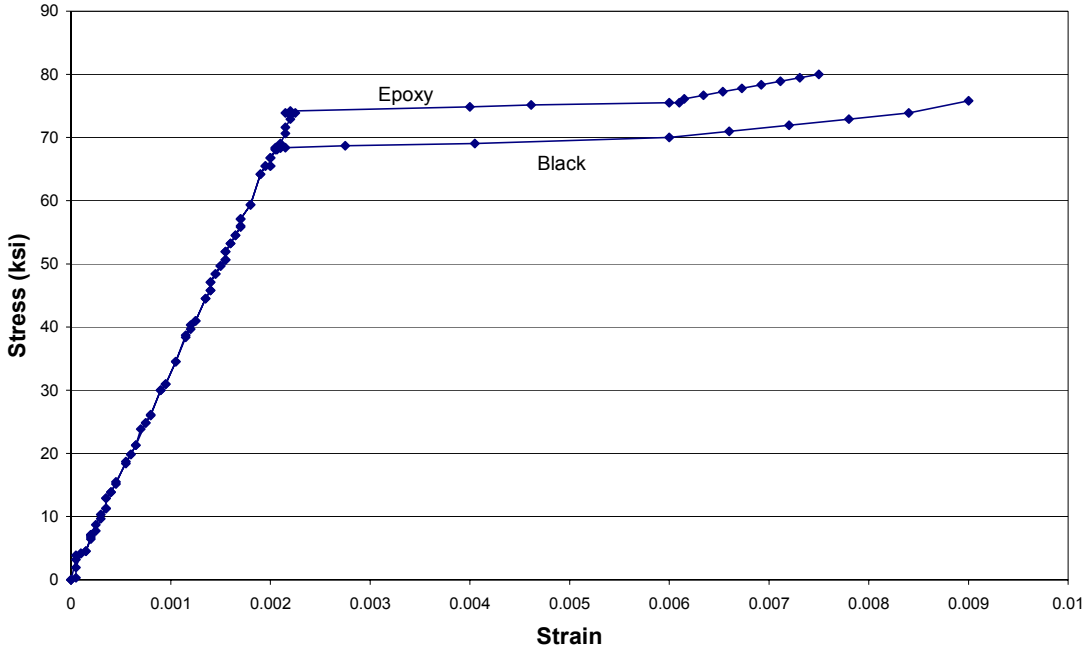

Figure 6.6: Reinforcement Stress-Strain Curve

6.3.2.1 Epoxy Coatings

The epoxy coated reinforcing bars were obtained from MidWest Pipe. The bars were specified to be coated to a thickness of 6, 12, and 18 mils. Because the process of applying epoxy to the reinforcement is not exact, the bars were not all accurately coated with the specified epoxy thickness. After receiving the reinforcing bars, the coating thickness was measured using a Microprocessor Coating Thickness Gage (Electro-Physik, Mini Test 3001). The epoxy thickness was measure in five different locations along the length of each bar. These measurements as well as the average and standard deviations for each bar are presented in Table 6.6. Table 6.7 presents the overall average and standard deviations of the epoxy coating thickness for the reinforcement included in each specimen.

Table 6.6: Reinforcing Bars Epoxy Coating Thickness

Specimen	Bar	Epoxy Coating Thickness (mils)						
		Measurement Location					AVG	SD
		1	2	3	4	5		
E12-6	1	16.3	17.2	12.6	11.3	10.5	13.6	2.7
	2	11.5	11.4	10.4	11.8	11.5	11.3	0.5
	3	11.7	14.8	15.2	13.4	13.8	13.8	1.2
	4	16.0	15.3	11.5	13.9	14.2	14.2	1.5
	5	14.8	16.8	13.7	14.5	12.6	14.5	1.4
	6	14.7	9.1	10.6	12.8	11.9	11.8	1.9
E12-9	1	12.3	11.0	11.5	10.5	12.0	11.5	0.7
	2	11.5	12.1	11.4	15.1	13.8	12.8	1.4
	3	12.7	12.7	17.5	11.3	8.7	12.6	3.0
	4	11.6	11.8	13.1	12.0	10.4	11.8	0.9
E12-12	1	16.3	17.2	12.6	11.3	10.5	13.6	2.7
	2	14.0	14.3	11.3	10.5	12.2	12.5	1.5
	3	11.9	12.1	12.9	12.5	11.8	12.2	0.4
E12-18	1	11.5	11.9	11.7	12.9	13.3	12.3	0.7
	2	14.6	18.2	17.5	13.3	12.3	15.3	2.1
E6-9	1	8.9	7.5	9.5	8.2	7.9	8.4	0.7
	2	8.3	8.1	8.8	9.4	8.8	8.7	0.5
	3	8.3	7.0	7.2	8.0	9.7	8.0	1.0
	4	12.6	11.2	9.9	9.1	10.0	10.6	1.2
E18-9	1	19.0	20.6	21.5	20.7	18.5	20.1	1.1
	2	17.7	16.0	19.5	17.0	21.8	18.4	2.0
	3	18.4	19.2	17.7	19.0	18.2	18.5	0.5
	4	18.4	16.9	17.5	16.8	18.3	17.6	0.7

Table 6.7: Reinforcement Epoxy Coatings

Specimen	Epoxy Coating Thickness (mils)							
	Bar 1	Bar 2	Bar 3	Bar 4	Bar 5	Bar 6	AVG.	SD
E12-6	13.6	11.3	13.8	14.2	14.5	11.8	13.2	1.33
E12-9	11.5	12.8	12.6	11.8	-	-	12.2	0.62
E12-12	13.6	12.5	12.2	-	-	-	12.8	0.74
E12-18	12.3	15.3	-	-	-	-	13.8	2.12
E6-9	8.4	8.7	8.0	10.6	-	-	8.9	1.15
E18-9	20.1	18.4	18.5	17.6	-	-	18.7	1.05

The difference in epoxy thickness along the lengths of the bars may affect bond in different regions of the bars. However, the variations measured were considered representative of typical coating practice. It should be noted that the coating thickness of the bars specified as 6 mils were not very accurate; consequently, the specimen design to contain a 6 mil coating (E6-9) was actually closer to 9 mils. This result is also representative of typical coating practice, as manufacturers do not want to coat below the ASTM minimum epoxy thickness.

6.4 Model Construction

The specimens were constructed in two casting operations due to limited laboratory space. Series I specimens were cast first while Series II specimens were cast second (Table 6.2). All formwork was built with ¾ in., grade B-B plyform reinforced with 2 in. by 4 in. lumber. To limit leakage of concrete during casting, the forms were caulked. Formwork is shown in Figures 6.7 and 6.8. The forms were reused for the second casting operation.

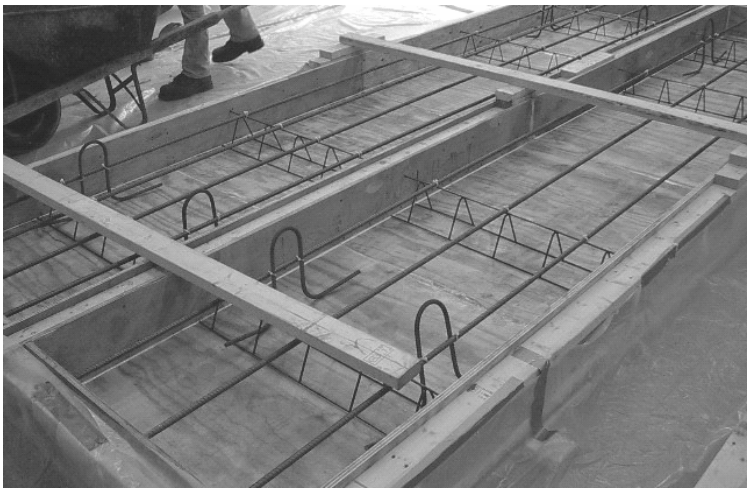

Figure 6.7: Specimen Formwork

Figure 6.8: Specimen Formwork

After the formwork was constructed, reinforcing bars were placed. The #5 bars were set on 5-7/8 in. chairs leaving 1-½ in. clear cover over the reinforcement. The bars were then tied to the chairs to minimize movement during the placement of the concrete. Cross braces, constructed from 2 in. by 4 in. lumber, were also installed to reduce wall deflection during the placement of the wet concrete. To limit the effect of the chairs on the slab cracking pattern, the chairs were placed at 2 ft and 5 ft from the ends of the slabs (Figure 6.9). At these locations, the largest possible unobstructed span could be obtained, while still providing proper support for the reinforcement.

To easily move the slabs after curing, four lifting hooks (two at each end) were placed approximately 2'-6" from the end (Figures 6.8 and 6.9). The hooks were fabricated from #4 reinforcing bars. Finally, all formwork (including test cylinders) were covered with form oil to ensure easy removal after curing.

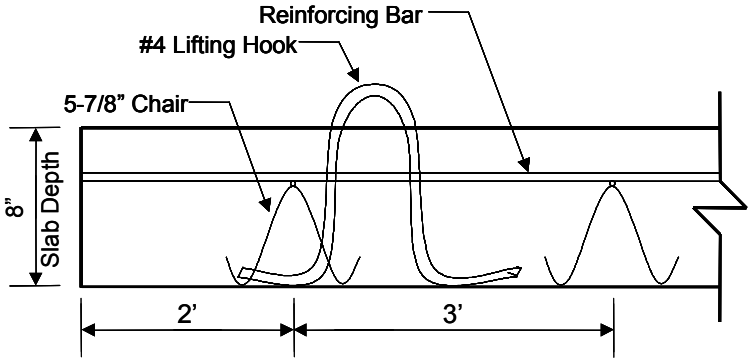

Figure 6.9: Elevation View of Slab Specimen End

6.5 Casting and Curing

The test specimens were cast at two different times. Series I specimens were cast on November 27, 2001, while Series II specimens were cast on January 10, 2002. After the concrete had been placed in the forms, the specimens were screeded and finished with trowels (Figure 6.10). The specimens were then allowed to set for two and half hours before wet burlap and plastic were used to cover the exposed top surfaces of the deck models. Table 6.8 presents the time-line of events for the placement and curing of the specimens.

Figure 6.10: Finishing the Slab Specimens

Table 6.8: Sequence of Events for Casting and Curing

	Casting Series I		Casting Series II	
Arrival of Concrete	11/27/01	10:00 AM	01/10/02	10:00 AM
Slump Test	11/27/01	10:10 AM	01/10/02	10:15 AM
Start Pour Sequence	11/27/01	10:20 AM	01/10/02	10:20 AM
End Pour Sequence	11/27/01	11:00 AM	01/10/02	10:55 AM
Screeded and Finished	11/27/01	11:45 AM	01/10/02	11:45 AM
Placed Burlap/Plastic	11/27/01	3:15 PM	01/10/02	3:15 PM
Burlap Wetted	11/27/01	3:25 PM	01/10/02	3:25 PM
Burlap Rewetted	11/27/01	8:30 PM	01/10/02	9:15 PM
Removal of Burlap/Plastic	12/4/01	10:00 AM	01/17/02	9:30 AM

To minimize early-aged shrinkage, a seven day wet cure was used for both the slab specimens and concrete cylinders (Table 6.7). This curing time was used to minimize both the magnitude of residual tension caused by shrinkage as well as shrinkage cracking on the surface. Wet curing consisted of covering the deck models and test cylinders with saturated burlap and plastic sheeting (Figure 6.11). The burlap was maintained constantly saturated over the seven day curing period, soaking daily.

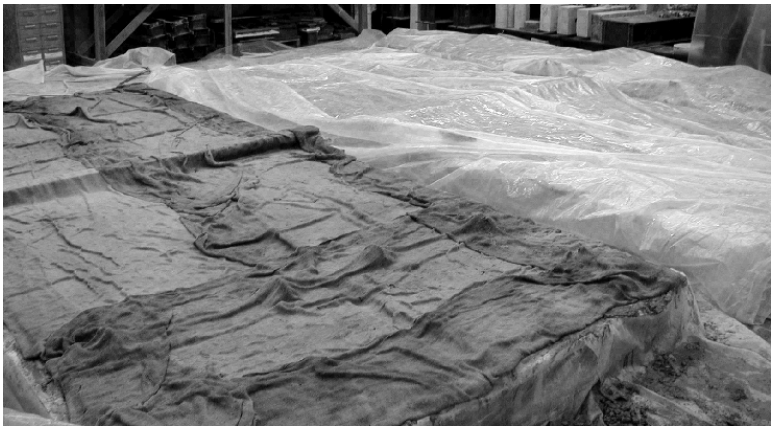

Figure 6.11: Specimen Curing

6.6 Testing Setup

A hand pumped hydraulic system was used to load the specimens. Load was applied with two hydraulic cylinders at each end (Figure 6.12). The two hydraulic cylinders reacted against a 3 ft long stiffened W8x15 section to distribute the load across the width of the specimen and produce a concentrated line load (Figure 6.12).

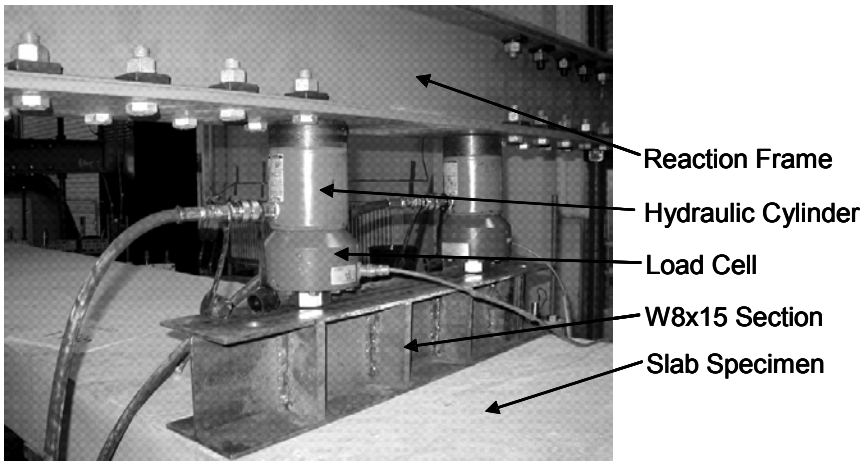

Figure 6.12: Hydraulic Loading System

The four hydraulic cylinders (30 Tons each) were fed from the same pump through a manifold to ensure even pressure to each cylinder. Applied loads were measured by four load cells placed between the hydraulic cylinder and reaction beam (Figures 6.12 and 6.13). The loading frame consisted of two 14x25 channels bolted together with a ½ in. x 8 in. plate on the top and bottom and attached to two 2-1/4 in. threaded dowels. These threaded dowels were anchored to the laboratory strong floor.

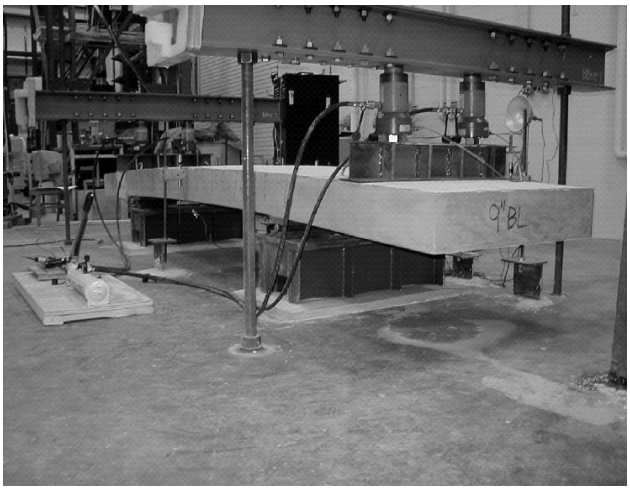

Figure 6.13: Load Reaction Frame

6.6.1 Supports

The specimens were simply supported in the test setup. One support was designed to simulate a pin while the other was designed to simulate a roller. The pinned connection was constructed using two 3 ft long steel plates. The pin assembly consisted of a 1 in. thick top plate and a 1-1/4 in. thick bottom plate that was grooved on one side to accommodate a 1-1/2 in. diameter rod. The roller support was constructed primarily the same, but neither plate was grooved and both were 1 in. thick. The bottom plates of both the roller and pin connections were welded on top of the 3 ft long steel supports. These support sections were hydrostoned to the ground to restrict movement (Figure 6.14).

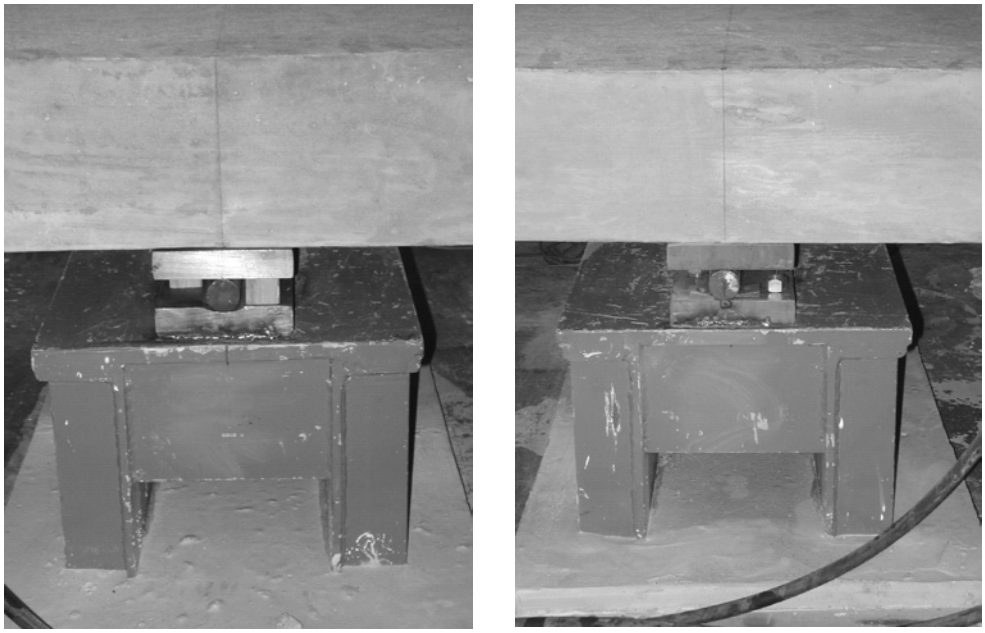

Pin **Roller**

Figure 6.14: Support Conditions

6.7 Instrumentation

Three different types of instrumentation were used during the testing of the experimental program. Linear voltage displacement transducers (LVDTs) measured deflections, load cells measured the applied loads from the four hydraulic cylinders, and two 50X Direct Measuring Edmund microscopes were used to measure the crack widths during testing.

6.7.1 LVDTs

LVDTs were used to monitor the beam deflection. Each of the LVDTs used for the experimental program were calibrated before testing with an accuracy of 0.001 in. To allow adequate capacity to measure both midspan and end span deflections past yielding in the constant moment region, 2 in. LVDTs were deemed sufficient after preliminary deflection calculations.

The LVDTs were set on stands, which were hydrostoned to the ground as shown in Figure 6.15. The LVDT cores were attached to small angles that were then epoxied to the bottom of each of the specimens. LVDTs were positioned to monitor deflections at the load points, midspan, and supports. These locations are shown in Figure 6.16. LVDTs were placed on either side of the specimen at midspan to ensure that the specimens did not twist during loading.

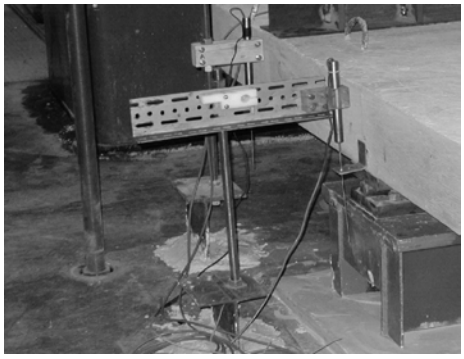

Figure 6.15: LVDT Support

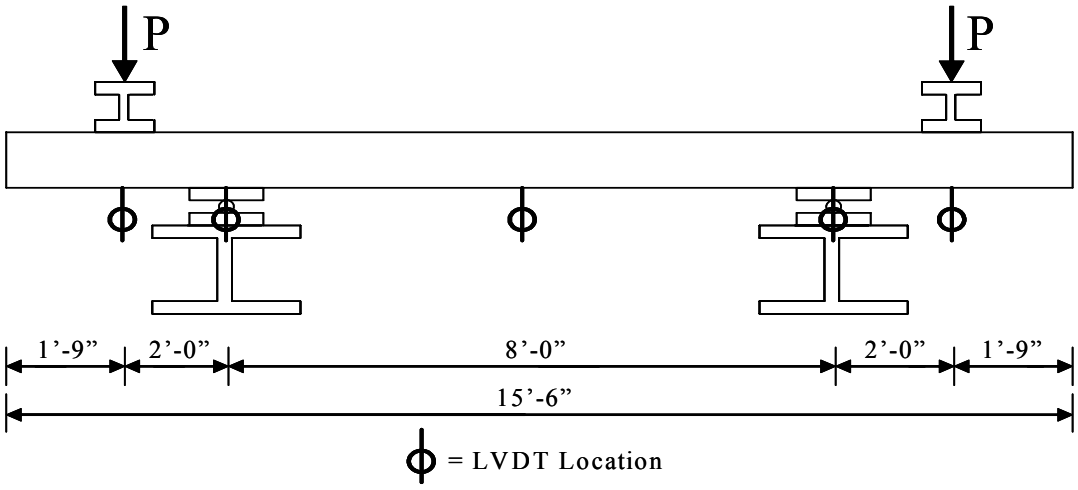

Figure 6.16: Location of the LVDTs

6.7.2 Load Cells

Four 20 kip Lebow load cells were placed under the hydraulic cylinders to measure the applied load (Figure 6.12). These four load cells were calibrated prior to testing.

6.7.3 Crack Measurements

Crack widths were measured during testing using an Edmund Direct Measuring 50X microscope. The microscopes could be read within an accuracy of 1 mil (1/1000 of an inch).

6.8 Loading Procedure

The loading procedure was similar for all specimens. In general, monotonic loading was applied up to flexural cracking of the specimens. Following cracking, loading was increased in predetermined increments depending on the specimen tested. For specimens with reinforcement at 6 in. and 9 in. spacing, 1 kip increments were used. For specimens with reinforcement spaced at 12 in. and 18 in., ½ kip increments were used. At cracking and after each load stage, cracks were marked and photographs were taken. In addition, crack widths were measured while the load was maintained.

Different load increments were used since the flexural yield capacities of the specimens varied. As shown in Table 6.9, the calculated cracking load for all specimens was approximately the same. However, the calculated yield capacities were considerably different. In order to provide an adequate number of crack width measurements at different stress levels, the load interval was varied.

Table 6.9: Calculated Cracking and Yield Load of Slab Specimens

Bar Spacing (in.)	Mcr (ft*kips)	Cracking Load, P (kips)	My (ft*kips)	Yield Load, P (kips)
18	18.9	9.3	18.1	9.0
12	19.1	9.5	26.8	13.4
9	19.2	9.6	35.3	17.7
6	19.5	9.8	55.2	26.1

Crack width measurements were discontinued when the steel stress reached above 55 ksi. However, loading of the specimens continued beyond the yield to fully describe the load-deflection behavior. Once the reinforcement in each of the specimens had fully yielded, the specimens were slowly unloaded to obtain the unloading behavior.

6.9 Data Collection

Data was collected using a Micro Measurements 5100 series data acquisition system. Data was recorded continuously during the test at 10-second intervals.

6.9.1 Crack Readings

The widths of primary cracks were measured using an Edmund Direct 50X microscope. A crack was considered primary if it traversed the full width of the specimen. The width of each primary crack was read in three different locations. These locations were chosen to provide a representative distribution of crack width and eliminate local anomalies. In general, measurements were taken directly above a reinforcing bar or midway between two reinforcing bars. Cracking that was found within the support region was not included within the data.

6.10 Results

6.10.1 General Behavior

Each of the slab specimens were loaded by the loading procedure explained in Section 6.8. The midspan load-deflection was continuously monitored during testing. These graphs are presented in Figures 6.17-6.20. Deck specimens with the same reinforcement spacing are plotted together. The load which corresponds to nominal yield (steel stress = 60 ksi) is also presented in each graph.

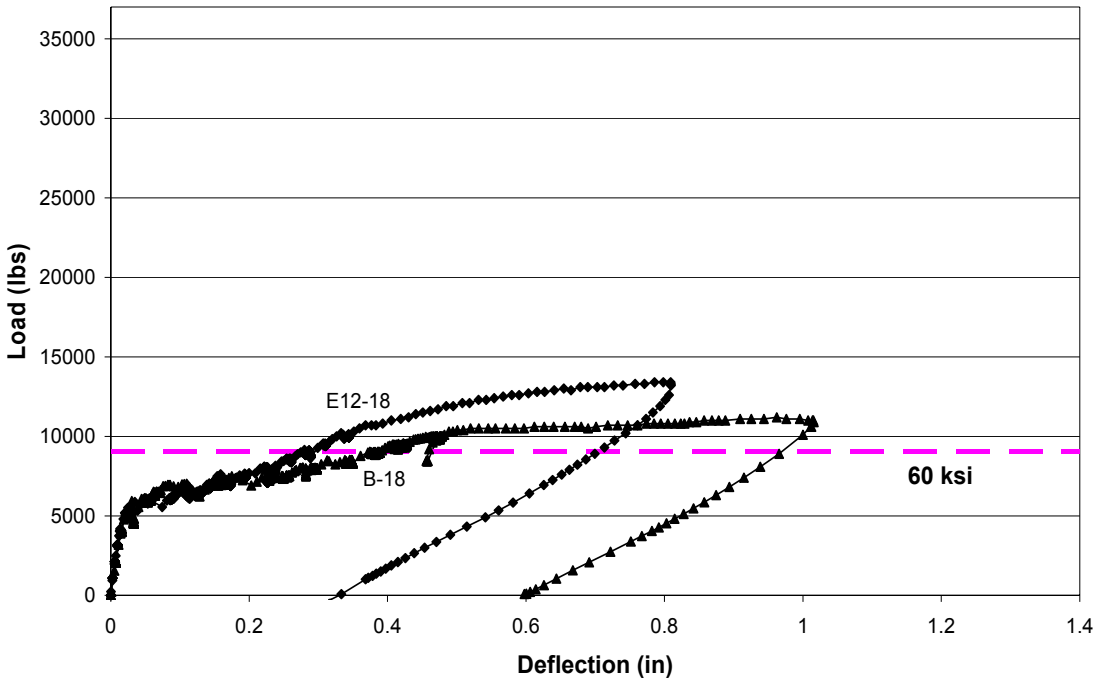

Figure 6.17: Load Deflection (18 in. Spacing)

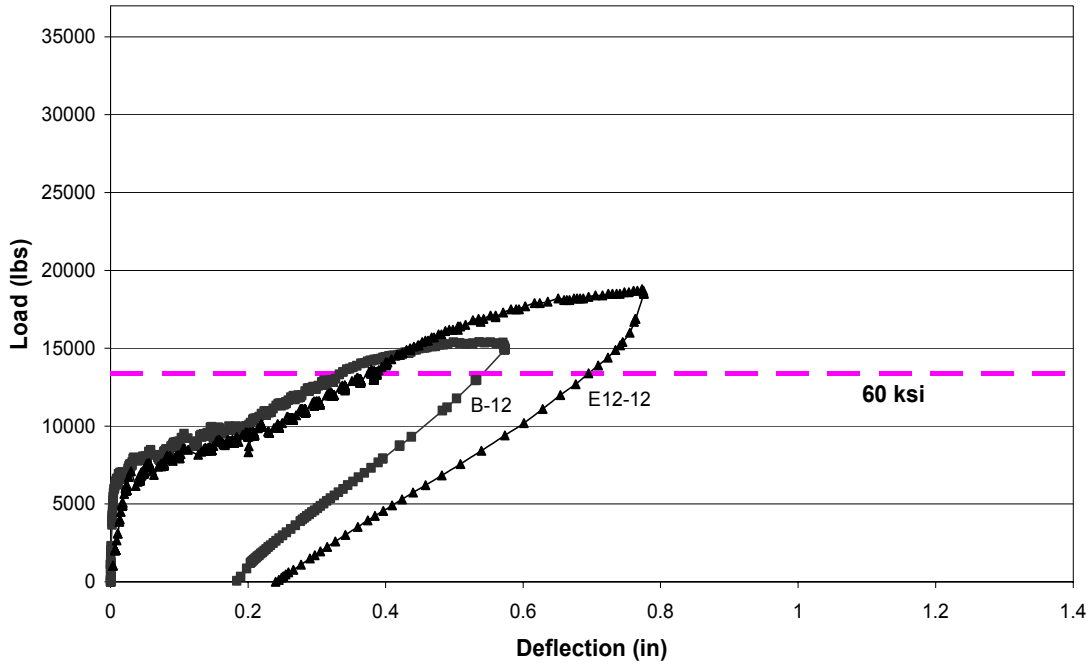

Figure 6.18: Load Deflection (12 in. Spacing)

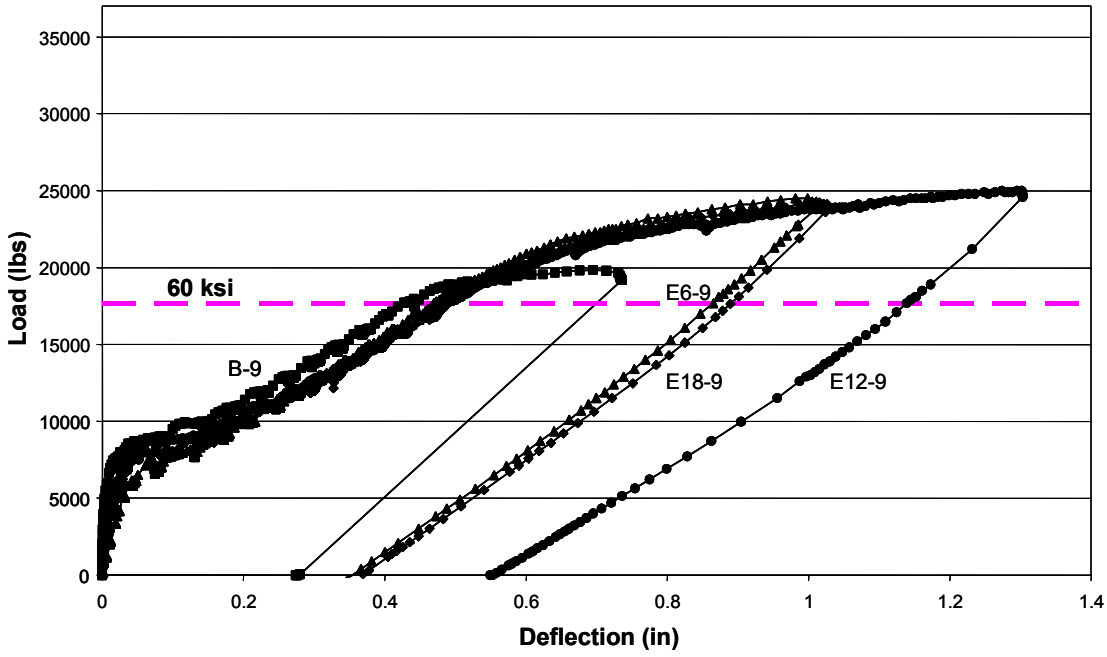

Figure 6.19: Load Deflection (9 in. Spacing)

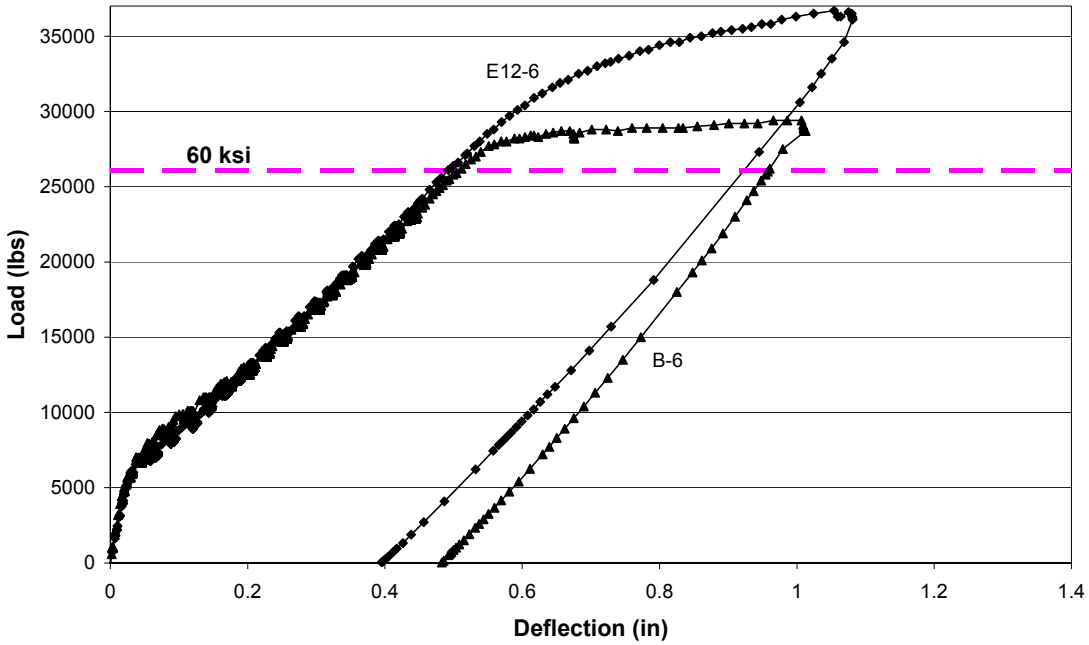

Figure 6.20: Load Deflection (6 in. Spacing)

Regardless of reinforcement spacing or epoxy coating thickness, each of the specimens behaved similarly up to first cracking. Midspan load-deflection was linear until this point. First cracking occurred in all specimens at approximately 6.5 kips. Variation in the cracking load was small because each slab specimen was constructed with similar concrete. Also, the differences in reinforcement ratios were not large enough to significantly change the transformed section moment of inertia.

As shown in the load-deflection curves, following cracking, the stiffness was reduced. As loading increased, the specimens with the same bar spacings behaved similarly until yielding of the reinforcement. However, the specimens with wider bar spacings displayed a larger reduction in stiffness than those with smaller reinforcement spacings as expected.

As discussed in Section 6.3.2, the yield capacities of the black reinforcing bars were smaller than that of the epoxy coated bars. This difference occurred since these bars were obtained from a different heat of steel. The specimens constructed with black bars yielded at a lower load than the specimens constructed with epoxy-coated bars. It is shown in the load-deflection curves that both types of bars yielded above the nominal yield of 60 ksi. Because the differences in load-deflections were similar for specimens with the same bar spacings up until reinforcement yielding, the epoxy coating did not seem to affect the overall behavior.

After yielding the reinforcement, load was slowly removed. The slope of the unloading curve was similar to the loading curve after cracking had occurred. In each case, the experimental data compared well with calculated load-deflection response.

6.10.2 Crack Patterns

During testing, the specimens were examined for cracks at each load increment up to yielding of the reinforcement (Figure 6.21). The growth of each crack was examined, and the crack spacings were determined.

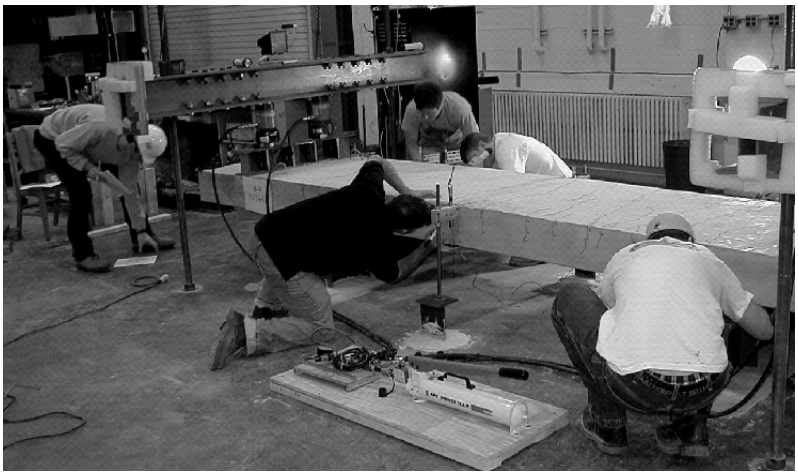

Figure 6.21: Marking Cracks During Testing (Specimen B-9)

Transverse cracking initiated near the supports. With only a small increase in load, transverse cracks occurred outside the support region. In each case, cracking developed more slowly in specimens with smaller reinforcement spacings (higher ρ). For the lightly reinforced sections (12 in. and 18 in. spacing) cracks crossed the full width of the slab upon initiation. However, transverse cracking in the more heavily reinforced sections (6 in. and 9 in. spacing) was more gradual. In several cases, an increase of 5 kips (5 load increments) was required to cause cracking across the full width of the specimen. In general, cracking of the specimens during testing was symmetrical about midspan.

Complete cracking patterns for each of the ten slab models after testing are presented in Appendix F. The crack patterns are shown for the constant moment region. Figure 6.22 depicts a typical cracking pattern in the constant moment region of the deck specimens.

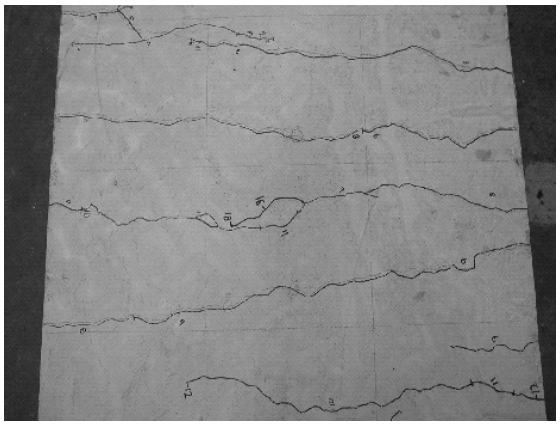

Figure 6.22: Typical Crack Pattern (Specimen B-9)

The average spacing of the primary cracks was calculated. A crack was considered primary if it traversed the full width of the specimen. The distance between these cracks was measured at mid-depth on each side face of the specimens. Cracking that occurred 8" from the centerline of the support was not included in the data. This region is often termed a D-region or discontinuity region. Cracking was considered to be in the D-region if it fell within 8 in. of a support. Cracks forming in this region are affected by the support and consequently do not provide representative crack widths and spacings. Table 6.10 presents the number of primary cracks and the average crack spacings found after the completion of each test.

Table 6.10: Number and Spacing of the Primary Cracks

Specimen	Number of Primary Cracks	Average Spacing of Primary Cracks (in.)	Standard Deviation (in.)	Max Spacing (in.)	Min Spacing (in.)
B-6	13	6.9	1.5	9.3	4.5
B-9	9	9.0	2.8	14.4	4.5
B-12	8	9.8	2.6	14.5	6.3
B-18	7	12.2	4.2	19.5	6.5
E12-6	13	6.7	1.4	9.2	4.5
E12-9	10	8.9	2.0	12.0	5.1
E12-12	8	10.1	4.3	17.5	5.3
E12-18	6	13.3	4.6	18.8	6.8
E6-9	11	8.0	2.0	11.9	5.5
E18-9	12	7.4	1.8	11.3	4.3

6.10.3 Longitudinal Cracking

Longitudinal cracks were found on the surfaces of Casting Series II specimens. These cracks were discovered prior to testing and were evident directly above of the reinforcement (Figure 6.23). It was concluded that these were settlement cracks which is a common form of cracking formed in the plastic stage of the concrete after initial consolidation. "Settlement crack are the natural result of heavy solids (i.e. reinforcing bars) settling in a liquid medium" (ACI 224 2001). These cracks were found primarily in the Casting Series II specimens.

Even though the longitudinal cracks were not of primary concern for this test, the widths of the cracks were measured before testing and at a steel stress of 60 ksi to determine if any crack growth occurred during loading. It was found that these cracks did not increase in width. However, when the specimens were loaded past reinforcement yielding, these cracks had a tendency to grow in length and width.

Because some of the longitudinal cracks were of substantial size (up to 13 mils), the effect of this type of cracking in a bridge deck should be of concern. Settlement cracking was not investigated in this study since its causes are known. Procedures outlined by ACI Committee 224 (2001) should be used to limit settlement cracking in a bridge deck.

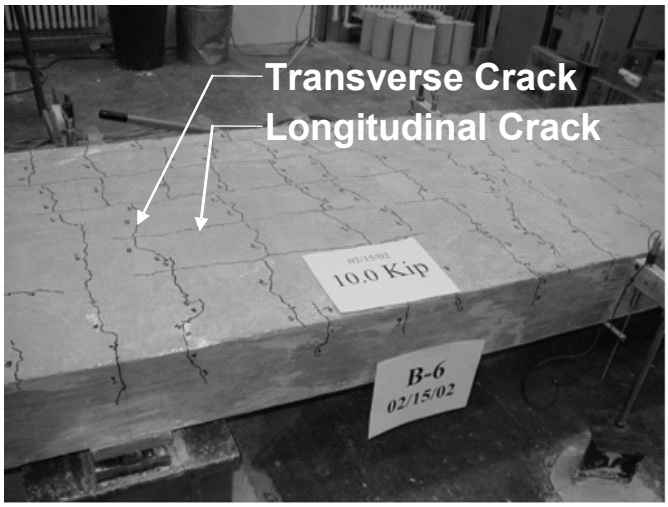

Figure 6.23: Cracking Pattern of Specimen B-6

6.11 Analysis

6.11.1 Crack Spacing

6.11.1.1 Spacing of Reinforcement

To directly investigate how the spacing of reinforcing bars in each slab specimen affected the spacing and number of primary cracks, the average number of primary cracks and their average spacings for each specimen with the same amount of reinforcement are presented in Table 6.11 and Figure 6.24. Both the black and epoxy coated bars were included in the analysis.

Table 6.11: Number and Spacings of Primary Cracks (Steel Stress 60 ksi)

Bar Spacing (in.)	Average Number of Primary Cracks	Average Spacings of Primary Cracks
6	13.0	6.8
9	10.5	8.3
12	8.0	9.9
18	6.5	12.7

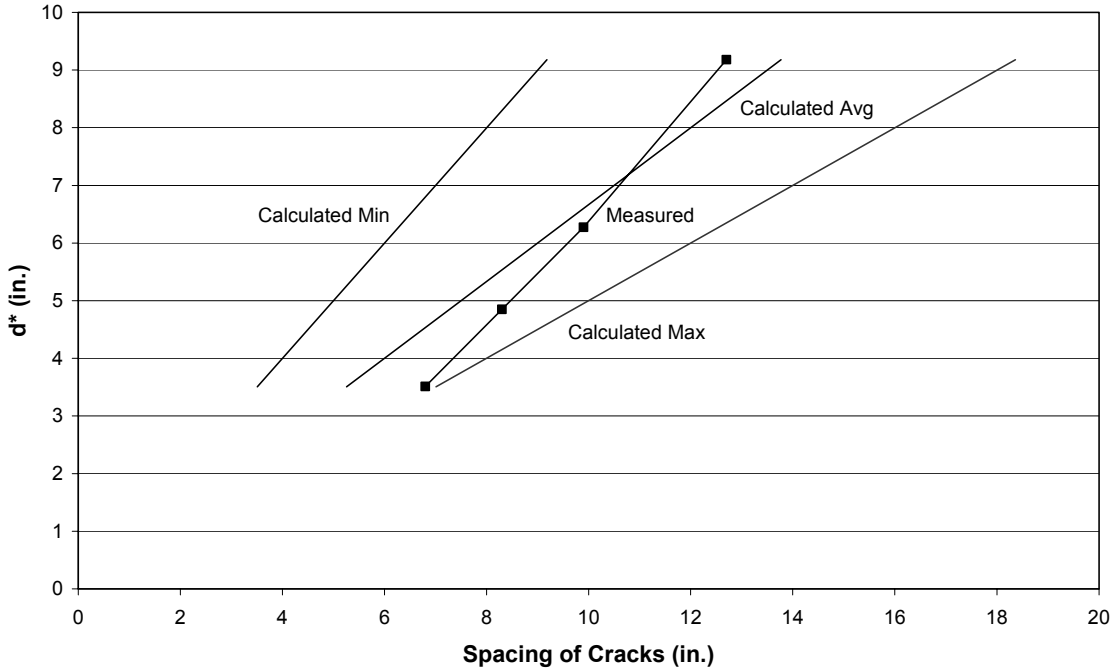

Figure 6.24: Measured and Calculated Crack Spacings vs. d* (60 ksi Steel Stress)

To compare the experimental results with the theoretical analysis (Frosch 1999), the spacings of the primary cracks compared to the maximum distance from a reinforcing bar (Table 6.12) to the tensile face of the slab specimens (d*) has also been plotted in Figure 6.24. The theoretical calculation of the minimum, average, and maximum crack spacings is discussed in Section 1.3.3.

Table 6.12: Maximum Distance from a Reinforcing Bar to the Tensile Face of the Slab (d*)

Number of Reinforcing Bars	Spacing of Reinforcement (in.)	d* (in.)
2	18	9.18
3	12	6.27
4	9	4.85
6	6	3.51

Figure 6.24 shows that as the spacing of the reinforcement increased, there was a corresponding increase in the spacing of the cracks. According to the measured crack spacings from the slab specimens, the relationship between crack spacings and bar spacing is nearly linear and falls within the calculated minimum and maximum. The data indicates that as the spacing of the reinforcement decreased, the calculated average crack spacings were lower than test results and as the spacing of the reinforcement increased, calculated crack spacings were higher than the measured values. Regardless, all measured crack spacings fell within the calculated range, and reaffirm that the crack spacings can be reasonably calculated.

6.11.1.2 Varying Epoxy Thickness

To examine the effect of epoxy thickness on the number and spacing of primary cracks, it is necessary to compare specimens with the same amount of reinforcement, but with varying epoxy thickness. Table 6.13 presents the number and spacing of cracks for each of the specimens designed with 9 in. spaced reinforcement.

Table 6.13: Epoxy Thickness Effect on Crack Spacings (9 in. Spacing)

Thickness of Epoxy (mils)	Number of Primary Cracks	Spacing of Primary Cracks (in)
Black	9	9.0
6	11	8.0
12	10	8.9
18	12	7.4

Even though there is not a large amount of data to confirm a trend, the data suggests that the thickness of the epoxy did affect the number and spacing of primary cracks in each specimen. The data suggests that as the epoxy thickness increased, the number of primary cracks also increased. Also, it seems that as the thickness of epoxy increased the spacings of the primary cracks decreased. This is opposite to prior expectations. It was assumed that a thicker epoxy coating would decrease bond and fewer cracks would develop within the constant moment region at similar loads. However, it must be noted that the differences in crack spacings are not large, indicating that there is not a significant effect between epoxy coating thickness and crack spacings. The variation in crack spacings is within the scatter inherent in cracking.

6.11.2 Crack Widths

6.11.2.1 Reinforcement Spacing

Two sets of specimens were designed to investigate the effect of reinforcement spacing on the widths of primary cracks. Four specimens were designed with varying spacings of black reinforcement (B-18, B-12, B-9, B-6), while four additional specimens were designed with varying spacings of 12 mil epoxy coated reinforcement (E12-18, E12-12, E12-9, E12-6). The steel stress is plotted versus the measured average and maximum crack widths in Figures 6.25-6.28. The reinforcement stress level was calculated using a cracked section analysis. The crack width measurements for these specimens at varying stress levels are provided in Appendix G.

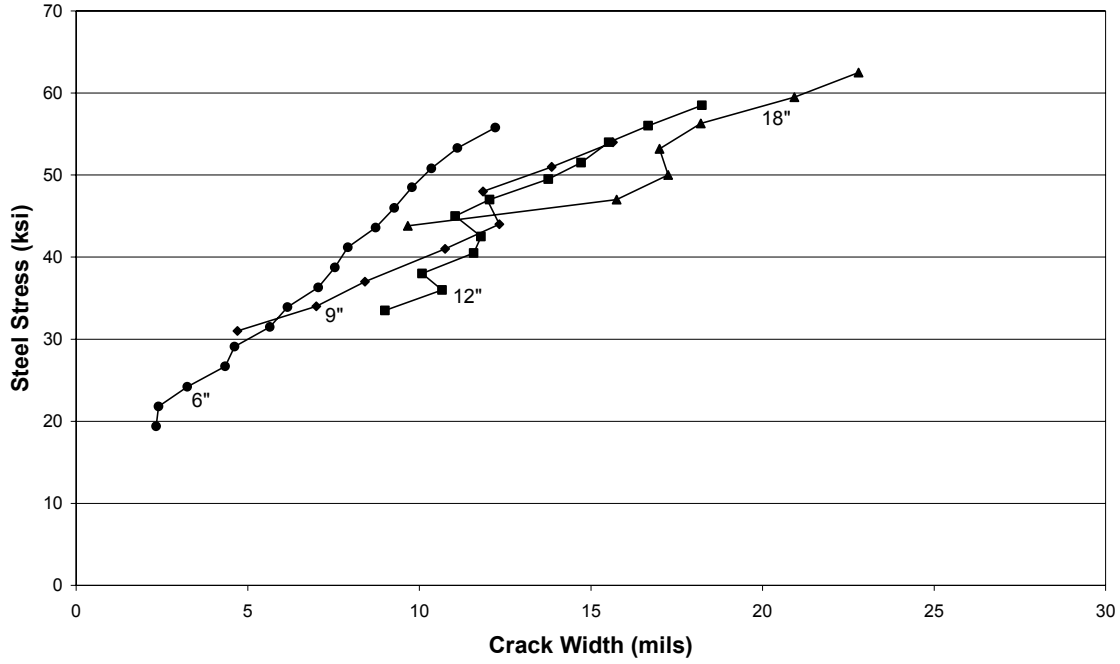

Figure 6.25: Average Crack Widths (Black Bars)

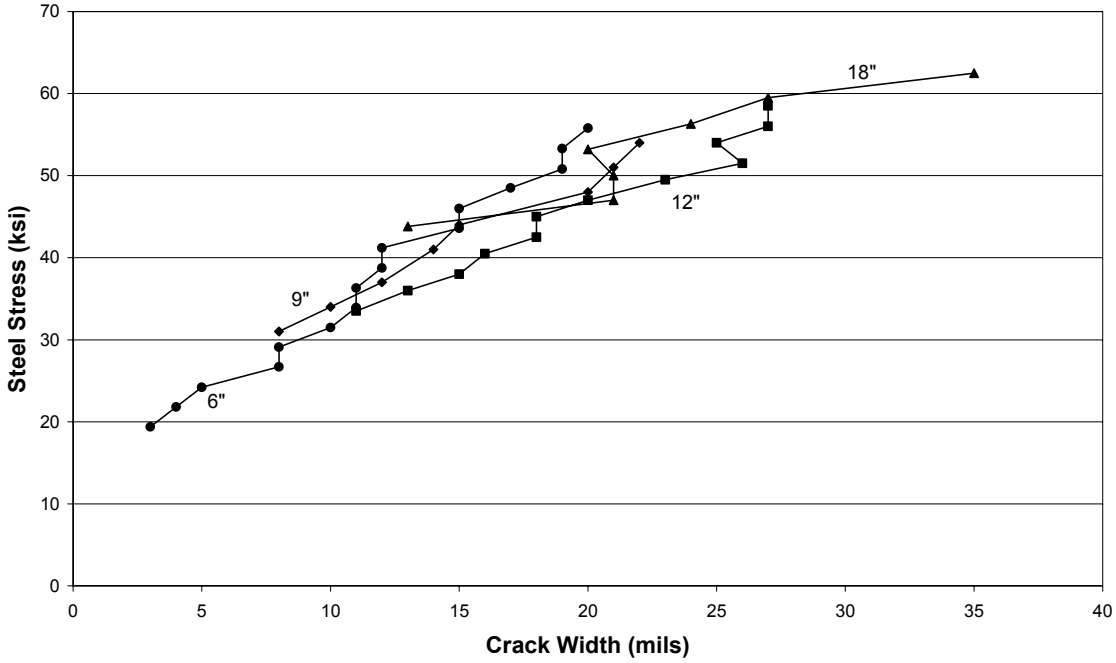

Figure 6.26: Maximum Crack Widths (Black Bars)

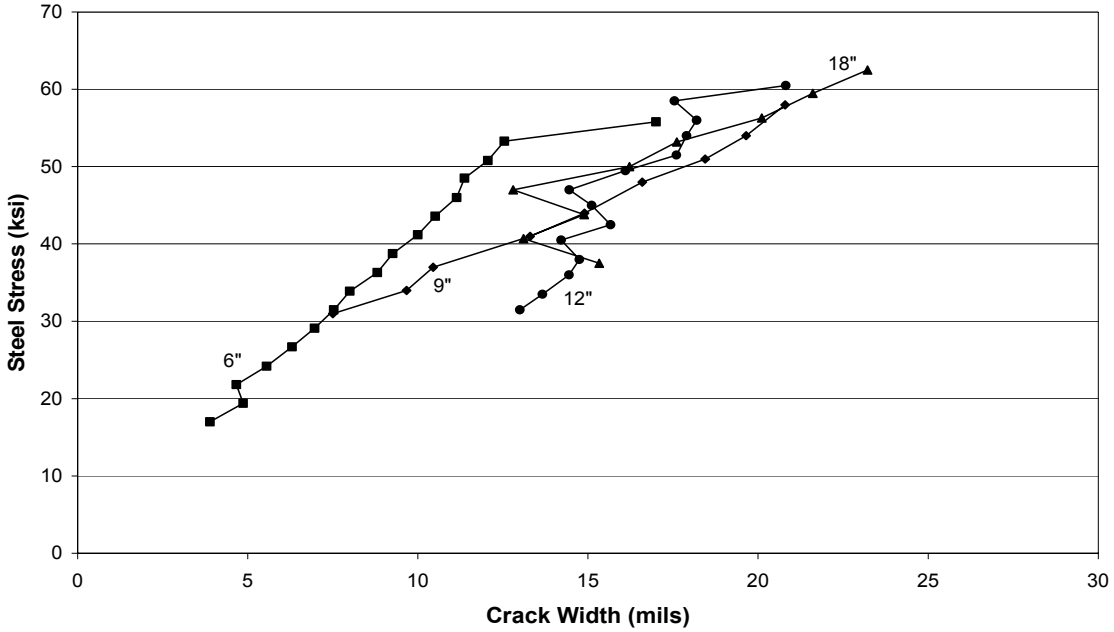

Figure 6.27: Average Crack Widths (12 mil Epoxy Coated Bars)

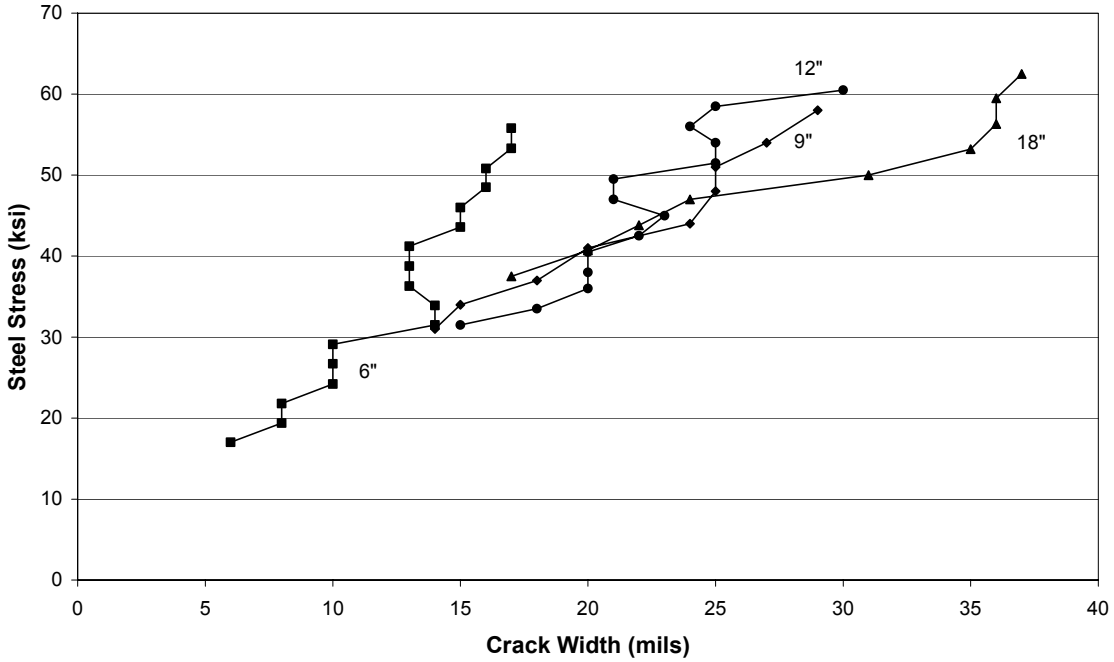

Figure 6.28: Maximum Crack Widths (12 mil Epoxy Coated Bars)

Each of the figures indicates similar trends. First, as the spacing of the reinforcement increased, there was a corresponding increase in crack width. Second, as the spacing of the reinforcement decreased, first cracking occurred at lower steel stress levels. Finally, it appears that the average crack width for specimens designed with black bars was less at every stress level than the specimens designed with epoxy coated (12 mil) bars.

To provide a clearer picture of the effect of the reinforcement spacing on the widths of the primary cracks, the average and maximum crack widths of specimens designed with black reinforcement and 12 mil epoxy coated bars are compared in Tables 6.14-6.17. At each steel stress level, the average and maximum crack widths were divided by the crack width measured in the specimen with a 6 in. reinforcement spacing (B-6 or E12-6) at the same stress level to determine an influence factor. The bolded values represent the largest influence factors computed, while the italicized crack readings represent crack widths that exceed the generally accepted crack width of 16 mils (ACI 318-99). Average influence factors are also presented.

Table 6.14: Average Crack Widths of Specimens (Black Bars)

Steel Stress	Spacing of Reinforcement (in.)							
	6		9		12		18	
(ksi)	w_6 (mils)	w_6/w_6	w_9 (mils)	w_9/w_6	w_{12} (mils)	w_{12}/w_6	w_{18} (mils)	w_{18}/w_6
30	4.9	1.00	-	-	-	-	-	-
35	6.5	1.00	7.5	1.15	10.2	1.57	-	-
40	7.6	1.00	10.0	1.32	11.4	1.50	-	-
45	9.1	1.00	10.6	1.16	11.0	1.21	11.3	1.24
50	10.2	1.00	13.1	1.28	14.0	1.37	*17.3*	**1.70**
55	11.9	1.00	15.6	1.31	*16.1*	1.35	*17.9*	1.50
Avg.	-	1.00	-	1.25	-	1.40	-	1.48

Note: Bold indicates the largest influence factors computed.
Italic indicates crack readings exceeding the typical maximum crack limit.

Table 6.15: Maximum Crack Widths of Specimens (Black Bars)

Steel Stress	Spacing of Reinforcement (in.)							
	6		9		12		18	
(ksi)	w_6 (mils)	w_6/w_6	w_9 (mils)	w_9/w_6	w_{12} (mils)	w_{12}/w_6	w_{18} (mils)	w_{18}/w_6
30	9	1.00	-	-	-	-	-	-
35	11	1.00	10	0.91	12	1.09	-	-
40	12	1.00	13	1.08	15	1.25	-	-
45	15	1.00	*19*	1.27	*18*	1.20	15	1.00
50	*18*	1.00	*21*	1.17	*24*	**1.33**	*21*	1.17
55	*20*	1.00	*22*	1.10	*26*	1.30	*22*	1.10
Avg.	-	1.00	-	1.11	-	1.23	-	1.09

Note: Bold indicates the largest influence factors computed.
Italic indicates crack readings exceeding the typical maximum crack limit.

Table 6.16: Average Crack Widths of Specimens (12 mil Epoxy)

Steel Stress	Spacing of Reinforcement (in.)							
	6		9		12		18	
(ksi)	w_6 (mils)	w_6/w_6	w_9 (mils)	w_9/w_6	w_{12} (mils)	w_{12}/w_6	w_{18} (mils)	w_{18}/w_6
25	5.9	1.00	-	-	-	-	-	-
30	7.2	1.00	-	-	-	-	-	-
35	8.3	1.00	10.2	1.22	14.8	**1.78**	-	-
40	9.7	1.00	12.5	1.29	15.3	1.58	*16.7*	1.72
45	11.0	1.00	15.4	1.40	15.1	1.37	15.9	1.44
50	11.9	1.00	*17.8*	1.50	*16.6*	1.39	*16.2*	1.36
55	13.3	1.00	*20.1*	1.51	*18.2*	1.37	*21.8*	1.63
Avg.	-	1.00	-	1.38	-	1.50	-	1.53

Note: Bold indicates the largest influence factors computed.
Italic indicates crack readings exceeding the typical maximum crack limit.

Table 6.17: Maximum Crack Widths of Specimens (12 mil Epoxy)

Steel Stress	Spacing of Reinforcement (in.)							
	6		9		12		18	
(ksi)	w_6 (mils)	w_6/w_6	w_9 (mils)	w_9/w_6	w_{12} (mils)	w_{12}/w_6	w_{18} (mils)	w_{18}/w_6
25	10	1.00	-	-	-	-	-	-
30	10	1.00	-	-	-	-	-	-
35	14	1.00	*17*	1.21	*19*	1.36	-	-
40	14	1.00	*19*	1.36	*20*	1.43	*17*	1.21
45	15	1.00	*24*	1.60	*23*	1.53	*22*	1.47
50	16	1.00	*25*	1.56	*23*	1.44	*31*	1.94
55	*18*	1.00	*27*	1.50	*24*	1.33	*36*	**2.00**
Avg.	-	1.00	-	1.44	-	1.42	-	1.66

Note: Bold indicates the largest influence factors computed.
Italic indicates crack readings exceeding the typical maximum crack limit.

The data suggests that as the bar spacing increased, crack widths became larger. In the range of reinforcement spacings tested, average crack widths (Black bars) could be influenced by as much as 70% (B-18) and maximum crack width could be influenced by as much as 33% (B-12). When averaged over all stress levels, the influence dropped to 48% for average crack width, and 23% for maximum crack width. The data also indicates that the spacing of reinforcement affected crack widths more when 12 mil epoxy coated bars were used. Average crack widths (12 mil Epoxy) were influenced by

as much as 78% (E12-12) and maximum crack width was influenced by as much as 100% (E12-18). The difference in crack widths is significant and can affect the lifespan of an exposed concrete structure.

It is also interesting to note that both Specimens E12-9 and E12-12 exceeded the maximum crack width limitation at a steel stress level of 35 ksi. It was not until a steel stress of 45 ksi that any of the specimens designed with black bars (B-9 and B-12) exceeded this limit.

The measured crack widths can also be compared with the calculated values. Table 6.16 presents the ratio of the calculated crack width vs. measured crack width for each of the specimens designed with black reinforcing bars. Crack widths were calculated by the model presented by Frosch that was also presented in Chapter 1. It must be noted that the values given in Table 6.18 have been averaged over all stress levels. Individual calculation comparisons have been made for each specimen and are provided in Appendix H.

Table 6.18: Calculated and Measured Crack Width Relationship (Black Bars)

Reinforcement Spacing (in.)	Calculated Crack Width / Measured Crack Width	
	Average	Maximum
6	1.29	1.02
9	1.36	1.23
12	1.50	1.37
18	2.01	2.12

The calculated values for both average and maximum crack widths overestimated the measured crack width. The trend from Table 6.18 shows that as the bar spacing decreased, the estimated values became more accurate. Also, it appears that the calculation method provides a better estimation for maximum crack widths than the average crack widths.

To further examine the accuracy of the calculation method, the ratio of the calculated vs. measured crack widths (12 mils epoxy) are presented Table 6.19. The epoxy coating was not considered when calculating widths for the epoxy coated bars.

Table 6.19: Calculated and Measured Crack Width Relationship (12 mils Epoxy)

Reinforcement Spacing (in.)	Calculated Crack Width / Measured Crack Width	
	Average	Maximum
6	0.99	0.91
9	0.98	0.87
12	1.17	1.14
18	1.64	1.52

The calculated crack widths for the specimens reinforced with bars coated with 12 mils of epoxy were more accurate than for the black bars. Because the calculated crack widths estimated were found to be large for specimens containing black bars, the ratio of calculated crack width vs. measured crack width became more accurate as the epoxy coating increased. The same trends observed from the black bars were also observed with the reinforcing bars coated with 12 mils of epoxy. As the spacing of the reinforcement decreased, the calculated values became more accurate. The results show that the maximum calculated/measured ratios were in all cases lower than average calculated/measured ratios.

6.11.2.2 Varying Epoxy Thickness

Of the ten specimens designed for the experimental program, four (B-9, E6-9, E12-9, E18-9) were designed specifically to determine the effect of epoxy coating thickness on crack width. All crack width measurements are available in Appendix G. Steel stress is plotted versus the measured average and maximum crack width in Figures 6.29 and 6.30.

It can be seen in general that the crack width increased as the thickness of the epoxy coating increased. For both average and maximum crack widths, it appears that the 6 mil epoxy coated bars behaved similar to the black reinforcing bars. In addition, the two specimens containing 12 and 18 mil epoxy thickness also behaved similarly.

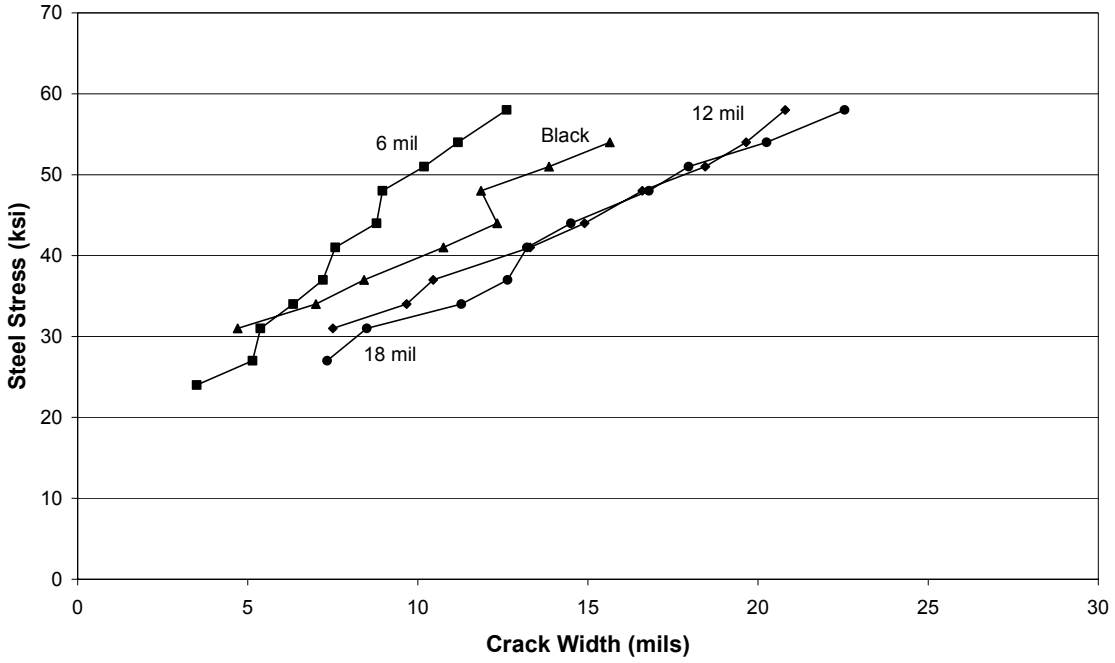

Figure 6.29: Average Crack Widths for Varying Epoxy Thickness (9 in. Spacing)

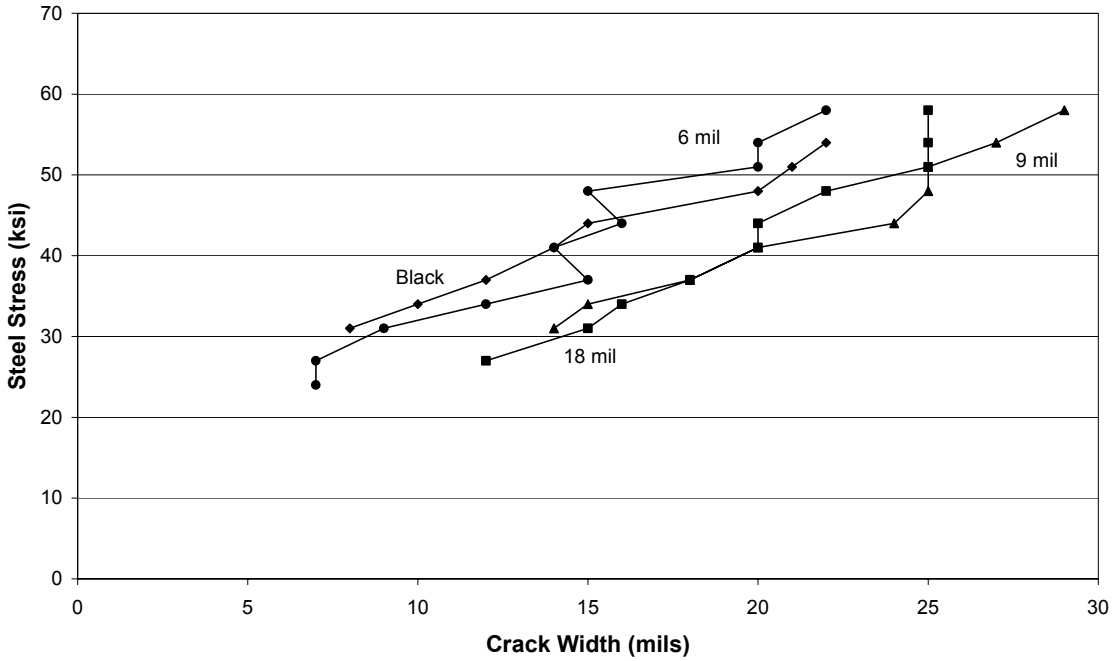

Figure 6.30: Maximum Crack Widths For Varying Epoxy Thickness (9 in. Spacing)

To provide further insight, the measured average and maximum crack widths are tabulated versus the corresponding steel stress. In addition, the crack widths are divided by the average or maximum crack width measured from Specimen B-9 to determine the influence of the epoxy coating thickness (Tables 6.20 and 6.21). Again, the bolded values represent the largest influence factors computed while the italicized crack readings represent crack widths that exceed the generally accepted crack width limit of 16 mils (ACI 318-99). Average values of the influence factors for each epoxy thickness are also presented.

Table 6.20: Average Crack Widths of Specimens (9 in. Bar Spacing)

Steel Stress	Thickness of Epoxy (mils)							
	Black		6		12		18	
(ksi)	w_b (mils)	w_b/w_b	w_6 (mils)	w_6/w_b	w_{12} (mils)	w_{12}/w_b	w_{18} (mils)	w_{18}/w_b
35	7.5	1.00	6.6	0.88	10.2	1.36	12.3	**1.64**
40	10.0	1.00	8.3	0.83	12.5	1.25	13.3	1.33
45	10.6	1.00	8.9	0.84	15.4	1.45	15.1	1.42
50	13.1	1.00	9.8	0.75	*17.8*	1.36	*17.6*	1.34
55	15.6	1.00	11.6	0.74	*20.1*	1.29	*20.9*	1.34
Avg.	-	1.00	-	0.81	-	1.34	-	1.42

Note: Bold indicates the largest influence factors computed.
Italic indicates crack readings exceeding the typical maximum crack limit.

Table 6.21: Maximum Crack Widths of Specimens (9 in. Bar Spacing)

Steel Stress	Thickness of Epoxy (mils)							
	Black		6		12		18	
(ksi)	w_b (mils)	w_b/w_b	w_6 (mils)	w_6/w_b	w_{12} (mils)	w_{12}/w_b	w_{18} (mils)	w_{18}/w_b
35	10	1.00	13	1.30	*17*	**1.70**	*17*	**1.70**
40	13	1.00	14	1.08	*19*	1.46	*20*	1.54
45	*19*	1.00	16	0.84	*24*	1.26	*20*	1.05
50	*21*	1.00	*18*	0.86	*25*	1.19	*23*	1.10
55	*22*	1.00	*20*	0.91	*27*	1.23	*26*	1.18
Avg.	-	1.00	-	1.00	-	1.37	-	1.31

Note: Bold indicates the largest influence factors computed.
Italic indicates crack readings exceeding the typical maximum crack limit.

The data suggests that for the range of epoxy coating thickness tested, the average crack width could be influenced by as much as 64% (E18-9) while the maximum crack width could be influenced by as much as 70% (E12-9 and E18-9). When averaged over all stress levels, the influence dropped to 42% for average crack width, and 37% for maximum crack width. It is interesting to note that the influence factor was largest, in both cases (average and maximum), at the lowest steel stress level (35 ksi). This steel stress level is well within working stress levels; therefore, crack widths in a bridge deck using epoxy coated reinforcement can be significantly higher than for uncoated reinforcement. Due to the scatter in the influence factor, the average values may not be indicative of the true influence.

More importantly than the influence values calculated at low stress levels in Specimens E12-12 and E12-18, upon first cracking, the primary crack width exceeded the crack width limit of 0.0016 in. Even Specimen B-9 exceeded the crack size limit at a steel stress of 45 ksi.

The crack widths measured during the experimental procedure can also be compared with the calculated values. To investigate if the calculated crack widths were affected by the epoxy coating thickness, the average and maximum calculated crack widths have been normalized by the measured crack readings and are presented in Table 6.22. The number of observations for each comparison has also been presented in the table. An observation refers to one crack reading (average or maximum) at a given stress level for each specimen. Figures 6.31–6.34 presents histograms of the average and maximum calculated crack width divided by the measured crack width for both black and epoxy coated bars.

Table 6.22: Crack Width Due to Epoxy Coating

Bar Coating Type	Calculated Crack Width / Measured Crack Width				
	Avg.	S.D.	Max	S.D	Number of Observations
Black	1.54	0.34	1.44	0.48	20
Epoxy	1.24	0.34	1.11	0.26	34

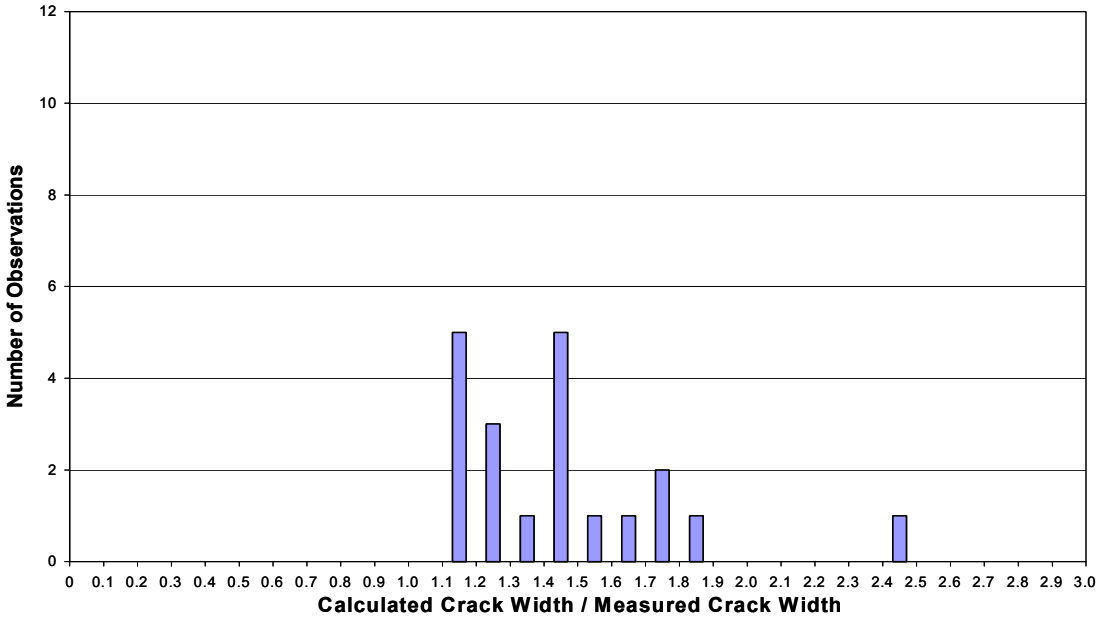

Figure 6.31: Calculated / Measured Average Crack Width (Black Bars)

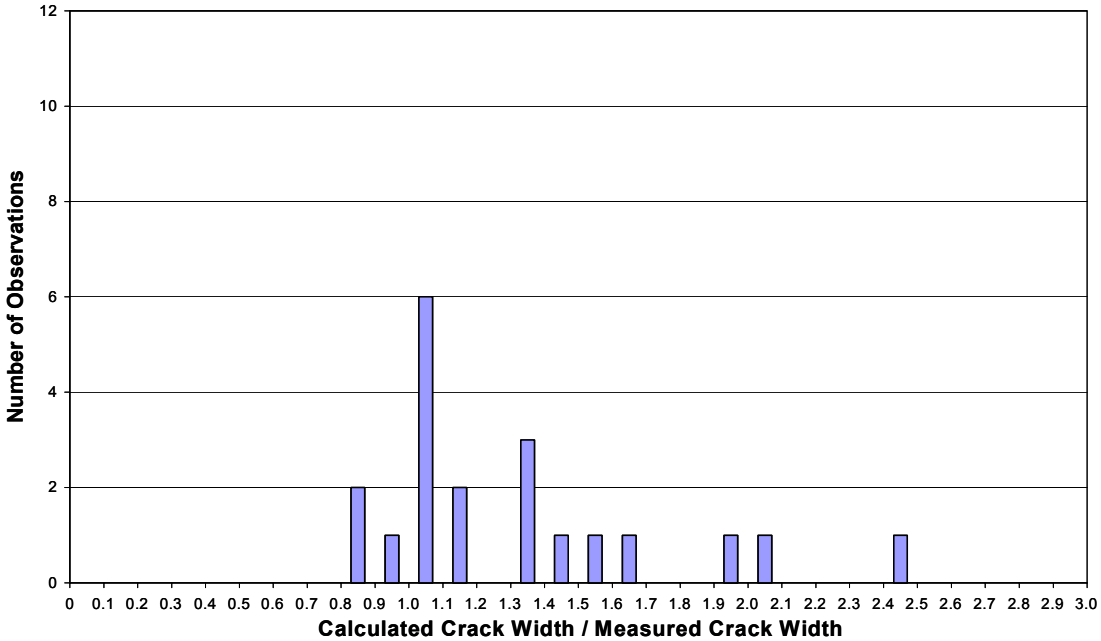

Figure 6.32: Calculated / Measured Maximum Crack Width (Black Bars)

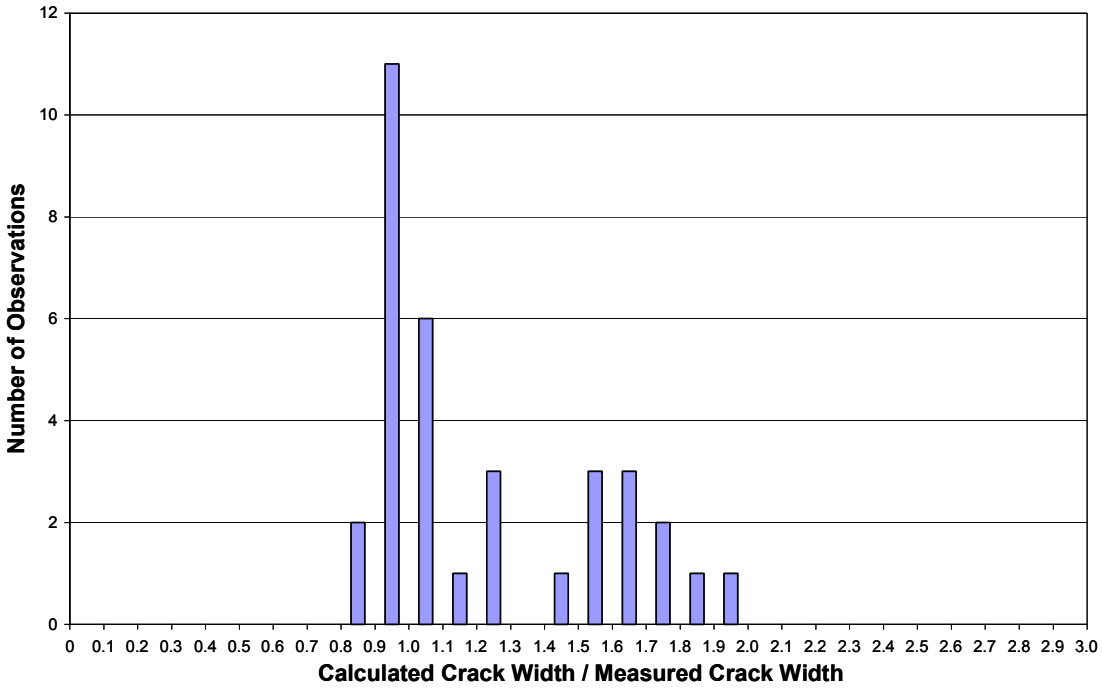

Figure 6.33: Calculated / Measured Average Crack Width (Epoxy Coated Bars)

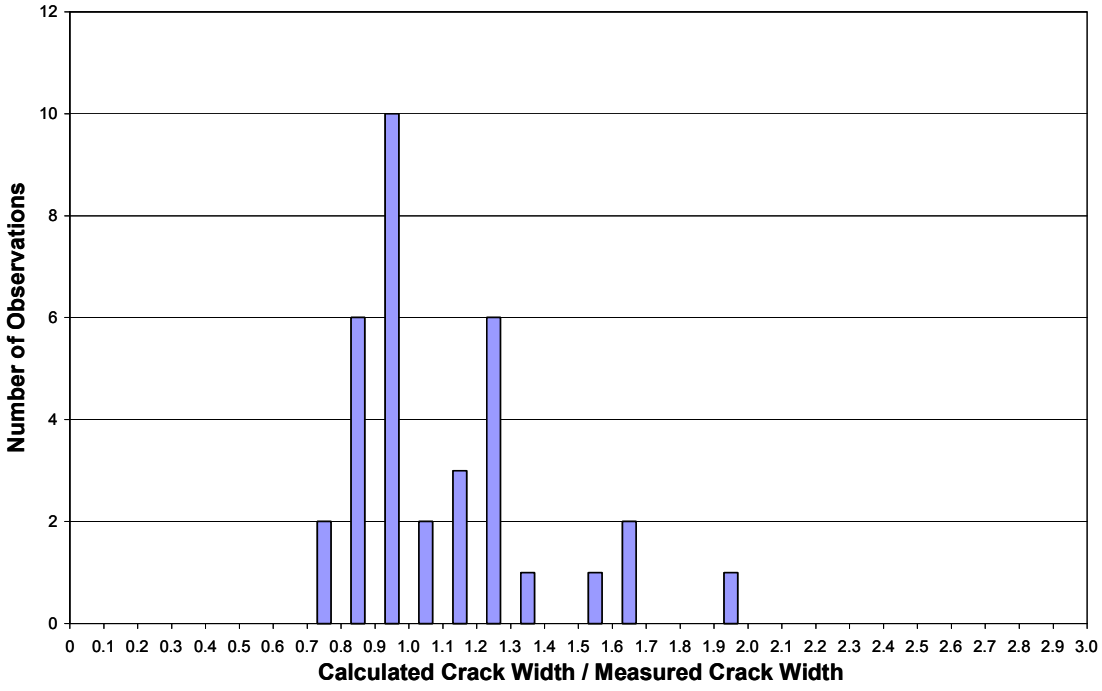

Figure 6.34: Calculated / Measured Maximum Crack Width (Epoxy Coated Bars)

From these results, it can be seen that both the average and maximum cracks widths, for both the black and epoxy coated bars, on average were overestimated. The maximum crack widths were calculated closer to the actual than were the average values. The scatter depicted in the histograms is similar to what has been found using other crack calculation methods (Frosch 1999). The accuracy of the calculation was also evaluated by comparing the results of varying epoxy-coating thickness. Table 6.23 presents calculated/measured average and maximum crack width ratios.

Table 6.23: Calculated and Measured Crack Width Relationship

Epoxy Thickness (mils)	Calculated Crack Width / Measured Crack Width			
	Avg.	S.D.	Max	S.D.
Black	1.54	0.34	1.44	0.48
6	1.68	0.15	1.32	0.19
12	1.20	0.26	1.11	0.28
18	0.95	0.06	0.92	0.04

Again, the average calculated/measured width ratios were estimated larger than the maximum crack widths ratios. Up to an epoxy thickness of 12 mils, the calculated maximum crack widths overestimated the actual readings, except from Specimen E18-9, where the crack widths measured were underestimated. These results indicate that, in order to calculate crack widths with the same factor of safety as when black bars are used, the calculation must have a multiplier that accounts for the epoxy coating thickness. Within the range of epoxy coating thickness currently accepted by ASTM, the data suggests that a crack width multiplier of 1.3 would ensure a factor of safety similar to that computed when black bars are used. According to the data, if an epoxy coating thickness of 18 mils were used, a multiplier of 1.6 would be necessary to retain a similar factor of safety as found when using black bars. Consequently, the multiplication factor proposed by Frosch (2.0), overestimated crack widths measured from specimens designed with epoxy coated bars and can be decreased (Frosch 1999).

CHAPTER 7
SUMMARY AND CONCLUSIONS

7.1 Introduction

Many bridges in the state of Indiana have been identified to have cracking in the concrete deck. Cracking has been identified in the negative and positive moment regions of bridges on both the top and bottom surfaces. In some structures, only top surface cracking is visible due to the use of stay-in-place steel forms. The cracking can appear before or shortly after the opening of the structure to live loads. Significant crack widths and various degrees of cracking exist in different bridge systems including both concrete and steel superstructures.

The objective of this research project was to determine the factors affecting transverse and longitudinal bridge deck cracking in Indiana, as well as, to develop design recommendations that minimize or prevent these types of cracking in bridge decks. The research focused on the design and construction of new bridge decks. For bridge decks being rehabilitated with overlays, overlay cracking can also be of concern. Therefore, for completeness, recommendations to minimize this type of cracking are provided in Section 1.6.2.

7.2 Research Conclusions

This research project was divided into five phases. The results of each phase are presented below.

7.2.1 Phase 1: Field Investigation

The first phase was a field evaluation of 20 bridge locations to investigate the scope of the problem experienced in Indiana. From the data obtained in the first phase, the following conclusions were made:

1. Bridge decks cast monolithically with a concrete superstructure had the fewest cracks.
2. The restraint of the concrete deck on steel superstructure bridges, through the use of composite action and/or stay-in-place steel forms, induced more transverse cracking than those not incorporating composite action and/or stay-in-place steel forms.
3. Transverse cracks were observed on more bridges with a steel girder superstructure than bridges with a concrete superstructure. Precast, prestressed concrete superstructure bridges likely behave similar to the monolithic concrete bridges and shrink with the deck instead of restraining the shrinkage when the concrete girders and deck are close in age.

7.2.2 Phase 2: Field Instrumentation

Using the information gathered from the first phase, the second phase consisted of the instrumentation of a typical bridge structure to provide an understanding of the behavior of transverse cracks in a concrete bridge deck. From the data obtained in the second phase, the following conclusions were made:

1. The I65 over SR25 bridge experienced longitudinal deck cracking within 9 days after deck casting and transverse cracks 19 days after deck casting.
2. The leg of the cold-rolled angle turned into the deck to support the stay-in-place steel forms causes a discontinuity and crack initiation location. This construction feature caused longitudinal deck cracking in the bridge investigated. It is noted that the contractor did not construct the formwork in accordance with the approved formwork drawings. The short leg rather than the long leg should have been turned into the deck. However, either detail will cause a discontinuity and crack initiation location.
3. Based on the recorded data, the peak temperature of the deck due to the heat of hydration was reached roughly 14 hours after the deck was cast and continued to generate heat for approximately 48 hours. The temperature development during the heat of hydration did not contribute to the development of transverse cracks.
4. Based on the recorded data, the occurrence of transverse cracking was not influenced by live loads or the vibrations caused by live loads.
5. The channels in the stay-in-place steel forms create shear keys in the bottom surface of the deck, which may restrict the concrete during drying shrinkage. In addition, the vertical component of the stay-in-place steel forms induces a crack initiation location.
6. For longitudinal deck reinforcement with #4 top bars and #5 bottom bars spaced at 11 13/16-in. on center, the reinforcing steel yielded once the deck developed transverse cracks.

7.2.3 Phase 3: Laboratory Models

With the findings from the previous two phases, the third phase conducted a laboratory investigation to study the effects of shrinkage and restraint of a concrete deck and to determine the contribution of stay-in-place steel forms to the formation of transverse cracking. Two models were constructed, instrumented, and monitored. From the data obtained in the third phase, the following conclusions were made:

1. Based on the recorded data, the peak temperature of the deck models due to the heat of hydration was reached 13 ½ hours after the models were cast and continued to generate heat for approximately 72 hours. The temperature and duration were similar to that experienced in the field. The heat of hydration had a dramatic initial influence on the measured strains and deflections. However, the heat of hydration did not contribute to transverse cracking.
2. Once the curing process was terminated, moisture loss and drying shrinking commenced.

From the findings in the first three phases, the primary cause of deck cracking is the restraint of the drying shrinkage of the concrete. Methods that reduce the restraint or

minimize drying shrinkage are recommended to reduce the development of transverse cracking.

7.2.4 Phase 4: Laboratory Shrinkage Models

Shrinkage strains and displacements were monitored in ten laboratory deck models for two months. The models were designed to determine the effects of form type on the magnitude of shrinkage, curling, and early-age bridge deck cracking. The following conclusions were made:

1. The stiffness of SIP deck pans in restraining shrinkage is not significant. The stiffness of the deck pans oriented in the transverse direction affected neither the curling nor the total magnitude of shrinkage of the specimens. The stiffness of the SIP deck pans oriented in the longitudinal direction did not affect the curling of the specimens, but the total magnitude of shrinkage was slightly reduced.
2. Sealing the bottom surface of a bridge deck was found to significantly influence deck shrinkage. When compared to a wood formed deck model, sealed specimens both decreased the total shrinkage magnitude (up to 23%) and increased curling (up to 60%).
3. Reinforcement significantly affected the total magnitude of shrinkage and curling. Less shrinkage was measured from specimens designed with reinforcement (up to 11%). However, the non-symmetric layout of the reinforcement caused those specimens to curl approximately 15% more than similar specimens designed without reinforcement.
4. Increased deck thickness affected the total magnitude of shrinkage. The specimens designed with an increased thickness (8-7/8 in. vs. 7-7/8 in.) shrank 16% less at the surfaces.
5. Hydration temperatures were not affected by form type.

7.2.5 Phase 5: Reinforced Concrete Slab Models

Ten reinforced concrete slab models were constructed to determine the effects of bar spacing and epoxy coating thickness on crack widths and spacings. Each model was subjected to a constant moment region. Slab specimens were reinforced with 6, 9, 12, and 18 in. spaced reinforcement. Epoxy coating thicknesses ranged from 0 mils (Black) to 18 mils. Cracks were measured at incremental steel stress levels up to 60 ksi. The measured crack widths and spacings were also compared to calculated crack widths and spacings. The following conclusions were made:

1. Load-deflection behavior was not affected by epoxy coating thickness. Regardless of reinforcement spacing or epoxy coating thickness, first cracking for each specimen occurred at approximately the same load. Behavior, beyond cracking was similar.
2. Spacing of reinforcement significantly affected the widths and spacings of cracks. As the reinforcement spacing decreased, the spacing of primary cracks decreased and the number of primary cracks increased. As the reinforcement spacing increased, there was a corresponding increase in crack width. This trend is consistent with generally accepted behavior.

3. Epoxy coating thickness significantly affected the widths and spacings of primary cracks. In general, as epoxy coating thickness increased, both average and maximum crack widths also increased. Specimens designed with 6 mil epoxy coated bars behaved similarly to specimens designed with black reinforcing bars; however, the data indicated that crack widths in specimens designed with thicker epoxy coatings (12 and 18 mils) could be affected up to 70% when compared to similar specimens designed with black bars.
4. To calculate crack widths of epoxy coated bars, the calculation procedure must account for epoxy coating thickness. Crack widths for epoxy coated bars can be computed by multiplying a factor times the crack width computed for black bars. Within the range of epoxy coating thicknesses currently accepted by ASTM (6-12 mils), the data indicated that a crack width multiplier of 1.3 is necessary. Furthermore, a multiplier of 1.6 is necessary if 18 mil epoxy coated bars are used.

7.3 Recommendations

Based on the research investigation, transverse deck cracking is caused by restrained shrinkage of the concrete deck. Since reduction of restraint is not possible due to the economic advantages of composite construction, the following recommendations to minimize deck cracking are made based on both the research and literature survey.

1. The requirement in the *INDOT Standard Specifications* (1999) for a minimum of 96 hours of wet curing of the concrete deck is insufficient. A minimum 7 day wet curing process is recommended to reduce drying shrinkage cracking by reducing overall shrinkage strains.
2. Drying shrinkage of the concrete mix should be minimized. Measures that reduce the shrinkage tendency of the mix should be encouraged. This can be achieved through mix design and materials selection. As an example, proper aggregate selection and gradation can produce lower shrinkage mixes.
3. Concrete compressive strength should be minimized. Strengths higher than specified by design are not required and can exacerbate deck cracking. Higher concrete strengths affect cracking in several ways. Higher compressive strengths resulting from additional cement can produce higher shrinkage concretes. Furthermore, higher compressive strength concretes have a higher tensile strength that can increase the likelihood of reinforcement yielding as well as a higher modulus of elasticity that provides additional internal restraint. Current INDOT class C concrete requires 659 lbs/yd^3 of cement which is regularly producing strengths in excess of 6,000 psi. This cement requirement can be reduced for bridge decks as only 4000 psi is required by design.
4. Current code requirements for shrinkage and temperature reinforcement do not place sufficient limits on bar spacings to control early-age bridge deck cracking. To produce maximum crack widths in the range of 16 mils, a maximum bar spacing of 6 in. is necessary when using current cover requirements and currently accepted epoxy thicknesses (6 to 12 mils). It should be noted that during this

study, INDOT increased the required thickness to the range of 8 to 13 mils which falls approximately in the range investigated here. If epoxy coating thicknesses are increased beyond these values in the future, smaller bar spacings would be required to achieve similar crack widths.

5. Additional reinforcement above current practice is required to control the crack widths in concrete decks. The total amount of reinforcing steel recommended is:

$$A_s = \frac{6\sqrt{f_c'}}{f_y} A_g$$

where:

A_g = gross area of section, in.^{2}
A_s = area of reinforcement in cross-section, in.^{2}
f_c' = specified compressive strength of concrete, psi.
f_y = specified yield strength of reinforcement, psi.

The purpose of this reinforcement is to prevent yielding of the reinforcement that can result in uncontrolled crack growth. For 4,000 psi concrete and 60,000 psi reinforcement, this requirements results in 0.63% steel in the deck cross-section.

6. Alternatives to stay-in-place (SIP) forms should be considered. From the experimental investigation, SIP forms produce curling that can exacerbate cracking on the top surface of the deck, provide for a crack initiation location due to the pan shape, as well as prevent visual inspection of the bottom deck surface. Removable formwork with a flat surface eliminates these problems.
7. Support of formwork through the use of an angle leg turned into the deck should be discontinued. The leg of the angle included in the deck causes a discontinuity and crack initiation location producing longitudinal girder edge cracking. As an alternative, the angle can be turned down to eliminate this discontinuity.

REFERENCES

ACI Committee 207, 1995, "Effect of Restraint, Volume Change, and Reinforcement on Cracking in Mass Concrete," American Concrete Institute, Farmington Hills, MI, 26 pp.

ACI Committee 224, 1998, "Causes, Evaluation, and Repair of Cracks in Concrete Structures (ACI 224.1R-93)," American Concrete Institute, Farmington Hills, MI, 22 pp.

ACI Committee 224, 2001, "Control of Cracking in Concrete Structures (ACI 224R-01)," American Concrete Institute, Farmington Hills, MI, 46 pp.

AASHTO, 1998, *AASHTO LRFD Bridge Design Specifications*, 2nd Edition, American Association of State Highway and Transportation Officials, Washington, D.C..

AASHTO, 1996, *AASHTO Standard Specification for Highway Bridges*, 16th Edition, American Association of State Highway and Transportation Officials, Washington, D.C.

Babaei, K. and Fouladgar, A.M., 1997, "Solutions to Concrete Bridge Deck Cracking," *Concrete International*, v. 19, n. 7, July 1997, pp 34-37.

Beer, F. P., and Johnston, Jr. R., 1992, "Mechanics of Materials 2nd Edition," McGraw-Hill Inc., New York.

Blackman, D., 2002, "Evaluation of Design Methods for the Control of Early Age Bridge Deck Cracking," Masters Thesis, School of Civil Engineering, Purdue University, May 2002.

Broms, B., 1965, "Crack Width and Crack Spacing in Reinforced Concrete Members," *Journal of the American Concrete Institute*, October 1965, pp. 1237-1255.

Cady P.D.; Carrier R.E., Bakr, T.A.; and Theisen, J.C., 1971, "Final Report of the Durability of Bridge Deck Concrete," The Pennsylvania State University, Dec. 1971.

Carrier, R.E., and Cady, 1975, "Moisture Distribution in Concrete Bridge Decks and Pavements," *Durability of Concrete* SP-47, American Concrete Institute, Farmington Hills, MI, pp. 169-192.

Clark, A.P., 1956, "Cracking in Reinforced Concrete Flexural Members." *Journal of the American Concrete Institute,* April 1956, pp. 851-863.

Cleary, D.B., and Ramirez, J.A., 1993, "Epoxy-Coating Reinforcement Under Repeated Loading," *ACI Structural Journal,* July-Aug. 1993, pp. 451-458.

Concrete Society, 1982, "Non-structural Cracks in Concrete," Technical Report No. 22, London, December, pp. 3-25.

Franco, R.J., 2001, "To Limit the Effects of Drying Shrinkage," *Structure,* June 2001, pp. 46-49.

French, C.E., Eppers, L.J., Le, Q.T.C. and Hajjar, J.F., 1999, "Transverse Cracking in Bridge Decks: Summary Report," Mn/DOT Final Report, January 1999, 37 pp.

Frosch, R.J., 1999, "Another Look at Cracking and Crack Control in Reinforced Concrete," *ACI Structural Journal*, May-June 1999, pp. 437-355.

Gergely, Peter and Lutz, Leroy A., 1968, "Maximum Crack Width in Reinforced Concrete Flexural Members, Causes, Mechanisms, and Control of Cracking in

Concrete," SP-20. American Concrete Institute, Farmington Hills, MI, pp. 87-117.
Gilbert, R.I., 1992, "Shrinkage Cracking in Fully Restrained Concrete Members," *ACI Structural Journal*, March-April 1992, pp. 141-149.
Healy, R.J. and Lawrie, R.A., 1998, "Bridge Cracking: A DOT Experience and Perspective," *Concrete International*, Sept. 1998, pp. 37-40.
Hughes, B.P. and Mahmood, A.T., 1998, "Early thermal cracking in end-restrained thick reinforced concrete members," Proc. Instrn. Civl. Engrs., Part 2, June 1998, pp. 305-315.
INDOT, 1992, Inter-Department Communication. *Bridge Design Memorandum #233 Revised*. Indiana Department of Transportation, Indianapolis, Indiana, November 2, 1992.
INDOT, 1999, *Standard Specifications*, Indiana Department of Transportation, Indianapolis, Indiana.
Issa, M., 1999, "An Investigation of Cracking in Concrete Bridge Decks At Early Ages," *Journal of Bridge Engineering,* May 1999, pp. 116-124.
Johnston, D.W., and Zia, P., 1982, "Bond Characteristics of Epoxy Coated Reinforcing Bars," Report No. FHWA/NC/82-002, Department of Civil Engineering, North Carolina State University, Raleigh, Aug.
Kaar, P.H. and Mattock, A.H., 1963, "High Strength Bars as Concrete Reinforcement - Part 4: Control of Cracking," *Journal of the PCA Research and Development Laboratories,* V. 5, No. 1, Jan. 1963, pp. 15-38.
Krauss, P.D. and McDonald, D.B., 1995, "Reducing Transverse Cracking in New Concrete Bridge Decks," *Concrete Construction*, Sept. 1995, pp. 735-738.
Krauss, P.D. and Rogalla, E.A., 1996, "Transverse Cracking in Newly Constructed Bridge Decks." *NCHRP Report No. 380, Transportation Research Board, National Report Council*, Washington D. C., 126 pp.
Larson, T.D., and Malloy J.J., 1966, "Durability of Bridge Deck Concrete – Report 3," Vol. 1, Pennsylvania State University, Mar. 1966, 188 pp.
Love, Jr., J.S.; Barnoff, R.M. and; Larson, T.D., 1967, "Composite Action form Corrugated Bridge Deck Forms," The Pennsylvania State University, Mar. 1967, 37 pp.
MacGregor, J.G., 1997, "Reinforced Concrete," 3rd Edition, Prentice Hall, Upper Saddle River, New Jersey, 385 pp.
McDonald, D.B., Krauss, P.D. and Rogalla, E.A., 1995, "Early-Age Transverse Deck Cracking," *Concrete International*, v. 17, n. 5, May 1995, pp. 49-51.
Measurements Group, Inc., Micro-Measurements, 2000, "CATALOG 500 – Precision Strain Gages," June 2000, pp. 4.
Micro Measurements, 1996, "Strain Gage Applications with M-Bond GA-61 Adhesive," Measurements Group, INC, Raleigh, NC.
Mindess, S. and Young, F.J., 1991, "Concrete," Prentice-Hall, Inc., Englewood Cliffs, New Jersey, pp. 481-523 and pp. 326-330.
Nabar, S., and Mendis, P., 1997, "Experience with Epoxy Polymer Concrete Bridge Deck Thin Overlays in Service for Over 10 Years," *In-Place Performance of Polymer Concrete Overlays (SP-169)*, American Concrete Institute, Farmington Hills, MI, pp. 1-10.

PCA, 1970*, Final Report – Durability of Concrete Bridge Decks – A Cooperative Study*, Portland Cement Association, 35 pp.

Pfeifer, D.W.; Landgren, J.R.; and Krauss, P.D., 1992, Investigation for CRSI on CRSI-Sponsored Corrosion Studies at Kenneth C. Clear, Inc, CRSI.

Purvis, R., Babaei, K., Udani, N., Qanbari, A., and Williams, W., 1995, "Premature Cracking of Concrete Bridge Decks: Causes and Methods of Prevention." Pennsylvania Department of Transportation, Fourth International Bridge Engineering Conference, Washington, D.C., pp. 163-175.

Radabaugh, R.D., 2001, "Investigation of Early Age Bridge Deck Cracking," Masters Thesis, School of Civil Engineering, Purdue University, May 2001.

Schmitt, T.R. and Darwin, D., 1995, "Cracking in Concrete Bridge Decks," *Report No. K-TRAN:KU-94-1*, Kansas Department of Transportation, April 1995, 151 pp.

Suprenant, B.A., 2002, "Why Slabs Curl," *Concrete International,* Mar. 2002, pp. 56-61.

Treece, R.A., and Jirsa, J.O., 1989, "Bond Strength of Epoxy-Coated Reinforcing Bars," *ACI Materials Journal*, V. 86, No. 2, Mar.-April 1989, pp. 167-174.

Wiegrink, K.; Shashidhara, M.; and Surendra, S., 1996, "Shrinkage Cracking of High-Strength Concrete," *ACI Materials Journal,* V. 93, n. 5, Sept.-Oct. 1996, pp. 409-415.

Weiss, J.W.; Yang, W.; and Shah, S.P., 1998, "Shrinkage Cracking of Restrained Concrete Slabs," *Journal of Engineering Mechanics,* July 1998, pp. 765-773.

Wiss, J., Elstener Associates Inc., 1992, "Report on the Blackfoot Bridge, Montana," Montana Department of Transportation, Oct. 1992.

APPENDIX A

BRIDGE INSPECTION REPORTS

Figure A.1.1: Bridge Elevation

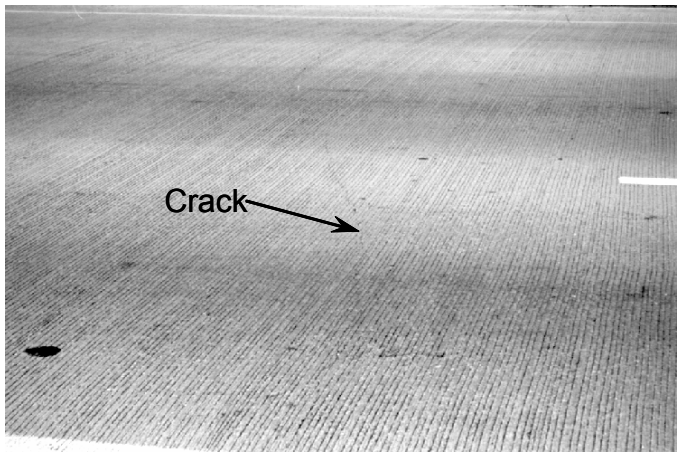

Figure A.1.2: Transverse Crack in Bridge

Bridge Reference Number: 1 **Sheet:** 1 of 2

INDOT Structure No.: I-65-118-4915C

Location: I65 over White River

Date Inspected: 9/23/99

Date Constructed: 1969

Date Rehabilitated: 1996 – New Deck

Superstructure Type: Steel Girders

Skew Angle: 20^{o}

Bridge Concerns: Longitudinal cracks near the white lane edge line of the road were observed. Transverse cracks were also observed near the end abutments parallel to the skew of the bridge.

	Yes	No	N/A	Unknown
Continuous	☐	✎	✎	✎
Composite	☐	✎	✎	✎
Stay-in-Place Steel Forms Used	☐	✎	✎	✎

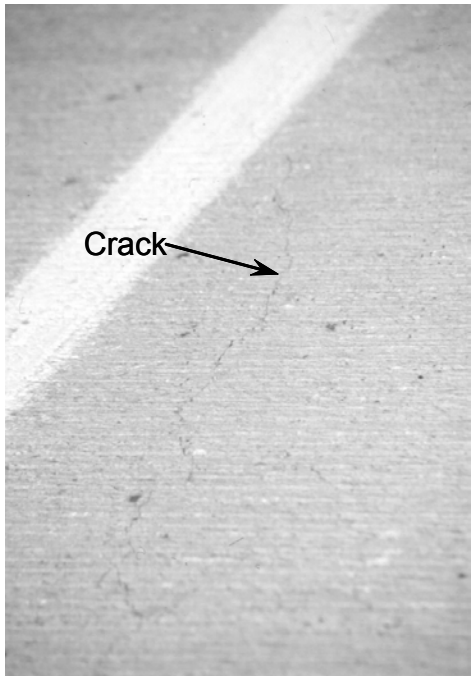

Figure A.1.3: Longitudinal Crack near Lane Edge Line

Figure A.2.1: Bridge Elevation

Figure A.2.2: Transverse Cracking in Bridge

Bridge Reference Number: 2 **Sheet:** 1 of 1

INDOT Structure No.: I-65-118-4838B NBL

Location: I65 over Crooked Creek

Date Inspected: 9/23/99

Date Constructed: 1964

Date Rehabilitated: 1996 – Widened Bridge

Superstructure Type: Steel Girders

Skew Angle: 17°

Bridge Concerns: Minor transverse cracks in the deck were obvious from observation of the concrete barrier wall.

	Yes	No	N/A	Unknown
Continuous	☐	✎	✎	✎
Composite	☐	✎	✎	✎
Stay-in-Place Steel Forms Used	☐	✎	✎	✎

Figure A.3.1: Bridge Elevation

Figure A.3.2: Steel I-Beam Superstructure with Stay-in-Place Forms

Bridge Reference Number: 3 **Sheet:** 1 of 2

INDOT Structure No.: I-65-119-4839B

Location: Kessler Road over I65

Date Inspected: 9/23/99

Date Constructed: 1964

Date Rehabilitated: 1997 – New Deck

Superstructure Type: Steel Girders

Skew Angle: -

Bridge Concerns: Regular transverse cracks running the entire length of the bridge were noted both in the positive and negative moment regions.

	Yes	No	N/A	Unknown
Continuous	☐	✎	✎	✎
Composite	☐	✎	✎	✎
Stay-in-Place Steel Forms Used	☐	✎	✎	✎

Figure A.3.3: Transverse Cracking in Bridge

Figure A.4.1: Bridge Elevation

Figure A.4.2: Unseated Rocker Support for Steel I-Beam Girder of Bridge

Bridge Reference Number: 4 **Sheet:** 1 of 1

INDOT Structure No.: I-465-116-4500A SBL

Location: I465S over 10th Street

Date Inspected: 9/23/99

Date Constructed: 1966

Date Rehabilitated: 1999 – New Deck

Superstructure Type: Steel Girders

Skew Angle: 7°

Bridge Concerns: No cracking was noted on this bridge when inspected; however, there were several loose rockers supporting the steel I-beam girders.

	Yes	No	N/A	Unknown
Continuous	☐	✎	✎	✎
Composite	☐	✎	✎	✎
Stay-in-Place Steel Forms Used	☐	✎	✎	✎

Figure A.5.1: Bridge Elevation

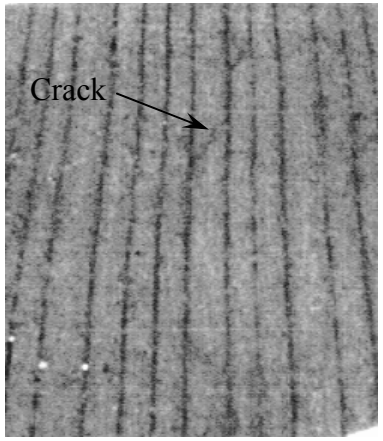

Figure A.5.2: Transverse Crack in Bridge

Bridge Reference Number: 5 **Sheet:** 1 of 1

INDOT Structure No.: I-465-116-4501A SBL

Location: I465S over US40

Date Inspected: 9/23/99

Date Constructed: 1965

Date Rehabilitated: 1999 – Widened Bridge

Superstructure Type: Steel Girders

Skew Angle: 3^{o}

Bridge Concerns: Minor transverse cracking in bridge deck were observed two months after the deck was placed.

	Yes	No	N/A	Unknown
Continuous	☐	✎	✎	✎
Composite	☐	✎	✎	✎
Stay-in-Place Steel Forms Used	☐	✎	✎	✎

Figure A.6.1: Map Cracking in Overlay of Bridge

Bridge Reference Number: 6 **Sheet:** 1 of 1

INDOT Structure No.: I-69-40-2304C NBL and SBL

Location: I69 North and South over railroad and CR 275W

Date Inspected: 9/23/99

Date Constructed: 1963

Date Rehabilitated: 1995 – Overlay on Deck

Superstructure Type: Steel Girders

Skew Angle: 11°

Bridge Concerns: Map cracking was noted in the approximately 2-in. thick overlay on both bridge decks.

	Yes	No	N/A	Unknown
Continuous	☐	✎	✎	✎
Composite	☐	✎	✎	✎
Stay-in-Place Steel Forms Used	✎	✎	✎	☐

Figure A.7.1: Bridge Elevation

Figure A.7.2: Steel Plate Girder Superstructure with Stay-in-Place Forms

Bridge Reference Number: 7 **Sheet:** 1 of 2

INDOT Structure No.: 58-42-7288

Location: IN 58 over White River

Date Inspected: 3/23/00

Date Constructed: 1996

Date Rehabilitated: N/A

Superstructure Type: Weathering Steel Plate Girders

Skew Angle: 30^{o}

Bridge Concerns: Regular transverse cracks on the deck were observed running the entire length of the bridge in both the positive and negative moment regions. The widths of the cracks were measured between 0.016 to 0.020 in. In the middle of the first span from the east, cracks were spaced at the following intervals: 40, 56, 36, 62, 36, 28, and 28 in. In the middle of the second span from the east, cracks were spaced at the following intervals: 34, 43, 41, 55, 36, 84, 90, 50, and 14 in. The average measured crack interval was 46 in.

	Yes	No	N/A	Unknown
Continuous	☐	✎	✎	✎
Composite	☐	✎	✎	✎
Stay-in-Place Steel Forms Used	☐	✎	✎	✎

Figure A.7.3: Transverse Cracks on Bridge

Figure A.8.1: Bridge Elevation

Figure A.8.2: Longitudinal Cracks on Bridge

Bridge Reference Number: 8 **Sheet:** 1 of 1

INDOT Structure No.: 58-42-3241A

Location: IN 58 over Gardner Ditch

Date Inspected: 3/23/00

Date Constructed: 1939

Date Rehabilitated: 1983 – Widened Bridge

Superstructure Type: Steel Girders

Skew Angle: 20^{o}

Bridge Concerns: Longitudinal cracks running the entire length of the bridge and minor transverse cracks were noted. The bridge did not use stay-in-place steel forms; therefore, the bottom of the bridge deck is exposed. The cracks could not be seen on the under side of the deck. The longitudinal cracks, however, could be located over the flanges of the girders.

	Yes	No	N/A	Unknown
Continuous	☐	✎	✎	✎
Composite	✎	☐	✎	✎
Stay-in-Place Steel Forms Used	✎	☐	✎	✎

Figure A.9.1: Bridge Elevation

Figure A.9.2: Transverse Crack with Delamination on Bridge

Bridge Reference Number: 9 **Sheet:** 1 of 1

INDOT Structure No.: 54-28-2538

Location: IN 54 at railroad near junction US231 and IN157

Date Inspected: 3/23/00

Date Constructed: 1982

Date Rehabilitated: N/A

Superstructure Type: Steel Girders

Skew Angle: 27°

Bridge Concerns: The bridge deck had a few transverse cracks and a large portion of the deck was delaminated.

	Yes	No	N/A	Unknown
Continuous	☐	✎	✎	✎
Composite	✎	☐	✎	✎
Stay-in-Place Steel Forms Used	✎	☐	✎	✎

Figure A.10.1: Bridge Elevation

Bridge Reference Number: 10 **Sheet:** 1 of 1

INDOT Structure No.: (50)37-47-3416JC East

Location: US50/IN37 over East Fork White River

Date Inspected: 3/23/00

Date Constructed: 1964

Date Rehabilitated: 1988 – Widened Bridge

Superstructure Type: Steel Girders

Skew Angle: -

Bridge Concerns: This bridge does not contain stay-in-place steel forms. Therefore, a few transverse cracks were observed on the underside of the bridge. The bridge contained an overlay, which prevented the transverse cracks to be seen on the top surface.

	Yes	No	N/A	Unknown
Continuous	☐	✎	✎	✎
Composite	✎	☐	✎	✎
Stay-in-Place Steel Forms Used	✎	☐	✎	✎

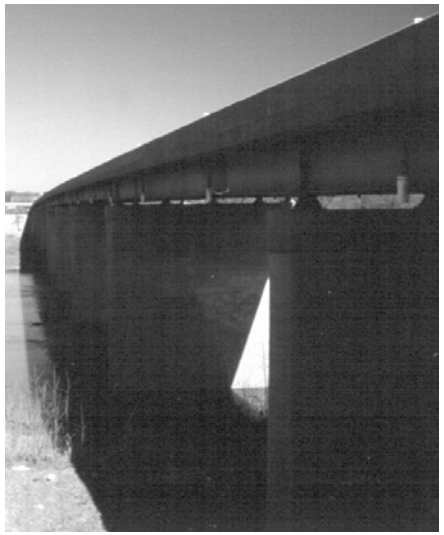

Figure A.11.1: Bridge Elevation

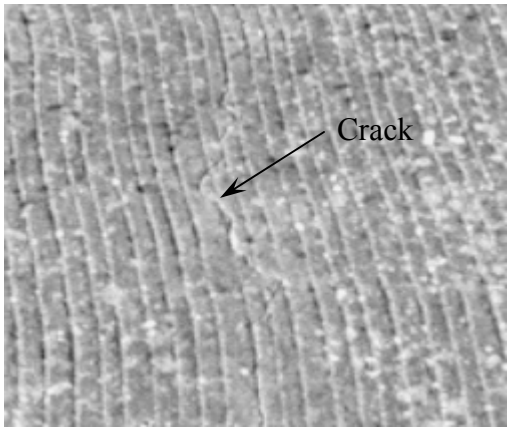

Figure A.11.2: Transverse Crack on Bridge

Bridge Reference Number: 11 **Sheet:** 1 of 1

INDOT Structure No.: (50)37-47-6615 West

Location: US50/IN37 over East Fork White River

Date Inspected: 3/23/00

Date Constructed: 1984

Date Rehabilitated: N/A

Superstructure Type: Steel Girders

Skew Angle: -

Bridge Concerns: Several few transverse cracks were observed on the top surface of the deck.

	Yes	No	N/A	Unknown
Continuous	☐	✎	✎	✎
Composite	☐	✎	✎	✎
Stay-in-Place Steel Forms Used	☐	✎	✎	✎

Figure A.12.1: Bridge Elevation

Figure A.12.2: Transverse Crack in Bridge

Bridge Reference Number: 12 **Sheet:** 1 of 1

INDOT Structure No.: I-70-82-5707B, JB EBL and WBL

Location: I70 over Pogues Run

Date Inspected: 9/23/99

Date Constructed: 1969

Date Rehabilitated: 1986 – Widened Bridge

Superstructure Type: Cast-in-place concrete

Skew Angle: 31°

Bridge Concerns: Transverse cracks were observed in the widened portion of the bridge. However, no cracks were observed in the original structure. It is likely that since the original structure had already experienced the majority of its shrinkage, the new portion, which was bonded directly to the old, was not allowed to shrink freely. The restraint of this shrinkage likely resulted in the transverse cracks in the widened portion.

	Yes	No	N/A	Unknown
Continuous	☐	✎	✎	✎
Composite	✎	✎	☐	✎
Stay-in-Place Steel Forms Used	✎	☐	✎	✎

Figure A.13.1: Bridge Elevation

Figure A.13.2: Precast Concrete I-Beam Superstructure with Stay-in-Place Forms

Bridge Reference Number: 13 **Sheet:** 1 of 2

INDOT Structure No.: I-465-111-4399C

Location: I465 over Hanna Ave.

Date Inspected: 9/23/99

Date Constructed: 1999

Date Rehabilitated: N/A

Superstructure Type: Precast, prestressed concrete I-beam girders

Skew Angle: -

Bridge Concerns: The bridge was under construction when inspected and not yet open to traffic. No cracks were observed.

	Yes	No	N/A	Unknown
Continuous	☐	✎	✎	✎
Composite	☐	✎	✎	✎
Stay-in-Place Steel Forms Used	☐	✎	✎	✎

Figure A.13.3: Bridge under Construction

Figure A.14.1: Bridge Elevation

Figure A.14.2: Precast Concrete Box Girder Superstructure

Bridge Reference Number: 14 **Sheet:** 1 of 2

INDOT Structure No.: I-465-109-4402B

Location: I465 over 9th Street

Date Inspected: 9/23/99

Date Constructed: 1999

Date Rehabilitated: N/A

Superstructure Type: Precast, prestressed concrete box girders

Skew Angle: 2°

Bridge Concerns: This bridge was under construction when inspected and not yet open to traffic. Longitudinal cracks were observed the full length of the bridge. A few transverse cracks were also noted in the negative moment region. The longitudinal cracks in the deck were located above the edge of the box girders. The cracking is likely due to the difference in height of adjacent box girders.

	Yes	No	N/A	Unknown
Continuous	☐	✎	✎	✎
Composite	☐	✎	✎	✎
Stay-in-Place Steel Forms Used	✎	☐	✎	✎

Figure A.14.3: Elevation Difference in Box Girders

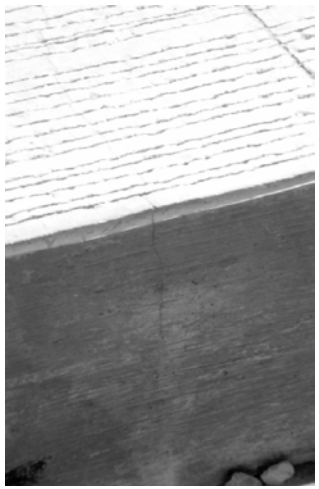

Figure A.14.4: Full Depth Longitudinal Crack at end of Bridge

No Photograph Available

Bridge Reference Number: 15 **Sheet:** 1 of 1

INDOT Structure No.: I-69-31-4740D NBL and SBL

Location: I69 over IN67

Date Inspected: 9/23/99

Date Constructed: 1963

Date Rehabilitated: 1995 – New Deck

Superstructure Type: Precast, prestressed concrete I-beam girders

Skew Angle: -

Bridge Concerns: No cracking was observed on this bridge when inspected.

	Yes	No	N/A	Unknown
Continuous	☐	✎	✎	✎
Composite	☐	✎	✎	✎
Stay-in-Place Steel Forms Used	☐	✎	✎	✎

Figure A.16.1: Bridge Elevation

Bridge Reference Number: 16 **Sheet:** 1 of 1

INDOT Structure No.: I-69-40-4746JD NBL
I-69-40-4746B SBL

Location: I69 over Killbuck Creek

Date Inspected: 9/23/99

Date Constructed: 1963

Date Rehabilitated: NBL – 1995, SBL – 1998 Overlays

Superstructure Type: Precast, prestressed concrete I-beam girders

Skew Angle: 11°

Bridge Concerns: Rehabilitation included the addition of an overlay approximately 2 in. thick latex-modified. Extensive map cracking was observed in the overlay over the entire length of both decks.

	Yes	No	N/A	Unknown
Continuous	☐	✎	✎	✎
Composite	☐	✎	✎	✎
Stay-in-Place Steel Forms Used	✎	☐	✎	✎

Figure A.17.1: Bridge Elevation

Figure A.17.2: Precast Concrete I-Beam Superstructure with Stay-in-Place Forms

Bridge Reference Number: 17 **Sheet:** 1 of 2

INDOT Structure No.: 67-28-7701

Location: IN67 over Black Creek

Date Inspected: 3/23/00

Date Constructed: 1994

Date Rehabilitated: N/A

Superstructure Type: Precast, prestressed concrete I-beam girders

Skew Angle: 20^{o}

Bridge Concerns: Longitudinal cracks running the entire length of the bridge were observed over both edges of the girders. Cracks widths were measured between 0.013 and 0.016 in.

	Yes	No	N/A	Unknown
Continuous	☐	✎	✎	✎
Composite	☐	✎	✎	✎
Stay-in-Place Steel Forms Used	☐	✎	✎	✎

Figure A.17.3: Longitudinal Cracks in Bridge

Figure A.18.1: Bridge Elevation

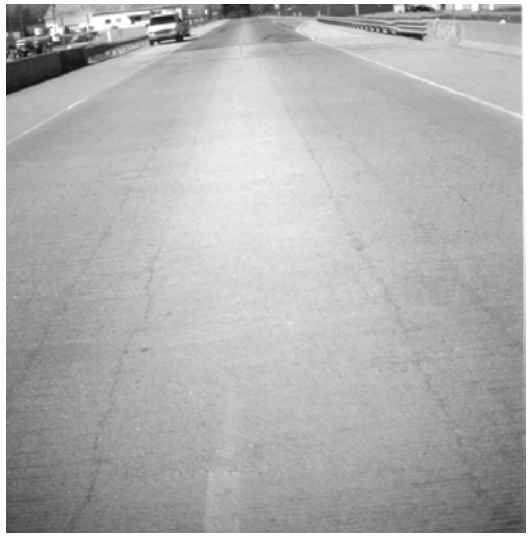

Figure A.18.2: Longitudinal Cracks in Bridge

Bridge Reference Number: 18 **Sheet:** 1 of 1

INDOT Structure No.: 231-28-2571

Location: US231 over abandoned railroad

Date Inspected: 3/23/00

Date Constructed: 1994

Date Rehabilitated: N/A

Superstructure Type: Precast, prestressed concrete girders – 2 spans of I-beams and 3 spans of T-beams

Skew Angle: Varies

Bridge Concerns: Longitudinal cracks running the entire length of the bridge were observed over both edges of the girders.

	Yes	No	N/A	Unknown
Continuous	☐	✎	✎	✎
Composite	☐	✎	✎	✎
Stay-in-Place Steel Forms Used	☐	✎	✎	✎

Figure A.19.1: Bridge Elevation

Figure A.19.2: Transverse Cracks in Bridge

Bridge Reference Number: 19 **Sheet:** 1 of 1

INDOT Structure No.: 54-47-6829

Location: IN54 over Spring Creek

Date Inspected: 3/23/00

Date Constructed: 1987

Date Rehabilitated: N/A

Superstructure Type: Precast, prestressed concrete I-beam girders

Skew Angle: 50^{o}

Bridge Concerns: The bridge has a large skew of 50^{o}. Transverse cracks were observed under the deck.

	Yes	No	N/A	Unknown
Continuous	☐	✎	✎	✎
Composite	☐	✎	✎	✎
Stay-in-Place Steel Forms Used	✎	☐	✎	✎

Figure A.20.1: Bridge Elevation

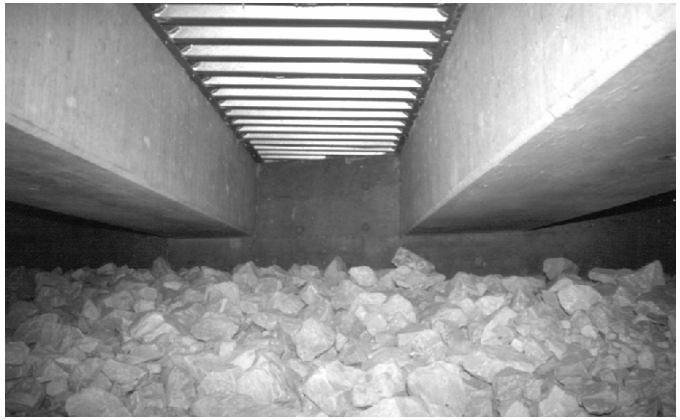

Figure A.20.2: Precast Spread Box Girder Superstructure with Stay-in-Place Forms

Bridge Reference Number: 20 **Sheet:** 1 of 2

INDOT Structure No.: 58-47-7178

Location: IN58 over Leatherwood Creek

Date Inspected: 3/23/00

Date Constructed: 1991

Date Rehabilitated: N/A

Superstructure Type: Precast, prestressed spread concrete box girders

Skew Angle: 23°

Bridge Concerns: Longitudinal cracks running the entire length of the bridge were observed. A few transverse cracks parallel to the skew were noted near the abutments of the bridge.

	Yes	No	N/A	Unknown
Continuous	☐	✎	✎	✎
Composite	☐	✎	✎	✎
Stay-in-Place Steel Forms Used	☐	✎	✎	✎

Figure A.20.3: Longitudinal Cracks in Bridge

APPENDIX B

I65 OVER SR25 BRIDGE PLANS

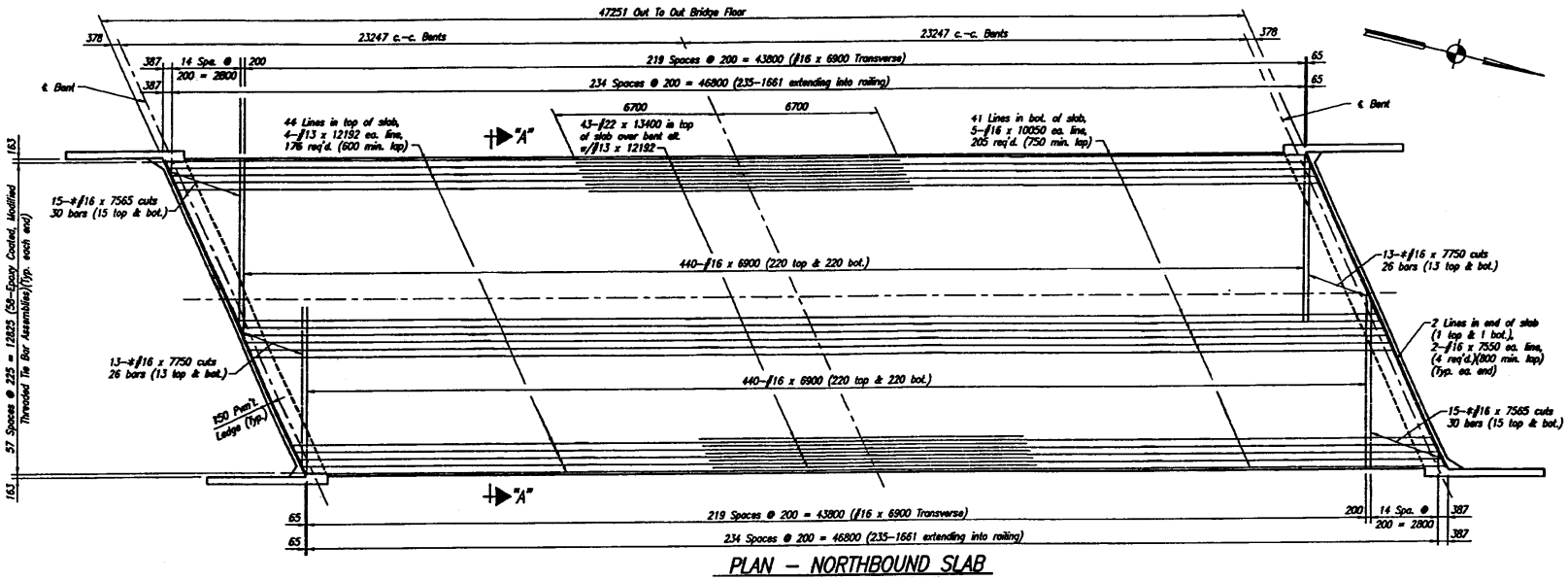

Figure B.1: Reinforcement Layout for I65 over SR 25 Bridge

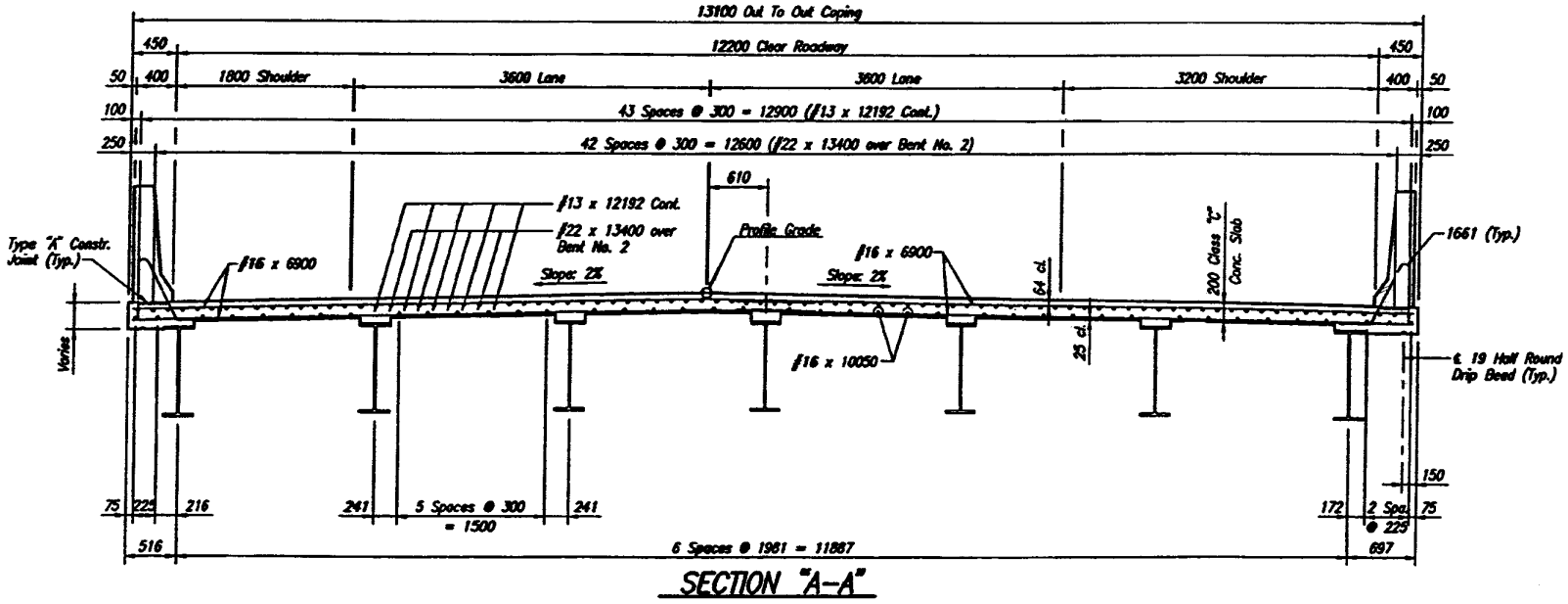

Figure B.2: Cross Section of I65 over SR 25 Bridge

APPENDIX C

INSTRUMENTATION SPECIFICATIONS

C.1 Introduction

All data obtained from the gages was acquired through a data acquisition system. Provided below are complete technical details for the strain gages and thermocouples used throughout this research as well as the datalogger system used for the field instrumentation.

C.2 Strain Gages

Strain gages were placed on both the reinforcing steel and the steel bridge girders to record the strain of the reinforcement and the girders. Micro-Measurements foil type electrical resistive precision strain gages, surface-cleaning chemicals, tape, adhesive, and protective coatings were selected for use in this research. For the field instrumentation, Style CEA-06-125UN-350 (0.125-in.) strain gages were used on the reinforcing steel and CEA-06-250UN-350 (0.250-in.) strain gages were installed on the steel girders. For the laboratory models, Style CEA-06-250UN-350 (0.250-in.) strain gages were installed on both the reinforcing steel and steel girders. Table C.1 describes the designation system for these strain gages.

Table C.1: Micro-Measurements Strain Gage Designation System (Measurements Group 2000)

Item	Description
CE	Encapsulated flexible gage with large, copper-coated soldering tabs providing optimum capability for direct leadwire attachment
A	Constantan alloy in self-temperature-compensated form
06	Approximate thermal expansion coefficient in ppm/^{o}F of the structural material in which the gage is to be attached
125 or 250	Active grid length in mils
UN	Grid and tab geometry
350	Resistance of the gage in Ohms

C.3 Thermocouples

Thermocouples were placed on the reinforcing steel and the steel girders to record the temperature of the deck and the girders. Omega Type T (copper-constantan) 24 AWG solid thermocouple wire was used in both the field investigation and the laboratory models. Each conductor as well as the overall jacket was insulated with fused Teflon tape.

C.4 Datalogger System

To monitor the strain gages and thermocouples in the field investigation, a data acquisition system was required. Based on the quantity of instrumentation on this bridge, 2 Campbell Scientific datalogger systems were selected. One datalogger system was placed at each end of the bridge.

A CR10X with extended memory was selected as the base datalogger system. Each datalogger required a 12 Volt direct current (Vdc) power source and had 6

differential analog inputs, 3 switched excitation channels, and 8 digital input/output channels. The differential analog inputs measured voltage differences across instruments. The excitation channels were programmable over a ± 2500 mV range. The digital input/output channels were used to read peripherals.

A PS12LA supplied power to the datalogger. The PS12LA included a 12 Vdc sealed rechargeable battery and a charging regulator. The 7 amp-hour battery was charged through the regulator in the unit using a Campbell Scientific Model 9591, 18 Vdc, 1.2 Amp wall charger.

AM416 multiplexers were added to increase the capacity of the datalogger to read and record additional gages. Each multiplexer had 16 differential channels that allowed 16 strain gages or 32 thermocouples to be read. Multiplexers wired for strain gages used one of the differential analog inputs of the datalogger, but a multiplexer wired for thermocouples used two differential analog inputs.

The data acquisition system recorded values for full resistive bridge measurements; however, the strain gages used were only ¼ of the Wheatstone Bridge. To complete the other ¾ of the Wheatstone Bridge, a 350-Ohm, 4-Wire Full Bridge Module (4WFB350) was required for each strain gage.

For the datalogger to record temperature readings from the thermocouples, a 107-L temperature probe was necessary. The temperature probe was a thermistor that acted as a reference temperature gage at the datalogger allowing for the determination of the temperature at the end of the thermocouple at the bridge. Without a reference temperature, thermocouples are incapable of measuring temperature.

Programs for the datalogger were written using Campbell Scientific PC208W software. By establishing a communication link between the datalogger and a laptop computer, the program was downloaded to the datalogger. To create this link a SC32A 9-pin optically isolated interface was connected between the datalogger and the 25-pin serial port on the laptop computer. This interface allowed for the transfer of the programs to the datalogger and the collected data to the laptop computer.

APPENDIX D

STRAIN GAGE APPLICATION

D.1 Strain Gage Application

The strain gages used for the experimental study were applied using the installation directions provided by Mirco Measurements (Micro Measurements 1996). Strain gages for both the reinforcing bars and deck pans were applied in the same manner.

Before the strain gage was applied to a reinforcing bar or deck pan, the surface was cleaned. In the case of the reinforcing bars, three lugs of the epoxy were removed on one side of the bar using an air powered grinder. Next, the area where the gage was applied was sprayed with CSM-1A degreaser to remove all oil from the surface. After being wiped clean with gauze, this step was repeated. The application area was then wet sanded with 400-grit Silicon Carbon paper with Conditioner A. This step was then repeated at least twice, and finally cleaned with gauze. Afterwards, Neutralizer 5A was applied to the surface and wiped dry using a cotton-swab. This step was also repeated until no discoloration was visible on the swab.

To apply the strain gage accurately, it was first taped to the cleaned area. Without removing the full length of tape, one side of the tape was pulled back until the strain gage just lifted off the bar/pan. M-Bond 200 Catalyst-C was then applied to the gage and allowed to dry. Subsequently, M-Bond 200 Adhesive was applied to the cleaned surface and the gage was pressed against the cleaned area under constant pressure for at least one minute. Finally, the tape was completely removed after the adhesive had ample time to set (at least 5-minutes).

After the gage had been adequately applied to the bar/pan, a three conductor lead wire (26 AWG) was soldered to the two strain gage terminals (Figures D.1 and D.2). A three conductor lead wire was used to provide temperature compensation. The lead wires and terminals were fluxed (m-flux), soldered, and cleaned with RSK Rosin Solvent to remove any excess flux. To protect the strain gage from damage during pouring, the bar/pan gages were covered with wax to prevent water intrusion and covered with M Coat J (Figure D.3)

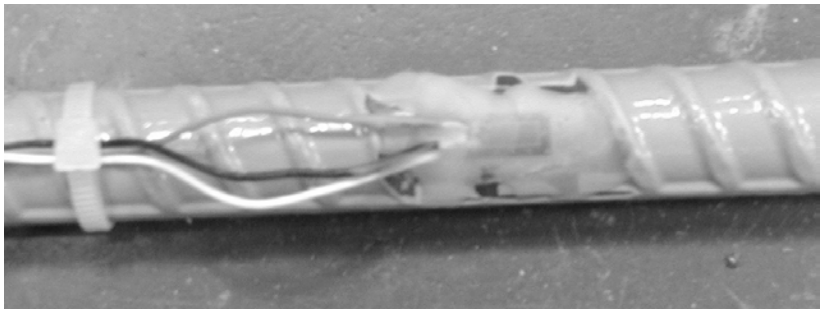

Figure D.1: #5 Epoxy Coated #5 Reinforcing Bar With an Applied Strain Gage

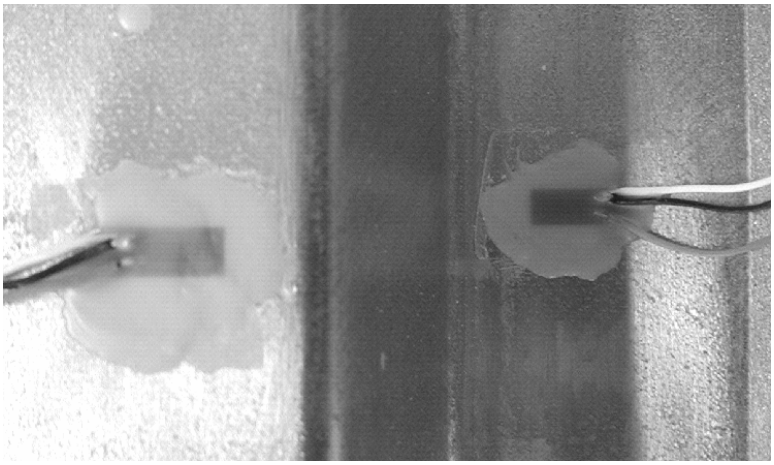

Figure D.2: Strain Gage Applied to a Deck Pan and Protected with Wax

Figure D.3: Applied Strain Gage Protected with M-Coat J

APPENDIX E

SHRINKAGE SPECIMEN MEASUREMENTS

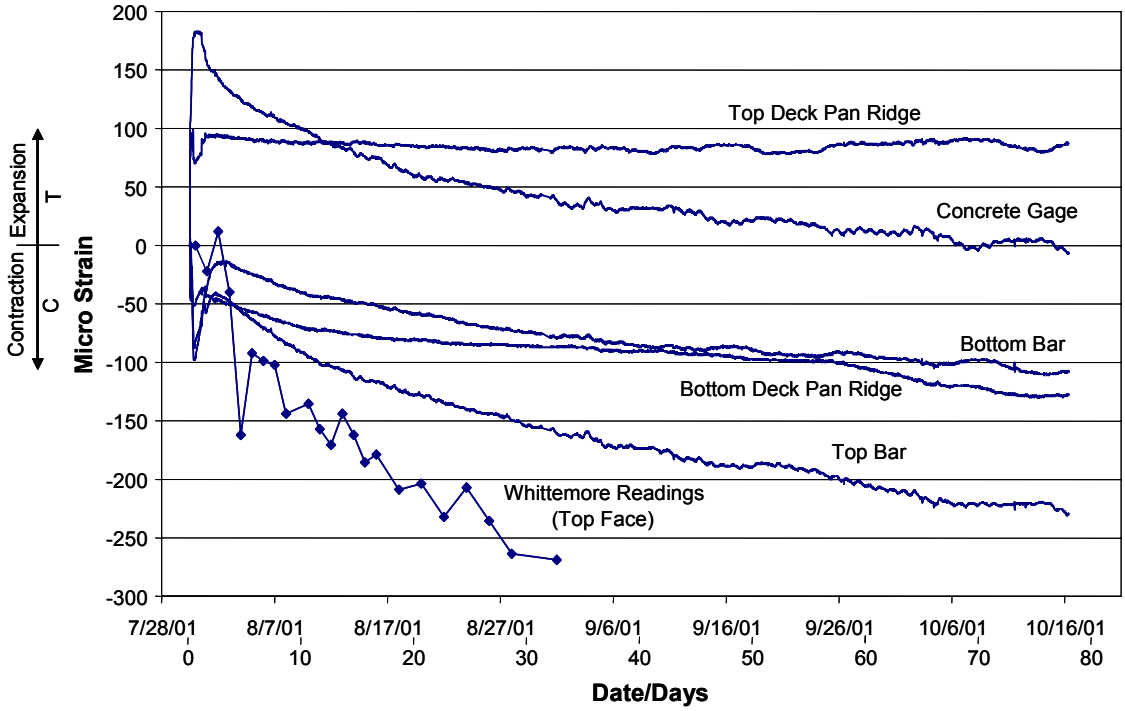

Figure E.1: Specimen 1

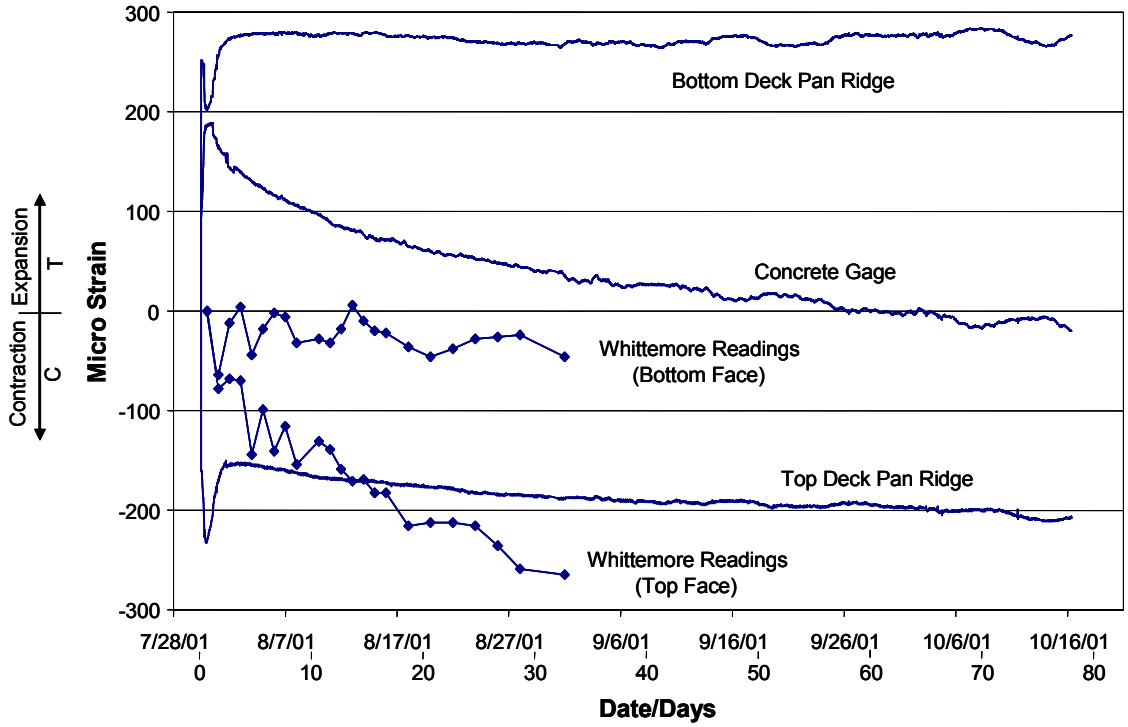

Figure E.2: Specimen 2

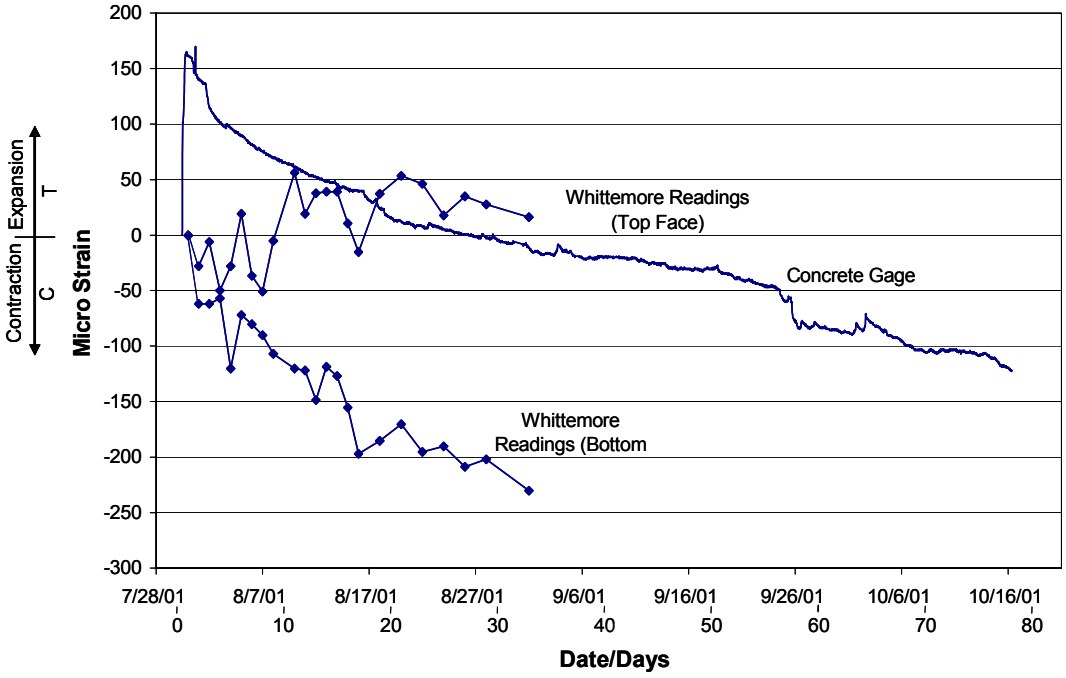

Figure E.3: Specimen 3

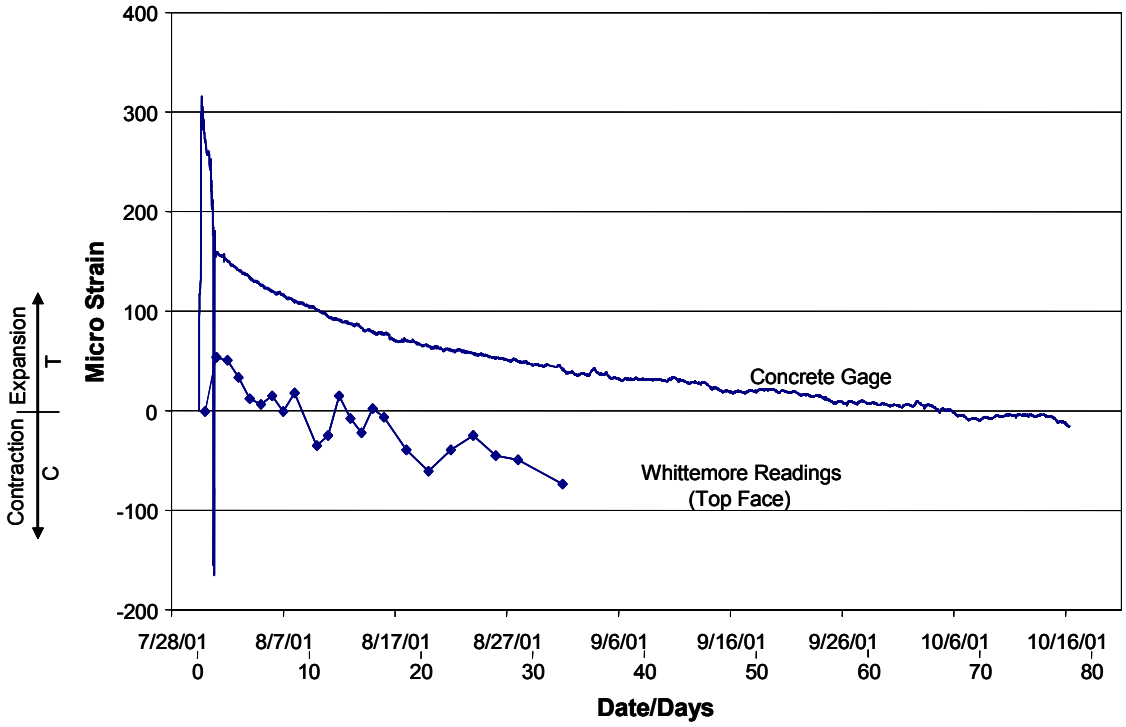

Figure E.4: Specimen 4

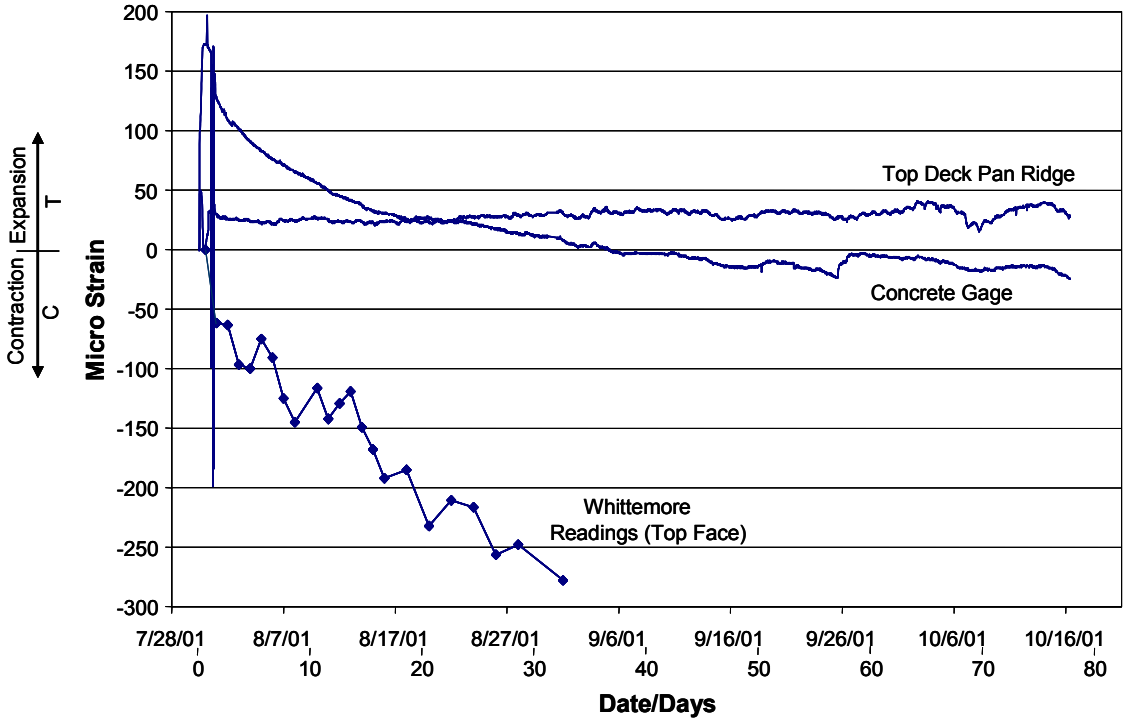

Figure E.5: Specimen 5

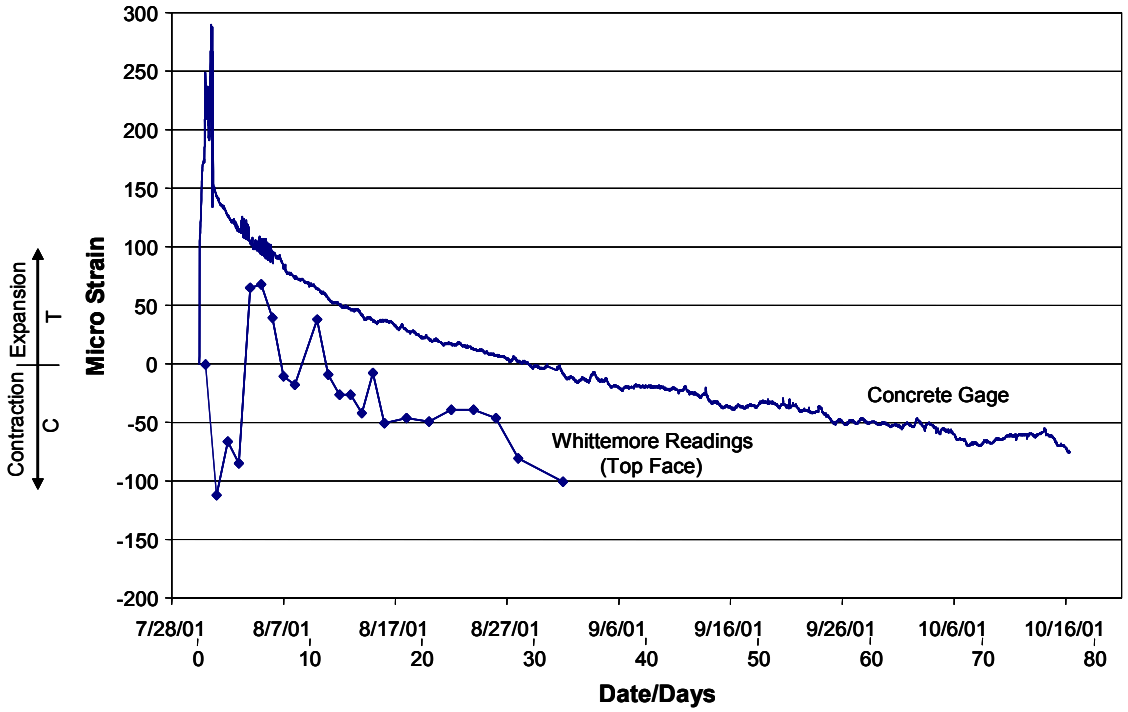

Figure E.6: Specimen 6

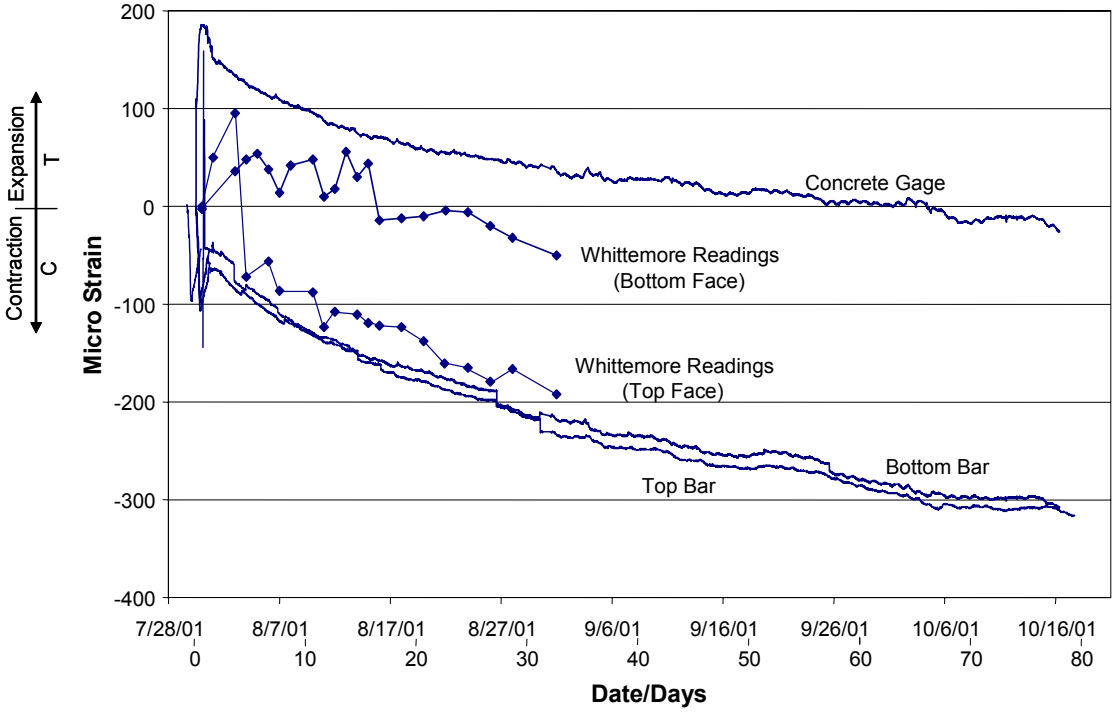

Figure E.7: Specimen 7

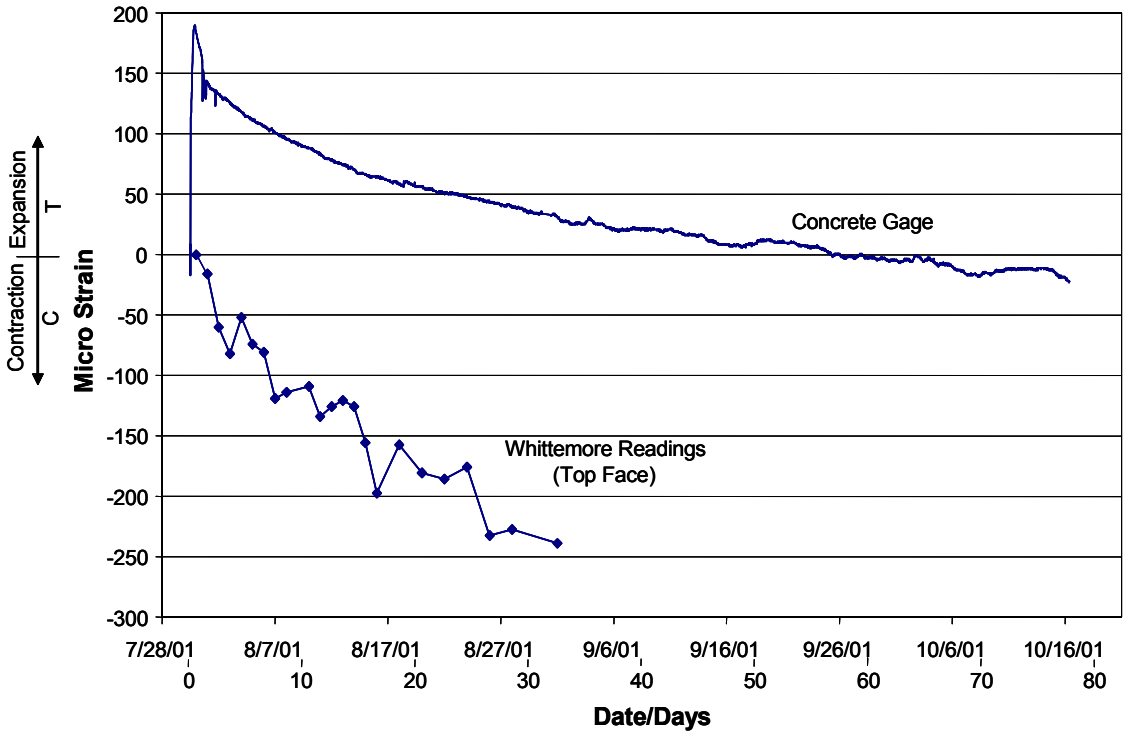

Figure E.8: Specimen 8

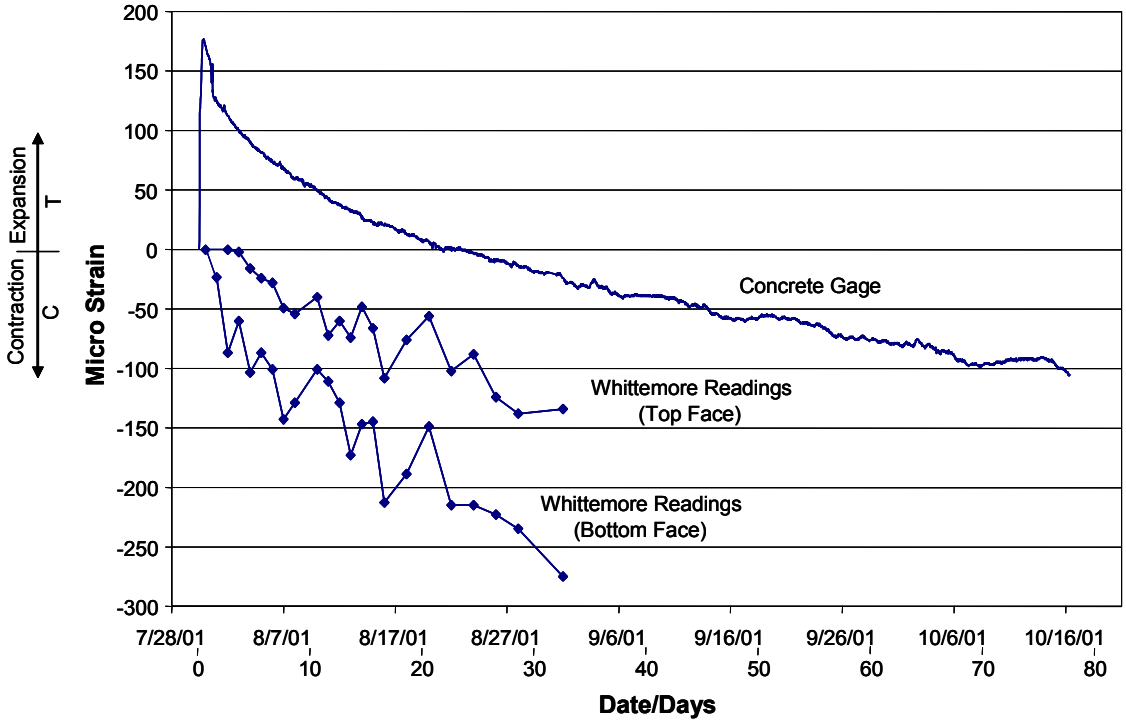

Figure E.9: Specimen 9

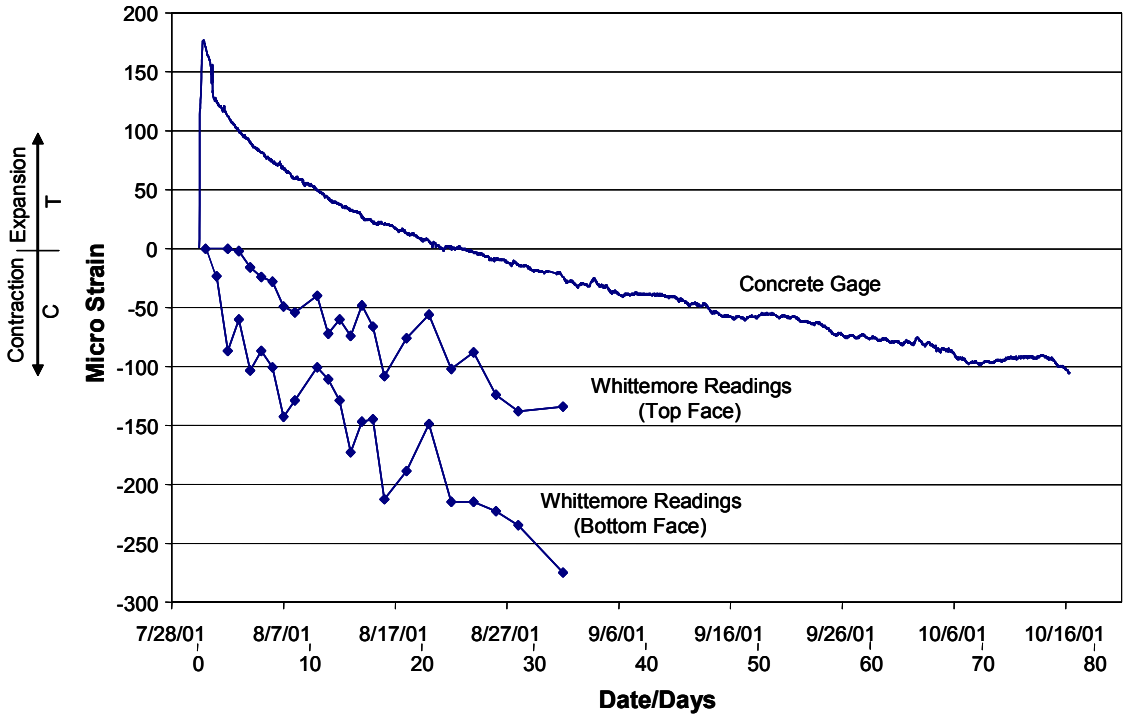

Figure E.10: Specimen 10

APPENDIX F

CRACK PATTERNS

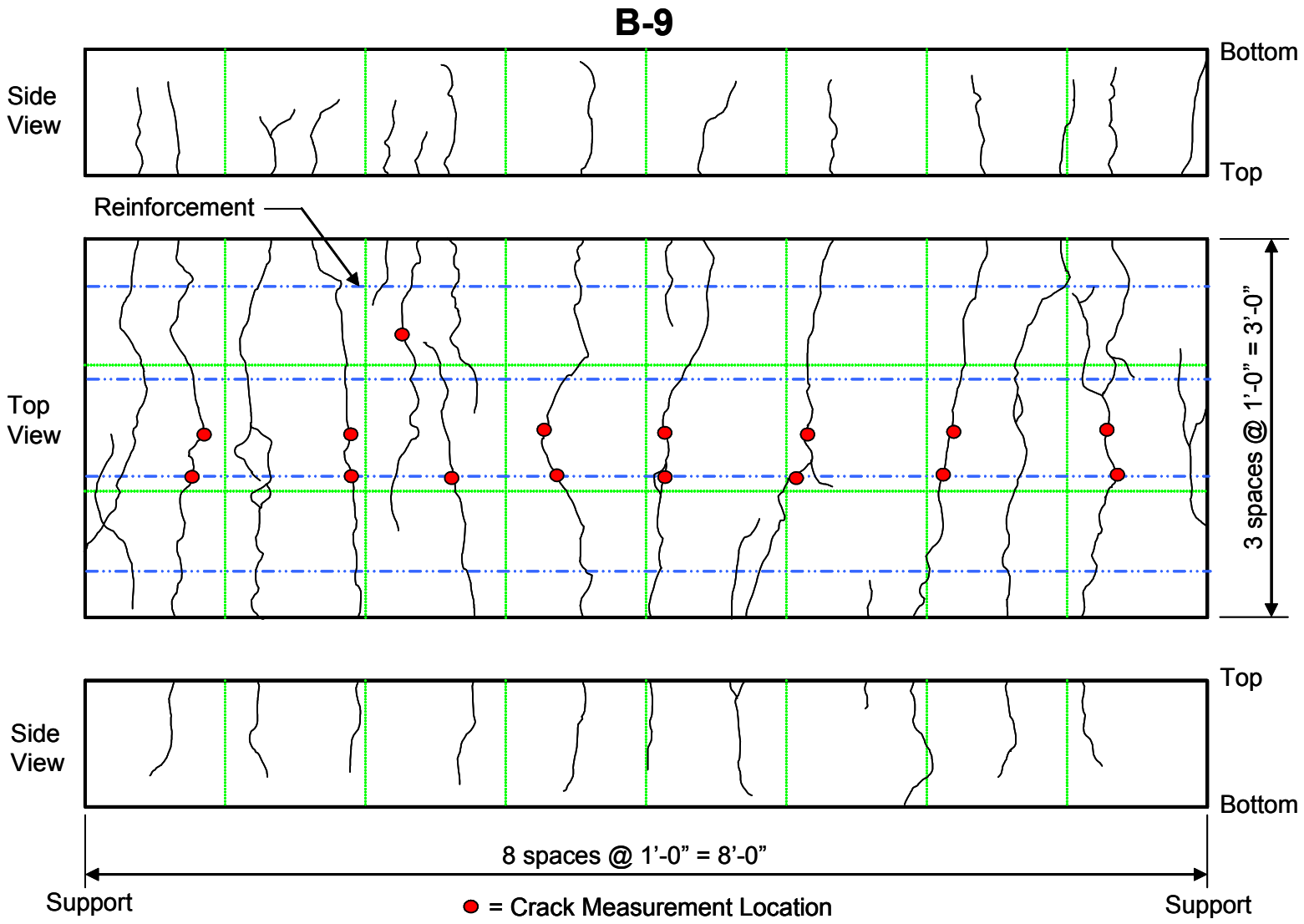
B-9
Side View
Bottom
Top
Reinforcement
Top View
3 spaces @ 1'-0" = 3'-0"
Top
Side View
Bottom
8 spaces @ 1'-0" = 8'-0"
Support
= Crack Measurement Location
Support

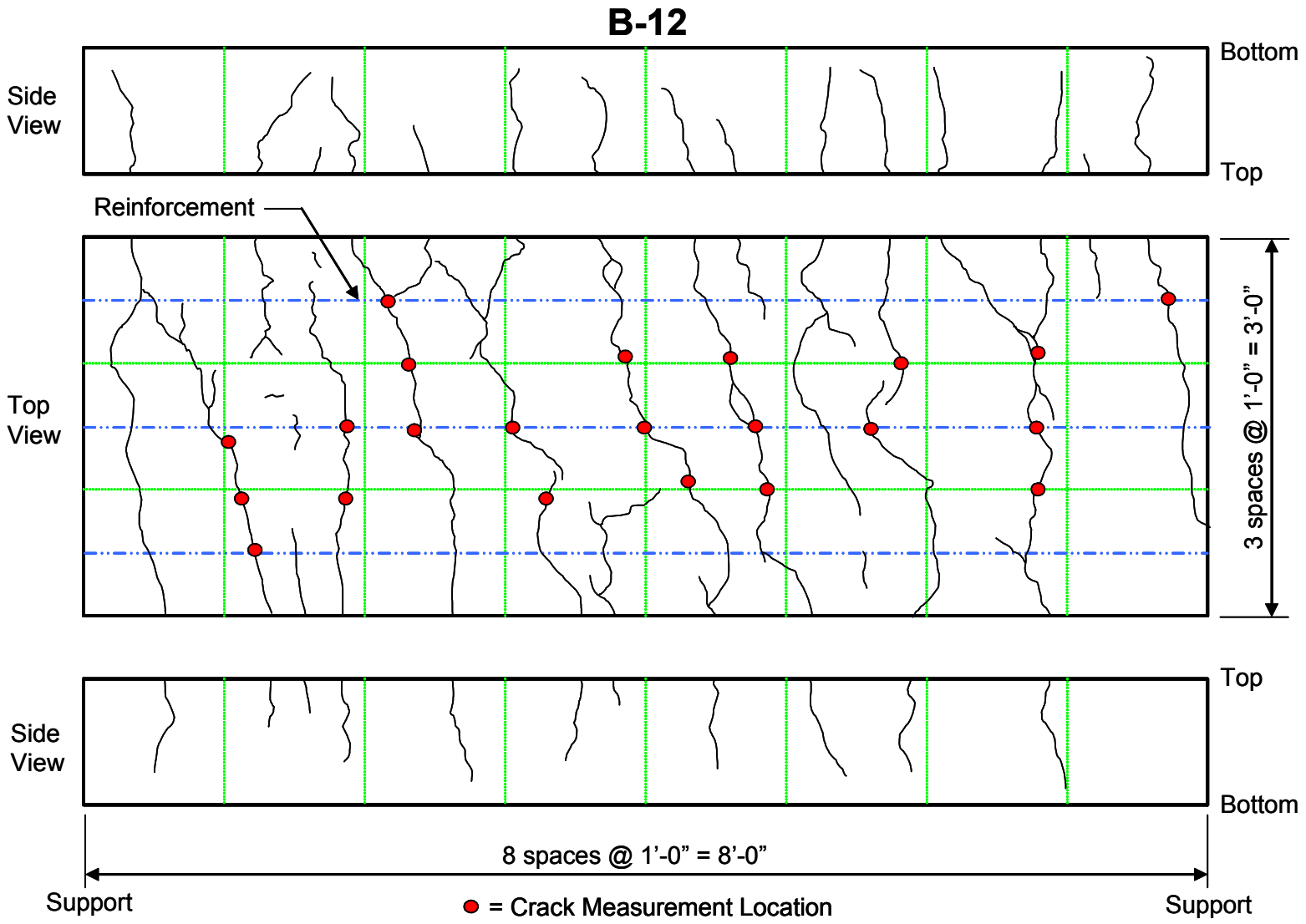
B-12
Side View
Bottom
Top
Reinforcement
Top View
3 spaces @ 1'-0" = 3'-0"
Top
Side View
Bottom
8 spaces @ 1'-0" = 8'-0"
Support
= Crack Measurement Location
Support

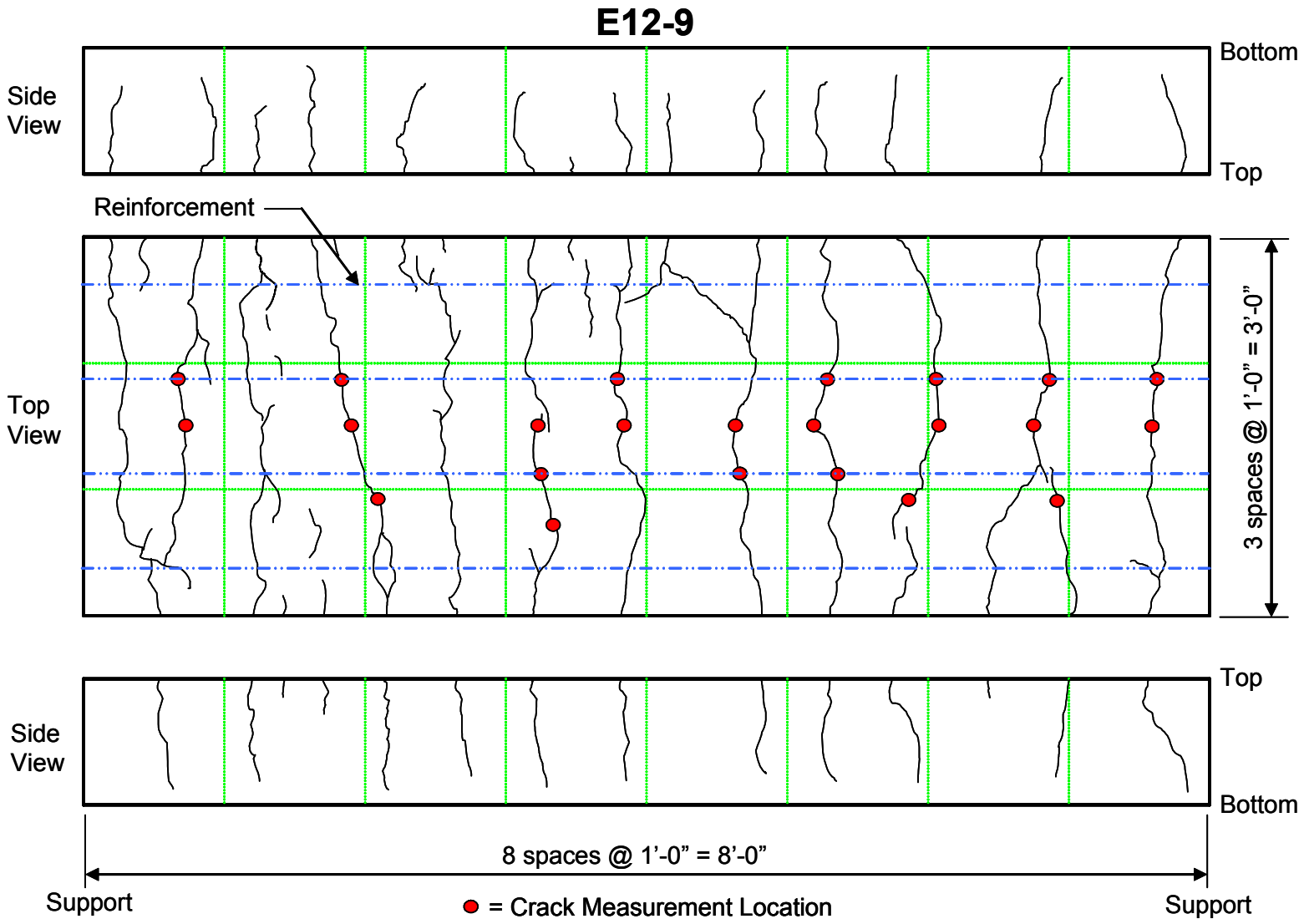
E12-9
Side View
Bottom
Top
Reinforcement
Top View
3 spaces @ 1'-0" = 3'-0"
Top
Side View
Bottom
8 spaces @ 1'-0" = 8'-0"
Support
= Crack Measurement Location
Support

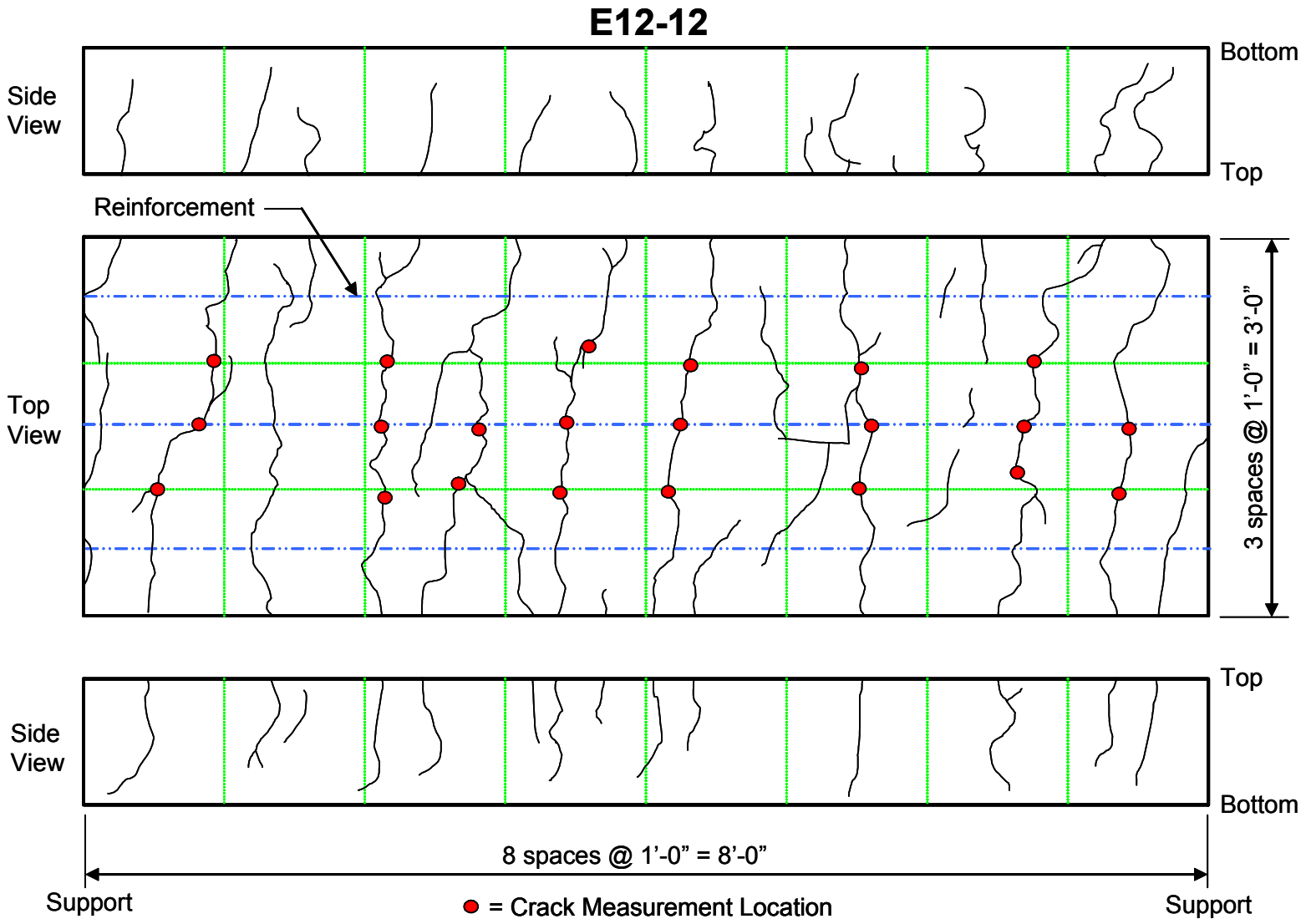
E12-12
Side View
Bottom
Top
Reinforcement
Top View
3 spaces @ 1'-0" = 3'-0"
Top
Side View
Bottom
8 spaces @ 1'-0" = 8'-0"
Support
= Crack Measurement Location
Support

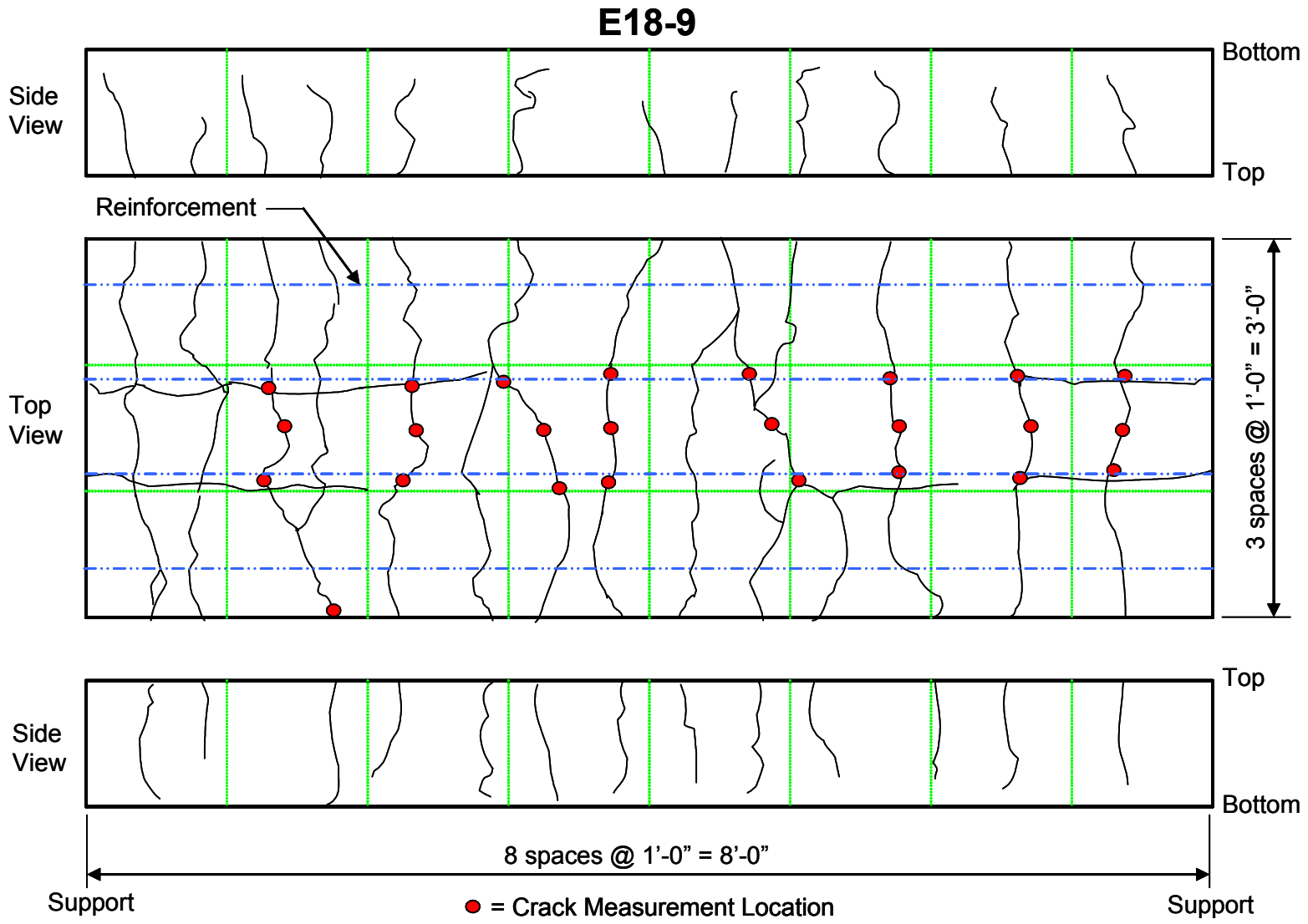
E18-9
Side View
Bottom
Top
Reinforcement
Top View
3 spaces @ 1'-0" = 3'-0"
Top
Side View
Bottom
8 spaces @ 1'-0" = 8'-0"
Support
= Crack Measurement Location
Support

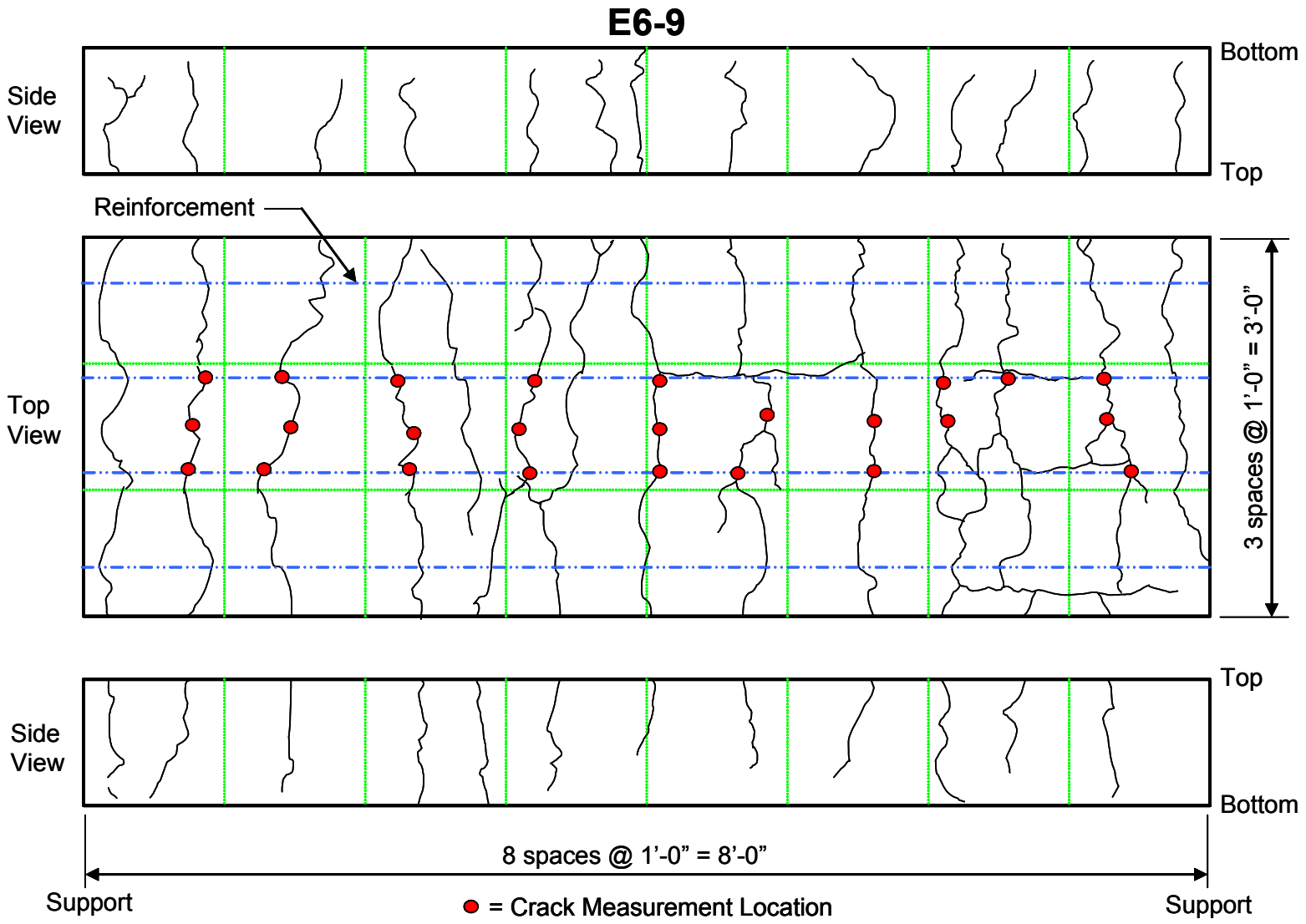
E6-9
Side View
Bottom
Top
Reinforcement
Top View
3 spaces @ 1'-0" = 3'-0"
Top
Side View
Bottom
8 spaces @ 1'-0" = 8'-0"
Support
= Crack Measurement Location
Support

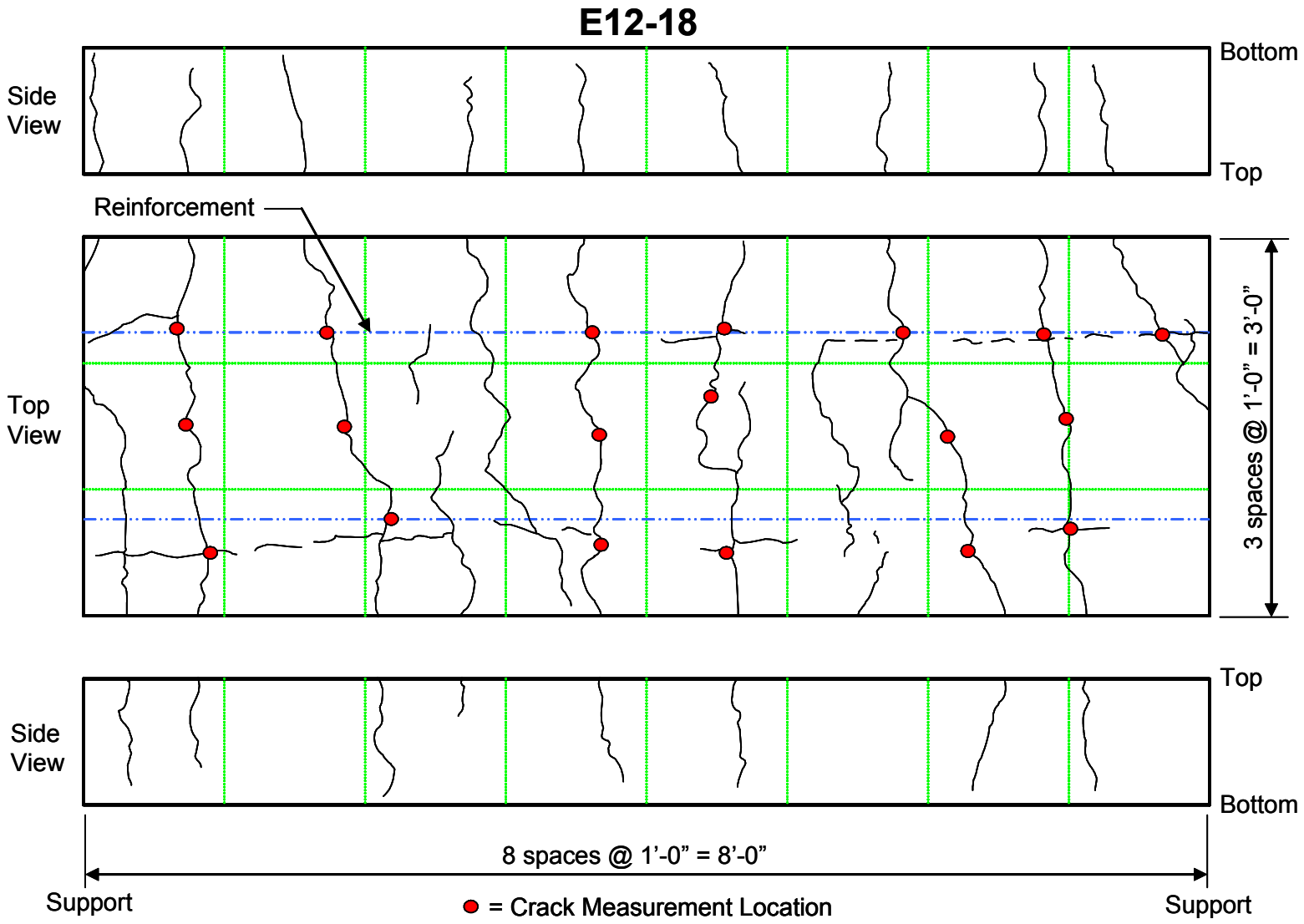
E12-18
Side View
Bottom
Top
Reinforcement
Top View
3 spaces @ 1'-0" = 3'-0"
Top
Side View
Bottom
8 spaces @ 1'-0" = 8'-0"
Support
= Crack Measurement Location
Support

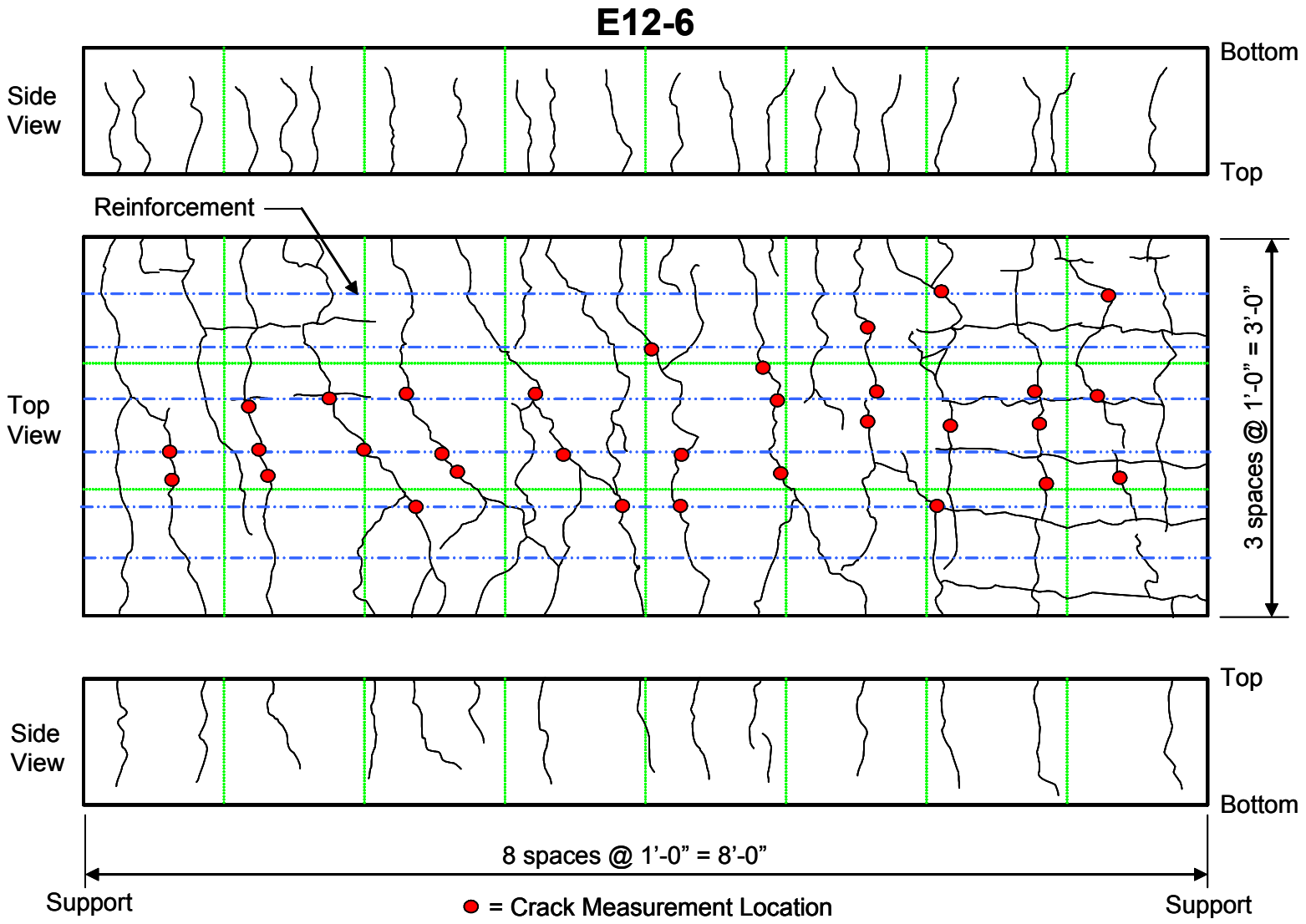
E12-6
Side View
Bottom
Top
Reinforcement
Top View
3 spaces @ 1'-0" = 3'-0"
Top
Side View
Bottom
8 spaces @ 1'-0" = 8'-0"
Support
= Crack Measurement Location
Support

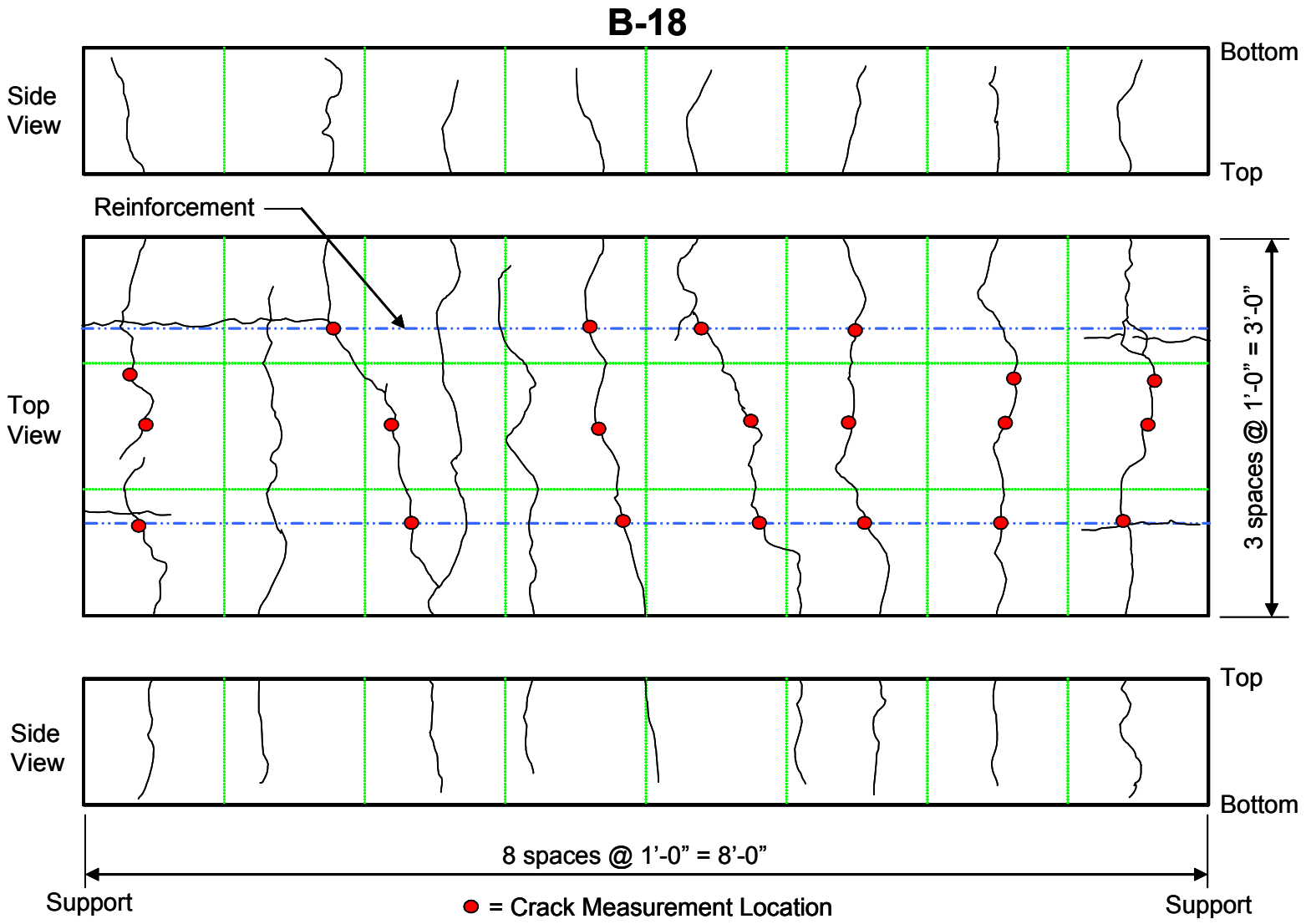
B-18
Side View
Bottom
Top
Reinforcement
Top View
3 spaces @ 1'-0" = 3'-0"
Top
Side View
Bottom
8 spaces @ 1'-0" = 8'-0"
Support
= Crack Measurement Location
Support

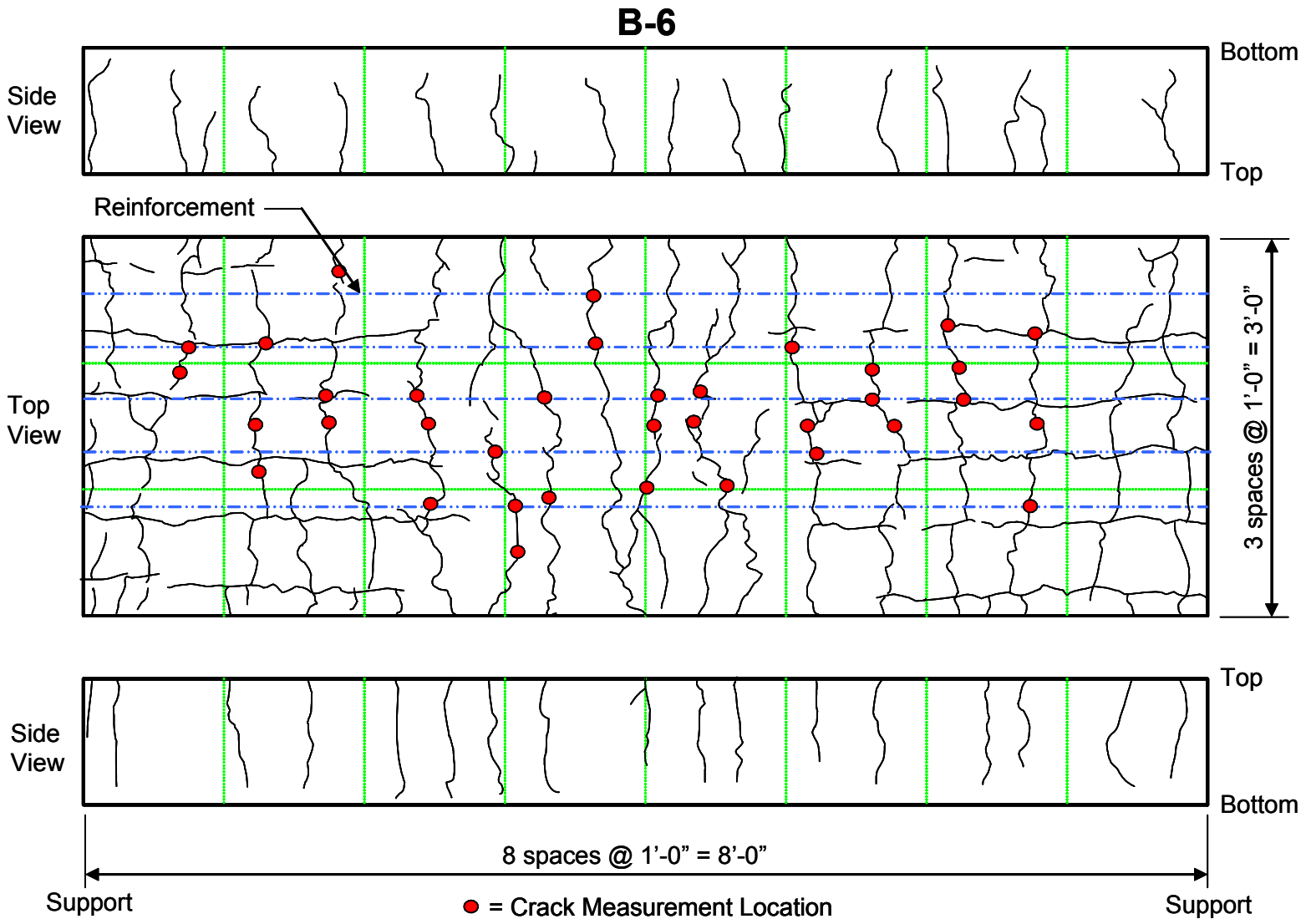
B-6
Side View
Bottom
Top
Reinforcement
Top View
3 spaces @ 1'-0" = 3'-0"
Top
Side View
Bottom
8 spaces @ 1'-0" = 8'-0"
Support
= Crack Measurement Location
Support

APPENDIX G

CRACK WIDTHS

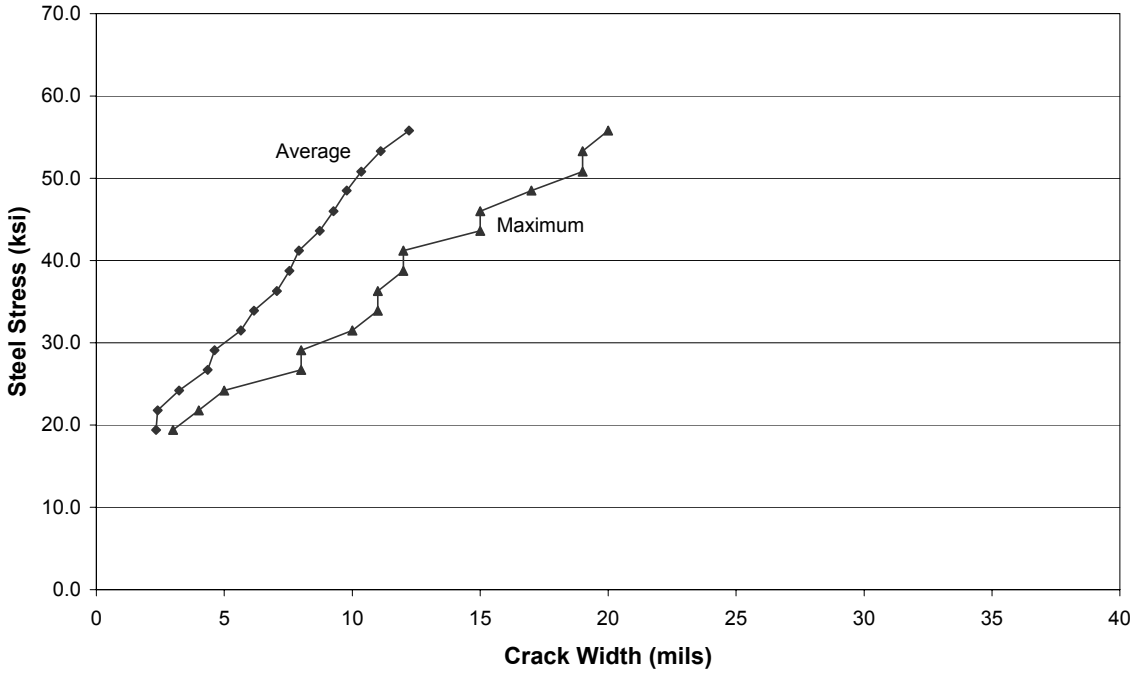

Figure G.1: Average and Max Crack Size Growth (B-6)

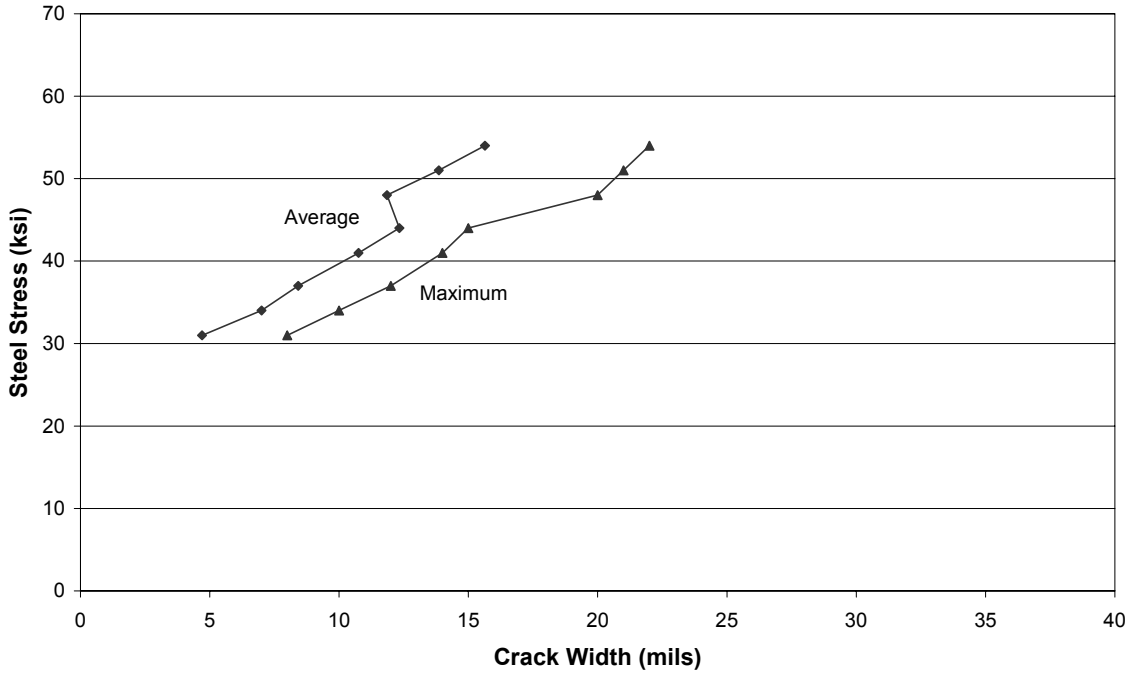

Figure G.2: Average and Max Crack Size Growth (B-9)

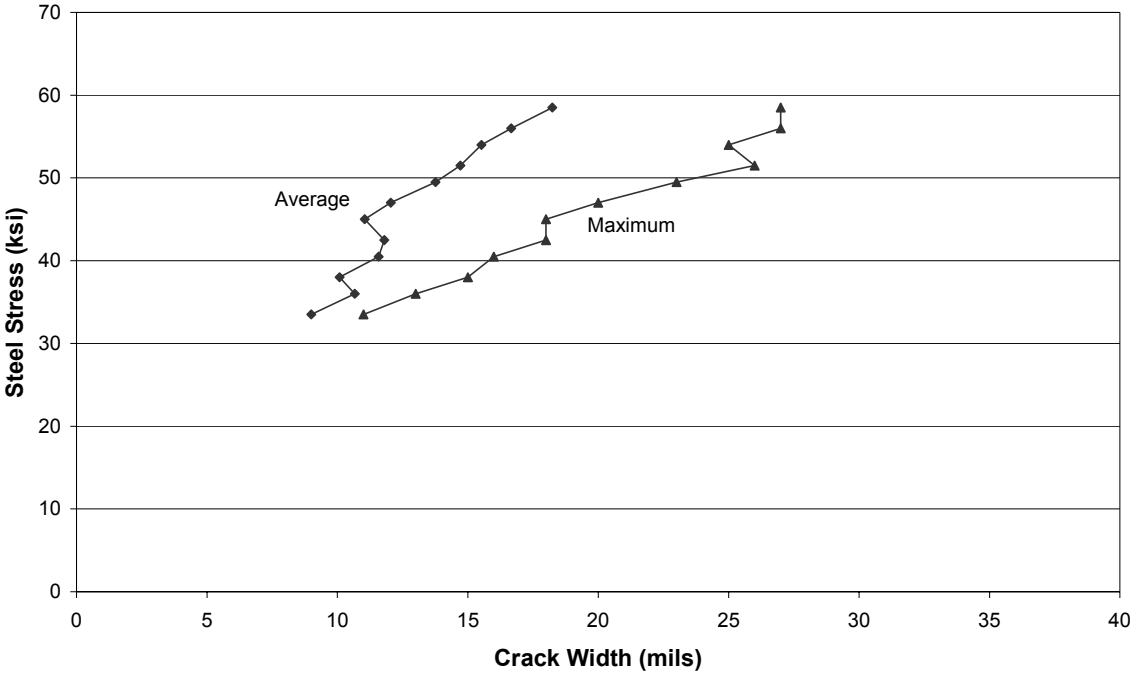

Figure G.3: Average and Max Crack Size Growth (B-12)

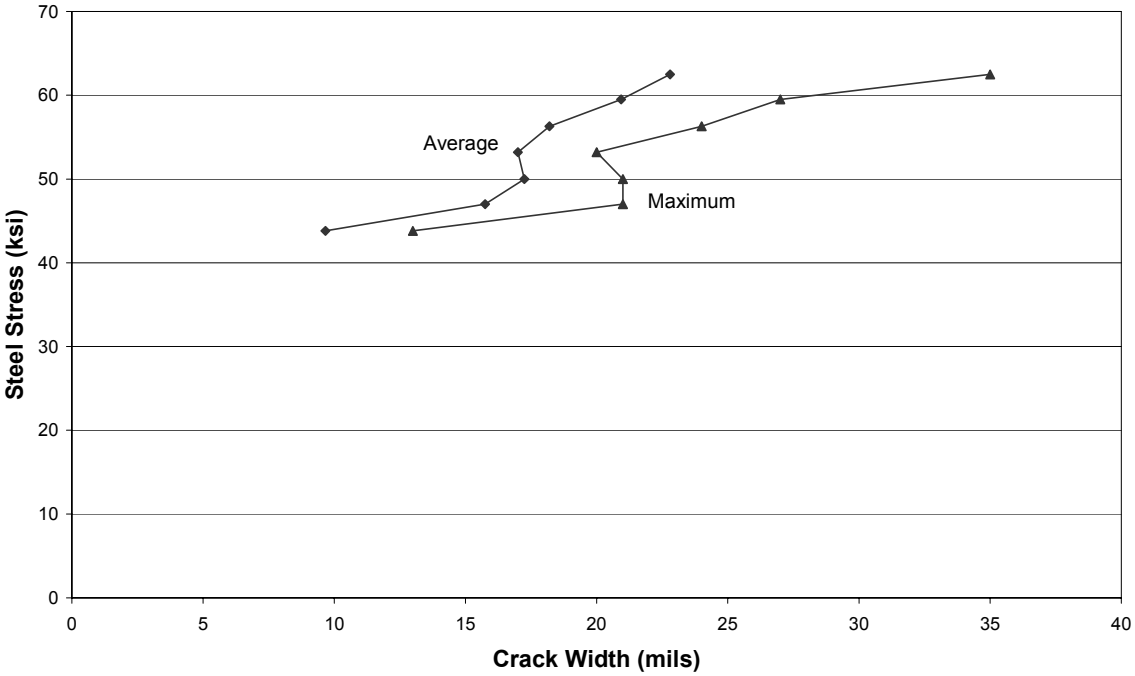

Figure G.4: Average and Max Crack Size Growth (B-18)

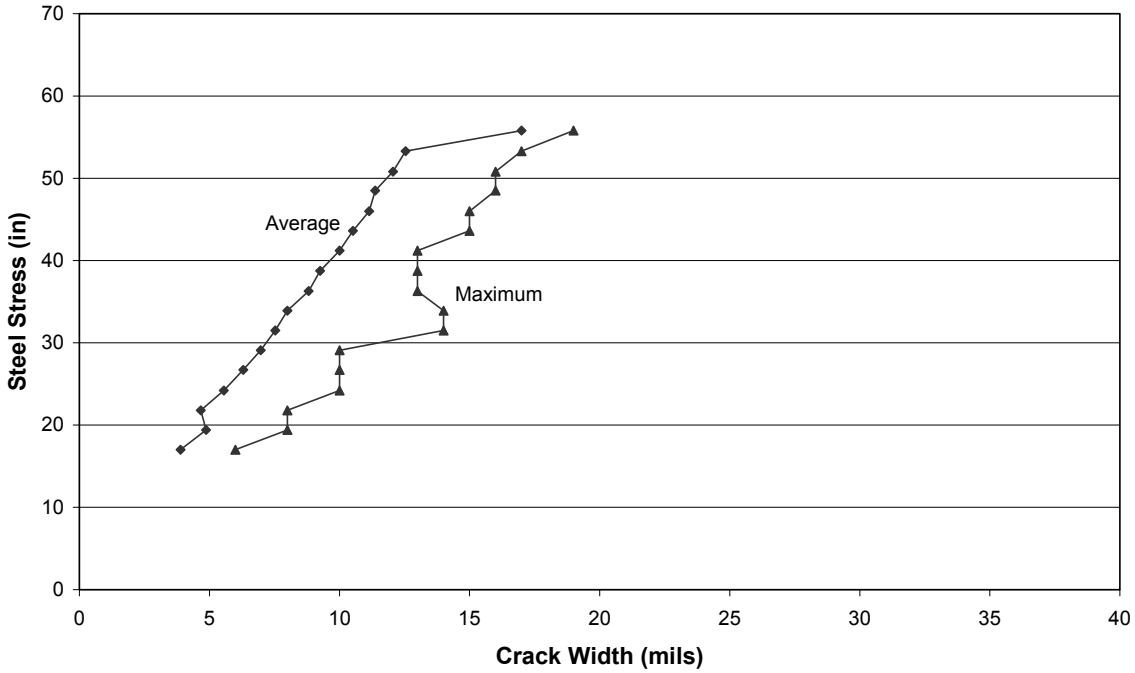

Figure G.5: Average and Max Crack Size Growth (E12-6)

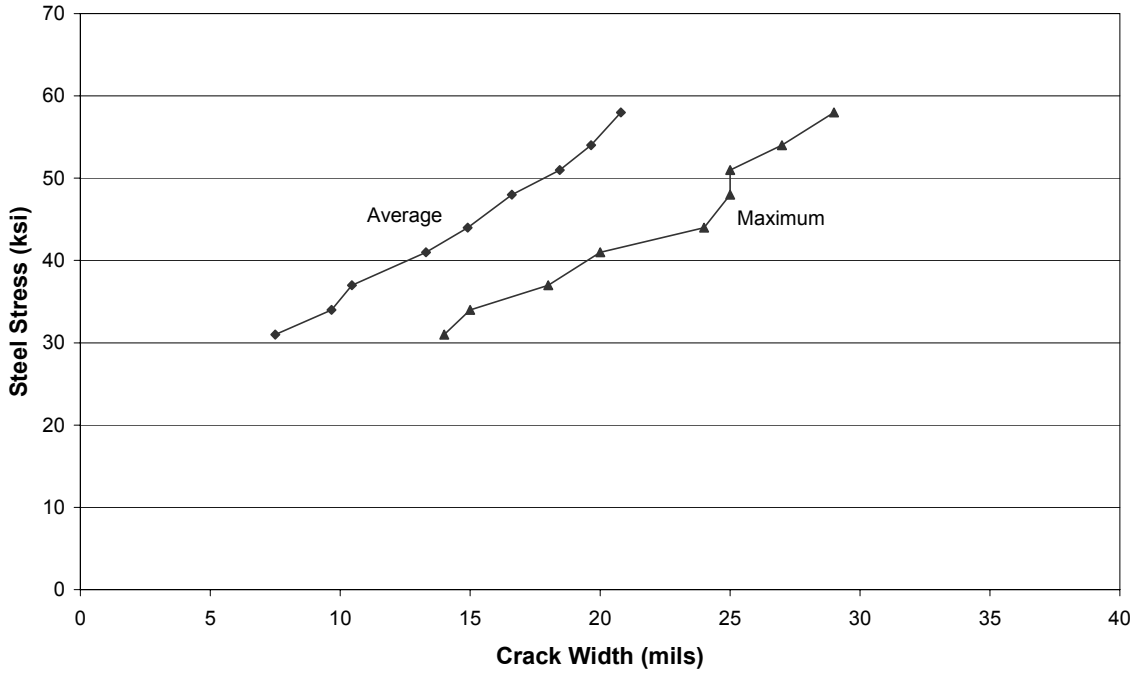

Figure G.6: Average and Max Crack Size Growth (E12-9)

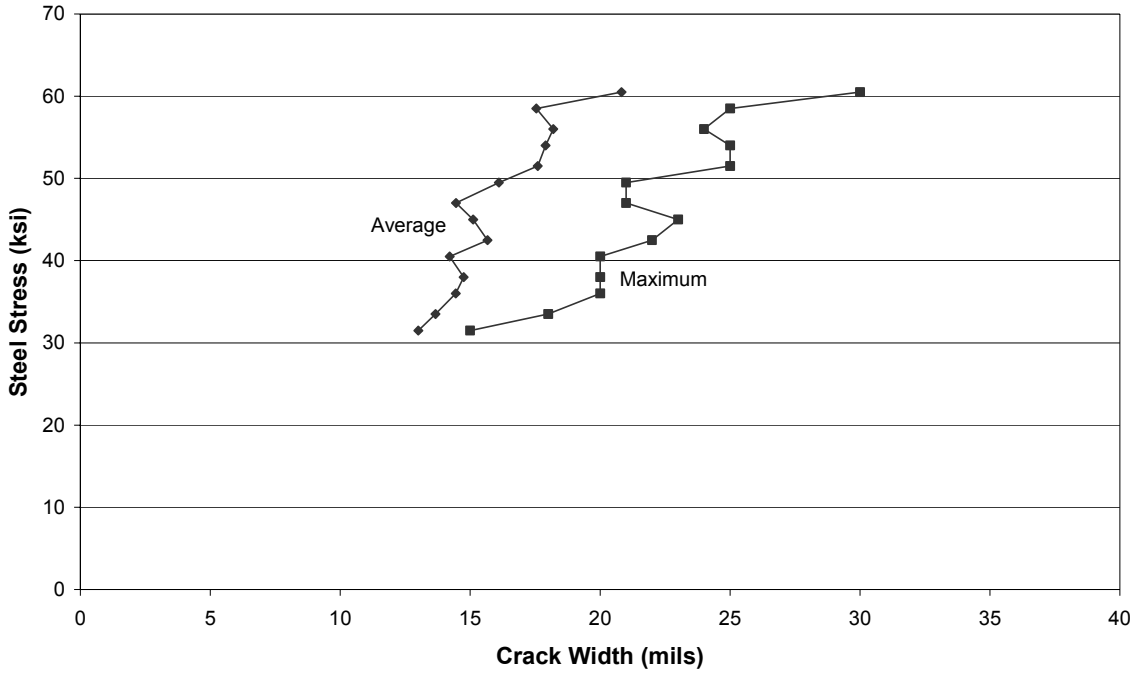

Figure G.7: Average and Max Crack Size Growth (E12-12)

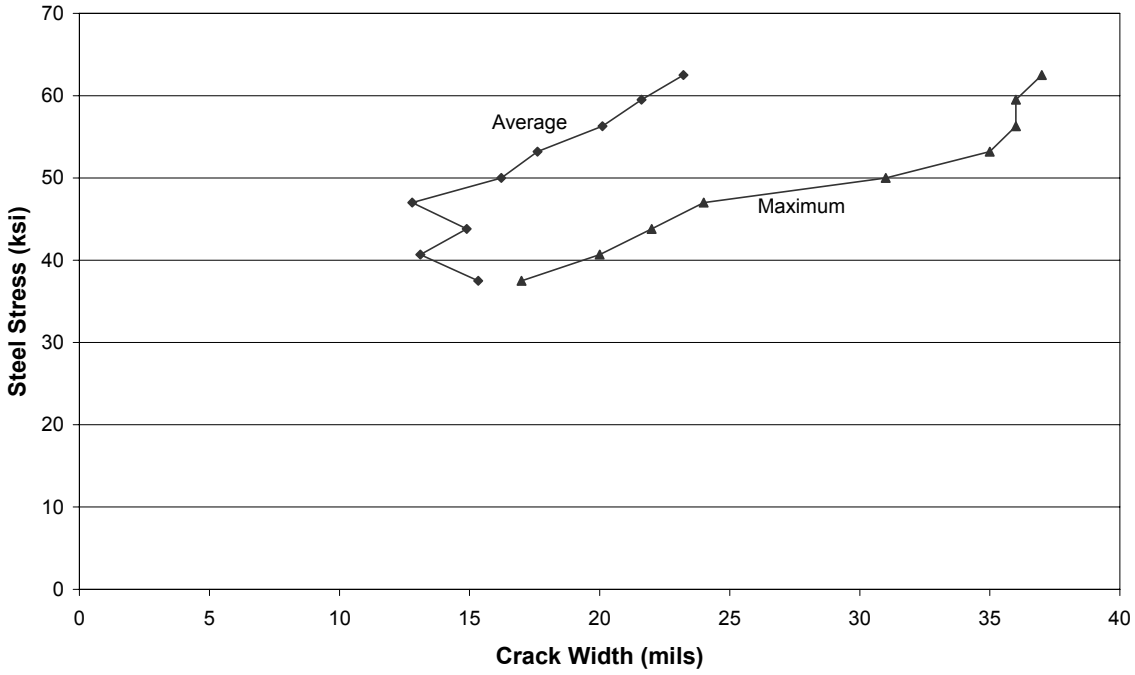

Figure G.8: Average and Max Crack Size Growth (E12-18)

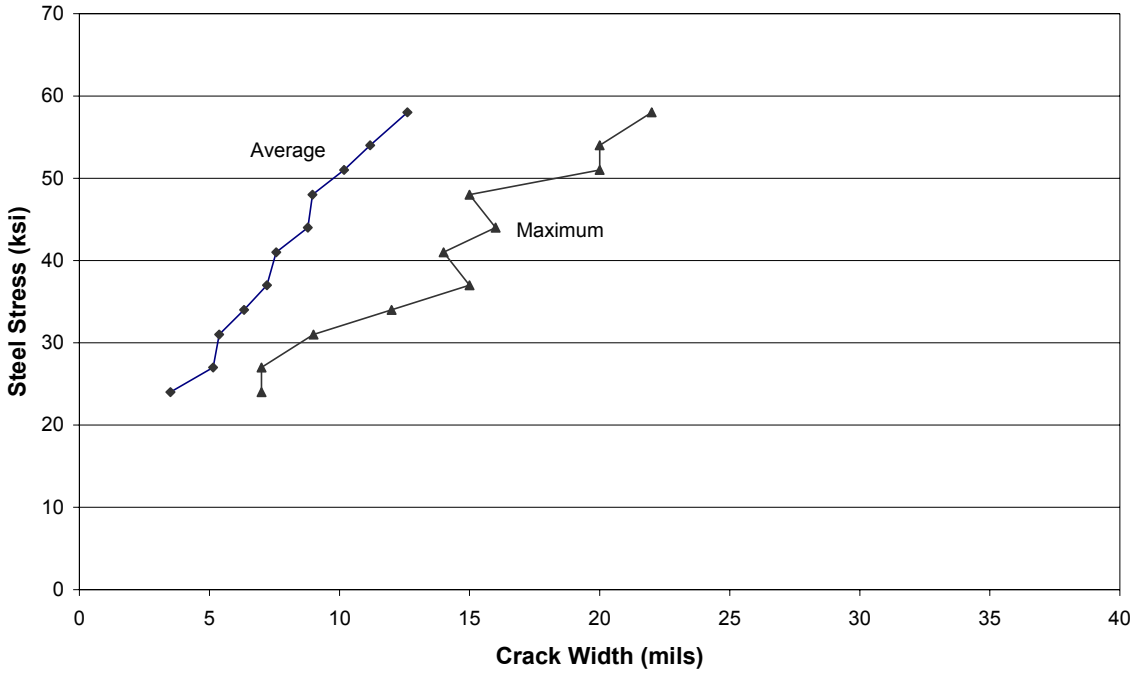

Figure G.9: Average and Max Crack Size Growth (E6-9)

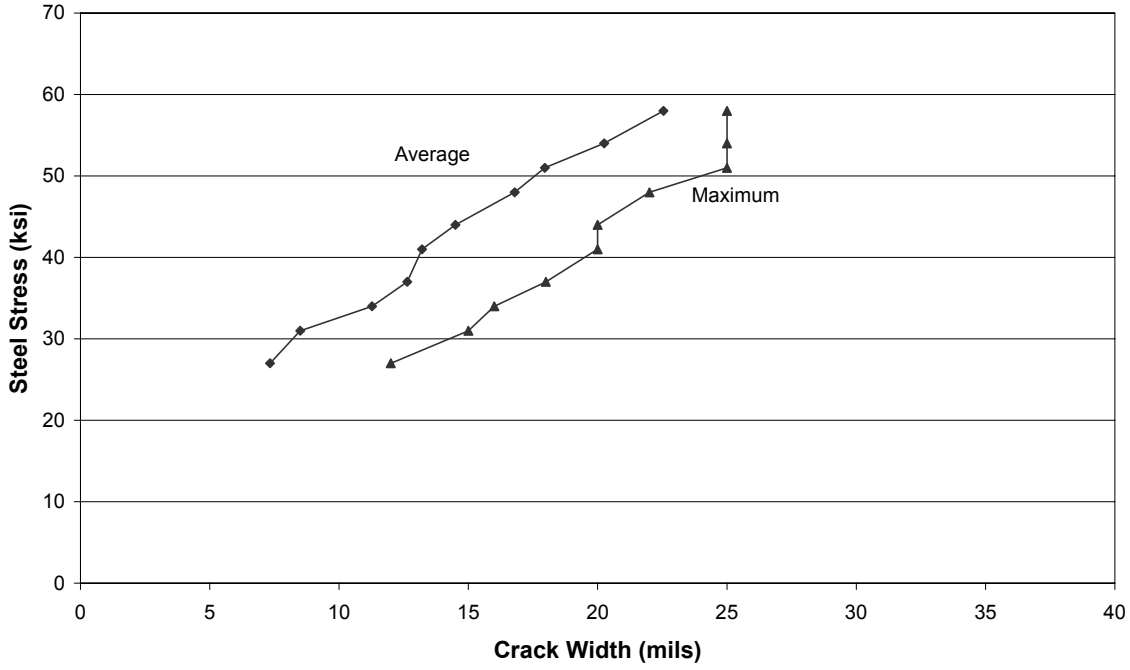

Figure G.10: Average and Max Crack Size Growth (E18-9)

APPENDIX H

CRACK WIDTH CALCULATION COMPARISIONS

Table H.1: Calculated and Measured Crack Widths (Specimen B-6)

Steel Stress (ksi)	Calculated Crack Width (mils)		Measured Crack Width (mils)			Calc/Measured Crack Width	
	Avg.	Max.	Avg.	SD	Max.	Avg.	Max.
20	4.8	6.4	2.3	0.5	3	2.07	2.12
25	6.0	7.9	3.7	1.2	6	1.61	1.32
30	7.2	9.5	4.9	1.9	9	1.46	1.06
35	8.3	11.1	6.5	2.0	11	1.28	1.01
40	9.5	12.7	7.6	2.2	12	1.25	1.06
45	10.7	14.3	9.1	2.3	15	1.18	0.95
50	11.9	15.9	10.2	2.9	18	1.17	0.88
55	13.1	17.5	11.9	3.2	20	1.10	0.87
60	14.3	19.1	-	-	-	-	-

Table H.2: Calculated and Measured Crack Widths (Specimen B-9)

Steel Stress (ksi)	Calculated Crack Width (mils)		Measured Crack Width (mils)			Calc/Measured Crack Width	
	Avg.	Max.	Avg.	SD	Max.	Avg.	Max.
20	6.5	8.7	-	-	-	-	-
25	8.1	10.9	-	-	-	-	-
30	9.8	13.0	-	-	-	-	-
35	11.4	15.2	7.5	2.2	10	1.52	1.52
40	13.0	17.4	10.0	1.9	13	1.30	1.34
45	14.7	19.5	10.6	2.6	19	1.38	1.03
50	16.3	21.7	13.1	2.7	21	1.24	1.03
55	17.9	23.9	-	-	-	-	-
60	19.5	26.0	-	-	-	-	-

Table H.3: Calculated and Measured Crack Widths (Specimen B-12)

Steel Stress (ksi)	Calculated Crack Width (mils)		Measured Crack Width (mils)			Calc/Measured Crack Width	
	Avg.	Max.	Avg.	SD	Max.	Avg.	Max.
20	8.4	11.1	-	-	-	-	-
25	10.4	13.9	-	-	-	-	-
30	12.5	16.7	-	-	-	-	-
35	14.6	19.5	10.2	1.7	12	1.43	1.62
40	16.7	22.3	11.4	2.1	15	1.47	1.48
45	18.8	25.1	11.0	4.2	18	1.71	1.39
50	20.9	27.8	14.0	4.2	24	1.49	1.16
55	23.0	30.6	16.1	4.5	26	1.43	1.18
60	25.1	33.4	-	-	-	-	-

Table H.4: Calculated and Measured Crack Widths (Specimen B-18)

Steel Stress (ksi)	Calculated Crack Width (mils)		Measured Crack Width (mils)			Calc/Measured Crack Width	
	Avg.	Max.	Avg.	SD	Max.	Avg.	Max.
20	12.1	16.2	-	-	-	-	-
25	15.2	20.2	-	-	-	-	-
30	18.2	24.3	-	-	-	-	-
35	21.2	28.3	-	-	-	-	-
40	24.3	32.3	-	-	-	-	-
45	27.3	36.4	11.3	3.2	15	2.41	2.43
50	30.3	40.4	17.3	2.9	21	1.75	1.92
55	33.3	44.5	17.9	3.4	22	1.86	2.02
60	36.4	48.5	21.2	5.1	32	1.72	1.52

Table H.5: Calculated and Measured Crack Widths (Specimen E12-6)

Steel Stress (ksi)	Calculated Crack Width (mils)		Measured Crack Width (mils)			Calc/Measured Crack Width	
	Avg.	Max.	Avg.		Max.	Avg.	Max.
20	4.8	6.4	5.0	1.2	8	0.95	0.79
25	6.0	7.9	5.9	1.8	10	1.01	0.79
30	7.2	9.5	7.2	1.8	10	0.99	0.95
35	8.3	11.1	8.3	1.9	14	1.01	0.79
40	9.5	12.7	9.7	1.9	14	0.98	0.91
45	10.7	14.3	11.0	2.0	15	0.98	0.95
50	11.9	15.9	11.9	2.4	16	1.00	0.99
55	13.1	17.5	13.3	2.8	18	0.99	0.97
60	14.3	19.1	-	-	-	-	-

Table H.6: Calculated and Measured Crack Widths (Specimen E12-9)

Steel Stress (ksi)	Calculated Crack Width (mils)		Measured Crack Width (mils)			Calc/Measured Crack Width	
	Avg.	Max.	Avg.	SD	Max.	Avg.	Max.
20	6.5	8.7	-	-	-	-	-
25	8.1	10.9	-	-	-	-	-
30	9.8	13.0	-	-	-	-	-
35	11.4	15.2	10.2	3.0	17	1.12	0.89
40	13.0	17.4	12.5	3.8	19	1.04	0.91
45	14.7	19.5	15.4	3.6	24	0.95	0.81
50	16.3	21.7	17.8	4.0	25	0.91	0.87
55	17.9	23.9	20.1	3.9	27	.89	0.88
60	19.5	26.0	-	-	-	-	-

Table H.7: Calculated and Measured Crack Widths (Specimen E12-12)

Steel Stress (ksi)	Calculated Crack Width (mils)		Measured Crack Width (mils)			Calc/Measured Crack Width	
	Avg.	Max.	Avg.	SD	Max.	Avg.	Max.
20	8.4	11.1	-	-	-	-	-
25	10.4	13.9	-	-	-	-	-
30	12.5	16.7	-	-	-	-	-
35	14.6	19.5	14.8	2.6	19	0.99	1.03
40	16.7	22.3	15.3	2.4	20	1.09	1.11
45	18.8	25.1	15.1	3.9	23	1.24	1.09
50	20.9	27.8	16.6	5.0	23	1.26	1.21
55	23.0	30.6	18.2	5.1	24	1.26	1.28
60	25.1	33.4	20.1	5.7	28	1.25	1.19

Table H.8: Calculated and Measured Crack Widths (Specimen E12-18)

Steel Stress (ksi)	Calculated Crack Width (mils)		Measured Crack Width (mils)			Calc/Measured Crack Width	
	Avg.	Max.	Avg.	SD	Max.	Avg.	Max.
20	12.1	16.2	-	-	-	-	-
25	15.2	20.2	-	-	-	-	-
30	18.2	24.3	-	-	-	-	-
35	21.2	28.3	-	-	-	-	-
40	24.3	32.3	16.7	1.9	17	1.45	1.90
45	27.3	36.4	15.9	5.8	22	1.72	1.65
50	30.3	40.4	16.2	6.8	31	1.87	1.30
55	33.3	44.5	21.8	6.6	36	1.53	1.24
60	36.4	48.5	-	-	-	-	-

Table H.9: Calculated and Measured Crack Widths (Specimen E6-9)

Steel Stress (ksi)	Calculated Crack Width (mils)		Measured Crack Width (mils)			Calc/Measured Crack Width	
	Avg.	Max.	Avg.	SD	Max.	Avg.	Max.
20	6.5	8.7	-	-	-	-	-
25	8.1	10.9	4.1	1.2	7	1.99	1.55
30	9.8	13.0	6.0	1.4	8	1.63	1.63
35	11.4	15.2	6.6	2.6	13	1.73	1.17
40	13.0	17.4	8.3	2.3	14	1.57	1.24
45	14.7	19.5	8.9	2.8	16	1.65	1.22
50	16.3	21.7	9.8	2.9	18	1.66	1.21
55	17.9	23.9	11.6	3.2	20	1.54	1.19
60	19.5	26.0	-	-	-	-	-

Table H.10: Calculated and Measured Crack Widths (Specimen E18-9)

Steel Stress (ksi)	Calculated Crack Width (mils)		Measured Crack Width (mils)			Calc/Measured Crack Width	
	Avg.	Max.	Avg.	SD	Max.	Avg.	Max.
20	6.5	8.7	-	-	-	-	-
25	8.1	10.9	-	-	-	-	-
30	9.8	13.0	9.6	3.2	14	1.02	0.93
35	11.4	15.2	12.3	3.0	17	0.93	0.89
40	13.0	17.4	13.3	3.4	20	0.98	0.87
45	14.7	19.5	15.1	3.8	20	0.97	0.98
50	16.3	21.7	17.6	3.9	23	0.93	0.94
55	17.9	23.9	20.9	3.8	26	0.86	0.92
60	19.5	26.0	-	-	-	-	-